ABSTRACT

Title of Document: FLEXURAL FATIGUE BEHAVIOUR OF FIBER-REINFORCED CONCRETE BASED ON DISSIPATED ENERGY MODELING

Ehsan Aramoon, Ph.D Civil Engineering, 2014

Directed By: Associate Professor, Dr. Dimitrios Goulias, Department of Civil and Environmental Engineering

After a century of study of fatigue phenomena in concrete, most of the proposed models for predicting the fatigue life of concrete are not sufficiently precise. The traditional models for predicting fatigue life of concrete are only based on the strength-related parameters such as stress level. The high variation of concrete's strength has led to highly scattered fatigue test result and, consequently, reduced the predictive quality of fatigue models.

Recently, several studies have focused on incorporation of new damping-related parameters in fatigue life models to improve the predictability of these models. Damping properties have a crucial effect on dynamic motion and energy dissipation capacity in fatigue life, and therefore they seem to be an important factor in characterizing fatigue as a dynamic motion.

The general objective of this research was to acquire a comprehensive understanding of the fatigue behavior of concrete in terms of energy dissipation and, consequently, develop a more statistically reliable approach to characterize the fatigue properties of concrete such as fatigue life. To achieve this purpose, damping properties of several concrete mixtures, with or without fiber reinforcement, were studied. A fatigue model based on dissipated energy concept was developed. The new model is then compared to traditional model. The results show that the new fatigue model has better predictive quality than the traditional approach.

FLEXURAL FATIGUE BEHAVIOUR OF FIBER-REINFORCED CONCRETE BASED ON DISSIPATED ENERGY MODELING

By

Ehsan Aramoon

Dissertation submitted to the Faculty of the Graduate School of the

University of Maryland, College Park in partial fulfillment

of the requirement for the degree of

Doctor of Philosophy

2014

Advisory Committee:

Dr. Dimitrios Goulias, Chair
Dr. M. Sherrif Aggour
Dr. Amade M. Amde
Dr. Ahmet H. Aydilek
Dr. Sung Lee, Dean's Representative

Dedication

I would like to dedicate this dissertation to my dear family and supportive, beautiful wife.

Acknowledgments

I would like to express my deepest appreciation to my advisor, Dr. Dimitrios Goulias, for his patience and guidance throughout this challenging journey.

I am also deeply thankful to the members of committee, Dr. M. Sherrif Aggour, Dr. Made M. Amde, Dr. Ahmet H. Aydilek and Dr. Sung Lee for providing comments and thoughts for my dissertation.

I am deeply grateful to Dr. Haejin Kim for his support by providing materials and testing equipment. Special thanks to my brother, Amin Aramoon, for helping me with computer programming. I would like to extend my appreciation to Mr. Alfred Bituin, Mr. Rongjin Hong, Ms. Sarah Saxon, Mr. Konnor Burrsow, and Ms. Sadaf Khosravifar for their help with experimental work.

Finally, I would like to thank my parents and wife for their endless support and sacrifices.

Table of Contents

DEDICATION… II

ACKNOWLEDGMENTS III

LIST OF TABLES IX

LIST OF FIGURES XV

CHAPTER 1. INTRODUCTION 1

1.1. RESEARCH MOTIVATION 1

1.2. OBJECTIVE OF THIS RESEARCH 3

1.3. RESEARCH APPROACH 4

1.4. ORGANIZATION OF DISSERTATION 5

CHAPTER 2. LITERATURE REVIEW 6

2.1. INTRODUCTION 6

2.2. EFFECT OF LOADING CHARACTERISTICS ON THE FATIGUE LIFE OF CONCRETE 6

2.2.1. MODELS INCORPORATING STRESS LEVEL (S) 7

2.2.2. MODELS INCORPORATING STRESS RATIO (R) 10

2.2.3. MODELS INCORPORATING LOADING FREQUENCY (F) 13

2.3. PROBABILISTIC FATIGUE MODELS 16

2.4. ENERGY APPROACH TO CHARACTERIZING FATIGUE BEHAVIOR OF CONCRETE 18

2.4.1. FACTORS IMPACTING THE TOTAL DISSIPATED ENERGY IN FATIGUE OF CONCRETE 18

2.4.2. HEAT GENERATION IN THE FATIGUE PROCESS 21

2.4.3. FATIGUE LIFE PREDICTIONS FOR CONCRETE USING THE ENERGY-DISSIPATION CONCEPT 23

2.5. THE IMPACT OF FROST DAMAGE ON THE FATIGUE PERFORMANCE OF CONCRETE 25

2.5.1. THE FROST DAMAGE MECHANISM 25

2.5.2. Effect of Frost Damage on the Physical Properties of Plain and Fiber-Reinforced Concrete 26
2.5.3. Combined Effects of Freeze-thaw and Fatigue 29

CHAPTER 3. MATERIAL, MIX DESIGN AND TESTING 35

3.1. Material 35
3.1.1. Aggregate 35
3.1.2. Cement 36
3.1.3. Chemical Admixtures 37
3.1.4. Synthetic Fiber 37
3.2. Mixture Design 37
3.3. Sample Preparation (Casting and Curing) 39
3.4. Testing Program 39
3.4.1. Fresh Concrete Testing 39
3.4.2. Hardened Concrete Testing 42
3.5. Mix Characteristics 46
3.5.1. Fresh Concrete Properties 46
3.5.2. Hardened Concrete Test Results 47

CHAPTER 4. METHODOLOGY, RESULTS AND DISCUSSION 51

4.1. Methodology 51
4.1.1. Fatigue Failure Definition 51
4.1.2. Fatigue Test as a Forced Vibration 52
4.1.3. Energy Dissipation in the Fatigue Process 57
4.1.4. Terminology 64
4.2. Fatigue Test Results and Discussion 65
4.2.1. Effect of Stress Level on Fatigue Life 66

4.2.2. Effect of Loading Frequency on Fatigue Life 70
4.2.3. Effect of Fiber Addition on Fatigue Life 72
4.3. Dissipated Energy per Cycle of Loading 73
4.3.1. Energy Dissipation during the Course of Fatigue Life 75
4.3.2. Effect of Fiber Addition on Energy Dissipation Properties during Fatigue 78
4.3.3. Factors Influencing Damping Force 79
4.3.4. Averaged-dissipated energy per loading cycle 88
4.3.5. Total Dissipated Energy per Cycle of Loading 93
4.3.6. Deformational Characteristics 99
4.4. Combined Effect of Fatigue and Freeze-Thaw 116
4.4.1. Volumetric Analysis of Samples Exposed to Freeze-Thaw 117
4.4.2. Ultrasonic Pulse Velocity Result 125
4.4.3. Effect of Freeze-Thaw Exposure on Fatigue Life 126
4.4.4. Effect of Freeze-Thaw Exposure on Averaged and Total Dissipated Energy 127
4.4.5. Effect of Freeze-Thaw Exposure on Damping Force 130
4.4.6. Effect of Freeze-Thaw Exposure on Deformational Characteristics 133

CHAPTER 5. RESEARCH ANALYSIS AND MODELING 140

5.1. Introduction 140
5.2. Least Squares Methods 141
5.3. Fatigue Life Modeling 141
5.3.1. Fatigue Life Prediction Using ADE 143
5.3.2. Linear Model 143
5.3.3. Exponential Model 145
5.3.4. Power Model 158
5.3.5. Traditional S-N_F Approach versus ADE-N_F Approach 163
5.3.6. Fatigue life prediction model incorporating fiber content 179

5.4. LOADING CHARACTERISTICS AND ADE RELATIONSHIP 184

5.4.1. LINEAR MODEL 184

5.4.2. EXPONENTIAL MODEL 189

5.4.3. POWER MODEL 193

5.4.4. EVALUATING THE EFFECT OF FREQUENCY OF LOADING ON ADE 197

5.5. COMBINED EFFECT OF FREEZE-THAW AND FATIGUE 198

5.5.1. APPLICATION OF ADE IN FATIGUE LIFE PREDICTION MODEL OF FREEZE-THAW EXPOSED CONCRETE 199

5.5.2. EXPONENTIAL MODEL (FREEZE-THAW EXPOSED SAMPLES) 199

5.5.3. PREDICTION MODEL INCORPORATING FREEZE-THAW CYCLES AND ADE 202

5.5.4. PREDICTION MODEL INCORPORATING VOID CONTENT AND ADE 204

5.6. PREDICTION MODEL FOR PLASTIC DEFORMATION ACCUMULATION OF MIXTURE WITH VARIOUS AMOUNTS OF FIBER CONTENT (%F) 206

5.7. RELATION BETWEEN DYNAMIC MOTION PARAMETERS AND FATIGUE LIFE AND STRESS LEVEL 213

5.8. ENDURANCE LIMIT 218

5.8.1. TRADITIONAL APPROACH TO DETERMINING ENDURANCE LIMIT 218

5.8.2. LOAD-DEFORMATION CURVE AND ENDURANCE LIMIT 220

CHAPTER 6. CONCLUSIONS AND RECOMMENDATIONS 226

6.1. CONCLUSIONS 226

6.2. RECOMMENDATIONS FOR FUTURE RESEARCH 233

APPENDIX A… 235

APPENDIX B…. 240

APPENDIX C… 244

REFERENCES.. 259

List of Tables

TABLE 2-1: CALIBRATION PARAMETERS FOR PLAIN CONCRETE AT DIFFERENT SURVIVAL PROBABILITIES (SHI, FWA AND TAN 1993) 12

TABLE 2-2: CALIBRATION PARAMETERS FOR STEEL FIBER-REINFORCED CONCRETE AT DIFFERENT SURVIVAL PROBABILITIES (SINGH AND KAUSHIK 2003) 13

TABLE 2-3: TEST CONDITIONS (FORGERON AND TROTTIER 2004) 30

TABLE 2-4: FLEXURAL STRENGTH AND STIFFNESS OF PLAIN CONCRETE AT DIFFERENT COMBINATIONS OF FREEZE-THAW AND FATIGUE (FORGERON AND TROTTIER 2004) 31

TABLE 2-5: FLEXURAL STRENGTH AND STIFFNESS OF FRC AT DIFFERENT COMBINATIONS OF FREEZE-THAW AND FATIGUE (FORGERON AND TROTTIER 2004) 31

TABLE 2-6. LOADING AND ENVIRONMENTAL CONDITIONS (LI, SUN AND JIANG 2011) 32

TABLE 3-1: FINE AGGREGATE PROPERTIES 35

TABLE 3-2: COARSE AGGREGATE PROPERTIES 36

TABLE 3-3: PHYSICAL AND CHEMICAL PROPERTIES OF CEMENT 36

TABLE 3-4: PROPERTIES OF POLYPROPYLENE FIBER 37

TABLE 3-5: MIX PROPORTION 38

TABLE 3-6: MD #7 MIX REQUIREMENT 38

TABLE 3-7: TESTING PROGRAM AND NUMBER OF SAMPLES 46

TABLE 3-8: FRESH CONCRETE PROPERTIES OF CONCRETE MIXTURES 46

TABLE 4-1: FATIGUE LIFE AND STRESS LEVEL OF FRC8 SAMPLES (LOADING FREQUENCY=5) 67

TABLE 4-2: FATIGUE LIFE AND STRESS LEVEL OF FRC8 SAMPLES (LOADING FREQUENCY=10) 68

TABLE 4-3: VARIABILITY ASSESSMENT OF FATIGUE LIFE AT DIFFERENT LOADING CONDITIONS (FRC8 SAMPLES) 70

TABLE 4-4: EFFECT OF POLYPROPYLENE FIBER ADDITION ON FATIGUE LIFE (FRC8, FRC4 AND CONTROL MIXTURES) 73

TABLE 4-5: CYCLIC STIFFNESS DURING FATIGUE LIFE (KN/M) (EFFECT OF LOADING CHARACTERISTIC, FRC8 SAMPLES) 85

TABLE 4-6: CYCLIC STIFFNESS DURING FATIGUE LIFE (KN/M) (EFFECT OF FIBER REINFORCEMENT) 86

TABLE 4-7: DIMENSIONLESS HYSTERESIS DAMPING CONSTANT. (EFFECT OF LOADING CHARACTERISTICS. FRC8 SAMPLES) 87

TABLE 4-8: DIMENSIONLESS HYSTERESIS DAMPING CONSTANT (EFFECT OF FIBER REINFORCEMENT) 88

TABLE 4-9: β_K (KN/M) (EFFECT OF FIBER REINFORCEMENT) 88

TABLE 4-10: DAMPING CONSTANT $C=\beta_K/2\pi f$ (N.SEC/M) (EFFECT OF LOADING CHARACTERISTICS, FRC8 SAMPLES) 91

TABLE 4-11: VARIABILITY ASSESSMENT OF ADE (EFFECT OF FIBER REINFORCEMENT) 93

TABLE 4-12: TOTAL DISSIPATED ENERGY OF FRC8 SAMPLES AT DIFFERENT LOADING CONDITION 95

TABLE 4-13: TOTAL DISSIPATED ENERGY AT S=0.7 AND LOADING FREQUENCY =5 (EFFECT OF FIBER REINFORCEMENT) 98

TABLE 4-14: MAXIMUM DEFLECTION AT FAILURE (EFFECT OF FIBER REINFORCEMENT) 110

TABLE 4-15: TDE, TOTAL PLASTIC ENERGY AND HEAT (FRC8 SAMPLES) 112

TABLE 4-16: RATIO OF TOTAL PLASTIC ENERGY TO TDE 113

TABLE 4-17: PLASTIC ENERGY DISSIPATION (EFFECT OF FIBER REINFORCEMENT) 113

TABLE 4-18: VOLUMETRIC DEFINITION OF ASTM C642 PARAMETERS 118

TABLE 4-19: DENSITY, WATER ABSORPTION AND %VOIDS OF FRC8 SAMPLES EXPOSED TO FREEZING AND THAWING CYCLE 121

TABLE 4-20: MASS LOSS DUE TO SCALING 123

TABLE 4-21: EFFECT OF FROST DAMAGE ON CYCLIC STIFFNESS (K) 131

TABLE 4-22: EFFECT OF FROST DAMAGE ON HYSTERESIS DAMPING CONSTANT 132

TABLE 4-23: MAXIMUM DEFLECTION AT FAILURE (EFFECT OF FROST DAMAGE) 136

TABLE 4-24: TDE, PLASTIC ENERGY AND HEAT (EFFECT OF FREEZE-THAW EXPOSURE, FRC8) 139

TABLE 5-1: FATIGUE MODELING DATASET 142

TABLE 5-2: LINEAR CORRELATION COEFFICIENT BETWEEN NF AND ADE 144

TABLE 5-3: ANALYSIS OF VARIANCE (EXPONENTIAL MODEL, NF-ADE, FRC8, 5 HZ, A=0.05) 146

TABLE 5-4: ANALYSIS OF VARIANCE (EXPONENTIAL MODEL, NF-ADE, FRC8, 10 HZ, A=0.05) 146

TABLE 5-5: CALIBRATION COEFFICIENTS AND *T*-TEST OF INDEPENDENT VARIABLE (EXPONENTIAL MODEL, N_F-ADE, FRC8, 5 HZ, A=0.05) 147

TABLE 5-6: CALIBRATION COEFFICIENTS AND *T*-TEST OF INDEPENDENT VARIABLE (EXPONENTIAL MODEL, N_F-ADE, FRC8, 10 HZ, A=0.05) 147

TABLE 5-7: OUTLIER DETECTION (EXPONENTIAL MODEL, NF VS ADE, 5 HZ) 153

TABLE 5-8: OUTLIER DETECTION (EXPONENTIAL MODEL, NF VS ADE, 10 HZ) 154

TABLE 5-9: MEASURE OF GOODNESS OF MODEL (EXPONENTIAL MODEL, NF VS ADE, 5 HZ) 156

TABLE 5-10: MEASURE OF GOODNESS OF MODEL (EXPONENTIAL MODEL, NF VS ADE, 10 HZ) 156

TABLE 5-11. LOO CV FOR EXPONENTIAL MODEL AT 5 HZ FREQUENCY (NF VS ADE) 158

TABLE 5-12 REGRESSION ANALYSIS OF THE POWER MODEL (NF VS. ADE, 5HZ, A=0.05) 160

TABLE 5-13 REGRESSION ANALYSIS OF THE POWER MODEL (NF VS. ADE, 10HZ, A=0.05) 161

TABLE 5-14 OUTLIER DETECTION (POWER MODEL, NF VS ADE, 5 HZ) 162

TABLE 5-15 OUTLIER DETECTION (POWER MODEL, NF VS ADE, 10 HZ) 163

TABLE 5-16: COMPARISON OF FATIGUE LIFE PREDICTION RESULTS USING ADE AND ADE (N) 172

TABLE 5-17: WOHLER'S EQUATION CALIBRATION (NF VS. S, 5 HZ, A=0.05) 174

TABLE 5-18: SHI'S EQUATION CALIBRATION (EN VS. S, 5 HZ, A=0.05) 174

TABLE 5-19: CALCULATION OF R^2 FOR SHI'S FORMULA (EQUATION 14) WHEN *LN NF* IS THE DEPENDENT VARIABLE 175

TABLE 5-20:CHI-SQUARE CALCULATION (WOHLER'S S-NF MODEL) 177

TABLE 5-21: CHI-SQUARE CALCULATION (SHI'S S-NF MODEL) 178

TABLE 5-22: CHI-SQUARE CALCULATION (ADE-NF MODEL) 179

TABLE 5-23: EXPONENTIAL MODEL (NF VS. ADE, FRC4, A=0.05) 180

TABLE 5-24: EXPONENTIAL MODEL (NF VS. ADE, FRC4 AND FRC8, A=0.05) 182

TABLE 5-25: EXPONENTIAL MODEL (NF VS. ADE, CONTROL, FRC4 AND FRC8, A=0.05) 183

TABLE 5-26: REGRESSION ANALYSIS FOR LINEAR MODEL (ADE VS. S, 5 HZ, A=0.05) 185

TABLE 5-27: OUTLIER DETECTION, LINEAR MODEL (ADE VS. S, 5 HZ) 186

TABLE 5-28: REGRESSION ANALYSIS FOR LINEAR MODEL (ADE VS. S, 10 HZ, A=0.05) 187

TABLE 5-29: OUTLIER DETECTION, LINEAR MODEL (ADE VS. S, 10 HZ) 188

TABLE 5-30: REGRESSION ANALYSIS FOR EXPONENTIAL MODEL (ADE VS. S, 5 HZ, A=0.05) 190

TABLE 5-31: OUTLIER DETECTION, EXPONENTIAL MODEL (ADE VS. S, 5 HZ) 190

TABLE 5-32: REGRESSION ANALYSIS FOR EXPONENTIAL MODEL (ADE VS. S, 10 HZ, A=0.05) 191

TABLE 5-33: OUTLIER DETECTION, EXPONENTIAL MODEL (ADE VS. S, 10 HZ) 192

TABLE 5-34: REGRESSION ANALYSIS FOR POWER MODEL (ADE VS. S, 5 HZ, A=0.05) 194

TABLE 5-35: OUTLIER DETECTION, POWER MODEL (ADE VS. S, 5 HZ) 194

TABLE 5-36: REGRESSION ANALYSIS FOR POWER MODEL (ADE VS. S, 10 HZ, A=0.05) 195

TABLE 5-37: OUTLIER DETECTION, POWER MODEL (ADE VS. S, 10 HZ) 196

TABLE 5-38: MULTIVARIATE REGRESSION ANALYSIS (ADE, S, AND F, A=0.05) 197

TABLE 5-39. FATIGUE TEST AND VOLUMETRIC ANALYSIS (REEZE-THAW EXPOSED SAMPLES) 198

TABLE 5-40: DATA POINTS FOR EXPONENTIAL MODEL, INCLUDING THE F/T EXPOSED SAMPLES 200

TABLE 5-41: REGRESSION ANALYSIS OF FREEZE-THAW EXPOSED SAMPLES (EXPONENTIAL MODEL, A=0.05) 201

TABLE 5-42: REGRESSION ANALYSIS OF FROST-DAMAGE SAMPLE (A=0.05) 203

TABLE 5-43 MULTIVARIATE LINEAR REGRESSION (NF, ADE, AND VOID RATIO) 205

TABLE 5-44 MULTIVARIATE REGRESSION ANALYSIS (NF, ADE, AND VOID RATIO, A=0.05) 205

TABLE 5-45: PLASTIC DEFORMATION POLYNOMIAL MODELS 207

TABLE 5-46: NORMALIZED DEFORMATION MODELS AT VARIOUS CYCLE RATIOS (I.E., SHIFT FACTORS) 208

TABLE 5-47: CALIBRATION COEFFICIENTS OF EQUATION 36 AT DIFFERENT CYCLE RATIOS 211

TABLE 5-48: DATA SET FOR FATIGUE MODELING USING DYNAMIC MOTION PARAMETERS (5 HZ) 216

TABLE 5-49: SUMMARY OF REGRESSION ANALYSIS OF PROPOSED MODELS (NF, ADE, S, K AND B, A=0.05) 217

TABLE A-1: ADE VS. DISSIPATED ENERGY AT CYCLE 1 237

TABLE C-1: REGRESSION ANALYSIS OF MODEL 1-TABLE 5.49 244

TABLE C-2: REGRESSION ANALYSIS OF MODEL 2-TABLE 5.49 245

TABLE C-3: REGRESSION ANALYSIS OF MODEL 3-TABLE 5.49 246

TABLE C-4: REGRESSION ANALYSIS OF MODEL 4-TABLE 5.49 247

TABLE C-5: REGRESSION ANALYSIS OF MODEL 5-TABLE 5.49 248

TABLE C-6: REGRESSION ANALYSIS OF MODEL 6-TABLE 5.49 249

TABLE C-7: REGRESSION ANALYSIS OF MODEL 7-TABLE 5.49 250

TABLE C-8: REGRESSION ANALYSIS OF MODEL 8-TABLE 5.49 251

TABLE C-9: REGRESSION ANALYSIS OF MODEL 9-TABLE 5.49 252

TABLE C-10: REGRESSION ANALYSIS OF MODEL 10-TABLE 5.49 253

TABLE C-11: REGRESSION ANALYSIS OF MODEL 11-TABLE 5.49 254

TABLE C-12: REGRESSION ANALYSIS OF MODEL 12-TABLE 5.49 255

TABLE C-13: REGRESSION ANALYSIS OF MODEL 13-TABLE 5.49 256

TABLE C-14: REGRESSION ANALYSIS OF MODEL 14-TABLE 5.49 256

TABLE C-15: REGRESSION ANALYSIS OF MODEL 15-TABLE 5.49 257

TABLE C-16: REGRESSION ANALYSIS OF MODEL 16-TABLE 5.49 257

TABLE C-17: REGRESSION ANALYSIS OF MODEL 17-TABLE 5.49 258

List of Figures

FIGURE 2.1: DARTER AND BARENBERG (DARTER AND BARENBERG 1977) 8

FIGURE 2.2: EFFECT OF STRESS RATIO ON CONCRETE FATIGUE LIFE (TEPFERS AND KUTTI, FATIGUE STRENGTH OF PLAIN, ORDINARY, AND LIGHTWEIGHT CONCRETE 1979) 11

FIGURE 2.3: S-N_F-PF CURVES FOR DIFFERENT COMBINATION OF POLYPROPYLENE AND STEEL FIBER REINFORCED CONCRETE (2011) 17

FIGURE 2.4: TOTAL DISSIPATED ENERGY (EFFECT OF CONCRETE STRENGTH) (PASKOVA AND MEYER 1997) 19

FIGURE 2.5: TOTAL DISSIPATED ENERGY (EFFECT OF STRESS LEVEL) (PASKOVA AND MEYER 1997)..... 19

FIGURE 2.6: EFFECT OF STEEL FIBER-REINFORCEMENT ON TOTAL DISSIPATED ENERGY (PASKOVA AND MEYER 1997) 20

FIGURE 2.7: EFFECT OF POLYPROPYLENE-FIBER-REINFORCEMENT ON TOTAL DISSIPATED ENERGY (PASKOVA AND MEYER 1997) 20

FIGURE 2.8: DEVELOPMENT OF HEAT IN THE FATIGUE PROCESS (TEPFERS, SJOSTROM, ET AL. 2011) 21

FIGURE 2.9: EFFECT OF STRESS LEVEL ON GENERATED HEAT IN FATIGUE (HOLMES AND SHULER 1990) 22

FIGURE 2.10: EFFECT OF LOADING FREQUENCY ON GENERATED HEAT IN FATIGUE (HOLMES AND SHULER 1990) 22

FIGURE 2.11: DISSIPATED ENERGY RATIO IN THE FATIGUE PROCESS (DANIEL AND BISIRRI 2005) 24

FIGURE 2.12: COMPARISON OF THE DER METHOD WITH TRADITIONAL METHODS (DANIEL AND BISIRRI 2005) 24

FIGURE 2.13: RELATIVE PULSE VELOCITY AND MASS LOSS (SAHMARAN, ET AL. 2012)..... 27

FIGURE 2.14: DETERIORATION DUE TO FROST DAMAGE (SAHMARAN, ET AL. 2012) 27

FIGURE 2.15: PULSE VELOCITY REDUCTION DUE TO FREEZE-THAW EXPOSURE (RICHARDSON, COVENTRY AND WILKINSON 2012) 28
FIGURE 2.16: MASS LOSS DUE TO FROST DAMAGE (RICHARDSON, COVENTRY AND WILKINSON 2012) 28
FIGURE 2.17: STRAIN AT LOWER AND UPPER POINTS OF BENDING BEAMS DURING FATIGUE LIFE (LI, SUN AND JIANG 2011) 33
FIGURE 2.18: STRAIN AT LOWER AND UPPER POINTS OF BENDING BEAMS DURING FATIGUE LIFE (LI, SUN AND JIANG 2011) 33
FIGURE 2.19. STRESS-STRAIN CURVE (COMBINED EFFECTS OF FATIGUE AND FREEZE-THAW) (HASAN, UEDA AND SATO 2008) 34
FIGURE 3.1: SLUMP TEST 40
FIGURE 3.2: INVERTED SLUMP TEST 41
FIGURE 3.3: FLEXURAL STRENGTH TEST (THIRD POINT LOADING CONFIGURATION) 43
FIGURE 3.4: COMPRESSIVE STRENGTH OF CONCRETE MIXTURES AT 28 DAYS 48
FIGURE 3.5: FLEXURAL STRENGTH OF CONCRETE MIXTURES AT 28 DAYS 48
FIGURE 3.6: LOAD-DEFLECTION CURVES OF CONCRETE SAMPLES IN FLEXURE 49
FIGURE 3.7: ELASTIC MODULUS OF CONCRETE MIXTURES 50
FIGURE 4.1: CONCEPT OF FATIGUE FAILURE 52
FIGURE 4.2: HARMONICALLY EXCITED SINGLE DEGREE OF FREEDOM VIBRATION 53
FIGURE 4.3: AMPLITUDE RATIO OF HYSTERESIS DAMPING SYSTEM 57
FIGURE 4.4: DEMONSTRATION OF DISSIPATED ENERGY PER LOADING CYCLE 59
FIGURE 4.5: EXAMPLE OF RECORDED DATA PER LOADING CYCLE 60
FIGURE 4.6: DEMONSTRATION OF TOTAL DISSIPATED ENERGY DUE TO PLASTIC DEFORMATION 63
FIGURE 4.7: STRESS LEVEL VS. FATIGUE LIFE (FRC8, LOADING FREQUENCY = 5) 68
FIGURE 4.8: STRESS LEVEL VS. FATIGUE LIFE (FRC8, LOADING FREQUENCY = 10) 69

FIGURE 4.9: COMPARISON OF S-N_F CURVES AT DIFFERENT LOADING FREQUENCY (FRC8 SAMPLES) 71

FIGURE 4.10: RATIO OF FATIGUE LIFE AT LOADING FREQUENCY OF 10 HZ TO FATIGUE LIFE AT LOADING FREQUENCY OF 5 HZ (FRC8 SAMPLES) 71

FIGURE 4.11: DISSIPATED ENERGY PER LOADING CYCLE THROUGHOUT THE ENTIRE FATIGUE LIFE (FRC8 SAMPLE) 74

FIGURE 4.12: NORMALIZED MOVING AVERAGE OF DISSIPATED ENERGY (LOADING FREQUENCY = 5, FRC8 SAMPLES) 77

FIGURE 4.13: NORMALIZED MOVING AVERAGE OF DISSIPATED ENERGY (LOADING FREQUENCY = 10, FRC8 SAMPLES) 77

FIGURE 4.14: NORMALIZED MOVING AVERAGE OF DISSIPATED ENERGY (EFFECT OF FIBER REINFORCEMENT) 79

FIGURE 4.15: CYCLIC STIFFNESS (K) VARIATION DURING FATIGUE LIFE (S=0.8, LOADING FREQUENCY=5, FRC8) 81

FIGURE 4.16: CYCLIC STIFFNESS (K) VARIATION DURING FATIGUE LIFE (S=0.8, LOADING FREQUENCY=10, FRC8) 82

FIGURE 4.17: CYCLIC STIFFNESS (K) VARIATION DURING FATIGUE LIFE (S=0.7, LOADING FREQUENCY=5, FRC8) 82

FIGURE 4.18: CYCLIC STIFFNESS (K) VARIATION DURING FATIGUE LIFE (S=0.7, LOADING FREQUENCY=10, FRC8) 83

FIGURE 4.19: CYCLIC STIFFNESS (K) VARIATION DURING FATIGUE LIFE (S=0.6, LOADING FREQUENCY=5, FRC8) 83

FIGURE 4.20: CYCLIC STIFFNESS (K) VARIATION DURING FATIGUE LIFE (S=0.6, LOADING FREQUENCY=5, FRC8) 84

FIGURE 4.21: AVERAGED-DISSIPATED ENERGY PER LOADING CYCLE (EFFECT OF LOADING CHARACTERISTICS, FRC8 SAMPLES) 91

FIGURE 4.22: EFFECT OF FIBER REINFORCEMENT ON AVERAGE DISSIPATED ENERGY PER LOADING CYCLE ... 92

FIGURE 4.23: EFFECT OF LOADING FREQUENCY ON TOTAL DISSIPATED ENERGY (FRC8 MIXTURE) 94

FIGURE 4.24: TOTAL DISSIPATED ENERGY (TDE) VS. FATIGUE LIFE (N_F) (FRC8 SAMPLES)..... 96

FIGURE 4.25: LOAD-DEFLECTION CURVE (S=0.8, FREQUENCY OF LOADING=5, FRC8) 100

FIGURE 4.26: LOAD-DEFLECTION HISTORY-FRC8 SAMPLE (S=0.8, LOADING FREQUENCY = 5)..... 103

FIGURE 4.27:LOAD-DEFLECTION HISTORY-CONTROL SAMPLE (S=0.7, LOADING FREQUENCY = 5)..... 103

FIGURE 4.28: PLASTIC DEFORMATION ACCUMULATION DURING FATIGUE LIFE (S=0.8, LOADING FREQUENCY = 5, FRC8 SAMPLES) 104

FIGURE 4.29: PLASTIC DEFORMATION ACCUMULATION DURING FATIGUE LIFE (S=0.7, LOADING FREQUENCY = 5, FRC8 SAMPLES) 105

FIGURE 4.30: PLASTIC DEFORMATION ACCUMULATION DURING FATIGUE LIFE (S=0.6, LOADING FREQUENCY = 5, FRC8 SAMPLES) 105

FIGURE 4.31: PLASTIC DEFORMATION ACCUMULATION DURING FATIGUE LIFE (S=0.8, LOADING FREQUENCY = 10, FRC8 SAMPLES) 106

FIGURE 4.32: PLASTIC DEFORMATION ACCUMULATION DURING FATIGUE LIFE (S=0.7, LOADING FREQUENCY = 10, FRC8 SAMPLES) 106

FIGURE 4.33: PLASTIC DEFORMATION ACCUMULATION DURING FATIGUE LIFE (S=0.7, LOADING FREQUENCY = 10, FRC8 SAMPLES) 107

FIGURE 4.34: PLASTIC DEFORMATION ACCUMULATION DURING FATIGUE LIFE (EFFECT OF FIBER REINFORCEMENT) 108

FIGURE 4.35: AMPLITUDE RATIO VARIATION DURING FATIGUE LIFE (S=0.7, LOADING FREQUENCY = 10, FRC8) 114

FIGURE 4.36: AMPLITUDE RATIO VARIATION DURING FATIGUE LIFE (S=0.8, LOADING FREQUENCY = 10)... 115

FIGURE 4.37: AMPLITUDE RATIO VARIATION DURING FATIGUE LIFE (S=0.8, LOADING FREQUENCY = 5, FRC8) 115

FIGURE 4.38: AMPLITUDE RATIO VARIATION DURING FATIGUE LIFE (S=0.8, LOADING FREQUENCY = 5, FRC8) 116

FIGURE 4.39: PHASE DIAGRAM OF CONCRETE 118

FIGURE 4.40: VARIATION OF APPARENT DENSITY DUE TO FROST DAMAGE (FRC8 SAMPLES) 120

FIGURE 4.41: RATIO OF THE VOLUME OF PERMEABLE VOIDS AFTER BOILING (V_B) TO THE VOLUME OF PERMEABLE VOIDS AFTER IMMERSION (V_I) (FRC8 SAMPLES) 123

FIGURE 4.42: ABSORPTION AFTER IMMERSION (FRC8 SAMPLES) 124

FIGURE 4.43: ABSORPTION AFTER BOILING (FRC8 SAMPLES) 124

FIGURE 4.44: ULTRASONIC PULSE VELOCITY VS. FREEZE-THAW EXPOSURE 125

FIGURE 4.45: VOID RATIO VS. FREEZE-THAW CYCLE 126

FIGURE 4.46: AVERAGE FATIGUE LIFE AT DIFFERENT FREEZE-THAW EXPOSURE (FRC8 SAMPLE) 127

FIGURE 4.47: AVERAGED DISSIPATED ENERGY PER LOADING CYCLE AT DIFFERENT FREEZE-THAW EXPOSURE (FRC8 SAMPLES) 128

FIGURE 4.48: TOTAL DISSIPATED ENERGY AT DIFFERENT FREEZE-THAW CYCLE (FRC8 SAMPLES) 129

FIGURE 4.49: ADE-N_F TREND (0 F/T VS. FROST-DAMAGED SAMPLES, FRC8) 130

FIGURE 4.50: HYSTERESIS DAMPING CONSTANT VS. FATIGUE LIFE (EFFECT OF FROST DAMAGE, FRC8) 132

FIGURE 4.51: LOAD-DEFLECTION HISTORY (0 F/T, FRC8) 134

FIGURE 4.52: LOAD-DEFLECTION HISTORY (200 F/T, FRC8) 134

FIGURE 4.53: LOAD-DEFLECTION HISTORY (400 F/T, FRC8) 135

FIGURE 4.54: LOAD-DEFLECTION HISTORY (400 F/T, FRC8) 135

FIGURE 4.55: CATEGORIZATION OF SEVERITY OF FROST DAMAGE BASED ON THE FATIGUE LIFE 138

FIGURE 4.56: PLASTIC DEFORMATION ACCUMULATION DURING FATIGUE LIFE (EFFECT OF FREEZE-THAW EXPOSURE, FRC8) 138

FIGURE 5.1: FATIGUE LIFE VS. ADE (FRC8) 144

FIGURE 5.2: ASSUMPTION OF LINEAR REGRESSION 148

FIGURE 5.3: RANKIT PLOT (EXPONENTIAL MODEL, NF VS. ADE, 5HZ) 150

FIGURE 5.4: RANKIT PLOT (EXPONENTIAL MODEL, NF VS. ADE, 10HZ) 150

FIGURE 5.5: EXPONENTIAL MODEL OF FATIGUE FOR SAMPLES TESTED AT A FREQUENCY OF 5 HZ 155

FIGURE 5.6:POWER MODEL (NF VS ADE, 5HZ) 160

FIGURE 5.7: RANKIT PLOT (POWER MODEL, NF VS. ADE, 5HZ) 161

FIGURE 5.8: RANKIT PLOT (POWER MODEL, NF VS. ADE, 10HZ) 162

FIGURE 5.9: NORMALIZED ADE(N) DURING THE FATIGUE LIFE (FRC8, S=0.6, 5HZ) 164

FIGURE 5.10: NORMALIZED ADE(N) DURING THE FATIGUE LIFE (FRC8, S=0.6, 5HZ) 164

FIGURE 5.11: NORMALIZED ADE(N) DURING THE FATIGUE LIFE (FRC8, S=0.7, 5HZ) 165

FIGURE 5.12: NORMALIZED ADE(N) DURING THE FATIGUE LIFE (FRC8, S=0.7, 5HZ) 165

FIGURE 5.13: NORMALIZED ADE(N) DURING THE FATIGUE LIFE (FRC8, S=0.8, 5HZ) 166

FIGURE 5.14: NORMALIZED ADE(N) DURING THE FATIGUE LIFE (FRC8, S=0.8, 5HZ) 166

FIGURE 5.15: NORMALIZED ADE (N) DURING THE FATIGUE LIFE (FRC8, 5HZ, AVERAGE OF 5 SAMPLES)... 167

FIGURE 5.16: RATIO OF LN NF FROM ESTIMATED ADE WITH ERROR TO LN NF FROM ACTUAL ADE..... 168

FIGURE 5.17: ALGORITHM TO FIND ADE (N) 170

FIGURE 5.18: ESTIMATION OF ADE FROM N-ADE(N) CURVE (FRC8,0.8-5-1) 170

FIGURE 5.19: ESTIMATION OF ADE FROM N-ADE(N) CURVE (FRC8,0.7-5-1) 171

FIGURE 5.20: ESTIMATION OF ADE FROM N-ADE (N) CURVE (FRC8, 0.6-5-3)..... 171

FIGURE 5.21: EFFECT OF M ON THE ABSOLUTE ERROR OF ADE (N) AND THE STOPPING TIME OF FATIGUE TEST 172

FIGURE 5.22: EXPONENTIAL MODEL (NF VS. ADE, FRC4) 181

FIGURE 5.23: EXPONENTIAL MODEL (NF VS. ADE, FRC4 AND FRC8) 182

FIGURE 5.24: EXPONENTIAL MODEL (NF VS. ADE, CONTROL, FRC4, AND FRC8)..... 184

FIGURE 5.25: LINEAR MODEL (ADE VS. S, FRC8, 5 HZ) 187

FIGURE 5.26: LINEAR MODEL (ADE VS. S, FRC8, 10 HZ) 188

FIGURE 5.27: EXPONENTIAL MODEL (ADE VS. S, FRC8, 5 HZ) 191

FIGURE 5.28: EXPONENTIAL MODEL (ADE VS. S, FRC8, 10 HZ) 192

FIGURE 5.29: POWER MODEL (ADE VS. S, FRC8, 5 HZ) 195

FIGURE 5.30: POWER MODEL (ADE VS. S, FRC8, 10 HZ) 196

FIGURE 5.31: EXPONENTIAL MODEL (NF VS. ADE, FREEZE-THAW EXPOSED SAMPLES) 201

FIGURE 5.32: EXPONENTIAL FATIGUE LIFE MODEL (FREEZE-THAW EXPOSED SAMPLES VS. UNDAMAGED SAMPLES) 202

FIGURE 5.33: PLASTIC DEFORMATION ACCUMULATION DURING FATIGUE LIFE (MIXTURES WITH VARIOUS FIBER CONTENTS) 206

FIGURE 5.34: NORMALIZED D/DMAX VS. FIBER CONTENT 210

FIGURE 5.35: CALIBRATION COEFFICIENT (A) VS. CYCLE RATIO 211

FIGURE 5.36: CALIBRATION COEFFICIENT (B) VS. CYCLE RATIO 212

FIGURE 5.37: COMPARISON OF DEFORMATION PREDICTION MODEL AND ACTUAL DATA 213

FIGURE 5.38: ENDURANCE LIMIT OF FRC8 SAMPLES TESTED AT FREQUENCIES OF 5 HZ AND 10 HZ 219

FIGURE 5.39: ENDURANCE LIMIT OF FRC8 SAMPLES TESTED AT FREQUENCIES OF 5 HZ AND 10 HZ EXPRESSED AS PERCENTAGE OF PLAIN CONCRETE FLEXURAL STRENGTH 220

FIGURE 5.40: LOAD-DEFLECTION ENVELOPE (FRC8, 0.8-10-1) 221

FIGURE 5.41: LOAD-DEFLECTION ENVELOPE (FRC8, 0.8-5-5) 222

FIGURE 5.42: LOAD-DEFLECTION ENVELOPE (FRC8, 0.7-10-3) 222

FIGURE 5.43: LOAD-DEFLECTION ENVELOPE (FRC8, 0.7-5-5) 223

FIGURE 5.44: ENVELOPE CURVE OF FRC8 MIXTURE TESTED AT A FREQUENCY OF 5 HZ 224

FIGURE 5.45: ENVELOPE CURVE OF FRC8 MIXTURE TESTED AT FREQUENCY OF 10 HZ 225

FIGURE A.1: ELASTO-PLASTIC DEFORMATION AT LOADING POINTS 235

FIGURE B.1: PROCESS OF OUTLIER DETECTION BASED ON CHAUVENET'S CRITERIA 241

FIGURE B.2: APPARENT DENSITY OF FREEZE-THAW EXPOSED SAMPLES (OUTLIER DETECTION) 241

FIGURE B.3: ABSORPTION AFTER IMMERSION OF FREEZE-THAW EXPOSED SAMPLES (OUTLIER DETECTION) 242

FIGURE B.4: ABSORPTION AFTER BOILING OF FREEZE-THAW EXPOSED SAMPLES (OUTLIER DETECTION) 242

FIGURE B.5: UPV OF FREEZE-THAW EXPOSED SAMPLES (OUTLIER DETECTION) 243

FIGURE B.6: VOID RATIO OF FREEZE-THAW EXPOSED SAMPLES (OUTLIER DETECTION) 243

FIGURE C.1: GRAPHICAL FORMAT OF MODEL 1-TABLE 5:49 244

FIGURE C.2: GRAPHICAL FORMAT OF MODEL 2-TABLE 5:49 245

FIGURE C.3: GRAPHICAL FORMAT OF MODEL 3-TABLE 5:49 246

FIGURE C.4: GRAPHICAL FORMAT OF MODEL 4-TABLE 5:49 247

FIGURE C.5: GRAPHICAL FORMAT OF MODEL 5-TABLE 5:49 248

FIGURE C.6: GRAPHICAL FORMAT OF MODEL 6-TABLE 5:49 249

FIGURE C.7: GRAPHICAL FORMAT OF MODEL 7-TABLE 5:49 250

FIGURE C.8: GRAPHICAL FORMAT OF MODEL 8-TABLE 5:49 251

FIGURE C.9: GRAPHICAL FORMAT OF MODEL 9-TABLE 5:49 252

FIGURE C.10: GRAPHICAL FORMAT OF MODEL 10-TABLE 5:49 253

FIGURE C.11: GRAPHICAL FORMAT OF MODEL 11-TABLE 5:49 254

FIGURE C.12: GRAPHICAL FORMAT OF MODEL 12-TABLE 5:49 255

Chapter 1. Introduction

1.1. Research Motivation

After a century of study of fatigue phenomena in concrete, most of the proposed models for predicting the fatigue life of concrete are not sufficiently precise. Numerous studies have focused on finding a new approach to characterize fatigue life and develop more reliable prediction models.

Traditionally, prediction models for the fatigue life of concrete incorporate fatigue test setup parameters as an independent variable. Stress level has been the most common independent variable used in the fatigue life prediction models. Wohler's fatigue model, which is a semi-logarithmic relationship between fatigue life and stress level, has been calibrated by several researchers for different type of concrete and various testing configurations (i.e., various loading conditions and sample shapes and sizes). Later, several fatigue life models incorporated the stress ratio as the second most important factor, with stress level as an independent variable.

The relatively low predictability of these models originates from highly scattered fatigue test results. High variation in fatigue test results can be attributed to significant uncertainty in the value of fatigue test setup parameters, such as stress level. The stress level is the ratio of maximum cyclic load to the strength of the material. High variation in the value of concrete strength, even in a controlled testing environment, is the reason for the existing uncertainty. For instance, a 16% difference (as stated in ASTM C78) in the result of two properly operated flexural strength tests is accepted as the maximum deviation, which in fact shows the high variability in the results of flexural strength tests.

These highly scattered fatigue test results led to the introduction of probabilistic approaches to fatigue prediction models.

The other deficiency of the existing models is that the process of calibration is very time-consuming. The large deviation in the fatigue life test results requires a large number of fatigue tests to be conducted at each stress level in order to develop a reliable model. This, along with the fact that each fatigue test can take several days to complete, makes the process of calibration long and tedious. Increasing the loading frequency of fatigue tests was evaluated as the first possible solution to reduce the time for fatigue testing. Many studies have focused on the effect of loading frequencies, and consequently several fatigue models have been developed, including using loading frequency as the third independent variable.

One of the disadvantages of using strength-related parameters in prediction models is that they cannot distinguish between samples with the same strength but different damping properties. Damping properties have a crucial effect on dynamic motion and energy dissipation capacity in fatigue life, and therefore they seem to be an important factor in characterizing fatigue as a dynamic motion. In a recent study, Bissiri and Daniel (2005) introduced the concept of dissipated energy ratio (DER)—which is the ratio of the change in dissipated energy from load cycle N to load cycle N+1 to the dissipated energy of load cycle N—to predict the fatigue life (N_f) of concrete. The proposed model was compared to existing fatigue models, and good agreement was observed between the results for predicted fatigue life.

In this study, it is attempted to examine the damping behavior of polypropylene fiber-reinforced concrete to obtain a better understanding of the damping properties of

concrete during fatigue tests. The damping behavior of concrete is described by the hysteresis model. Hysteresis loop parameters such as dissipated energy per cycle, cyclic stiffness, and the hysteresis damping constant have been studied at various loading conditions and with different mixtures. Potentially, the result would be a more reliable model that can be calibrated in less time and require fewer fatigue tests.

1.2. Objective of This Research

The general objective of this research was to acquire a comprehensive understanding of the fatigue behavior of concrete in terms of energy dissipation and, consequently, develop a more statistically reliable approach to characterize the fatigue properties of concrete such as fatigue life. To achieve this objective, several substudies were designed and incorporated in the study, with the following aims:

- Evaluate the effect of polypropylene fiber reinforcement on both the fresh properties and mechanical properties of concrete, such as flexural strength, compressive strength, and elastic modulus;
- Determine the effect of fatigue-test loading characteristics, such as stress level and loading frequency, on the fatigue life and damping properties of polypropylene fiber-reinforced concrete;
- Introduce a damping related parameter to characterize the fatigue behavior of concrete in a more statistically reliable manner, as a replacement for traditional parameters such as stress level;
- Evaluate the effect of fiber reinforcement on the fatigue properties of concrete, such as damping and fatigue life;
- Evaluate the effect of fiber reinforcement on variability of fatigue test results;

- Evaluate the effect of frost damage on the damping properties and fatigue life of polypropylene fiber-reinforced concrete;
- Evaluate the effect of frost damage on the variability of fatigue test results;
- Develop a deterministic fatigue life prediction model based on the damping properties of concrete;
- Compare the new model to traditional fatigue life model to assess the new model's strength.

1.3. Research Approach

Three concrete mixtures containing various amount of polypropylene fiber (0%, 0.4%, and 0.8%) were prepared to investigate the effect of fiber reinforcement on concrete properties such as flexural strength, compressive strength, static elastic modulus, fatigue life, and damping behavior. Flexural fatigue tests using a third-point loading configuration were performed at a stress level of 0.7, loading frequency of 5 Hz, and stress ratio of 0.15.

To evaluate the effect of fatigue-test loading characteristics on the fatigue life and damping behavior of concrete, samples containing 0.8% polypropylene fiber were tested at three different stress levels (0.6, 0.7, and 0.8) and with loading frequencies of 5 and 10 Hz and a constant stress ratio of 0.15.

To study the effect of frost damage on fatigue resistance and damping properties of fiber-reinforced concrete, samples containing 0.8% fiber were exposed to freezing and thawing cycles for up to 400 cycles, in accordance with ASTM C666. The fatigue properties of frost-damaged samples were studied at a stress level of 0.7 after evaluating the homogeneity of the concrete sample using the ultrasonic pulse velocity test.

Thereafter, the tested samples were used to perform density, absorption, and void content analyses in accordance with ASTM C642.

1.4. Organization of Dissertation

The dissertation has been organized into six chapters, as follows. Chapter 1 includes the research motivation, objective, and approach. The summary of studies related to the fatigue behavior of concrete and the combination of freeze-thaw and fatigue are presented in Chapter 2. Testing procedures, material properties, and mixture design, along with test results for fresh concrete, flexural strength, compressive strength, and elastic modulus are presented in Chapter 3. Chapter 4 contains a detailed description of principles, calculation methods, and terminology, as well as experimental results and discussion. Statistical analysis and modeling are presented in Chapter 5. Several models were developed and assessed, based on regression analysis. Chapter 6 includes research conclusions and recommendations for future studies.

Chapter 2. Literature Review

2.1. Introduction

Fatigue is progressive damage to material that occurs due to repeated loading. Many civil structures experience this phenomenon during their service life. Some of these structures, such as pavement and bridges, are subjected to millions of load replications; some, such as tall buildings, may be exposed to thousands of load cycles as a result of earthquakes. Therefore, fatigue failure has always been one of the main concerns for engineers and requires careful consideration in the design of structures.

Developing a statistically reliable model to predict fatigue life has always been a major area of interest to researchers. Several fatigue life models have been proposed, and efforts are still being made to incorporate new variables to increase the accuracy of prediction models.

This chapter presents some of the major work performed in the fatigue modeling of concrete.

2.2. Effect of Loading Characteristics on the Fatigue Life of Concrete

The fatigue loading characteristic has been the most common parameter used in fatigue life prediction models. Fatigue loading is cyclic, and is usually characterized by stress level (S), stress ratio (R), and frequency of loading (f).

Stress level (S) is the ratio of maximum cyclic stress (peak of cyclic load) to the ultimate strength of material, stress ratio (R) is the ratio of minimum cyclic stress to

maximum cyclic stress, and loading frequency (f) is the number of loading cycles in a period of time.

The following section presents some of the previous studies, which have mainly focused on developing fatigue life prediction models for concrete beams and slabs exposed to flexural fatigue.

2.2.1. Models Incorporating Stress Level (S)

Many researchers have developed models that relate the fatigue life of the structure (Nf) to the stress level (S). Darter and Barenberg (1977) calibrated Equation 2.1, which is known as the Wholer equation, for a jointed plain concrete pavement based on fatigue test results conducted by Kesler (1953), Raithby and Galloway (1974), and Ballinger (1972). Figure 2.1 shows overall data collected from different studies. In the proposed model (Equation 2.2), fatigue failure is defined as the complete fracture of a concrete beam.

$$S = a + b\log(N_f) \quad \textbf{2.1}$$

$$\log(N_f) = 17.61 - 17.61\,S \quad \textbf{2.2}$$

Vesic and Saxena (1969) developed a power shape model (Equation 2.3) based on AASHO road test concrete sections. Terminal serviceability of 2.5 is considered to be the definition of fatigue failure.

$$N_f = 225000 \left(\frac{1}{S}\right)^4 \quad \textbf{2.3}$$

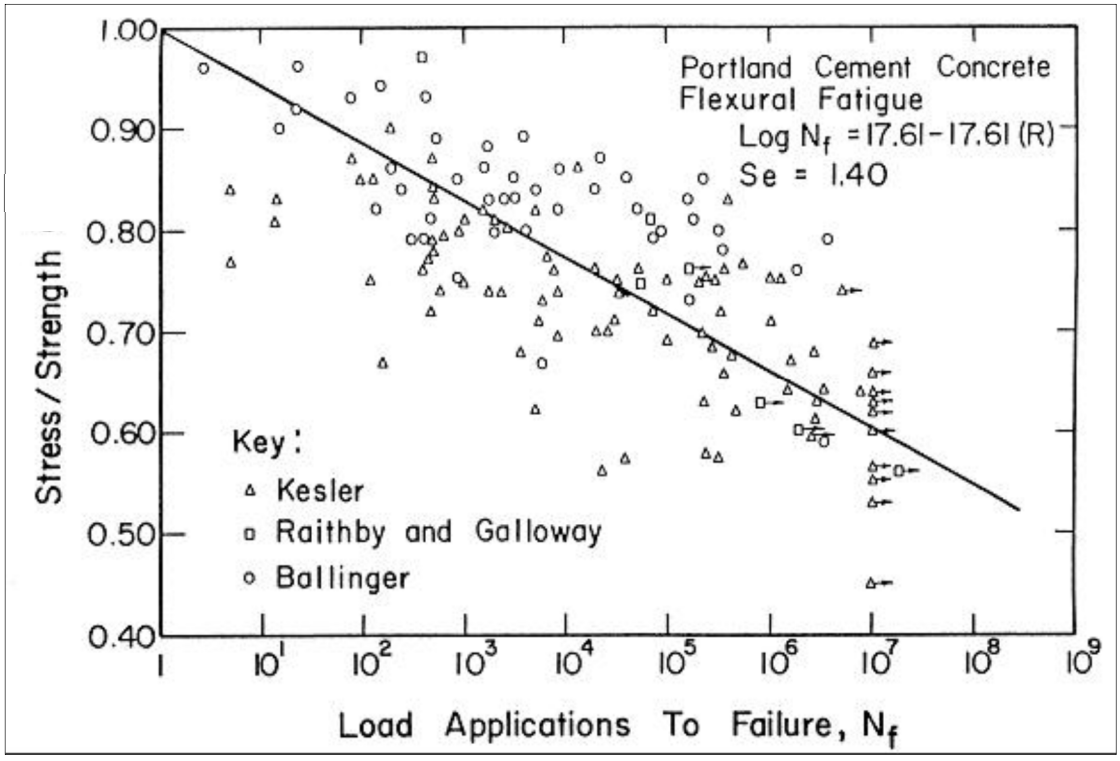

Figure 2.1: Darter and Barenberg (Darter and Barenberg 1977)

The effect of different supporting systems and load configurations were investigated by Roesler (1998). It was shown that results for a simply supported beam and fully supported beam have a good correlation with Darter's fatigue equation. Also, it was shown that existing beam fatigue models are very conservative in predicting concrete slab

fatigue. In other words, a concrete slab has a higher fatigue life than the predicted value when using the beam's fatigue equations. The following equation (Equation 2.4) was developed from his study on fully supported concrete slabs that are loaded at the edge.

$$N_f = \left(\frac{1.2968}{S}\right)^{32.57} \qquad \textbf{2.4}$$

Packard and Tayabji (1985) proposed the following equation based on flexural fatigue tests performed on concrete beams. The proposed model differentiates between fatigue tests performed at stress levels between 0.45 and 0.55 and fatigue tests performed at stress levels higher than 0.55. The model assumes that the fatigue life of concrete beam at a stress level below 0.45 is infinite.

$$\log \mathrm{N_f} = 11.737 - 12.077\ \mathrm{S} \quad \text{for} \quad \mathrm{S} > 0.55$$
$$\mathrm{N_f} = \left(\frac{4.2577}{\mathrm{S} - 0.4325}\right)^{3.268} \quad \text{for} \quad 0.45 < \mathrm{S} < 0.55 \qquad \textbf{2.5}$$

As can be seen in all proposed models, stress level has an indirect relationship with fatigue life whether the relation is defined by a linear semi logarithmic function or a power function. In other words, increasing the stress level is associated with a decrease in fatigue life of concrete. This is not surprising, considering that at higher stress levels, more plastic deformation is expected to be induced; hence, fatigue failure happens sooner.

2.2.2. Models Incorporating Stress Ratio (R)

Concrete structures are often exposed to changing loads, apart from their actual service load. A good example of this is the stress induced in a concrete pavement due to the temperature gradient. Temperature variation within the concrete slab results in curling. In the morning, when the temperature at the surface of the slab is higher than in the lower part, the slab has a convex upper shape. Therefore, the weight of the slab generates tensile stress on the lower slab fibers. This illustrates how a concrete pavement is exposed to a constant load apart from the traffic loading. In order to take into account this type of load's effect on fatigue behavior, the stress ratio (R) is introduced.

Murdok and Kesler (1958) were the first to investigate the effect of the stress ratio. Since then, many researchers have adopted a relationship that incorporate the effect of the stress ratio (R) on fatigue life of concrete. Equation 2.6 was proposed by Aas-Jakobsen (1970) to include the effect of the stress ratio (R) in fatigue life modeling.

$$S = 1 - b(1 - R)\log(N_f) \qquad \textbf{2.6}$$

The experimental coefficient (b) incorporated in this formula is determined to be 0.0640 (Aas-Jakobsen 1970) for a compressive fatigue test, 0.0685 (Tepfers and Kutti, Fatigue Strength of Plain, Ordinary, and Lightweight Concrete 1979) for a splitting tensile test of fatigue, and 0.0690 (Oh 1986) for a flexural fatigue test.

Figure 2.2 demonstrates the fatigue equation developed by Tepfers and Kutti (1979) for several stress ratios. As can be seen, at certain stress levels (S), increasing the

stress ratio (R) leads to fatigue life increase. In other words, as the minimum cyclic load increases—while the maximum cyclic load remains constant—fatigue life increases.

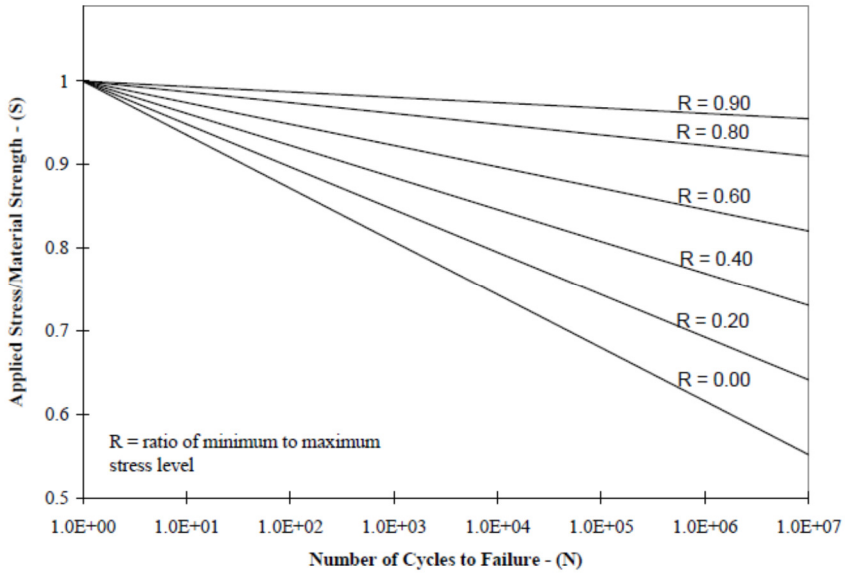

Figure 2.2: Effect of Stress Ratio on Concrete Fatigue Life (Tepfers and Kutti, Fatigue Strength of Plain, Ordinary, and Lightweight Concrete 1979)

The concept of equivalent fatigue life (EN) was introduced by Shi et al. (1993) to incorporate the stress ratio (R) into the fatigue life model. The definition of equivalent fatigue life is shown is Equation 2.7.

$$EN = {N_f}^{1-R} \qquad 2.7$$

The following fatigue model (Equation 2.8) was proposed based on the concept of equivalent fatigue life (EN), which takes into account the effect of stress level (S) and

stress ratio (R) on the fatigue life of concrete. Table 2-1 presents the calibration parameters (a and b) for the flexural fatigue of plain concrete (Shi, Fwa and Tan 1993). The proposed model is calibrated at different survival probabilities to incorporate a probabilistic point of view into the model. At a given survival probability and equivalent fatigue life (EN), the resulting stress level (S) shows the maximum stress level at which 95% of the time, the sample fails at an equivalent fatigue life larger than the given EN.

$$S = a\,(EN)^{-b} \qquad \textbf{2.8}$$

Table 2-1: Calibration Parameters for Plain Concrete at Different Survival Probabilities (Shi, Fwa and Tan 1993)

Survival Probability	a	b
0.95	0.9611	0.0419
0.90	0.9843	0.0423
0.80	1.0067	0.0424
0.70	1.0190	0.0423
0.60	1.0289	0.0422
0.50	1.0380	0.0422

Shi's fatigue formula was calibrated for steel fiber-reinforced concrete by Singh and Kaushik (2003).

Table 2-2: Calibration Parameters for Steel Fiber-reinforced Concrete at Different Survival Probabilities (Singh and Kaushik 2003)

Survival Probability	a	b
0.95	1.0261	0.0455
0.90	1.0434	0.0441
0.80	1.0573	0.0423
0.70	1.0658	0.0413
0.60	1.0736	0.0407
0.50	1.0786	0.0401

2.2.3. Models Incorporating Loading Frequency (f)

Developing a statistically reliable fatigue life model for concrete requires extensive testing at each stress level because of the high variability in fatigue testing. This becomes very long and tedious, particularly when fatigue life is studied at low stress levels, at which concrete has a very long fatigue life. Increasing the loading frequency (f) is one of the most common methods used to shorten the process of fatigue characterization.

Several investigators have studied the effect of loading frequency (f) on the fatigue strength of concrete. As cited by Kesler (1953), the flexural fatigue life of both medium- and high-strength concrete has not been significantly affected by loading frequencies that vary from 1.17 Hz to 7.3 Hz. In a review of research on the fatigue life of plain concrete, Murdok (1965) concluded that the effect of loading frequency within the range of 1 to 15 Hz on the fatigue life of concrete at stress levels below 0.75 is

insignificant (J. W. Murdock 1965). At higher frequencies, an increase in fatigue life is observed as the loading frequency increases (Awad and Hilsdorf 1971).

The influence of frequency can be attributed to the creep phenomenon. In lower frequencies, load applies in a longer period which result in higher creep deformation. Under such conditions, creep effects become more important and lead to a reduction in fatigue strength with decreasing loading rates (ACI Committee 215 1997).

Hsu (1981) was the first researcher to incorporate the effect of loading frequency in the fatigue life model. He extended fatigue model proposed by Aas and Jakobsen (1970) to include the effect of loading frequency on compression and flexural fatigue testing. The proposed models are as follows:

$$S = 1.2 - 0.2R - 0.133(1 - 0.779R)\log(N_f) - 0.053(1 - 0.445R)\log(\frac{1}{f}) \quad for \quad (N_f < 10^3)$$

$$S = 1 - 0.0662(1 - 0.556R)\log(N_f) - 0.0294\log(\frac{1}{f}) \quad for \quad (10^3 < N_f < 10^7) \qquad \textbf{2.9}$$

Furtak (1984) introduced a frequency influence coefficient and developed a new model (Equation 2.10) that includes the effect of loading rate, as shown below; a, b, c, d and e are experimental coefficients.

$$S = c\,{N_f}^a(1 + bR\log(N_f))\,C_f$$

$$C_f = 1 + d(1 - eR)\log f \qquad \textbf{2.10}$$

Recently, Chen (2009) introduced a correction factor (Equation 2.11) to relate the results of fatigue tests performed at frequencies higher than 100 Hz to tests of the fatigue life (N_f) of concrete performed at low frequencies. In Chen et al.'s model, the result of low-frequency fatigue can be estimated from the result of high-frequency fatigue by multiplying the high-frequency coefficient (φ) by a high-frequency fatigue formula.

$$\varphi = \varphi_0 \left(2N_f\right)^{\Delta b} \quad \textbf{2.11}$$

φ_0 and Δb are the experimental coefficients that can be determined using the Busquin fatigue model (Equation 2.12). According to the Busquin equation, amplitude of loading (σa) has a power relationship with fatigue life (N_f).

$$\sigma_a = c\left(2N_f\right)^b \quad \textbf{2.12}$$

φ is the ratio of amplitude of loading at a low frequency to the amplitude of loading at a high frequency.

$$\varphi = \frac{c_L}{c_H} \left(2N_f\right)^{b_L - b_H} \quad \textbf{2.13}$$

2.3. Probabilistic Fatigue Models

Scatter is an inherent characteristic of building materials, and concrete is not an exception. The fatigue life of similar concrete samples from the same batch under the same loading conditions can be significantly scattered. The variability in the fatigue life of concrete is unavoidable and can be attributed to many different sources, such as material variable properties, accuracy of testing equipment, testing environment, and so on.

McCall (1958) was one of the first researchers to apply probabilistic concepts to describe the variability in concrete beam fatigue failure. A theoretical model that incorporates probability of failure (P_f), stress level (S), and fatigue life (N_f) is proposed as follows.

$$(1 - P_f) = 10^{-aS^b(\log N_f)^c} \quad \textbf{2.14}$$

McCall's model generates a family of S-N_f-Pf curves. These graphs provide a probability of failure of concrete under a given loading condition (S) and fatigue life (N_f). Singh (2011) calibrated McCall's formula for hybrid fibrous concrete and produced a group of S-N-Pf curves (Figure 2.3) for different combinations of polypropylene- and steel-fiber-reinforced concrete. The S-N-Pf curve is the graphic format of McCall's model. At a given stress level and fatigue life (N_f), the probability that the sample will fail at a fatigue life equal to or smaller than N_f is shown in the graphs.

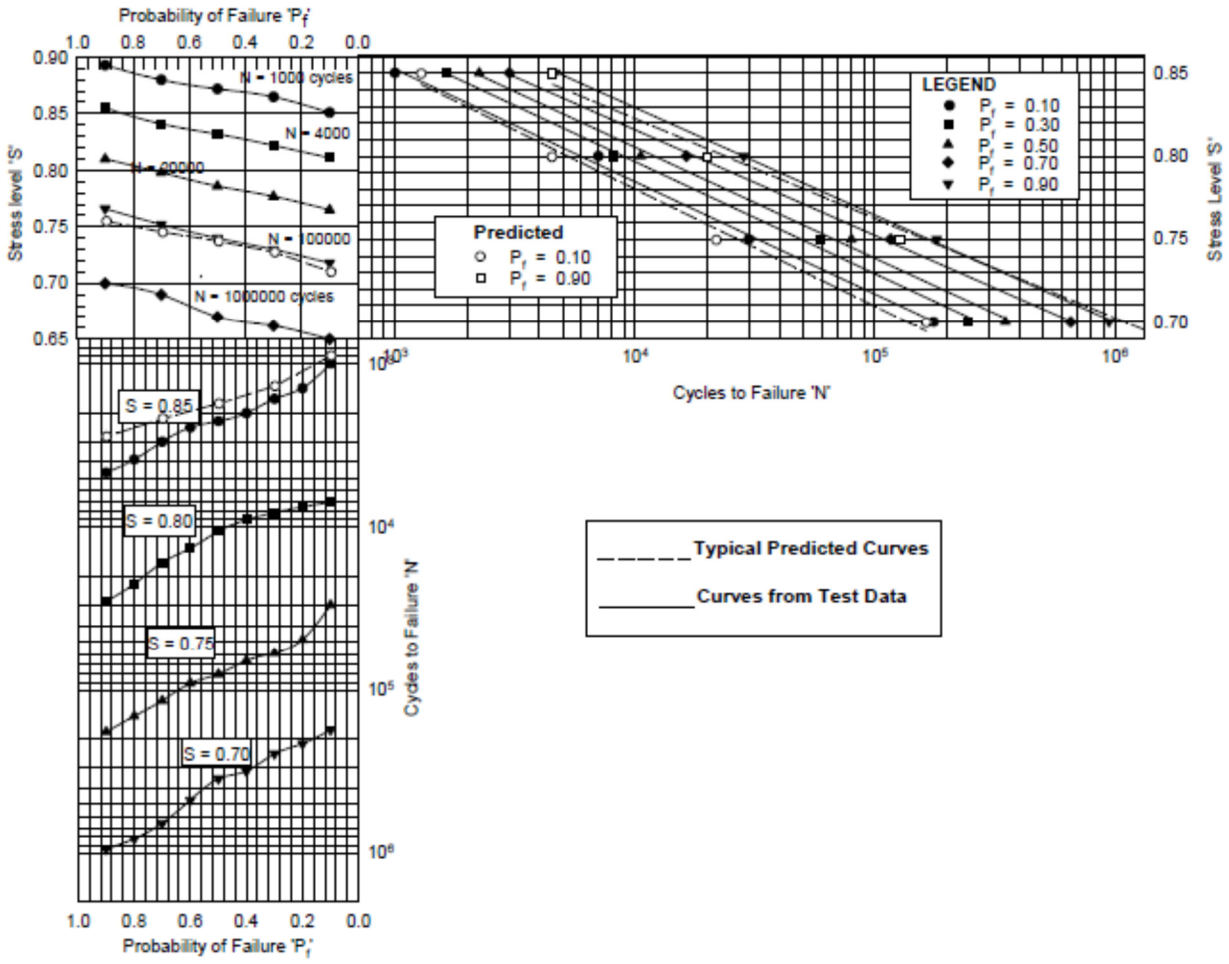

Figure 2.3: S-N_f-Pf Curves for Different Combination of Polypropylene and Steel Fiber Reinforced Concrete (2011)

Since the fatigue test results show considerable variability, the probability distribution function of fatigue life has received considerable attention in the literature. As cited by Kaushik and Mohammadi (2005), a two-parameter Weibull distribution was perfectly fit to the fatigue results for plain and fiber-reinforced concrete. This finding has also been reported by Singh et al. (2004).

2.4. Energy Approach to Characterizing Fatigue Behavior of Concrete

2.4.1. Factors Impacting the Total Dissipated Energy in Fatigue of Concrete

The energy absorption characteristic of concrete in the course of fatigue life has long been an area of interest for researchers. The energy absorption capacity of concrete due to its nonlinear hysteresis behavior under cyclic loading has been reported in many studies (Tepfers, Sjostrom, et al. 2011) (Paskova and Meyer 1997).

Paskova and Meyer (1997) found a direct relationship between the total energy dissipation of concrete during fatigue and its compressive strength (Figure 2.4). It is evident that at a given stress level, energy-dissipation capacity increases as the compressive strength increases. As shown in Figure 2.5, at a given compressive strength, more energy was dissipated during fatigue life as stress level decreases.

Application of steel and polypropylene fiber to concrete matrix has been found to be beneficial to the energy-dissipation capacity of concrete. As cited by Grzbowski and Meyer (1993) and Paskova and Meyer (1997), addition of 1% steel fiber can increase the energy absorption capacity of plain concrete by a factor of 10.2. The positive effect of polypropylene-fiber reinforcement has been seen at a lower stress level (Figure 2.6 and Figure 2.7).

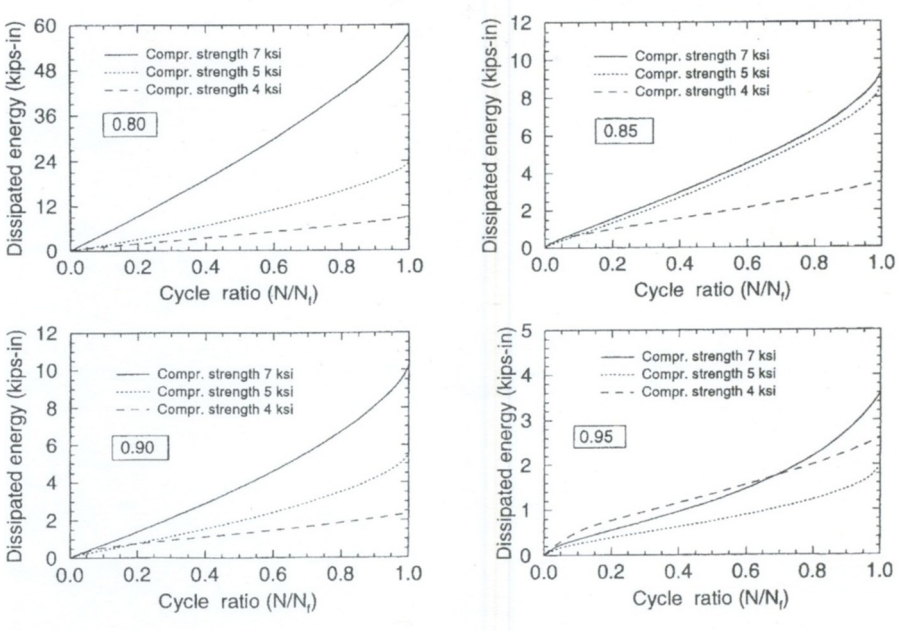

Figure 2.4: Total Dissipated Energy (Effect of Concrete Strength) (Paskova and Meyer 1997)

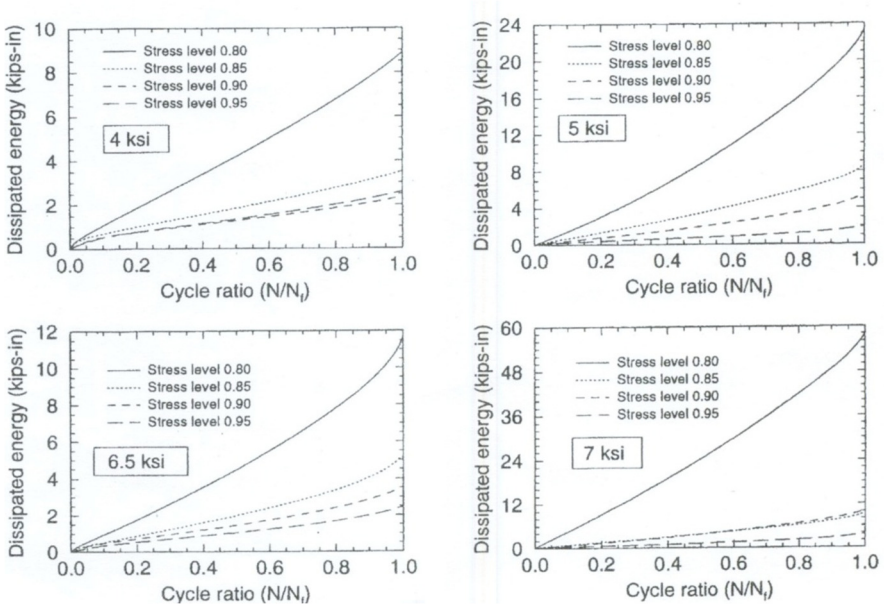

Figure 2.5: Total Dissipated Energy (Effect of Stress Level) (Paskova and Meyer 1997)

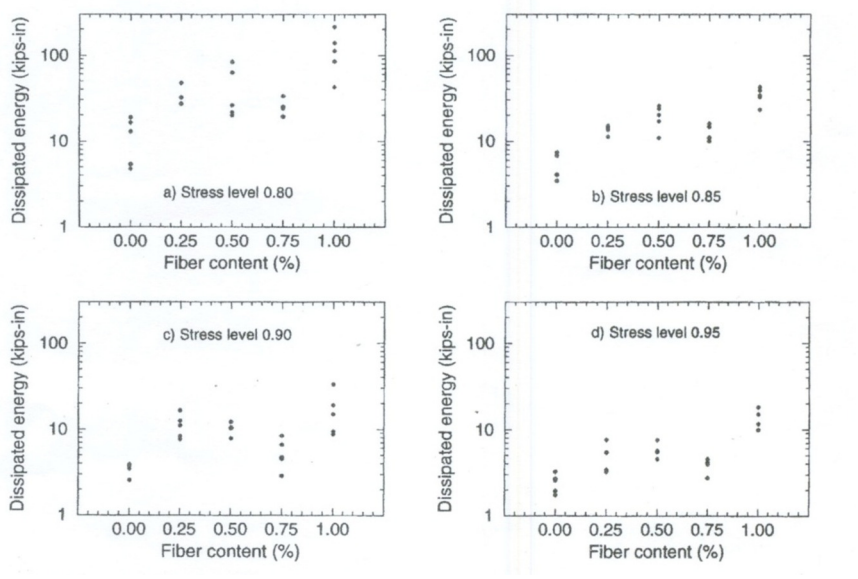

Figure 2.6: Effect of Steel Fiber-reinforcement on Total Dissipated Energy (Paskova and Meyer 1997)

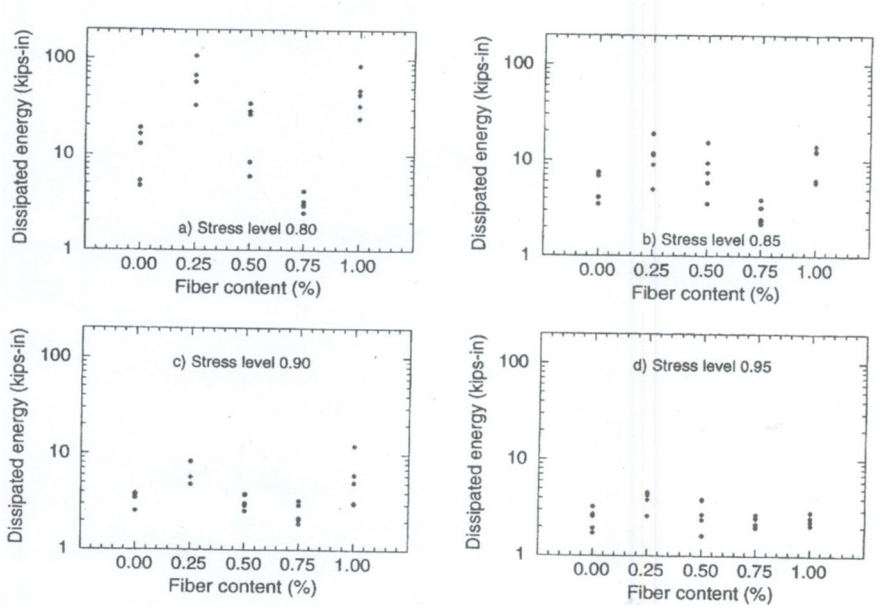

Figure 2.7: Effect of Polypropylene-fiber-reinforcement on Total Dissipated Energy (Paskova and Meyer 1997)

2.4.2. Heat Generation in the Fatigue Process

A significant amount of energy dissipation in the fatigue process of concrete occurs because of interplanar friction between different phases of concrete, which raises the concrete's temperature. Quantification of generated heat during the fatigue process was a purpose of the study conducted by Tepfers et al. (2011), which used a kind of insulation system and a series of thermocouples located around a cylindrical sample to measure generated heat during the compressive fatigue process of concrete. The development of heat energy during the course of fatigue life is presented in Figure 2.8. The transmitted energy shown in Figure 2.8 shows the heat exchange between sample and testing environment. The stored heat energy is the amount of heat energy that cannot be transmitted through insulation, and therefore increases the temperature of the sample during fatigue.

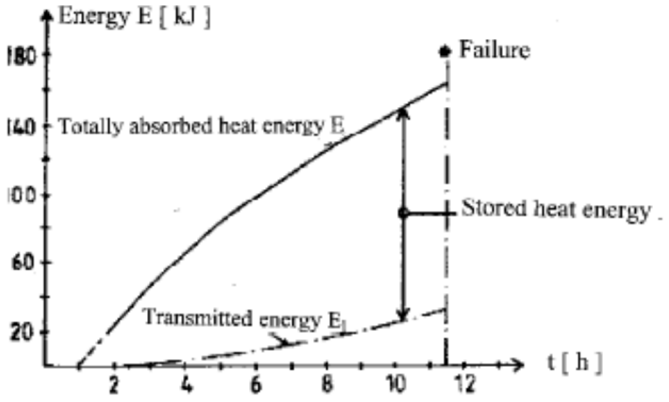

Figure 2.8: Development of Heat in the Fatigue Process (Tepfers, Sjostrom, et al. 2011)

Heat generation during fatigue is a typical phenomenon in all materials. As cited by Holmes and Shuler (1990), the temperature rise in fiber-reinforced ceramics is directly

related to fatigue-test loading characteristics such as stress level and loading frequency. As shown in Figure 2.9 and Figure 2.10, the temperature (T) caused by fatigue loading increases as stress level and loading frequency increase.

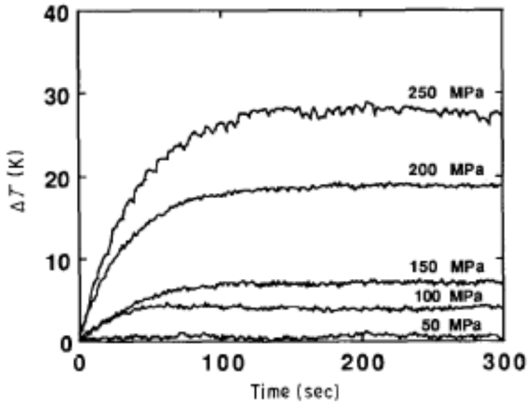

Figure 2.9: Effect of Stress Level on Generated Heat in Fatigue (Holmes and Shuler 1990)

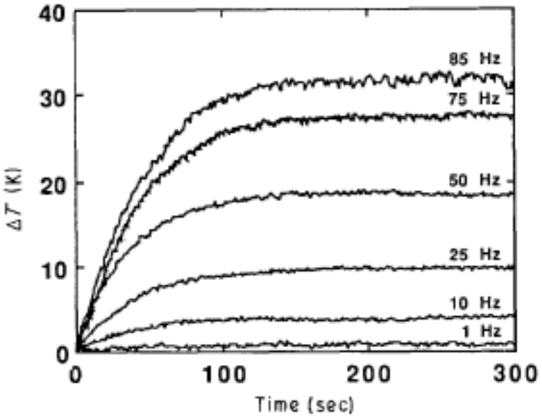

Figure 2.10: Effect of Loading Frequency on Generated Heat in Fatigue (Holmes and Shuler 1990)

2.4.3. Fatigue Life Predictions for Concrete Using the Energy-dissipation Concept

Studies have shown that the energy-dissipation characteristics of concrete during fatigue reveal less variability than seen in the fatigue life of concrete (Paskova and Meyer 1997). This has led to development of a more statistically reliable fatigue life prediction model based on energy-dissipation properties.

As cited by Paskova and Meyer (1997), the energy ratio, which is the ratio of total dissipated energy up to N cycles of fatigue to total dissipated energy up to failure, is a better indicator of the severity of damage to concrete than the traditional plastic strain measurement.

The disspated-energy ratio (DER) approach was first used by Carpenter and Jansen (1997) for hot mixed asphalt, then was proved to be valid for Portland Cement concrete by Daniel and Bissirri (2005). The DER is the ratio of change in the dissipated energy from load cycle i to load cycle i+1 (ΔDE) to the dissipated energy in load cycle i (DE) (Daniel and Bisirri 2005). The variation of dissipated energy during the course of fatigue life is presented in Figure 2.11.

As can be seen in Figure 2.11, the DER value becomes constant after several loading cycles, and rapidly increases at failure. The DER value when the dissipated energy ratio is constant—the so-called plateau value (PV)—has been shown to be a more reliable parameter in predicting fatigue life.

Fatigue life prediction using the PV has been shown to be more accurate than other traditional methods such as the Hsu Model (1981) and the Aas-Jackobson Model

(Aas-Jakobsen 1970). Figure 2.12 compares the DER method and other traditional models for predicting the fatigue life of concrete.

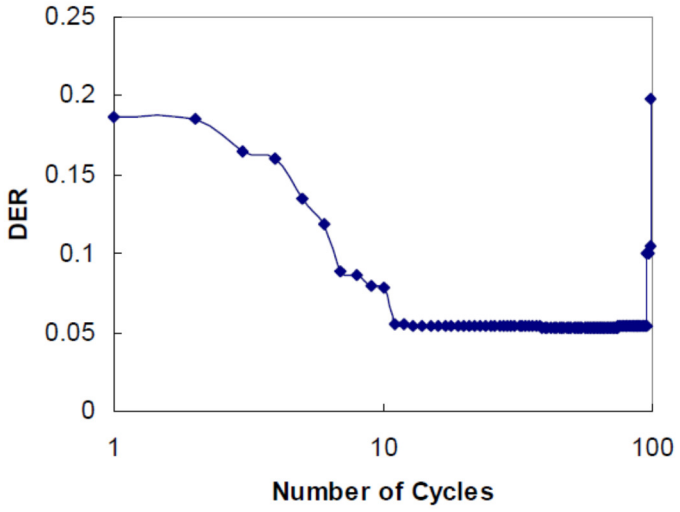

Figure 2.11: Dissipated Energy Ratio in the Fatigue Process (Daniel and Bisirri 2005)

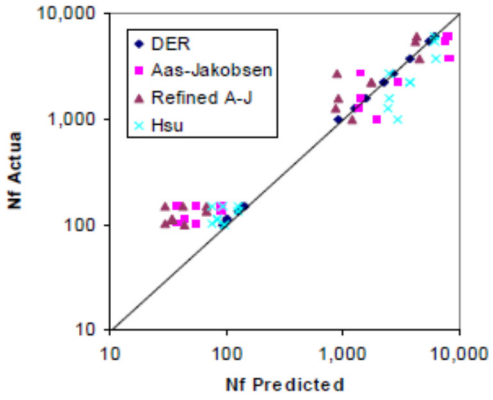

Figure 2.12: Comparison of the DER Method with Traditional Methods (Daniel and Bisirri 2005)

2.5. The Impact of Frost Damage on the Fatigue Performance of Concrete

2.5.1. The Frost Damage Mechanism

Concrete deterioration due to freeze-thaw cycles has been an interesting area of study for many years, but it remains poorly understood because of the complexity of the mechanism of freeze-thaw damage.

In early studies, Powers (1955) (1956) demonstrated that freeze-thaw damage can be attributed to the hydraulic pressure caused by the movement of water in capillary pores away from freezing zones (ACI Committee 201 2008). According to this theory, as water starts to freeze, it expands and pushes unfrozen water farther into capillary pores. Due to water movement, hydraulic pressure is induced along the walls of capillary pores. When this pressure exceeds the tensile strength of concrete, cracking is inevitable.

In more recent studies, Powers (1975) and Helmuth (1960a) (1960b) have shown that the water movement is actually *toward* freezing zones. According to this theory, as the temperature reaches the freezing point, water in the larger capillary pores starts to freeze; this tends to trigger formation of a zone with a higher concentration of solutes (dissolved ions in water). As a result, unfrozen water in adjacent capillary pores moves to the frozen area to equalize the solute concentration. This phenomenon is called osmosis. Therefore, induced pressure in concrete pores will be a combination of hydraulic pressure and osmosis pressure (ACI Committee 201 2008).

2.5.2. Effect of Frost Damage on the Physical Properties of Plain and Fiber-Reinforced Concrete

Formation of micro-cracks in concrete paste due to internal pressure caused by the freeze-thaw mechanism has a negative impact on the physical properties of concrete. Sahmaran et al. (2012) conducted a comprehensive study of the effect of freeze-thaw damage on the physical properties of plain and fiber-reinforced concrete. Loss of mass in concrete samples due to frost damage is evident (Figure 2.13). However, the addition of fibers and fly ash to the mixture considerably decreases loss of mass (Mass loss is the measure of scaling) in those samples compared to plain concrete. In addition, results of pulse velocity tests show that fiber reinforcement was beneficial in controlling frost damage; mixtures containing fibers showed a considerably smaller decrease in pulse velocity than mixtures without fiber reinforcement (Figure 2.13). Surface deterioration (scaling) of different concretes is shown in Figure 2.14. It is evident that the severity of frost damage on mixtures without fiber is greater.

Richardson et al. (2012) investigated the effectiveness of polypropylene-fiber reinforcement in improving the freeze-thaw resistance of concrete by testing the performance of four different mixtures of concrete—non-air-entrained, air-entrained, and two polypropylene fiber-reinforced—exposed to freeze-thaw cycles.

As shown in Figure 2.15 and Figure 2.16 , the addition of fiber is as effective as air entraining for controlling mass loss and pulse velocity in freeze-thaw-exposed samples. Plain concrete has severely deteriorated after 80 cycles of freeze-thaw exposure, whereas there no significant deterioration can be seen in either air-entrained or fiber-reinforced concrete.

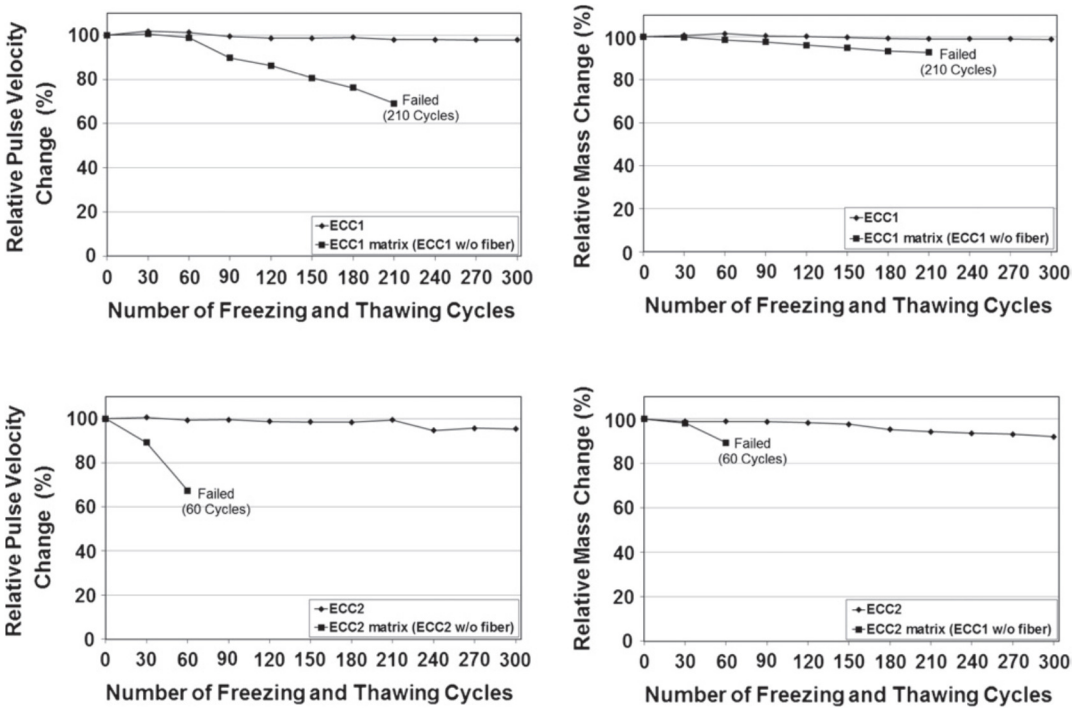

Figure 2.13: Relative Pulse Velocity and Mass Loss (Sahmaran, et al. 2012)

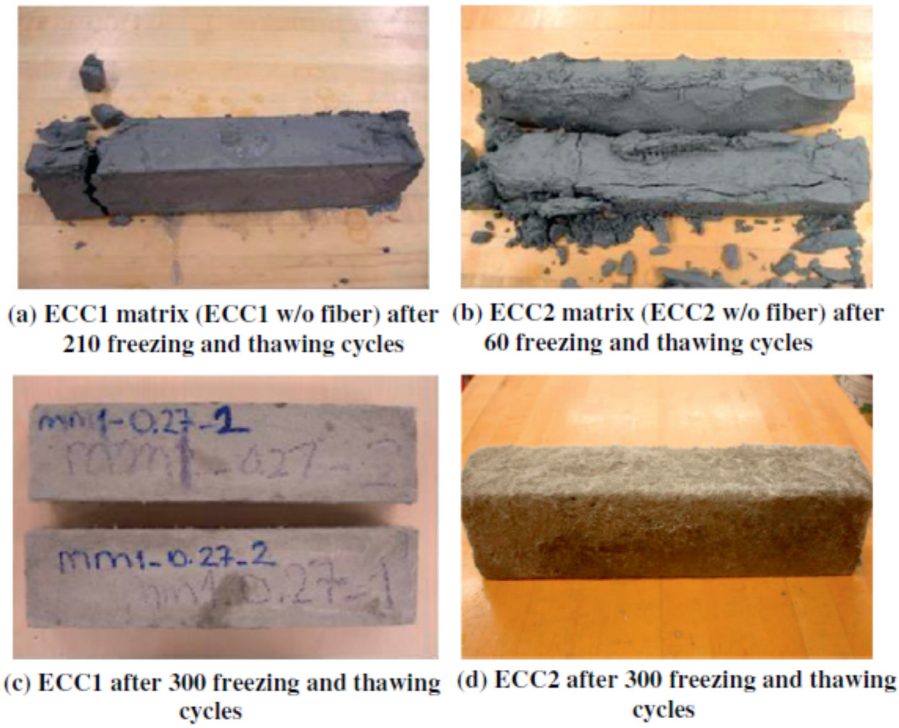

(a) ECC1 matrix (ECC1 w/o fiber) after 210 freezing and thawing cycles

(b) ECC2 matrix (ECC2 w/o fiber) after 60 freezing and thawing cycles

(c) ECC1 after 300 freezing and thawing cycles

(d) ECC2 after 300 freezing and thawing cycles

Figure 2.14: Deterioration Due to Frost Damage (Sahmaran, et al. 2012)

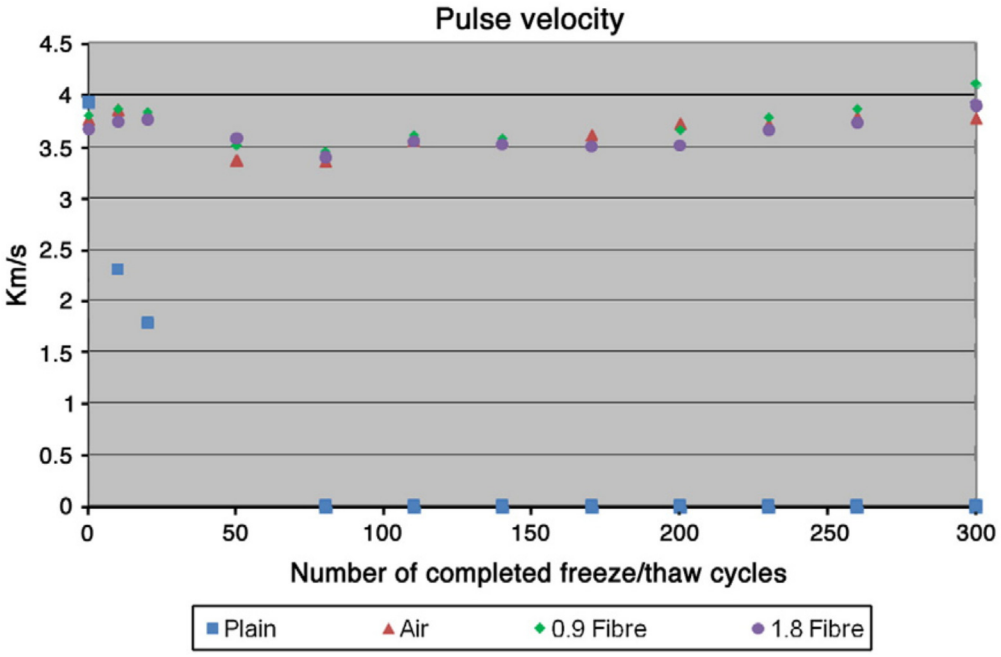

Figure 2.15: Pulse Velocity Reduction Due to Freeze-thaw Exposure (Richardson, Coventry and Wilkinson 2012)

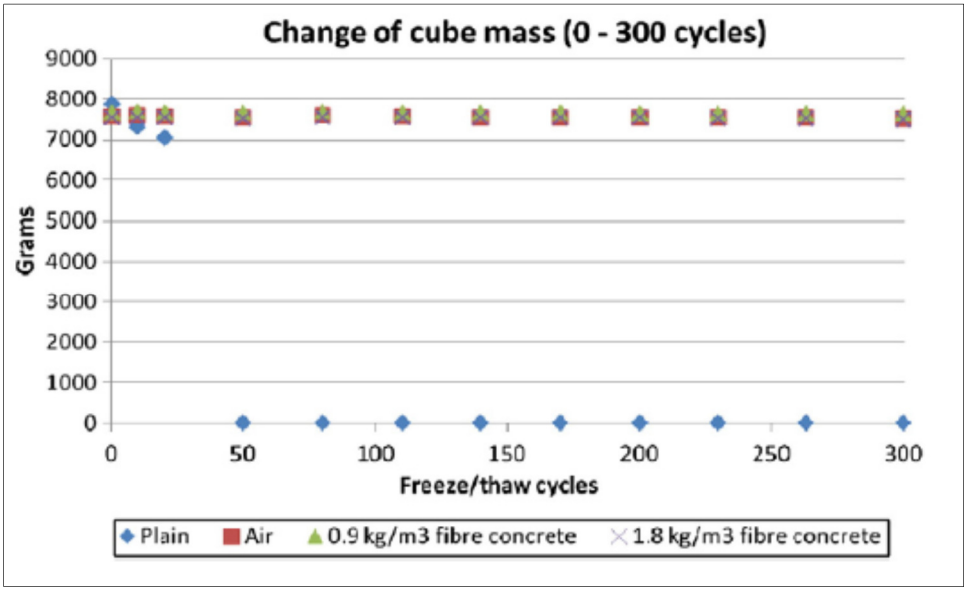

Figure 2.16: Mass Loss due to Frost Damage (Richardson, Coventry and Wilkinson 2012)

Richardson et al. (2012) also monitored the dynamic modulus of elasticity. Results for the durability factor revealed that the air-entrained concrete was 76 times more effective than non-air-entrained concrete, while polypropylene-fiber-reinforced concrete was 88 times more effective that non-air-entrained samples. The durability factor reflects changes in the dynamic modulus of elasticity after a given cycle of freezing and thawing; a detailed explanation can be found in ASTM C666/C666M. Also, the addition of polypropylene increased the ductility and compressive strength of samples exposed to freeze-thaw cycles by 16.01% and 26.56%, respectively, compared to air-entrained concrete.

2.5.3. Combined Effects of Freeze-thaw and Fatigue

Fatigue loading of concrete is accompanied by formation of progressive micro-cracks in the concrete matrix, which eventually results in concrete failure. Increasing the volume of micro-cracks during fatigue loading could make concrete more vulnerable to freeze-thaw attacks, since water can penetrate into these micro-cracks and exacerbate freeze-thaw damage. Civil structures such as bridges and highways are exposed to fatigue loading and freeze-thaw cycles simultaneously, and hence understanding the combined effects of freeze-thaw and fatigue is crucial.

A number of studies have evaluated the performance of concrete under the combined effects of fatigue and freeze-thaw. Fergeron and Trottier (2004) examined the residual mechanical properties of plain concrete (M0) and FRC (MF1, MF2, and MF3) after exposing them to combined flexural fatigue and freeze-thaw cycles. As shown in Table 2-3, different combinations of freeze-thaw exposure and fatigue were tested.

Table 2-3: Test Conditions (Forgeron and Trottier 2004)

Condition	Description
90-days	90 days of curing
F.Thaw	90 days curing + 300 cycles of freeze-thaw
Fatigue (10-40)	90 days curing + 2 million cycles of loading at (10% < stress level < 40%)
Fatigue (10-45)	90 days curing + 2 million cycles of loading at (10% < stress level < 45%)
F.Thaw + Fatigue (10-40)	90 days curing + 300 freeze-thaw cycles + 2 million cycles of loading at (10% < stress level < 40%)
F.Thaw + Fatigue (10-45)	90 days curing + 300 freeze-thaw cycles + 2 million cycles of loading at (10% < stress level < 45%)
Fatigue (10-45) + F.Thaw	90 days curing + 2 million cycles of loading at (10% < stress level < 45%) + 300 freeze-thaw cycles

As seen in Table 2-4 and Table 2-5, the flexural strength and stiffness of samples that experienced either fatigue loading or freeze-thaw cycles was lower than for samples with no freeze-thaw exposure or fatigue loading. However, the combined effects of freeze-thaw and fatigue were generally less destructive than separate effects for either freeze-thaw or fatigue loading.

Table 2-4: Flexural Strength and Stiffness of Plain Concrete at Different Combinations of Freeze-thaw and Fatigue (Forgeron and Trottier 2004)

Mixture	Condition	Flexural Strength (MPa)	Initial Flexural Stiffness (MPa/mm)
M0	90-day	6.60	173.8
	F.Thaw	4.65*	117.9*
	Fatigue(10-40)	4.78	137.6
	Fatigue(10-45)	5.34	157.5
	F.Thaw + Fatigue(10-40)	5.55	134.2
	F.Thaw + Fatigue(10-45)	5.75	146.2
	Fatigue(10-40) + F.Thaw	5.25*	127.6*

Table 2-5: Flexural Strength and Stiffness of FRC at Different Combinations of Freeze-thaw and Fatigue (Forgeron and Trottier 2004)

Mixture	Condition	Flexural Strength (MPa)	Initial Flexural Stiffness (MPa/mm)
MF1	90-day	7.09	160.0
	F.Thaw	6.11*	123.0*
	Fatigue(10-40)	5.34	117.9
	Fatigue(10-45)	7.06	117.0
	F.Thaw + Fatigue(10-40)	5.73	127.9
	F.Thaw + Fatigue(10-45)	4.93	133.2
	Fatigue(10-40) + F.Thaw	6.00*	99.0*
MF2	90-day	6.66	152
	F.Thaw	5.59*	126.3*
	Fatigue(10-40)	5.10	109.3
	Fatigue(10-45)	6.53	103
	F.Thaw + Fatigue(10-40)	6.30	122.9
	F.Thaw + Fatigue(10-45)	6.00	138.9
	Fatigue(10-40) + F.Thaw	5.51*	110*
MF3	90-day	6.55	149.8
	F.Thaw	5.51*	129.2*
	Fatigue(10-40)	4.76	108.9
	Fatigue(10-45)	N/A	N/A
	F.Thaw + Fatigue(10-40)	6.43	123.4
	F.Thaw + Fatigue(10-45)	6.21	135.2
	Fatigue(10-40) + F.Thaw	5.35*	116.4*

Li et al. (Li, Sun and Jiang 2011) conducted a study of the fatigue performance of concrete at three different environmental conditions (Table 2-6). The authors found that

the extent of damage caused by the combined effects of freeze-thaw and fatigue loading was 30.8% higher than the reference sample, which was only exposed to fatigue at 20° C (Figure 2.17).

Table 2-6. Loading and Environmental Conditions (Li, Sun and Jiang 2011)

Condition	Loading conditions
F(20)	Fatigue loading at 20 °C (reference)
F(−25)	Fatigue loading at −25 °C (frozen state)
F(F/T)	Simultaneous fatigue loading and freeze/thaw

Also, as seen in Figure 2.18, the formation of ice strengthened the concrete matrix; hence, the sample exposed to fatigue loading in the freezing condition 15.7% less damage than the reference sample. However, micro-cracks grew faster during the last 10% of the fatigue life cycle in frozen samples than in reference samples.

Hasan et al. (2008) studied the strain-stress relationship of samples under the combined effects of the freeze-thaw cycle and compressive fatigue loading. The cyclic load-deflection of samples are presented in Figure 2.19. The rate of plastic deformation accumulation increases as the number of freeze-thaw cycle increases. The first number in the sample label represents the number of freeze-thaw cycles and the second shows the stress level of fatigue test—i.e., “F-300-75” means that the sample experienced 300 freeze-thaw cycles followed by a fatigue test performed at a stress level of 75%.

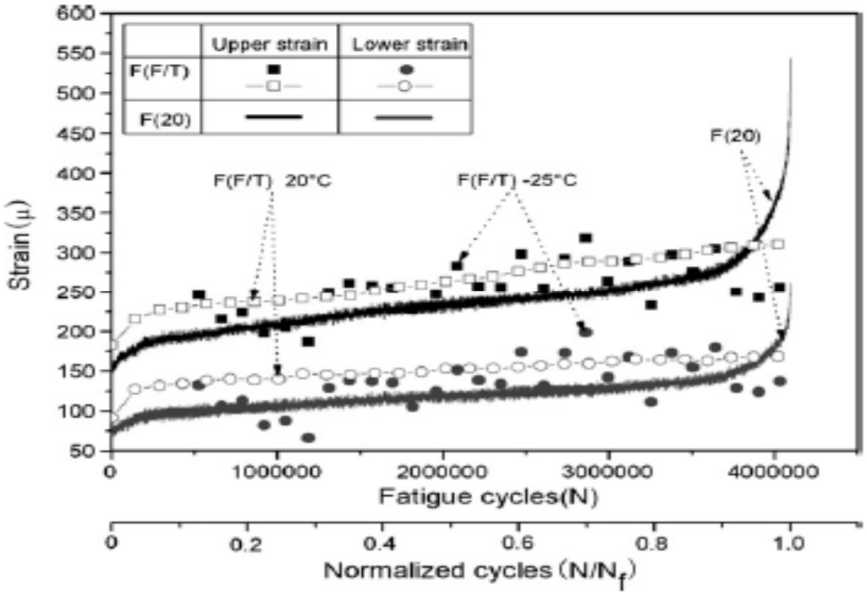

Figure 2.17: Strain at Lower and Upper Points of Bending Beams during Fatigue Life (Li, Sun and Jiang 2011)

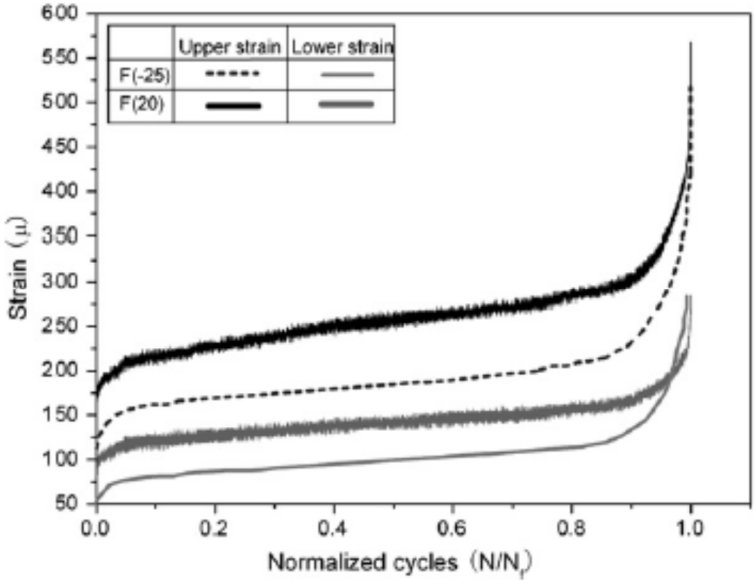

Figure 2.18: Strain at Lower and Upper Points of Bending Beams during Fatigue Life (Li, Sun and Jiang 2011)

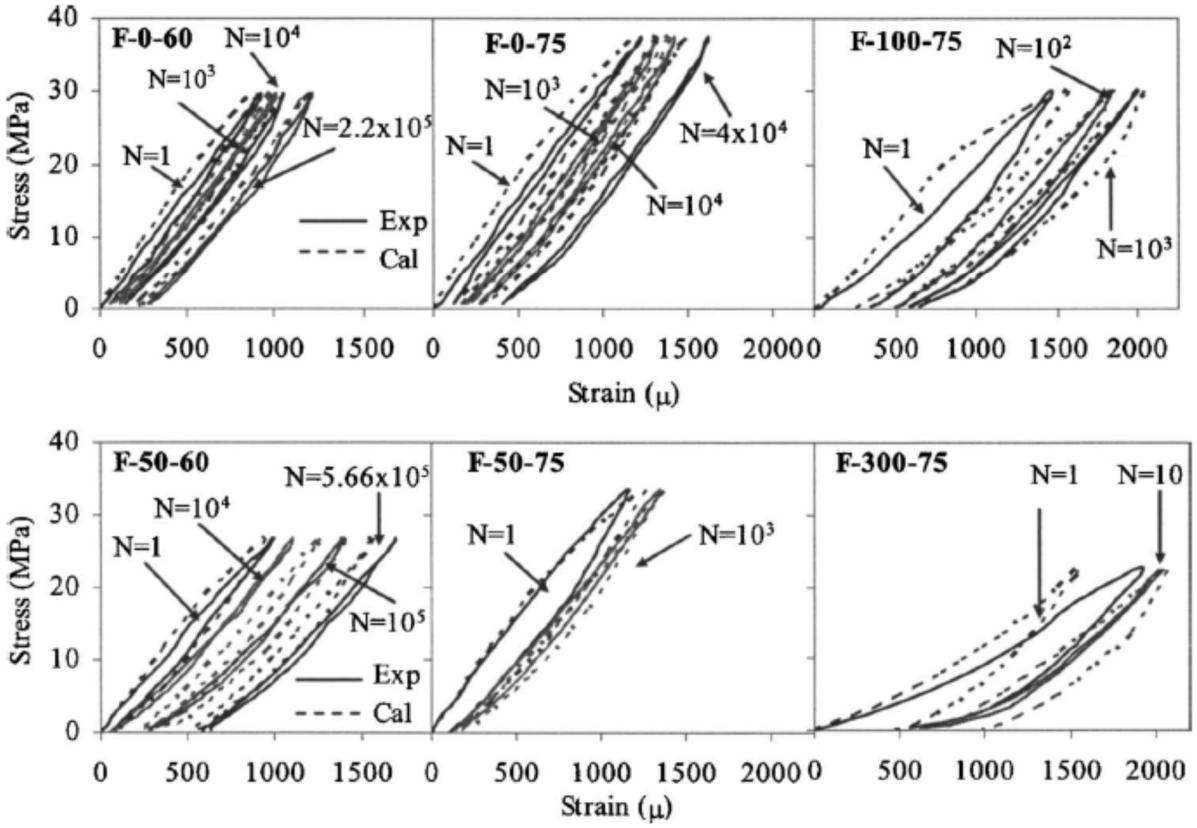

Figure 2.19. Stress-Strain Curve (Combined Effects of Fatigue and Freeze-thaw)

(Hasan, Ueda and Sato 2008)

Chapter 3. Material, Mix Design and Testing

3.1. Material

3.1.1. Aggregate

Sieve analysis has been conducted on both coarse and fine aggregate, in accordance with ASTM C136-05, and the gradation curves have been modified to meet ASTM C33 criteria. Crushed coarse aggregate #57 was used, with a maximum size of ¾". The maximum aggregate size is dictated by ASTM C192/C192M-07, which requires that the nominal maximum size of aggregate must be smaller than one-third of the minimum cross-sectional dimension of the mold. Natural, uncrushed fine aggregate has been provided from local sources in the State of Maryland. The absorption and specific gravity of aggregates have been determined using ASTM C127-04 and ASTM C128-04a. The properties of fine and coarse aggregate, as well as gradation criteria, are presented in Table 3-1 and Table 3-2, respectively.

Table 3-1: Fine aggregate properties

Fine Aggregate Properties		
SSD Specific Gravity	2.54	
Absorption (%)	0.63	
Fineness Modulus	2.61	
Particle Size Distribution		
Sieve #	Percent Passing	Limits (ASTM C33)
#4 (4.75 mm)	100	95-100
#8 (2.36 mm)	91	80-100
#16 (1.18 mm)	78	50-85
#30 (600 µm)	50	25-60
#50 (300 µm)	18	5-30
#100 (150 µm)	2	0-10

Table 3-2: Coarse aggregate properties

Coarse Aggregate Properties		
SSD Specific Gravity	2.86	
Absorption (%)	0.87	
Particle Size Distribution		
Sieve # (mm)	Percent Passing	Limits (ASTM C33, #57)
25.4	100	95-100
19	100	***
12.7	60	25-60
8.5	35	***
4.75	0	0-10

3.1.2. Cement

Type I/II Portland Cement was used in this study, which meets the ASTM C150-04 requirement. This type of cement is used for general purposes, and provides a moderate resistance to sulfate attack. Its chemical and physical properties are presented in Table 3-3.

Table 3-3: Physical and chemical properties of cement

Chemical Properties (percent by weight)		ASTM C150-04 Limits
SiO_2	20.4	min 20
Al_2O_3	5.1	max 6
Fe_2O_3	3.2	max 6
CaO	62.5	***
MgO	3.8	max 6
SO_3	2.8	max 3
Loss On Ignition	1.02	max 3
Physical Properties		
Surface Area (cm^2/g)	3300	
Specific Gravity	3.15	

3.1.3. Chemical Admixtures

A high-range water reducer and an air-entrainer admixture were used to reach a suitable slump range for casting and to achieve the target air content. Both the water reducer and air entrainer meet the requirements of ASTM C494-04 type A and F for water reducers and ASTM C260-04 for air-entraining admixtures. The specific gravity of the water reducer and air entrainer are 1.1 and 1, respectively.

3.1.4. Synthetic Fiber

A collated fibrillated polypropylene was used to reinforce the concrete samples. The fiber consists of 100% virgin homopolymer polypropylene; its physical properties are presented in Table 3-4.

Table 3-4: Properties of polypropylene fiber

Polypropylene Properties	
Specific Gravity	0.91
Tensile Strength (Mpa)	570-660
Color	White
Absorption	0
Length (mm)	19
Melting Point	163-168°c

3.2. Mixture Design

Three different concrete mixtures were made with 0%, 0.4%, and 0.8% (by unit volume) of fibrillated polypropylene fiber. Concrete mixtures were designed to meet the

requirements of MD #7 mix design, which is the typical concrete paving mixture in the State of Maryland. A high-range water reducer was applied to keep the slump within an acceptable range, and an air entrainer was used to reach the target air content specified by MD #7 mix criteria. Table 3-5 and Table 3-6 present mix proportions and MD #7 mix design requirements.

Table 3-5: Mix proportion

Mix ID	Fiber Content (%)	Cement (kg/m^3)	Fine Aggregate (kg/m^3)	Coarse Aggregate (kg/m^3)	Water (kg/m^3)	Admixture (kg/m^3)	
						Air-entrainer	Water reducer
Control	0	438.5	682.3	967	192.8	0.3	0.35
FRC4	0.4	438.5	671.6	967	192.8	0.3	0.59
FRC8	0.8	438.5	660.3	967	192.8	0.3	1.07

Table 3-6: MD #7 Mix requirement

MD#7 Mix Requirement	
Min 28 day Compressive Strength (Mpa)	30
Max Water/Cement	0.5
Min Cement Content (kg/m^3)	334
Aggregate #	57
Total Air Content (%)	8-May
Slump range (cm)	4 - 7.5
Concrete Temperature (°c)	21±11

3.3. Sample Preparation (Casting and Curing)

Several batches of concrete with a volume of approximately 63 liters were mixed in accordance with ASTM C192/C192M-07 by using a Gilson HM-220 portable concrete mixer. After completion of fresh concrete tests, the mixture was casted in 7.6×7.6×30.5 cm (3×3×12 in) oiled steel prism molds and 10.2×20.3 cm (4×8 in) plastic cylindrical molds. All samples were consolidated using a vibrating table until the surface of the concrete was smooth. Care was taken to avoid over consolidation, which leads to segregation of aggregate and fiber. Shortly after finishing, all the samples were covered with plastic wrap to avoid water evaporation from the surface. Samples were removed from the molds after 24 hours and transferred to a water storage tank and cured until test age.

3.4. Testing Program

3.4.1. Fresh Concrete Testing

All concrete batches were tested for workability and air content. Both the slump test, in accordance with ASTM C143/C143M-04, and the inverted slump test, in accordance with ASTM C995-01, were conducted to measure the workability of both the fiber-reinforced concrete and the conventional concrete. Air content of the batches was measured in accordance with ASTM C231-08b.

3.4.1.1. Slump Test

This is the most widely used test for the workability of conventional fresh concrete. The test device is a portion of a cone with a base 20.3 cm (8 inches) in diameter, a top diameter of 10.2 cm (4 inches), and a height of 30.5 cm (12 inches). According to ASTM C143/143M-04, the cone must be filled in three layers of equal volume, and each layer must be compacted with 25 strokes of a round, straight steel-tamping rod. The cone is then removed vertically and the slump measured—i.e., the difference between the height of the concrete before and after cone removal.

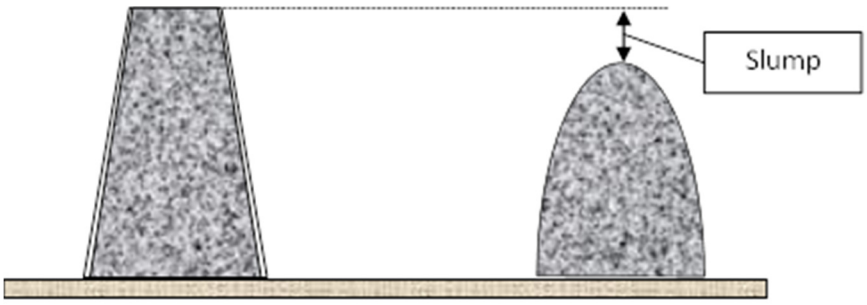

Figure 3.1: Slump test

3.4.1.2. Inverted Slump Test

The inverted slump test measures the workability of fiber-reinforced concrete. It is also applicable for any concrete mix containing coarse aggregate with a maximum size of 38 mm. This is a better method for use with fiber-reinforced concrete mixtures, because slump for fiber-reinforced concrete is usually low; therefore, the original slump test may not be a good indicator of workability. The testing apparatus consists of a slump

cone, an internal vibrator, and a bucket. A positioning device holds the slump cone upside down in the bucket and maintains the top of the cone at 10.1±0.6 cm from the bottom of the bucket. According to ASTM C995-01, the cone must be filled with three layers of concrete without any compaction. The internal vibrator is then inserted vertically from the top of the concrete and moved down until it touches the bottom of the bucket in 3±1 sec. The time it takes for the cone to become empty is recorded as the inverted slump time.

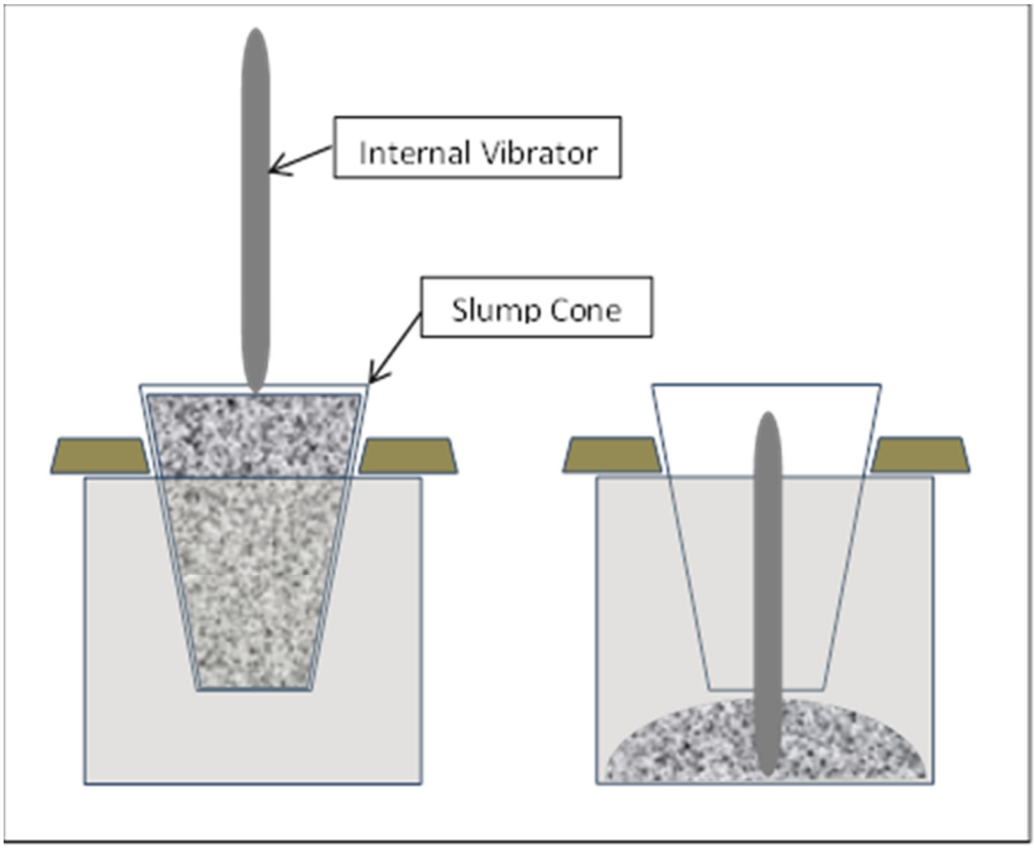

Figure 3.2: Inverted slump test

3.4.1.3. Air-content Test

The pressure method was used to determine the air content of freshly mixed concrete in accordance with ASTM C231-08b. This method measures air content by observing the sample's change in volume as the pressure is increased. It should be noted that the air content of hardened concrete may be slightly higher or lower than the amount determined by the pressure meter, depending on the vibration technique used and the extent of efforts to consolidate the specimen.

3.4.2. Hardened Concrete Testing

3.4.2.1. Compressive Strength Test

Compressive strength of the concrete mixtures was measured at the age of 28 days using 10.2×20.3 cm (4×8 in) cylindrical samples in accordance with ASTM C39/C39M-05. The rough ends of the samples were sawed to make them plain and smooth. Care was taken to keep the samples moist after removal from the water tank. The compressive strength was defined as the average for the three samples.

3.4.2.2. Elastic Modulus Test

The elastic modulus of concrete mixtures was measured at the age of 28 days in accordance with ASTM C469-02. The test was performed immediately after removal from the water storage tank. The reported modulus of elasticity was the average of three 10.2×20.3 cm (4×8 in.) cylindrical samples.

3.4.2.3. Flexural Strength Test

The flexural strength of the concrete mixtures was measured in accordance with ASTM C78-04 using simple beams with a third-point loading configuration, as seen in Figure 3.3. Three to five 7.6×7.6×30.5 cm (3×3×12 in.) samples with 0.8% fiber content were tested at 28, 40, 54, 60, 74, and 120 days. The flexural strength of other mixtures was measured at 28 days. Since moisture content could result in a reduction in flexural strength, samples were tested immediately after removal from the water tank.

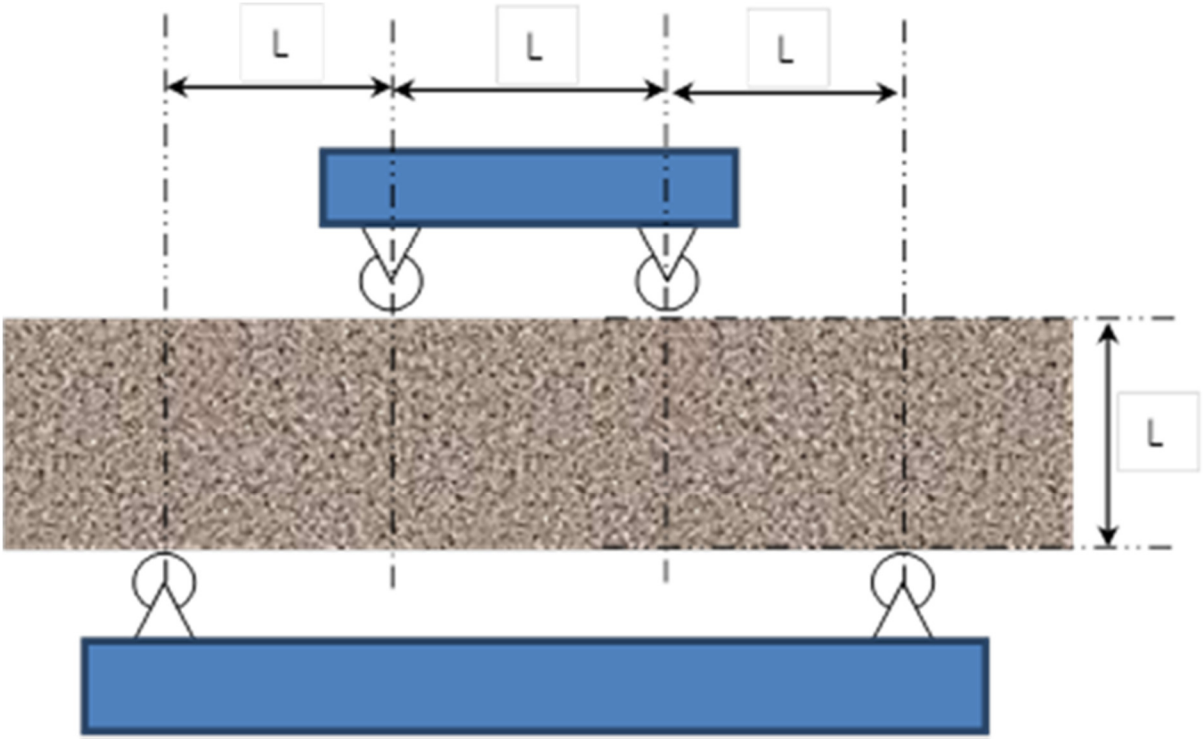

Figure 3.3: Flexural strength test (Third point loading configuration)

3.4.2.4. Rapid Freeze-Thaw Test

The rapid freeze-thaw test is designed to determine the resistance of concrete exposed to rapid freeze-thaw cycles. ASTM C666/C666M-03 procedure A was followed, and the samples underwent up to 200-400 cycles of freezing and thawing. A Humboldt H3185-B rapid freeze-thaw machine was used, which is capable of testing 17 samples simultaneously. The machine is equipped with both heating and cooling systems, and can cycle between two temperatures. It was set to produce freezing and thawing cycles between -18 and 4°C (0 to 40°F) over a period of approximately 4 hours. Concrete samples measured 7.6×7.6×30.5 cm (3×3×12 in.) after 28 days of moist curing.

3.4.2.5. Density, Absorption, and Voids in Hardened Concrete

Density, percent absorption, and void ratios of concrete samples exposed to freeze-thaw cycles were measured to evaluate the severity of deterioration due to freeze-thaw cycles. Tests were performed on 7.6×7.6×30.5 cm (3×3×12 in.) samples at 0, 200, and 400 cycles of freeze-thaw in accordance with ASTM C642-97.

3.4.2.6. Fatigue Test

A full factorial design for the fatigue test and number of samples are presented in Table 3-7. The following is a description of the fatigue test set-up, the testing machine, and loading characteristics.

3.4.2.7. Loading Set-up

In this study, the flexural fatigue test was used to evaluate the fatigue life of concrete, which is the most common test used to characterize concrete pavement. The set-up conformed with the ASTM C78-04 loading configuration (Figure 3.3).

3.4.2.8. Testing Machine

An Instron servohydraulic machine, which is capable of creating sinusoidal loads at different loading frequencies, was used for the fatigue test. An Instron FastTrack 8800 data acquisition system was used to record load and deflection along the loading points at prescribed intervals.

3.4.2.9. Loading Characteristics

A constant-amplitude sinusoidal type of loading was used; this load shape is widely used to simulate traffic loading. Fatigue tests were conducted on the samples with 0.8% fiber reinforcement at frequencies of 5 and 10 Hz and at stress levels of 0.6, 0.7, and 0.8. Fatigue tests performed on other mixtures were at a frequency of 5 Hz and a stress level of 0.7. The stress level is defined as the ratio of maximum cyclic stress to flexural strength of the sample. The stress ratio, which is the ratio of minimum cyclic stress to maximum cyclic stress, remained constant and equal to 0.15 for all tests.

3.4.2.10. Combination of fatigue and freeze-thaw

Fatigue tests were conducted on beam samples, which were exposed to freeze-thaw cycles to study the effect of freeze-thaw deterioration on the fatigue life of samples. All samples were tested at the same maximum load corresponding to the 0.7 stress level of control samples, which had not experienced any freeze-thaw cycles. The frequency and stress ratio were 5 and 0.15, respectively.

Table 3-7: Testing program and number of samples

Mix ID	FRC8								FRC4	Control
Loading Frequency	5					10			5	5
Stess Level	0.6	0.7			0.8	0.6	0.7	0.8	0.7	0.7
Freeze-thaw Cycle	0	0	200	400	0	0	0	0	0	0
Number of Samples	6	10	9	7	6	6	6	5	6	6

3.5. Mix Characteristics

3.5.1. Fresh Concrete Properties

The properties of fresh concrete mixtures are shown in Table 3-8. Workability was consistent for all batches of the same mixture. No segregation of aggregate was observed. Fibers were evenly distributed in the mixtures, and no balling was observed. Results confirm that the slump and air content of mixtures met the MD #7 mixture requirement. Even though the amount of water reducer is increased in the FRC mixture to avoid slump loss, FRC mixtures are still less workable than the control mixture.

Table 3-8: Fresh concrete properties of concrete mixtures

Mixture ID	Batch#	Slump (cm)	Inverted Slump Time (sec)	Air-Content (%)	Mixing Temperature (°c)
Control	1	7.5	----	5.1	23.9
FRC4	1	6.5	9	6	23.3
FRC8	1	5.5	11	5.8	23.3
	2	5	10	5.1	22.2
	3	4.5	12	6.1	22.2
	4	5.5	10	6.2	22.8

3.5.2. Hardened Concrete Test Results

3.5.2.1. Compressive Strength Test Results

Figure 3.4 presents the compressive strength of mixtures at age 28 days, which is the average for 5 samples. As can be seen, the compressive strength of concrete without polypropylene is considerably higher than that of FRC mixtures. Fiber reinforcement has two effects on the concrete matrix. It can slow the process of crack growth by bridging cracks, and hence improve the mechanical properties of concrete matrix. On the other hand, fiber reinforcement can cause local defects in the matrix and reduce the strength: The presence of fiber in fresh concrete hinders the movement of entrapped air to the surface, and therefore more air is entrapped in the matrix. The entrapped air causes local weak points in the concrete matrix and hence reduces the strength of concrete. Results demonstrate that the second effect is prominent for the FRC4 and FRC8 samples, and hence compressive strength is reduced.

3.5.2.2. Flexural Strength Test Result

Four 7.6×7.6×30.5 cm (3×3×12 in.) samples were tested according to ASTM C78-04 at 28 days flexural strength for all three mixtures. The average flexural strength of concrete mixtures is presented in Figure 3.5. The results indicate that the addition of fibers up to 0.4% has no significant effect on flexural strength, but beyond 0.4% the flexural strength decreases by 20%. Reduction in the flexural strength of FRC samples could be caused by the increase in entrapped air due to the addition of fibers. Load-deflection curves for several samples are shown in Figure 3.6. Though the addition of fiber has decreased the flexural strength, post-peak behavior is enhanced compared to the

control mixture. It can be seen that the FRC8 mixture has higher ductility compared to the other mixtures. The bridging effect may be the main reason for the higher ductility in the FRC8 samples.

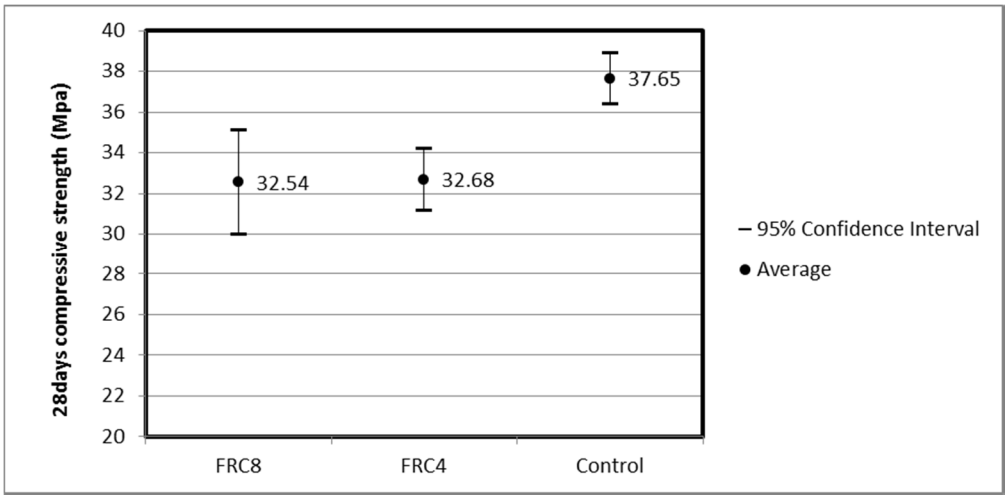

Figure 3.4: Compressive strength of concrete mixtures at 28 Days

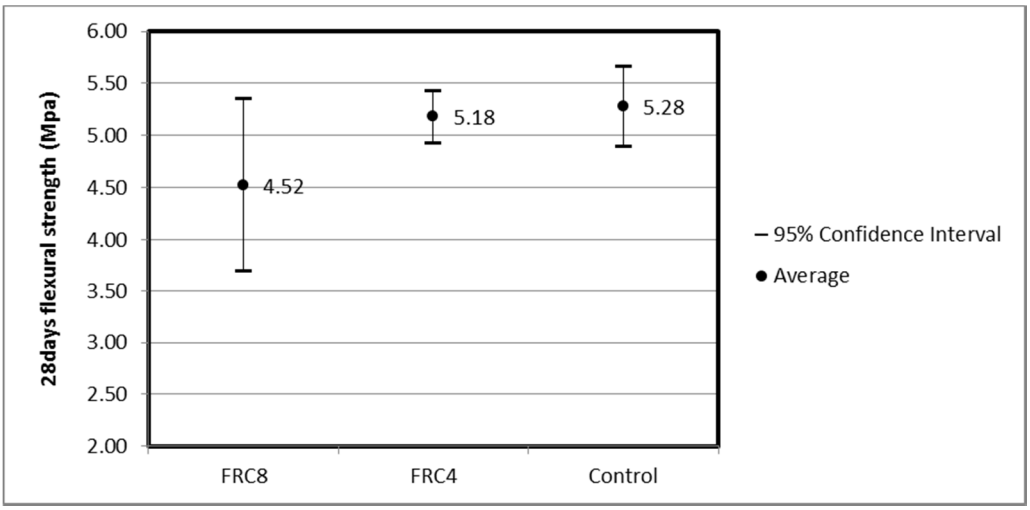

Figure 3.5: Flexural strength of concrete mixtures at 28 days

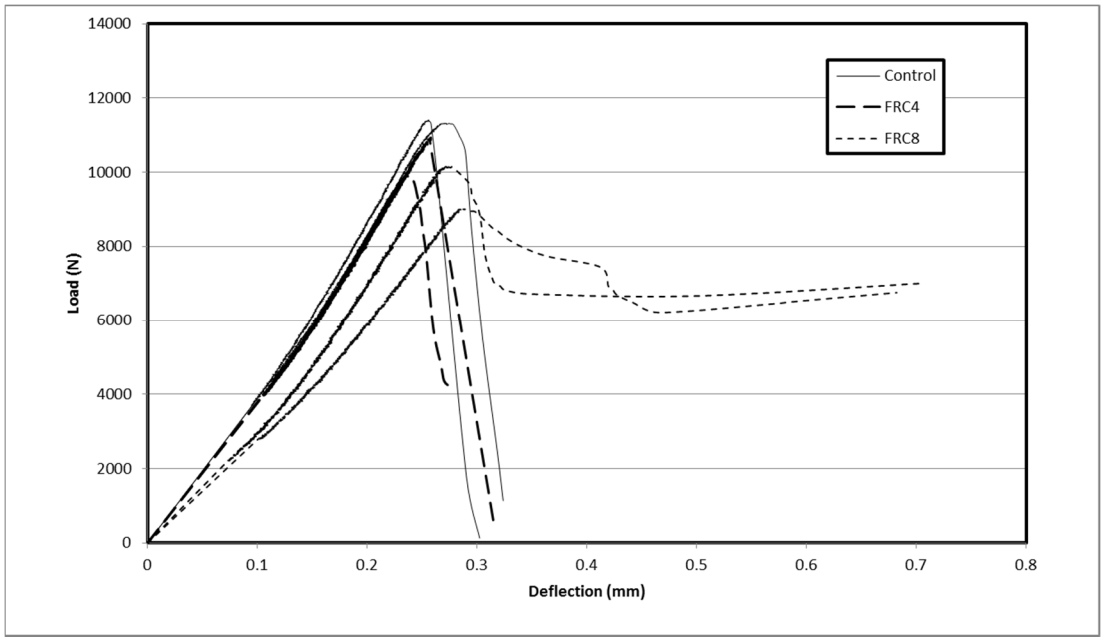

Figure 3.6: Load-deflection Curves of Concrete Samples in Flexure

3.5.2.3. Elastic Modulus Test Result

Results for the elastic modulus test are plotted in Figure 3.7. The elastic modulus of concrete containing 0.4% polypropylene is almost the same as that of the control mixture. On the other hand, increasing the polypropylene fiber content from 0.4% of 0.8% reduced the elastic modulus. The application of polypropylene fiber, which has a low elastic modulus compared to the concrete matrix, cannot be beneficial for increasing the elasticity of concrete (Manolis, et al. 1997). The elastic modulus of a polypropylene fiber (3.5 to 4.9 Gpa; from (Zheng and Feldman 1995)) is 3 times lower than that of a typical elastic modulus of concrete matrix (14 to 40 Gpa). Therefore, the elastic modulus of the composite mixture decreases as the amount of fiber increases. Moreover, the

increase in entrapped air of the mixture containing fiber may be another reason for elastic modulus reduction in FRC samples.

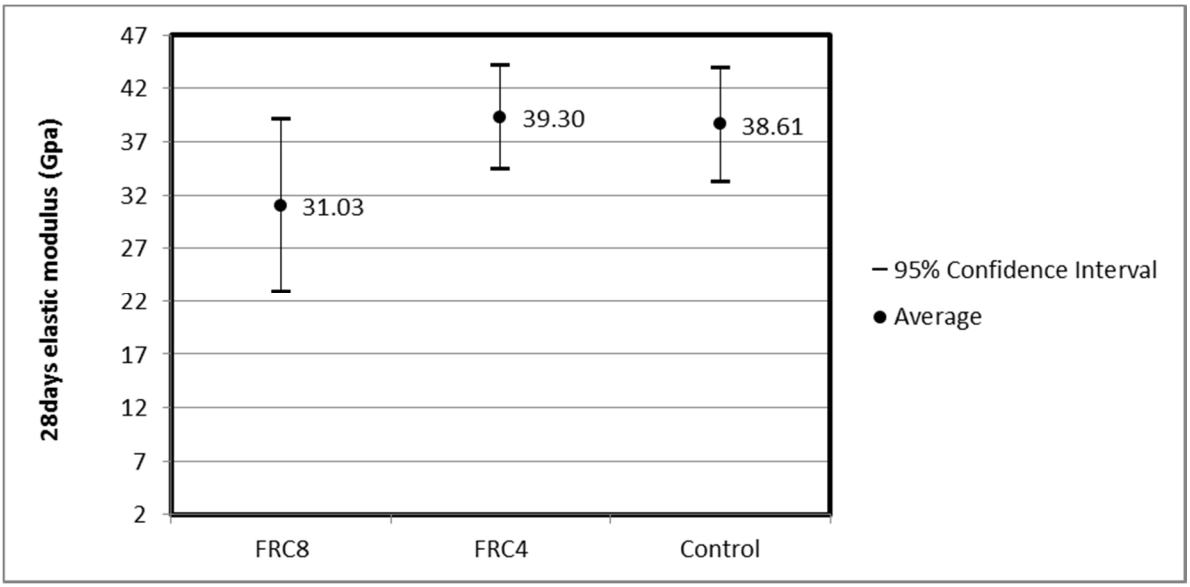

Figure 3.7: Elastic modulus of concrete mixtures

Chapter 4. Methodology, Results and Discussion

4.1. Methodology

In this section, detailed descriptions of the principles, calculation methods and definitions used in this study are presented.

4.1.1. Fatigue Failure Definition

Fatigue degradation is a progressive accumulation of damage in the material due to application of repeated loads less than the ultimate strength of the material. In this process, each cycle of loading is associated with the formation of micro-cracks. Eventually, as a result of micro-crack accumulation, the material matrix becomes unstable and fails.

Any attempt to study the fatigue behavior of concrete should begin with a clear-cut definition of fatigue failure. In the context of this study it is assumed that fatigue failure happens when the sample is not capable of taking the maximum cyclic load. In other words, an application of maximum cyclic load on a failed sample results in sudden growth in the size of the micro-crack network and, consequently, failure. Therefore, determining the number of loading cycles a sample can take before failure—its so-called fatigue life (N_f)—requires a precise study of the cyclic load-deflection curve. The concept of fatigue failure is demonstrated schematically in Figure 4.1.

It must be mentioned that fatigue failure does not necessarily happen simultaneously with the physical failure of the sample. In other words, when a sample is

considered to have failed at a certain stress level, it can still take more loading cycles at a lower stress level. This behavior will be discussed in Section 4.3.6.

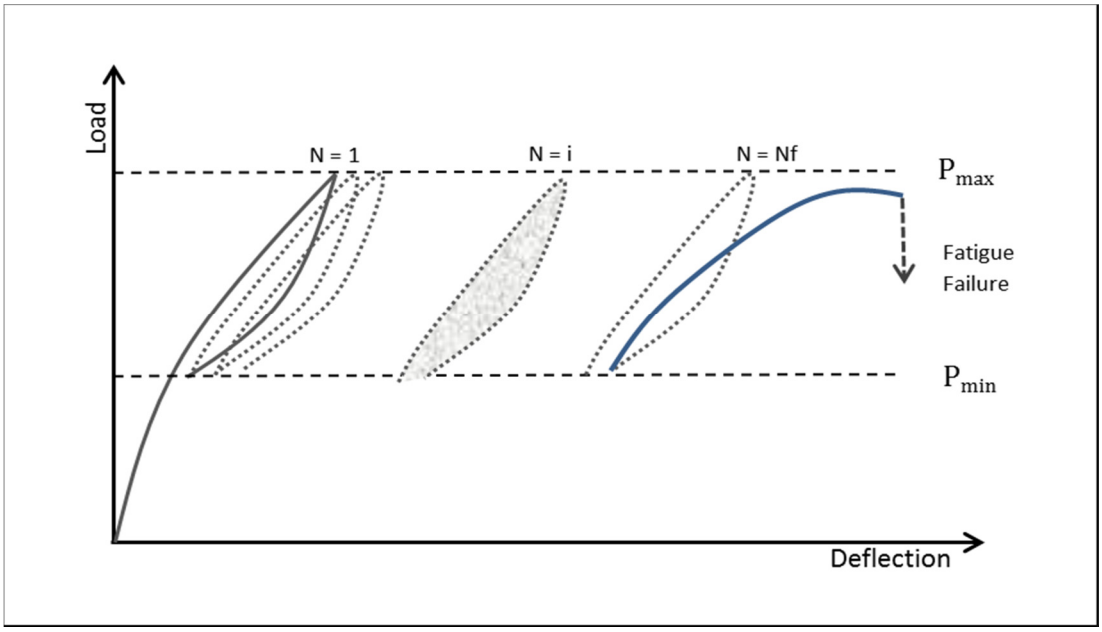

Figure 4.1: Concept of fatigue failure

4.1.2. Fatigue Test as a Forced Vibration

In this study, the flexural fatigue test is simulated by a harmonically excited single degree of freedom in which a concentrated mass M is connected to a spring-damper system and forced by a sinusoidal load with a frequency of f (Figure 4.2). It should be noted that the single degree of freedom system is not the perfect model to simulate this motion, since the weight of the concrete beam is spread over the length of the beam instead of being concentrated in the middle of the beam, but it can be used for the purpose of simplifying the analysis.

The motion equation of a single degree of freedom system excited by a sinusoidal harmonic force is given by Equation 4.1 (Rao 1990).

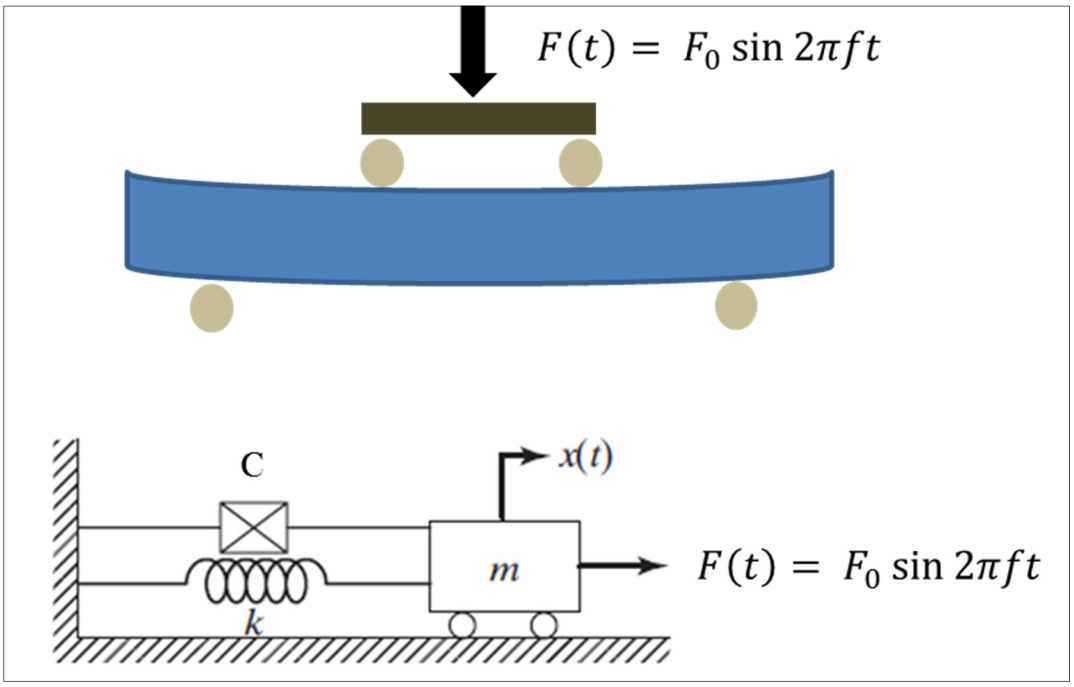

Figure 4.2: Harmonically excited single degree of freedom vibration

$$m\ddot{x} + c\dot{x} + kx = F_0 \sin 2\pi ft \qquad \textbf{4.1}$$

In the above equation, the cyclic stiffness of the system is denoted by k, the damping constant is denoted by c, the mass of the system is denoted by m, F_0 is the maximum cyclic load, and x represents the location of mass during the cyclic load.

Stiffness is defined as the amount of load that causes a unit deflection. In the case of a bending beam, stiffness is highly related to the elastic modulus (E) and the moment of inertia (I) of the bending section. On the other hand, the damping constant (c) is a material property that is influenced by material composition and loading characteristic.

Different models are developed to describe the damping behavior of materials such as viscous damping, coulomb damping, and hysteresis damping. Viscous damping originates from shear stress caused by the laminar flow of viscous fluids. The important characteristic of viscous damping is that the damping force is proportional to the velocity of vibration. Coulomb damping, or dry friction, is caused by friction force that develops between two dry surfaces as they move relative to each other. This type of damping is constant throughout the vibration. Finally, hysteretic damping is caused by inter-planar friction as well as molecular vibration caused by cyclic movement. (Steidel 1989)

The best model to describe the damping behavior of concrete is the hysteresis model. Hysteresis refers to a load-deflection curve in which the loading and unloading curves do not follow the same track.

Although an ideal hysteresis model does not incorporate plastic deformation (Steidel 1989), it can be used to model plastic materials in which the contribution of plastic damping to total damping force is small. As we shall see in Section 4.3.6., in the case of concrete, the contribution of plastic energy to total damped energy is insignificant compared to other sources of damping, and hence the damping model of concrete can be approximated by a hysteresis model.

Considering the hysteresis model for concrete damping behavior, the motion equation will change to the following format (Equation 4.2), in which β is the dimensionless hysteresis damping constant and $\frac{\beta k}{2\pi f}\dot{x}$ denotes the damping force.

$$m\ddot{x} + \frac{\beta k}{2\pi f}\dot{x} + kx = F_0 \sin 2\pi f t \qquad \textbf{4.2}$$

An ongoing change in concrete properties due to the formation of micro-cracks during a fatigue test is what distinguishes a real fatigue test from an ideal harmonically excited motion. As can be seen, damping force—which only exists when there is velocity in the motion—is directly related to material behavior, such as k and β. As concrete properties change during the course of fatigue life, damping behavior will also change.

In other words, a more accurate form of the motion equation for concrete could be written as follows (Equation 4.3), where β and k change as the fatigue test continues.

$$m\ddot{x} + \frac{\beta(t)k(t)}{2\pi f}\dot{x} + k\,(t)x = F_0 \sin 2\pi f t \qquad \textbf{4.3}$$

4.1.2.1. Cause of fatigue failure from the vibrational point of view

Fatigue failure can be attributed to the movement of the system toward resonance due to a decrease in the system's natural frequency. Resonance is a phenomenon in which the amplitude of vibration tends to become greater; in the case of hysteresis damping, this happens when the system's natural frequency and the loading frequency are equal. As Figure 4.3 shows, the amplitude ratio, which is the ratio of maximum cyclic deflection (X) to the maximum static deflection (F_0/k), gets larger as the system's natural frequency

(ω_n) and loading angular frequency (ω) get closer (Rao 1990). Static deflection is the amount of beam deflection under a static load F_0.

The natural frequency of a simply supported beam is approximated by Equation 4.4. Where n denotes the Nth natural frequency, l denotes the length of beam, ρ is the density of material, and A is the cross-sectional area. As shown in Equation 4.4, natural frequency is directly related to the stiffness of the bending beam (EI); therefore, it is expected to change due to fatigue deterioration of the concrete matrix.

$$\omega_n = n^4 \frac{\pi^2}{l^2} \sqrt{\frac{EI}{\rho A}} \qquad \textbf{4.4}$$

For this study, a 7.6×7.6×30.5 cm (3×3×12 inch) concrete beam with an average elastic modulus of 35 Gpa (5000 ksi) (extracted from Chapter 3), a density of 2400 kg/m^3 (150 lb/ft^3), is used which has a first mode natural frequency around 800. When the natural frequency is relatively larger than the loading frequency (5 and 10 Hz) which is the case in this study, the amplitude ratio is expected to be close to 1.

Accumulating fatigue damage reduces the stiffness (EI) of the beam, and consequently the natural frequency decreases. This simply means that the motion is moving toward resonance as the natural frequency of the beam gets closer to loading frequency, and hence the sample experiences greater cyclic deflection than during previous cycles. This process continues until the concrete matrix network becomes unstable and fails.

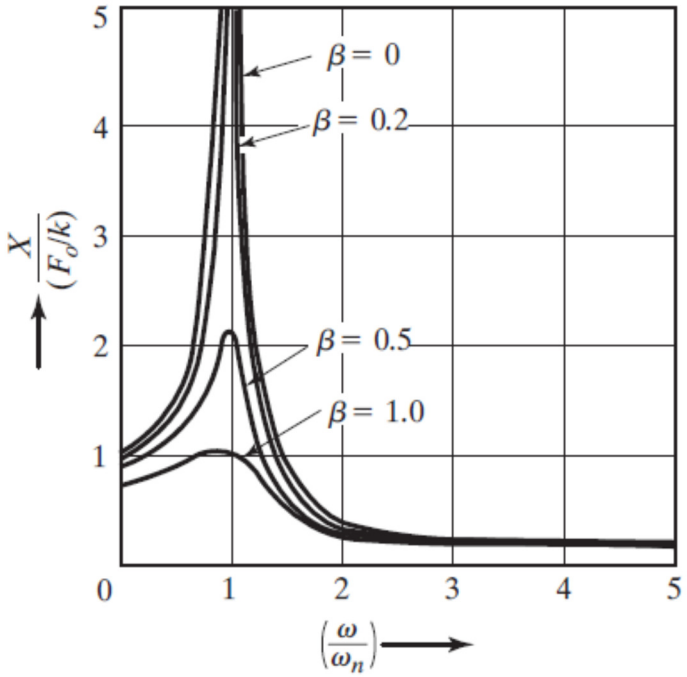

Figure 4.3: Amplitude ratio of hysteresis damping system

4.1.3. Energy Dissipation in the Fatigue Process

Fatigue testing is associated with transferring kinetic energy to energy stored in the body of the sample in the form of elasto-plastic deformation, in a periodic manner. Part of this energy dissipates due to damping forces that originate in the different mechanism of damping.

Energy dissipation in the fatigue process can be attributed to three distinctive mechanisms. First, energy dissipates due to the growth of macro-cracks. This type of energy dissipation is commonly called plastic dissipation. The second cause of energy dissipation in concrete fatigue is due to material damping. Material damping is the attenuation of energy waves generated from vibration as they travel through the volume of solid. Material damping is attributed to heterogeneity of the material. Finally, energy

loss due to inter-planar friction, so-called slip damping, is the third mechanism of energy dissipation. Slip damping—as opposed to material damping—originates from shear stress that develops between the boundaries of different phases in material (Torvik 2002).

4.1.3.1. Quantification of Dissipated Energy per Loading Cycle

As pointed out previously, concrete exhibits hysteretic behavior. The area underneath the loading portion represents the stored energy in the body of the sample. Once the load is removed, part of the stored energy transforms to kinetic energy. The area underneath the unloading portion of the load-deflection curve represents the released energy. The difference between these two areas is the amount of dissipated energy per loading cycle. Figure 4.8 shows the area that is considered to be dissipated energy per cycle.

As mentioned in the previous chapter, the data acquisition software is set to record load and deflection along the loading points at a rate of 20 to 24 data points per loading cycle. As an example, the raw data from a sample are plotted in Figure 4.9.

These data points are used as the input raw data to calculate dissipated energy per cycle. A macro written in Microsoft Excel reads input data from an Excel datasheet and calculates the dissipated energy per loading cycle. Equation 4.5 is used to calculate dissipated energy per loading cycle. The total number of data points recorded per loading cycle is denoted by n, and the *ith* recorded load and deflection are denoted by P_i and D_i, respectively.

$$Dissipated\ Energy\ per\ Loading\ Cycle = \sum_{i=1}^{n} \frac{(P_i + P_{i+1})}{2} (D_{i+1} - D_i) \qquad \textbf{4.5}$$

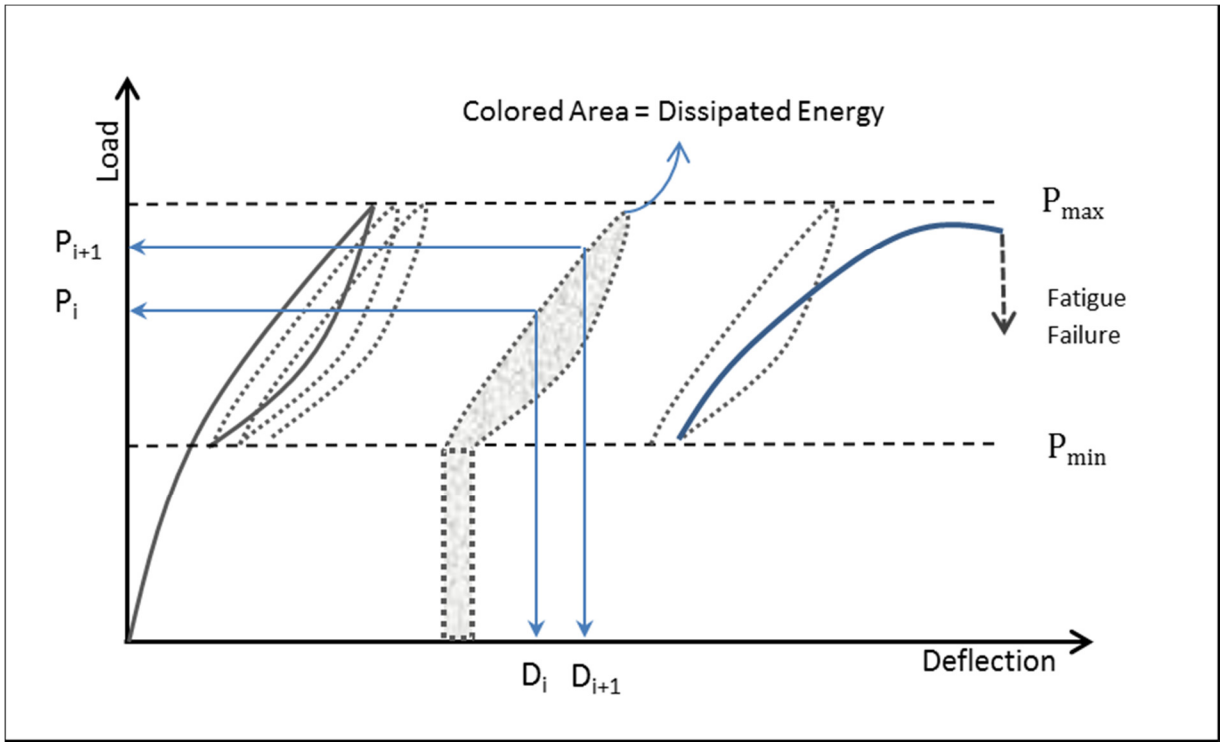

Figure 4.4: Demonstration of dissipated energy per loading cycle

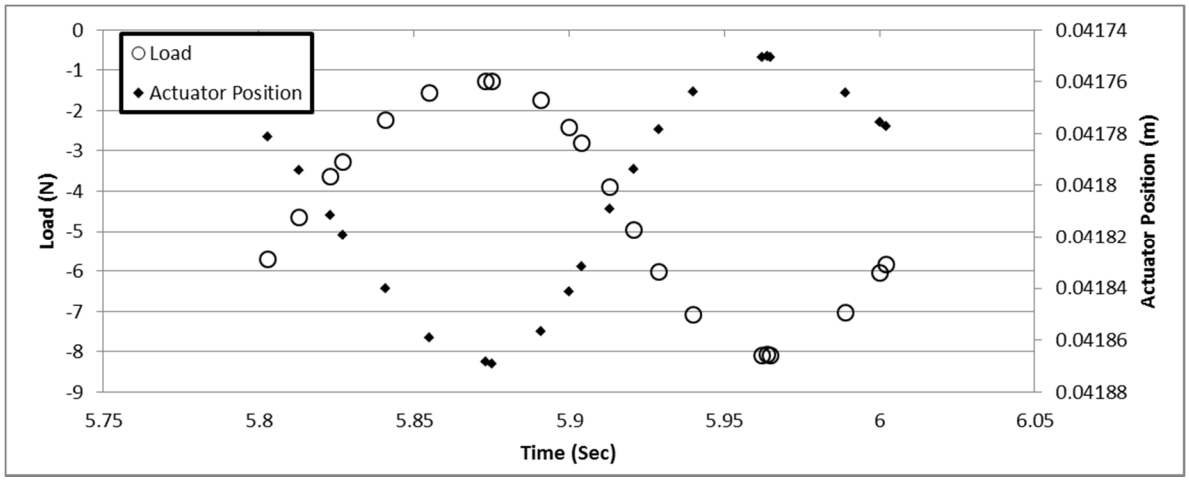

Figure 4.5: Example of recorded data per loading cycle

4.1.3.2. Quantification of Dimensionless Hysteresis Damping Constant (β) and Cyclic Stiffness (k)

If the hysteresis loop is considered as an inclined ellipse, the slope of the inclination is k. The cyclic stiffness (k) is the extent that a material deflects under applied cyclic load. In this study, cyclic stiffness is calculated by dividing the amplitude of the cyclic load by the amplitude of the cyclic deflection (Equation 4.)

$$t = tan^{-1}\left(\frac{\beta}{1-\frac{\omega^2}{{\omega_n}^2}}\right) * \frac{1}{2\pi f} \qquad \textbf{4.7}$$

It should be noted that due to the existence of damping force, there is always a time lag between the peak of deflection and load (Rao 1990). Therefore, maximum and minimum deflections do not happen at the same time as maximum and minimum cyclic load. Because of this, the proposed equation may not give an accurate stiffness value.

The time lag between cyclic load and cyclic deflection is quantified by Equation 4.7. In this equation, f denotes the frequency of loading. Considering that $\beta \approx 0.04$ (derived from Section 4.3.3.6), $\omega_n \approx 800$ and f=5, the time lag is significantly small ($t \approx 0.001$ sec) compared to the period of each cycle (T=1/f=0.2 sec), and hence for the purpose of calculating cyclic stiffness, it can be ignored.

$$k = \frac{Max\ Cyclic\ Load - Min\ Cyclic\ Load}{Max\ Cyclic\ Deflection - Min\ Cyclic\ Deflection} \quad \textbf{4.6}$$

$$t = tan^{-1}\left(\frac{\beta}{1 - \frac{\omega^2}{{\omega_n}^2}}\right) * \frac{1}{2\pi f} \quad \textbf{4.7}$$

As determined experimentally, the area enclosed in the hysteresis loop, the so-called dissipated energy, is equal to $\pi k \beta X^2$, where X is half of the peak-to-peak amplitude of the deflection (Rao 1990). Therefore the dimensionless hysteresis damping constant can be easily back-calculated from the dissipated energy using Equation 4.8.

$$\beta = \frac{Dissipated\ Energy\ per\ Cycle}{\pi k\ X^2} \quad \textbf{4.8}$$

4.1.3.3. Quantification of Plastic Energy in the Fatigue Process

As mentioned earlier in this chapter, plastic deformation is one of the causes of energy dissipation in concrete. In fact, plastic deformation plays a decisive role in the fatigue life of concrete samples, as fatigue failure occurs due to a loss of material strength due to the accumulation of plastic deformation.

Plastic deformation results from an irreversible process of micro-crack formation. Total energy dissipated in the fatigue process due to plastic deformation can be measured by the area underneath the load-deflection curve up to the failure point. The shaded area in Figure 4.6 represents the total dissipated energy in fatigue testing due to plastic deformation.

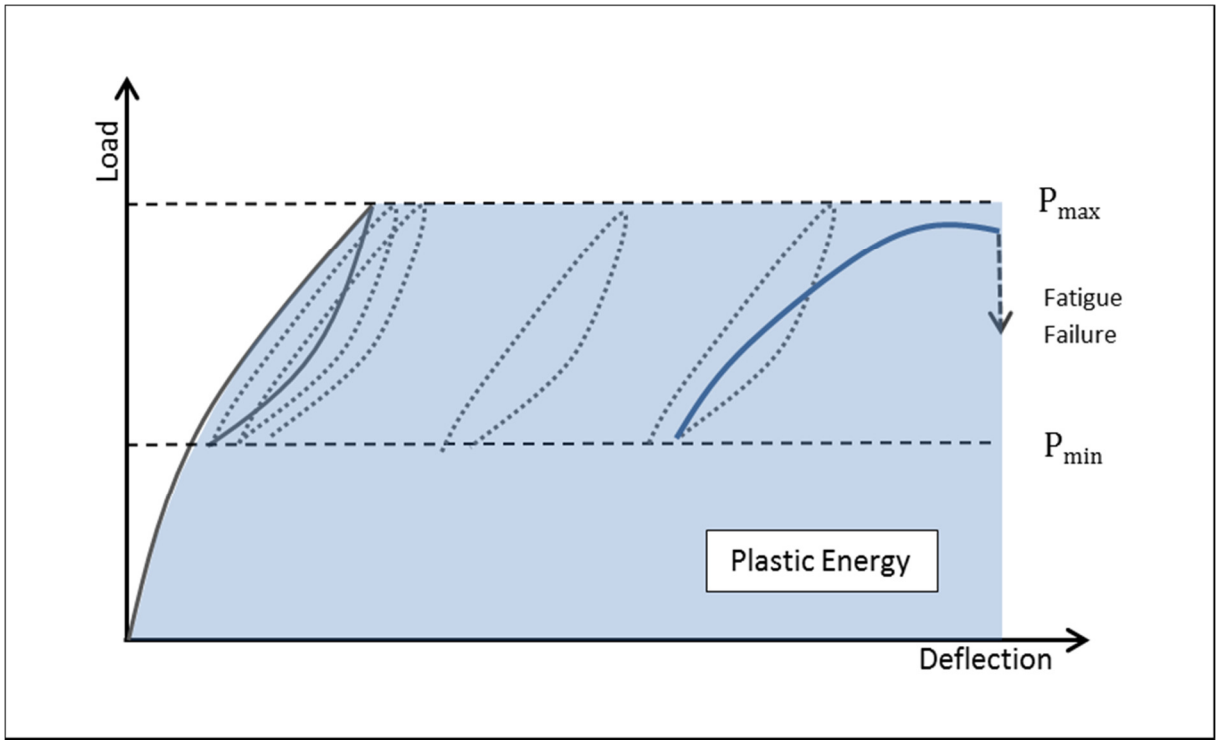

Figure 4.6: Demonstration of total dissipated energy due to plastic deformation

4.1.3.4. Heat Transformation in the Fatigue Process

Previous studies have shown that the fatigue process is associated with heat generation in the material. In fact, the majority of energy dissipation in fatigue is due to heat generation, which is caused by both material damping and slid damping.

Attenuation of energy waves caused by cyclic load in different phases of concrete is an indicator that one kind of energy is being transforming into another kind. As generated waves propagate through the concrete matrix, it creates a continuous vibration in all parts of the matrix and eventually increases the temperature of the material. Also generated friction due to the relative movement of different phases of the concrete matrix at their boundaries leads to energy dissipation through heat transformation.

The total dissipated energy balance (Equation 4.9) demonstrates that heat transformation can be quantified by measuring the total dissipated and total plastic energy.

$$\text{Total Dissipated Energy} = \text{Total Plastic Energy} + \text{Total Heat Energy} \quad \textbf{4.6}$$

4.1.4. Terminology

The following terms are used in this chapter:

Angular frequency of loading (ω): The ratio of the loading cycle in radian (each loading cycle is 2π radian) to time.

Averaged dissipated energy per loading cycle (ADE): The mean value of dissipated energy per loading cycle during the fatigue life.

Collapsing cycle: The loading cycle in which physical failure occurs.

Cycle ratio (N/N_f): The ratio of cycle count to fatigue life.

Cyclic stiffness (k): The ratio of amplitude of cyclic load to amplitude of cyclic deflection.

Fatigue life (N_f): The number of loading cycles a sample can withstand until failure occurs.

Frequency of loading (f): The number cyclic load applications per unit of time.

Heat transformation: Dissipated energy in the form of heat.

Hysteretic force: Refers to the term $\frac{\beta k}{2\pi f}\dot{x}$ in the movement equation of harmonically excited motion.

Material damping: The attenuation of energy waves generated from vibration as they travel through the volume of solid.

Natural frequency (ω_n): Frequency of unforced vibration.

Plastic damping: Energy dissipation through irreversible strains.

Plastic deformation: Change in the maximum cyclic deflection between cycle N=n and cycle N=m during fatigue life. In most cases, this refers to the change in cyclic deflection between N=1 and N=N_f.

Slid damping: A damping mechanism that originates from the shear stress that develops between the boundaries of different phases in material.

Stress level: The ratio of maximum cyclic load to the modulus of rupture.

Total dissipated energy (TED): Total energy dissipated during the fatigue process due to the damping mechanism.

4.2. Fatigue Test Results and Discussion

This section presents the results and analysis of the fatigue behavior of FRC concrete in terms of fatigue life, energy dissipation, and deformation characteristics. A series of fatigue tests was conducted on concrete mixtures containing 0.8% polypropylene fiber (FRC8) under different loading conditions. In addition, to evaluate

the effects of fiber reinforcement, two other mixtures with 0% (Control) and 0.4% (FRC4) fiber were prepared and tested at selected loading conditions (stress level of 0.7, loading frequency of 5 Hz).

4.2.1. Effect of Stress Level on Fatigue Life

The fatigue test on FRC8 samples was conducted according to the test set-up described in the previous chapter. Table 4-1 and Table 4-2summarize the results for fatigue life and stress level of FRC8 samples at loading frequencies of 5 and 10 Hz, respectively.

To arrive at a conclusion concerning the comparative relationship between stress level (S) and fatigue life (N_f), a linear regression line was fitted to each set of data in a semi logarithmic format. Regression lines are shown in Figure 4.7 and Figure 4.8.

Results show that fatigue life of the samples decreases as the stress level increases, in agreement with the results of other studies (ACI Committee 215 1997); stress level is considered to be the main factor affecting the fatigue life of concrete. At a higher stress level, concrete experiences more damage per loading cycle and thus failure occurs after a lower number of cycles.

Table 4-1: Fatigue life and stress level of FRC8 samples (loading frequency=5)

Stress Level-Frequency- ID#	Fatigue Life (N_f)	Stress Level (%)
0.8-5-1	15000	80.19
0.8-5-2	610	80.28
0.8-5-3	7950	80.36
0.8-5-4	1245	78.69
0.8-5-5	2310	78.95
0.8-5-6	30520	77.48
0.7-5-1	29120	70.58
0.7-5-2	153175	70.94
0.7-5-3	36475	70.6
0.7-5-4	7460	70.84
0.7-5-5	94110	70.72
0.7-5-6	41260	70.54
0.7-5-7	30640	69.7
0.7-5-8	42120	70.17
0.7-5-9	20000	70.22
0.7-5-10	66940	66.73
0.6-5-1	302620	59.43
0.6-5-2	272270	58.99
0.6-5-3	409800	59.09
0.6-5-4	118600	58.8
0.6-5-5	233900	58.56
0.6-5-6	775000	58.18

Table 4-2: Fatigue life and stress level of FRC8 samples (loading frequency=10)

Stress Level-Frequency- ID#	Fatigue Life (Nf)	Stress Level (%)
0.8-10-1	17150	77.44
0.8-10-2	11532	76.76
0.8-10-3	120928	76.07
0.8-10-4	24236	78.25
0.8-10-5	5352	77.43
0.8-10-6	15920	76.5
0.7-10-1	13090	68.93
0.7-10-2	5420	71.9
0.7-10-3	54840	70.38
0.7-10-4	22740	69.76
0.7-10-5	18340	68.28
0.7-10-6	128000	68.29
0.6-10-1	973500	59.18
0.6-10-2	300000	61.01
0.6-10-3	1736900	61.01
0.6-10-4	1277300	62.08
0.6-10-5	237000	62.12

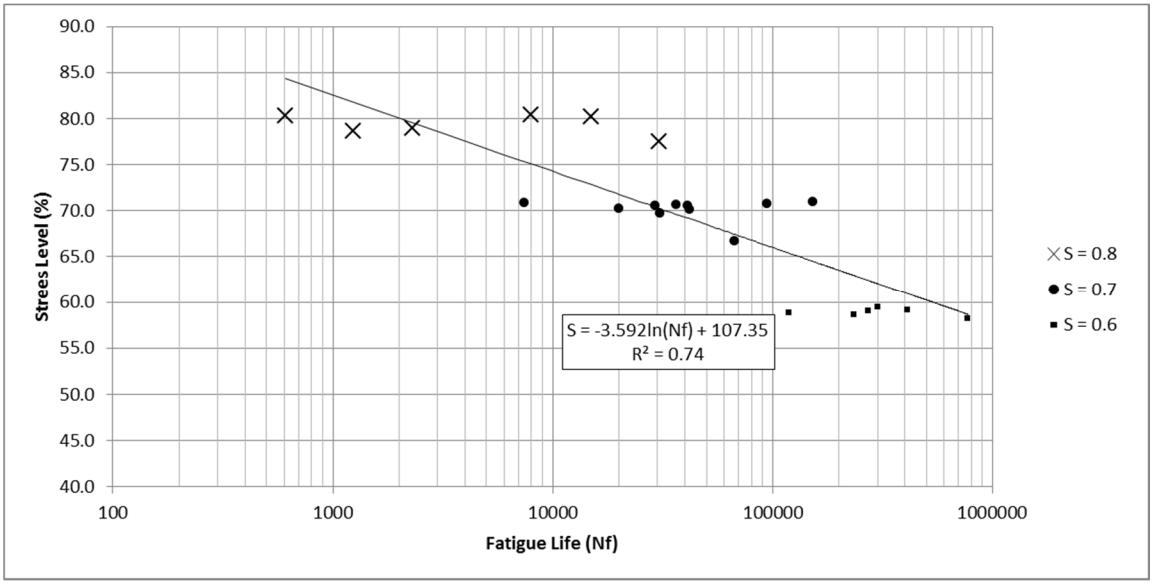

Figure 4.7: Stress level vs. fatigue life (FRC8, loading frequency = 5)

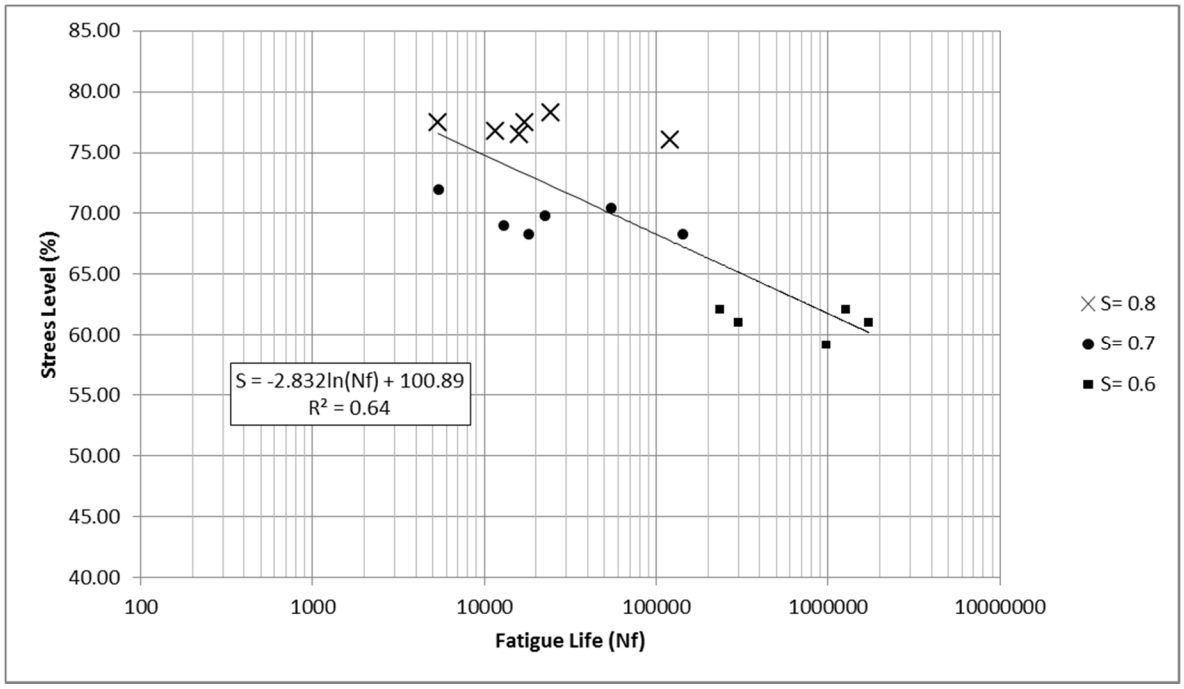

Figure 4.8: Stress level vs. fatigue life (FRC8, loading frequency = 10)

Variability assessment of fatigue life test results is presented in Table 4-3. High variability between the fatigue lives of concrete samples at different loading conditions is seen, which is not an unusual result and has been reported many times by other researchers (Kim 2003). Perhaps one of the main sources of excessive variation in fatigue life is the variation in the stress level of the concrete sample tested at each loading condition. The stress levels in Table 4-3 were calculated based on the average flexural strength of concrete. Knowing that the single operator coefficient of variation of third point loading can be 5.7% (derived from ASTM C78), and considering the increasing effect the addition of fiber has on the coefficient of variation, it can be conclude that the concrete samples were not tested at exactly the same stress level, which, in turn, caused excessive variation.

It is evident that loading rate is directly related to the variability of test results, as the fatigue test has shown higher variability at higher stress levels and loading frequencies.

Table 4-3: Variability assessment of fatigue life at different loading conditions (FRC8 samples)

Loading Frequency	5			10		
Stress Level	0.6	0.7	0.8	0.6	0.7	0.8
Average Nf	352032	52130	9606	904940	42972	32520
CV (%)	64.7	82.6	120.8	70.9	121.1	134.6

4.2.2. Effect of Loading Frequency on Fatigue Life

To study the effect of loading frequency on fatigue life, the S-N_f curves of FRC8 samples at loading frequencies of 5 and 10 Hz are combined in Figure 4.9. It can be seen that loading frequency has slightly influenced fatigue life. Generally, samples tested at a higher frequency have revealed higher fatigue life. This phenomenon can be attributed to creep deformation. Due to the longer duration of acting load at lower frequency, the concrete experiences higher creep deformation and failure occurs after fewer fatigue cycles. Figure 4.10 presents the ratio of average fatigue life at 10 Hz to average fatigue life at 5 Hz as a function of the stress level (i.e., considering the ratio of expected fatigue life in function of *S* from 5 Hz and 10 Hz testing, N_f10/N_f5 from Figure 4.9 in relation to stress level). It is evident that the impact of loading frequency on fatigue life (N_f) at lower stress levels is more noticeable.

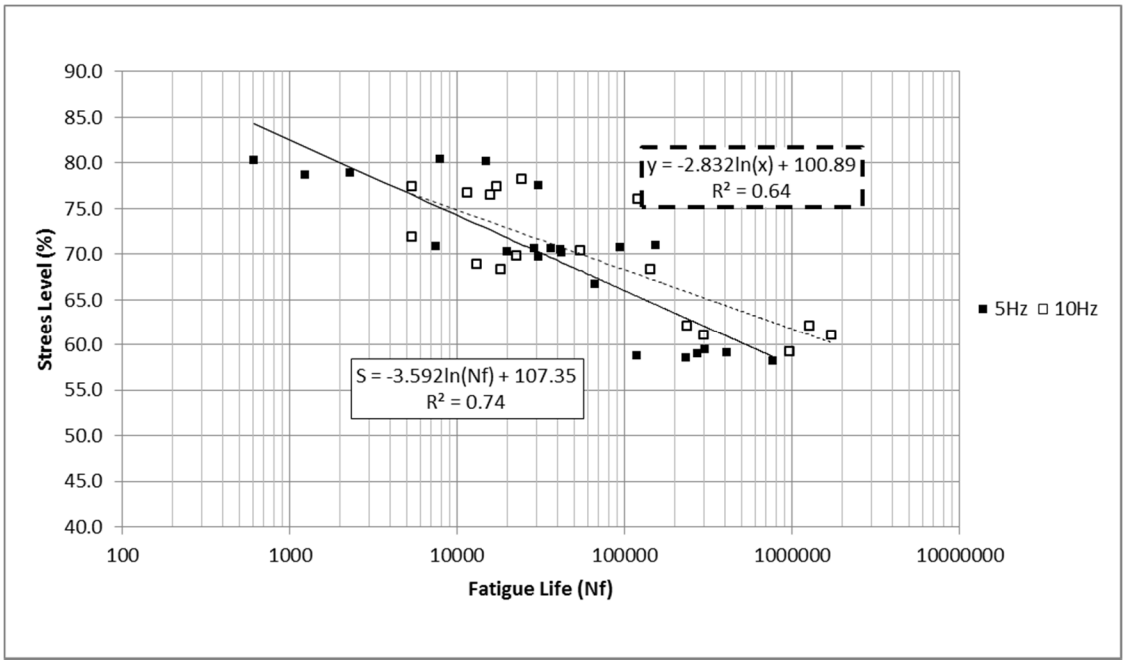

Figure 4.9: Comparison of S-N_f curves at different loading frequency (FRC8 samples)

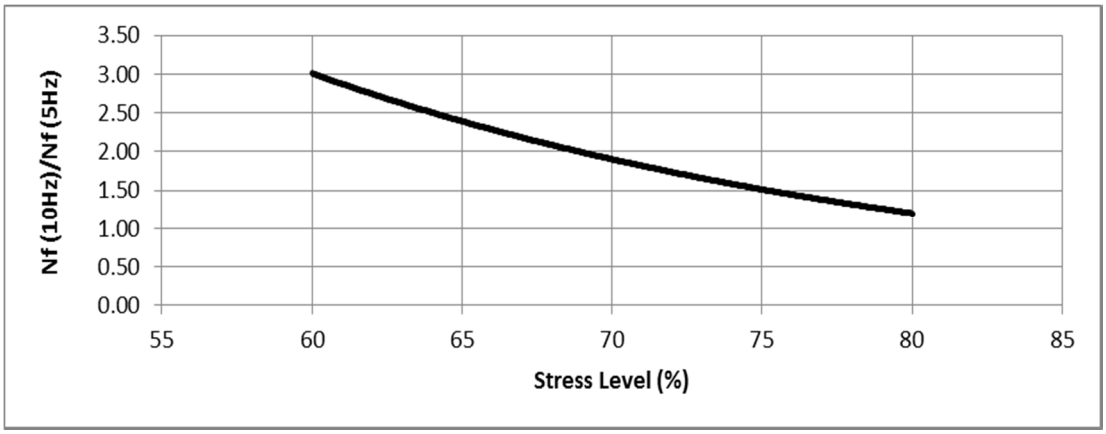

Figure 4.10: Ratio of fatigue life at loading frequency of 10 Hz to fatigue life at loading frequency of 5 Hz (FRC8 samples)

4.2.3. Effect of Fiber Addition on Fatigue Life

As mentioned at the beginning of this section, one part of this study is dedicated to investigating the effect of fiber reinforcement on the fatigue behavior of concrete. For this purpose, three concrete mixtures with fiber contents of 0, 0.4%, and 0.8% are prepared. Fatigue tests were conducted on all three mixtures at S=0.7 with a loading frequency of 5 Hz.

Table 4-4 shows the fatigue life of mixtures containing different amounts of fiber tested at the same stress level of 0.7. It can be seen that the fatigue life of the mixture containing 0.4% fiber is lower than the fatigue life of the control mixture, but this is not the case for the mixture containing 0.8% fiber. As seen in the previous chapter, the mixture containing 0.4% fiber has the same flexural strength as the control sample. On the other hand addition, of fibers up to 0.8% decreased the flexural strength by an average of 15%. In order to reach the same stress level as the control and FRC4 samples, the FRC8 samples were tested at the maximum stress, which is 15% less than the maximum stress applied to control and FRC4 samples.

Therefore, it can be concluded that polypropylene reinforcement is not beneficial when comparing the control sample with the FRC sample at the same maximum stress. When the comparison is made at the same stress level, however, fiber reinforcement does not have a negative effect on fatigue life.

Several studies have investigated the effect of polypropylene reinforcement on fatigue life, but there is no general consensus among researchers as to the optimum fiber volume that can be beneficial for enhancing the fatigue life of concrete.

As discussed in Section 4.2, the high variability in fatigue test results can be attributed to the inhomogeneity of concrete as well as variation in the stress level (due to variation in flexural strength), even in samples tested at the same stress levels.

Table 4-4: Effect of polypropylene fiber addition on fatigue life (FRC8, FRC4 and Control mixtures)

%Fiber	0	0.4	0.8
Fatigue Life (Nf)	120690	49160	29120
	85370	44920	41260
	23590	30170	30640
	7540	520	42120
	50220	22460	20000
	30210	420	66940
			153175
			36475
			7460
			94110
Average	52937	24608	52130
Coefficient of Variation (%)	80.5	85.6	82.6

4.3. Dissipated Energy per Cycle of Loading

Dissipated energy per loading was calculated for all specimens at each loading condition. As an example, the calculated dissipated energy per loading cycle of a FRC8 sample is plotted as a function of the cycle ratio (N/N_f) in Figure 4.11 . As the figure shows, dissipated energy values are dispersed throughout the entire fatigue life. This behavior is typical for all samples regardless of mixture type or loading condition.

The fact that the dissipated energy does not follow a pattern should not be surprising, given the concept of stress redistribution and the heterogeneous matrix of concrete. As mentioned previously, fatigue is associated with gradual formation of plastic deformation. During the fatigue cyclic loading, when the stress that causes plastic deformation is removed, residual stress induces in the material due to the elastic recovery of material. Therefore, subsequent loading produces a completely different stress distribution from the previous loading cycle. This phenomenon is called stress redistribution. This fact, along with the heterogeneity of mechanical characteristics throughout the concrete matrix, justifies the variable energy dissipation per cycle of loading during the fatigue process.

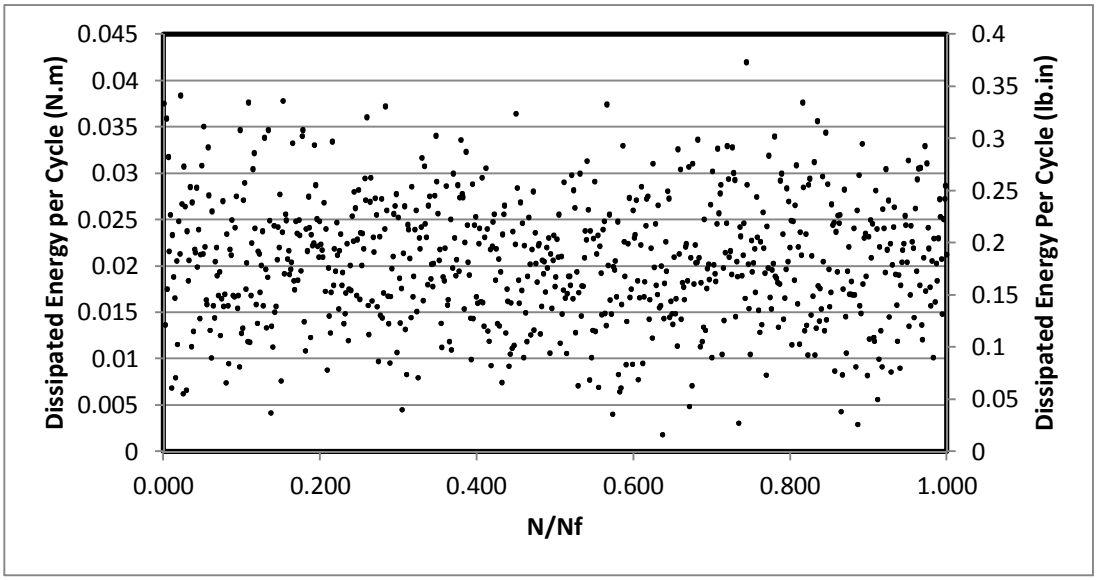

Figure 4.11: Dissipated energy per loading cycle throughout the entire fatigue life (FRC8 sample)

4.3.1. Energy Dissipation during the Course of Fatigue Life

Despite the randomness of energy dissipation per cycle of loading, the moving average of these values follows a meaningful pattern. The moving average is a technique to smooth out variation in data and accentuate the general pattern.

To illustrate energy dissipation at different stages of fatigue life, the moving average of the dissipated energy with subset size of 0.1 N_f is normalized by averaged-dissipated energy of the entire fatigue life (ADE) and plotted as a function of cycle ratio (N/N_f) in Figure 4.12 and Figure 4.13. The subset size of $0.1N_f$ indicates that each data point is the average of 0.1 N_f cycles. For example, the first data point in the moving average of a sample with a fatigue life of 1000 cycles is the average of the first 100 cycles.

The data points for Figure 4.12 and Figure 4.13 were obtained by averaging the data of at least 5 samples tested at frequencies of 5 and 10 Hz, respectively.

It is evident that the amount of dissipated energy changes at different stages of fatigue life. This can be explained by the load-carrying mechanism throughout the fatigue process of fiber-reinforced concrete. There are two distinctive load-carrying mechanisms for fiber-reinforced concrete. At the first stage of fatigue life, which is commonly called "first crack initiation," the load is carried through the concrete matrix. This stage is associated with the formation of micro-cracks in the concrete matrix. The load-carrying mechanism throughout the matrix is mainly influenced by concrete matrix properties such as cement paste strength and pore size distribution in the matrix. Fiber has no effect on the load carrying process until the first crack occurs in the matrix. Once the crack

occurs, the load carries through the bridging force of aggregate and fibers. Fiber properties such as length, surface texture, and fiber orientation can highly influence the load carrying capacity at this stage. Fibers will transfer the load to the matrix through interfacial bonding between fiber and matrix. As the cyclic load continues, the transferred load causes damage at the interface of fiber and matrix. This process continues until either the fibers mechanically fail or the bonding damage leads to fiber pull-out.

The contribution of any of the above load-carrying mechanisms to energy dissipation at different stages of fatigue life is under investigation. It is generally accepted that fiber pull-out's contribution to energy dissipation starts right after first crack initiation and increases at the end of the fatigue process.

The result shows that at the beginning and end of the fatigue test, the rate of energy dissipation is higher compared to average energy dissipation throughout the entire fatigue life. This is particularly noticeable in the case of the fatigue test performed at a loading frequency of 5 Hz. It is well accepted that the main mechanism of load carrying at the first stage of fatigue life is through the matrix. Therefore, the higher energy dissipation rate can be caused by formation of the first micro-cracks. At the final stage of fatigue life, the combination of bond failure at the matrix-fiber interface and the sudden increase in the size of micro-cracks could cause energy dissipation. Therefore, the higher energy dissipation rate at the beginning and end of fatigue life could be attributed to crack formation in the matrix.

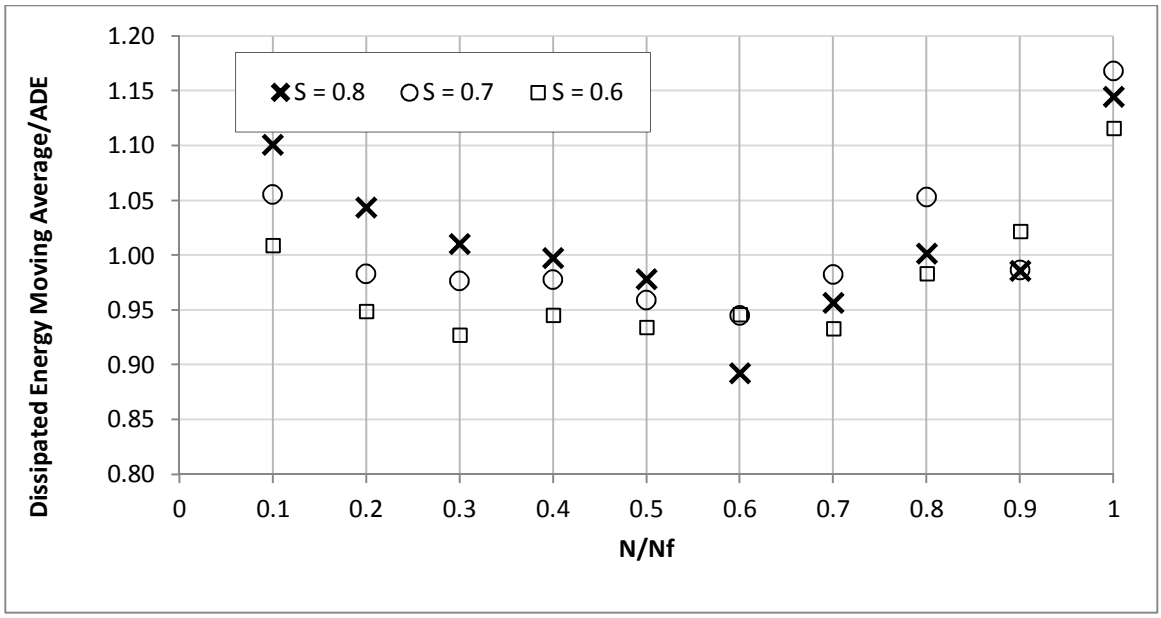

Figure 4.12: Normalized moving average of dissipated energy (loading frequency = 5, FRC8 samples)

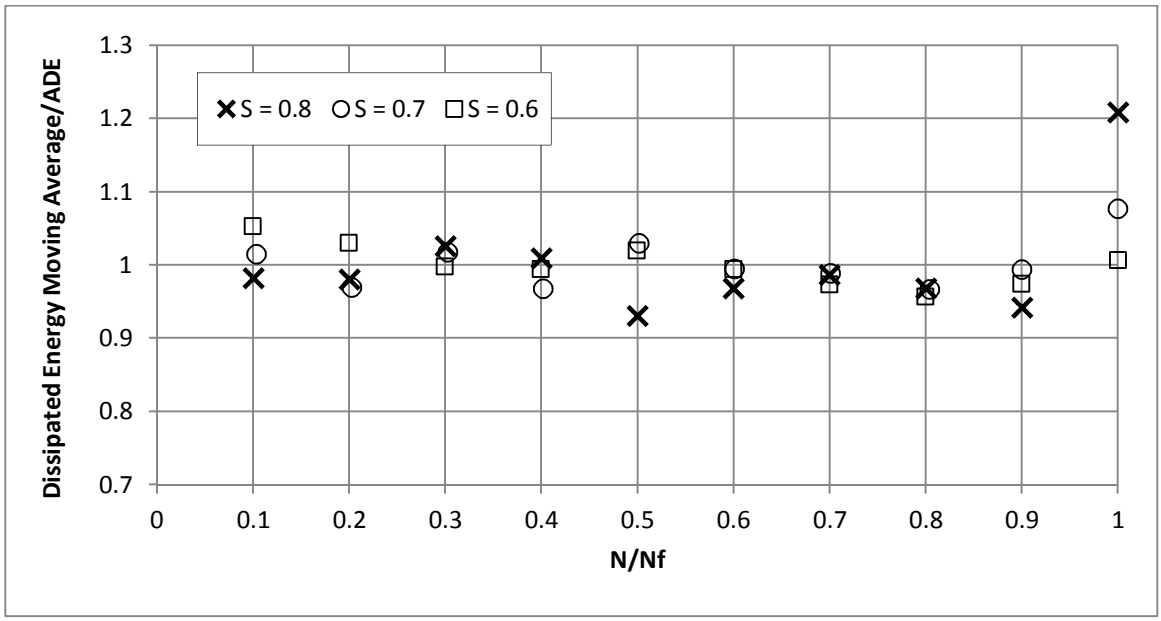

Figure 4.13: Normalized moving average of dissipated energy (loading frequency = 10, FRC8 samples)

4.3.2. Effect of Fiber Addition on Energy Dissipation Properties during Fatigue

To compare the amount of energy dissipation per loading cycle of mixtures containing polypropylene fiber to mixture without fiber, the normalized moving average of dissipated energy for each mixture is plotted as a function of cycle ratio (N/N_f) in Figure 4.14.

At the initial stage of fatigue life, the amount of energy dissipation per loading cycle for all three mixtures is higher than the averaged-dissipated energy (ADE) throughout the entire fatigue life, after which the rate of energy dissipation per loading cycle for all mixtures is around the averaged-dissipated energy. The final stage is associated with a higher rate of energy dissipation per loading cycle than ADE.

As can be seen, mixtures containing fiber have shown higher energy dissipation rates at the final stage compared to the control mixture. This could be attributed to the effect of fiber pullout on energy dissipation. Fiber pullout is the damage that occurs at the boundary between fiber and matrix, which leads to detachment of fiber from the matrix. Energy is dissipated in this process due to the friction force that develops between fiber and matrix when the fiber is being pulled out. Previous studies on fiber reinforced concrete has shown that energy dissipation due to fiber pullout is around 28% to 34% of total dissipated energy, while between 35% and 48% of energy is dissipated through matrix fracture (Trainor, Foust and Landis 2013). This implies that fiber pull-out make a significant contribution to energy dissipation, and therefore the addition of fiber can increase the amount of energy dissipation at the final stage.

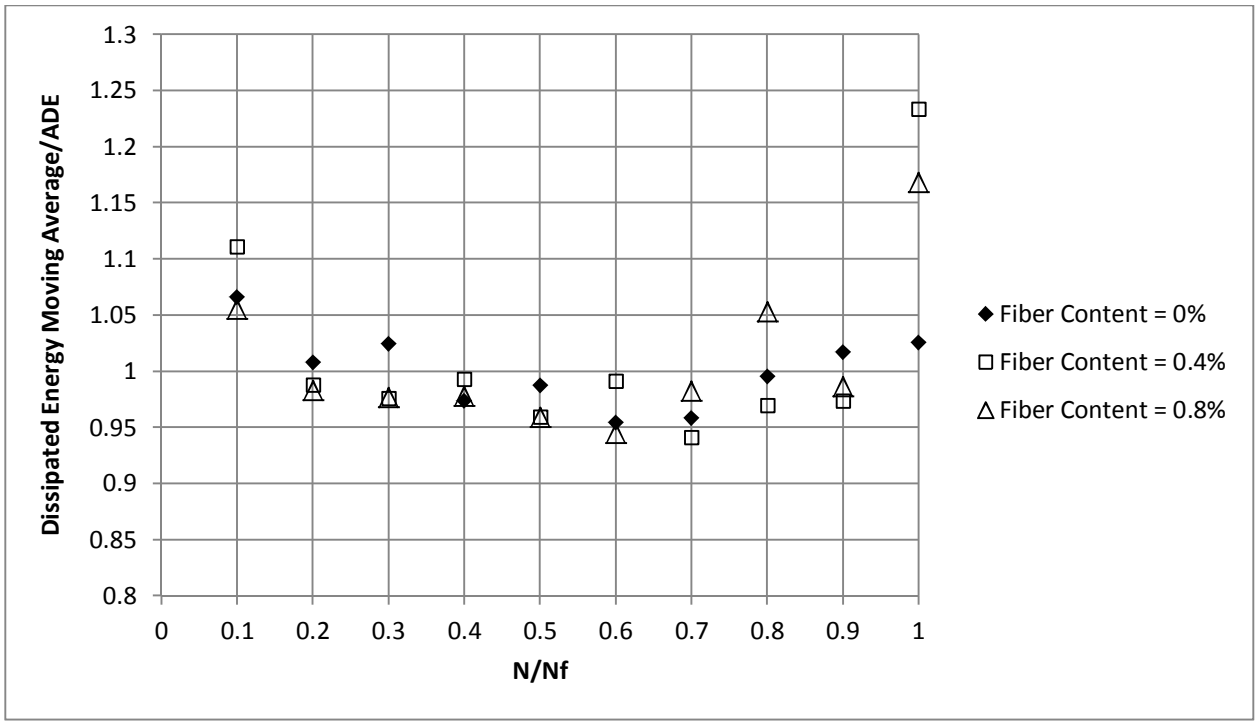

Figure 4.14: Normalized moving average of dissipated energy (effect of fiber reinforcement)

4.3.3. Factors Influencing Damping Force

4.3.3.1. Cyclic Stiffness of Beam

As mentioned at the beginning of this chapter, cyclic stiffness (k) is one of the main factors that directly affect damping force. Hence, studying the cyclic stiffness of the beam during the fatigue test can be helpful for understanding the amount of energy dissipation of concrete at different stages of fatigue life.

4.3.3.2. Cyclic Stiffness Change during the Course of Fatigue Life

The cyclic stiffness of a beam is highly influenced by the load-carrying mechanism; it depends on whether the load is transferred through the matrix, or the bridging effect of fibers, or a combination of these loading mechanisms. Since the load-carrying mechanism changes throughout the entire fatigue life, it is expected to observe different cyclic stiffness during the course of the fatigue test.

The following figures (Figure 4.15 to Figure 4.20) are some examples of calculated cyclic stiffness at different cycle counts. The cyclic stiffness is calculated by Equation 4.. The general trend for cyclic stiffness reveals that at the first 10% of fatigue life, cyclic stiffness is increasing. This stage is followed by a stage during which the change in cyclic stiffness is gradual, and finally, during the final 10% of fatigue life, a steep drop in stiffness is observed.

Perhaps the increase in cyclic stiffness at the first stage can be attributed to error in the measurement of flexural deflection. The measured deflection at the beginning of testing includes both flexural deflection and local deformation of the surface of the beam due to compression at the loading points. In a study done by El-Shakra and Gopalaratnam, the amount of extraneous surface deformation that is measured up to the first-crack load in a third-point loading flexural test is 200% of the net flexural deflection (EI-Shakra and Gopalaratnam 1993). Existence of the large irreversible surface deformation due to compression at loading points at the beginning of cyclic loading leads to cyclic stiffness values that are lower than the actual values. It should be noted that the amount of irreversible surface deformation is very large at the beginning of cyclic load

and gradually becomes small to the point of being negligible. Further explanation about surface deformation is presented on Appendix A.

Cyclic stiffness fluctuation at the second stage could be the result of change in the load-carrying mechanism due to micro-crack formation. Before the micro-cracks start growing, the load is mostly carried by the concrete matrix. As the number of micro-cracks in the matrix increases, the role of fiber bridging in transferring the load becomes more prominent. Given this and the difference in the stiffness of the matrix and polypropylene fibers, a change expected in the stiffness behavior of FRC once the micro-crack occurs.

Cyclic stiffness reduction at the final stage of fatigue life is not an unexpected result, since it is well known that the final stage is associated with micro-crack enlargement and instability of the concrete matrix.

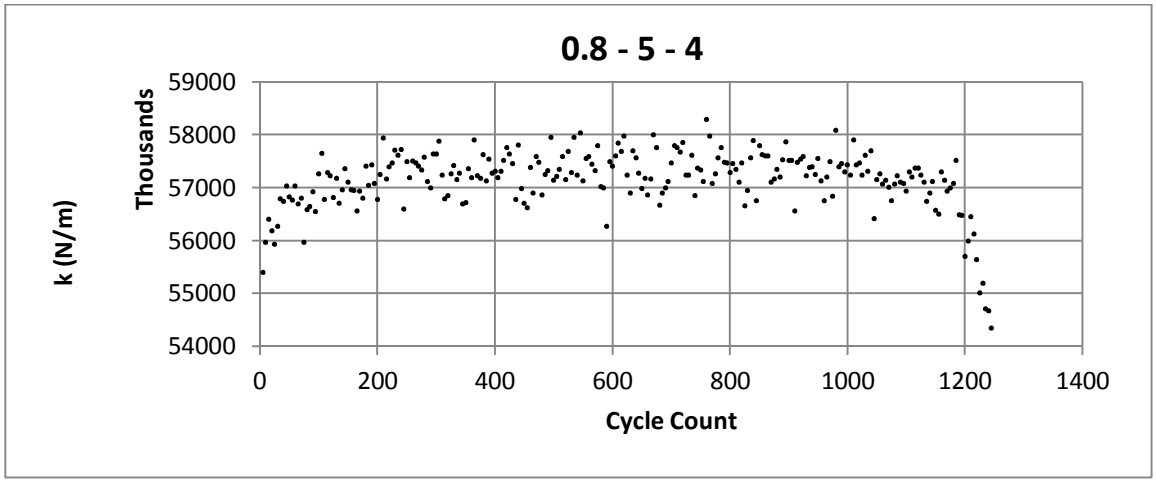

Figure 4.15: Cyclic stiffness (k) variation during fatigue life (S=0.8, loading frequency=5, FRC8)

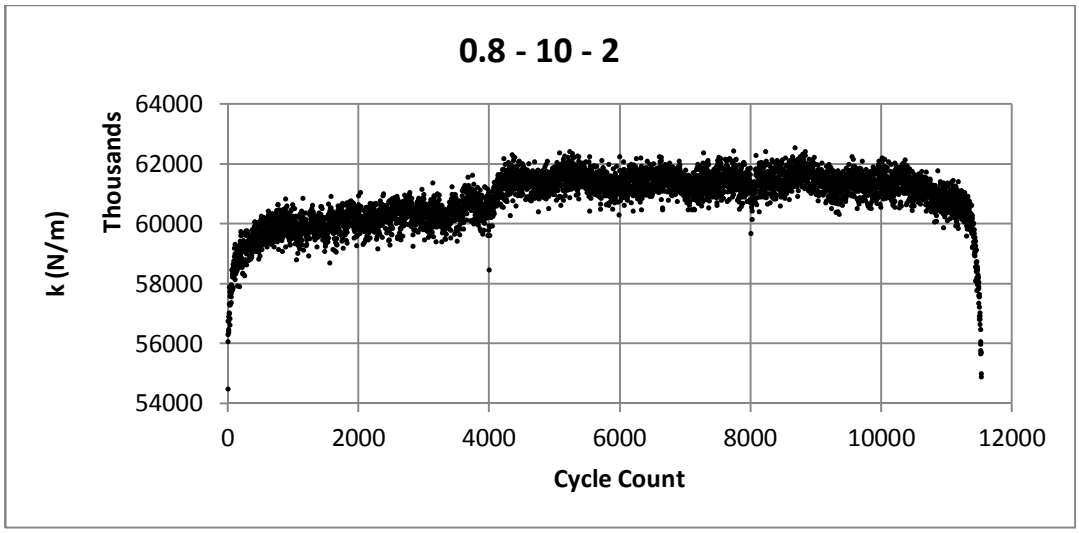

Figure 4.16: Cyclic stiffness (k) variation during fatigue life (S=0.8, loading frequency=10, FRC8)

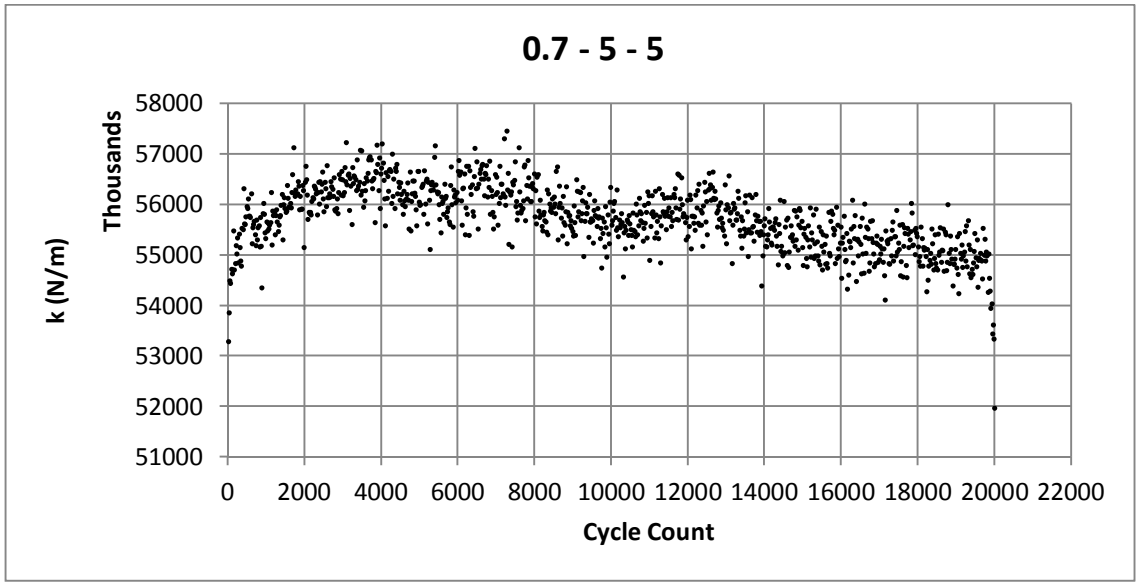

Figure 4.17: Cyclic stiffness (k) variation during fatigue life (S=0.7, loading frequency=5, FRC8)

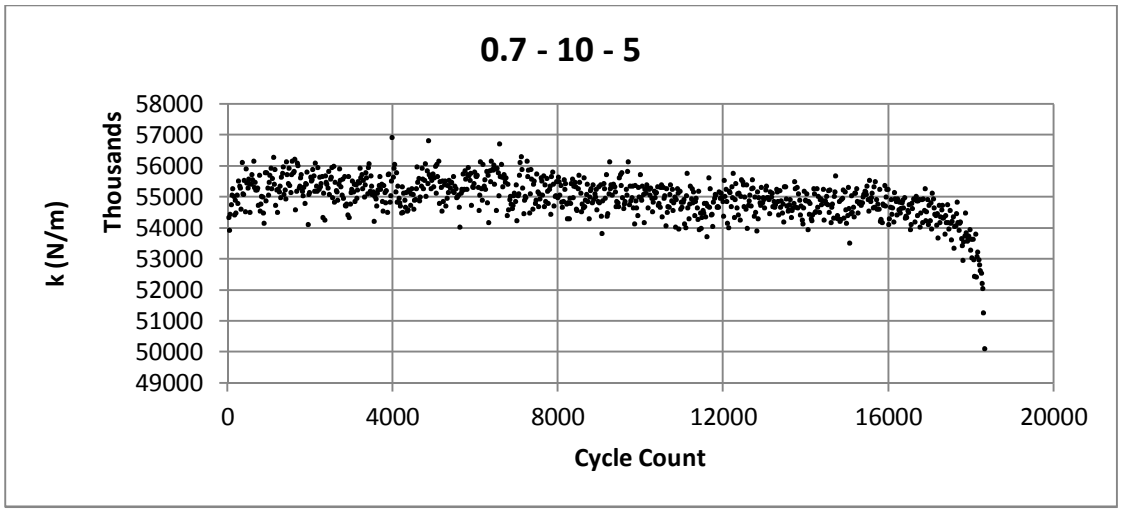

Figure 4.18: Cyclic stiffness (k) variation during fatigue life (S=0.7, loading frequency=10, FRC8)

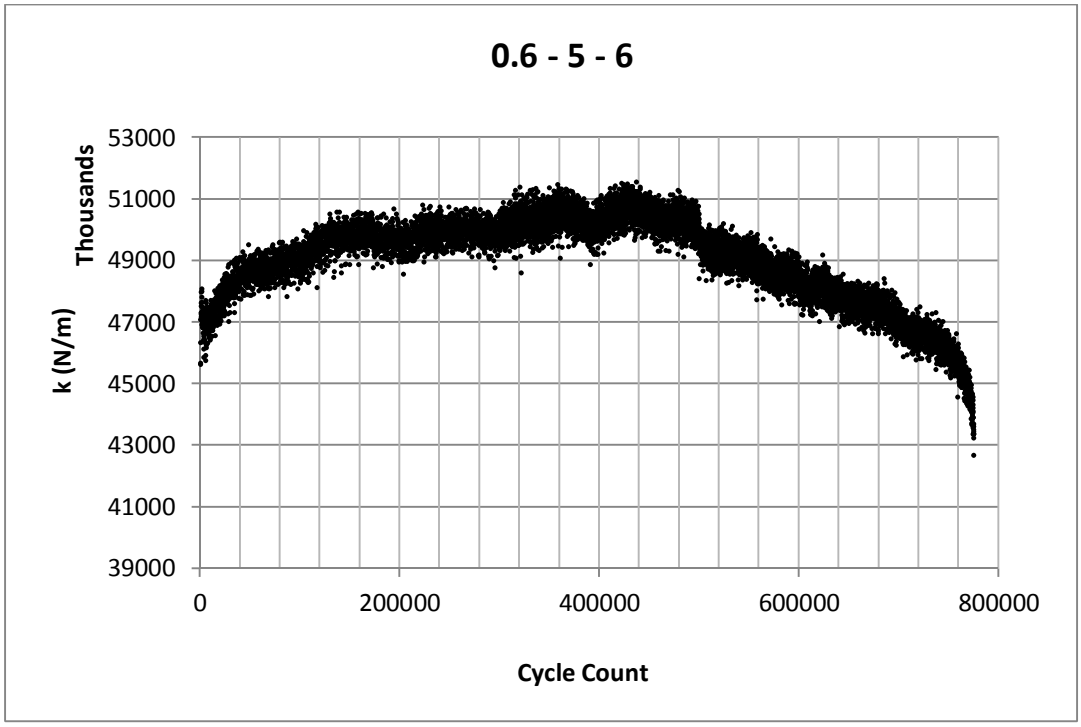

Figure 4.19: Cyclic stiffness (k) variation during fatigue life (S=0.6, loading frequency=5, FRC8)

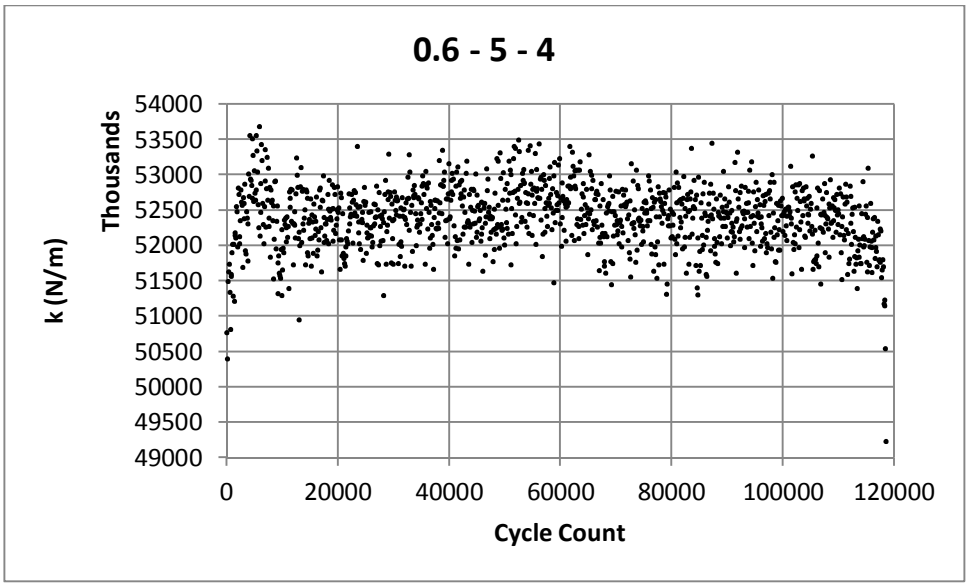

Figure 4.20: Cyclic stiffness (k) variation during fatigue life (S=0.6, loading frequency=5, FRC8)

4.3.3.3. Effect of Loading Characteristics on Cyclic Stiffness

The cyclic stiffness values in Table 4-5 represent the average values for cyclic stiffness of all samples tested at the same loading condition (i.e., same stress level and loading frequency). As can be seen, the higher the stress level and loading frequency, the greater the cyclic stiffness of the sample.

When stress level or loading frequency increases, the testing machine has to work with faster loading rates to be able to create a specified cycle of loading. Therefore, it can be concluded that cyclic stiffness has direct relationship with loading rate.

The dependence of concrete properties on loading rate has been observed and reported in several studies. It is well known that performing a mechanical properties test at higher loading rates leads to an increase in the mechanical properties of concrete, such

as compressive strength, flexural strength, and elastic modulus (Yan and Lin 2006) (Abd el Aty 2012)

Table 4-5: Cyclic stiffness during fatigue life (kN/m) (effect of loading characteristic, FRC8 samples)

Stress Level / Frequency	0.6	0.7	0.8
5	50090	55351	57160
10	56390	58726	59978

4.3.3.4. Effect of Fiber Addition on Cyclic Stiffness

The cyclic stiffness of all mixtures tested at S=0.7 and a loading frequency of 5 Hz is shown in Table 4-6. It seems that fiber reinforcement does not enhance the cyclic stiffness of the samples under dynamic loading. This is in accord with the static elastic modulus test discussed in Chapter 4, in which the FRC samples have revealed lower static elastic modulus. It can be concluded that polypropylene addition cannot enhance either the cyclic or compressive stiffness of concrete.

It is well accepted that the application of polypropylene fiber, which has a low elastic modulus, cannot be beneficial in increasing the elasticity of concrete (Manolis, et al. 1997) In fact, the elastic modulus of a polypropylene fiber (3.5 to 4.9 Gpa (from (Zheng and Feldman 1995)) is lower than a typical elastic modulus of concrete matrix (14 to 40 Gpa). Therefore, the elastic modulus of composite mixture decreases as the amount

of fiber increases. Also, the increase in entrapped air of the mixture containing fiber is another reason for lower elastic modulus.

Table 4-6: Cyclic stiffness during fatigue life (kN/m) (effect of fiber reinforcement)

Mix ID	Cyclic Stiffness
Control	58599
FRC4	56906
FRC8	55351

4.3.3.5. Dimensionless Hysteresis Damping Constant

Hysteresis force generated in the course of a fatigue test is influenced by the dimensionless hysteresis damping constant (β). Hysteresis force expressed by the term $\frac{\beta k}{2\pi f}\dot{x}$ in the movement equation of harmonically excited motion (Equation 4.2). The hysteresis damping constant is a material property and therefore is highly influenced by factors that impact the material's behavior, such as micro-crack formation, rate of loading, etc. Therefore, the value of β is expected to be influenced by loading history as well as loading characteristics.

4.3.3.6. Effect of Loading Characteristics on Hysteresis Damping Constant

Table 4-7 presents an average value of hysteresis damping constant per loading cycle of all samples that are tested at same loading conditions (i.e. the same stress level and loading frequency). As shown, the hysteresis damping constant is directly related to stress level and loading frequency. Therefore, it is expected that at a higher loading frequency and stress level, more energy dissipates per cycle of loading.

Table 4-7: Dimensionless hysteresis damping constant. (effect of loading characteristics. FRC8 samples)

Stress Level / Frequency	0.6	0.7	0.8
5	0.0272	0.0325	0.0342
10	0.0440	0.0481	0.0481

4.3.3.7. Effect of Fiber Addition on Dimensionless Hysteresis Damping Constant

In contrast to the decreasing effect of fiber addition on cyclic-stiffness, results show (Table 4-8) that addition of polypropylene fiber enhances the hysteresis damping constant of concrete. This could be attributed to the energy dissipation due to fiber pullout and the bridging effect.

As shown in Equation 4.2, damping force is directly related to the product of cyclic stiffness, k, and the dimensionless hysteresis damping constant, β, (i.e., βk) as well as loading frequency (f) and the velocity of motion ($\dot{x}$). To reach a definite conclusion regarding the effect of fiber reinforcement on the damping properties of concrete, the product of stiffness and the hysteresis damping constant is calculated and given in Table 4-9. It is evident that fiber reinforcement has improved the damping properties of the concrete matrix, since the βk value is larger.

Table 4-8: Dimensionless hysteresis damping constant (effect of fiber reinforcement)

Mix ID	β
Control	0.02693
FRC4	0.03012
FRC8	0.03252

Table 4-9: βk (kN/m) (effect of fiber reinforcement)

Mix ID	β.k
Control	1587
FRC4	1714
FRC8	1800

4.3.4. Averaged-dissipated energy per loading cycle

Averaged-dissipated energy per loading cycle (ADE), which is the sum of calculated dissipated energy per loading cycle divided by number of cycles to failure, is used as a representative value of dissipated energy per loading cycle of each sample.

As mentioned earlier in this chapter, the first cycle of loading is associated with not only flexural deformation but also a permanent surface deformation. Thus, the amount of energy dissipated in this cycle is usually much larger than the dissipated energy of the rest of cycles. Since the focus of this study is energy dissipation due to flexural bending, the dissipated energy of the first cycle of loading is excluded from ADE calculation. It should be mentioned that excluding the first cycle does not have a major effect on the ADE of samples with N_f>1000, but it can significantly affect the ADE of samples with N_f<1000.

4.3.4.1. Effect of Loading Characteristics on Averaged-Dissipated Energy per Loading Cycle

4.3.4.2. Stress level

ADE versus stress levels is plotted in Figure 4.21. It can be seen that the stress level has a direct relationship with ADE. As the stress level increases, the ADE also increases. The reasons for this are as follows.

First, it is well accepted that the amount of plastic deformation that occurs in a material has a direct relationship with the magnitude of the load. Beyond the elastic limit of the material, the magnitude of plastic deformation increases by increasing the magnitude of the load. Therefore, at higher stress levels, samples experience higher plastic deformation per cycle of loading and hence higher energy dissipation is anticipated.

Furthermore, the amount of damping through the slid damping mechanism at higher stress levels is expected to increase because shear stress at the interfaces of

different phases of concrete increases as maximum cyclic stress increases. Moreover, inhomogeneous strain distribution, which is the main cause of the relative movement of different phases of concrete, is larger at higher stress levels. Previous studies on concrete and other materials, such as fiber-reinforced ceramics, are in agreement with this finding (Holmes and Shuler 1990).

4.3.4.3. Loading Frequency

Figure 4.21 shows that ADE increases with increasing loading frequency. To compare the damping properties of a mixture at different loading frequencies, the damping constant (c), which is the ratio of the product of cyclic stiffness and the hysteresis damping constant to the loading frequency (i.e., $\frac{\beta k}{2\pi f}$ from Equation 4.2), is tabulated in Table 4-10. As can be seen, the damping constant of concrete at higher frequencies is decreased. It should be noted that damping force is not only related to the damping constant (c), but also is influenced by the velocity of movement ($\dot{x}$). Considering the results in Table 4-10 and the fact that the velocity of movement ($\dot{x}$) is almost doubled by increasing the frequency from 5 to 10 Hz, higher energy dissipation is anticipated at higher loading frequencies.

4.3.4.4. Effect of Fiber Reinforcement on Averaged-Dissipated Energy per Cycle

Figure 4.22 present the ADE of different mixtures tested at S=0.7 with a loading frequency of 5 Hz. As shown, polypropylene fiber improves the energy dissipation behavior of concrete. The increase in energy dissipation rate can be explained by an

increase in the work required to pull out the fibers. The bridging effect of fiber, along with the work required to pull out the fibers at the final stage of fatigue life, has increased the amount of energy dissipation in a loading cycle.

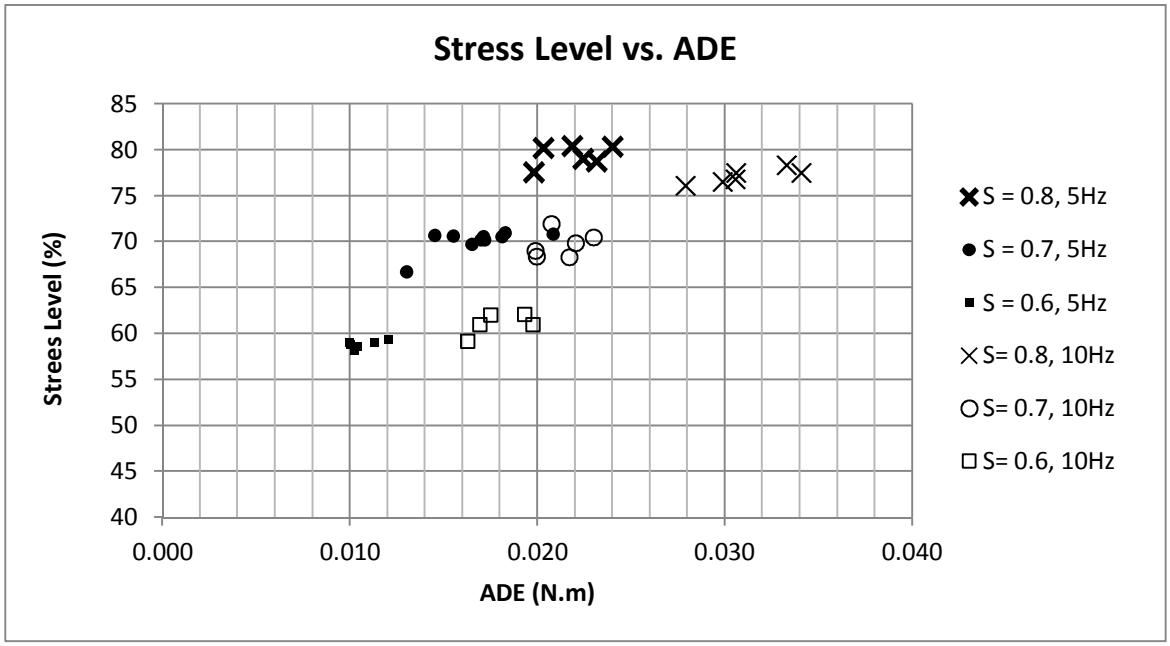

Figure 4.21: Averaged-dissipated energy per loading cycle (effect of loading characteristics, FRC8 samples)

Table 4-10: Damping constant $C=\beta k/2\pi f$ (N.Sec/m) (effect of loading characteristics, FRC8 samples)

Stress Level / Frequency	0.6	0.7	0.8
5	43373	57262	62225
10	39489	44956	45915

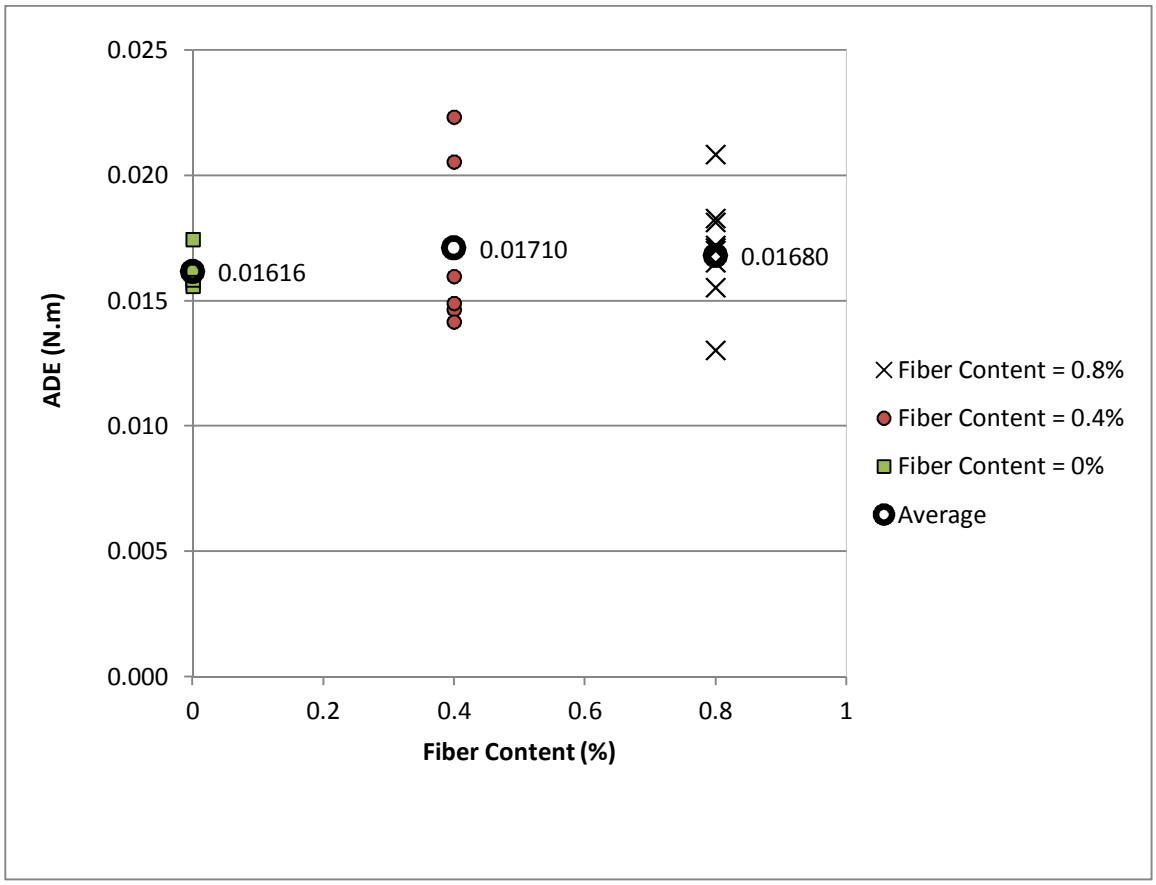

Figure 4.22: Effect of fiber reinforcement on average dissipated energy per loading cycle

Variability assessment of ADE is presented in Table 4-11. It is clear that the addition of fiber to the mixture increased the variability of ADE, which is not an unexpected result. Fiber addition acts as a source of heterogeneity and increases the variability of ADE. Heterogeneity caused by fiber originates from the random distribution of fibers within a sample, the random orientation of fibers, and the variability in fiber properties.

Table 4-11: Variability assessment of ADE (effect of fiber reinforcement)

%Fiber	0	0.4	0.8
ADE (N.m)	0.016028	0.014651	0.018286
	0.015746	0.014155	0.015520
	0.015588	0.014900	0.020826
	0.017451	0.022338	0.014505
	0.015836	0.015972	0.017101
	0.016288	0.020555	0.018117
			0.016502
			0.016988
			0.017191
			0.013015
Average	0.016156	0.017095	0.016805
Coefficient of Variation (%)	4.2	20.3	12.8

4.3.5. Total Dissipated Energy per Cycle of Loading

4.3.5.1. Effect of Loading Characteristics on Total Dissipated Energy

4.3.5.2. Stress Level

Total dissipated energy (TDE) is calculated by multiplying the ADE by the fatigue life of the sample (N_f). The results for FRC8 samples are summarized in Table 4-12. In spite of the greater energy dissipation per loading cycle at higher stress levels (Figure 4.21), samples tested at lower stress levels dissipate more energy during the fatigue process. By lowering the stress level, the fatigue life of the samples increases significantly, which compensates for the decreasing effect of change in the ADE.

If a damping mechanism is categorized as either a nondestructive damping mechanism (i.e., the mechanism is recoverable and causes no plastic deformation in the body of concrete, such as recoverable relative movement between different phases of concrete) or a destructive damping mechanism (i.e., it is associated with formation of

plastic strain due to micro-cracks), the contribution of non-destructive damping to total dissipated energy is greater at lower stress levels than at higher stress levels. The reason for that is that at low stress levels the rate of increasing plastic strain in the concrete is smaller than at high stress levels, and therefore the sample lasts for more cycles; hence, more energy dissipates due to non-destructive damping.

4.3.5.3. Loading Frequency

The increasing effect of loading frequency on total dissipated energy is observed in Figure 4.24. The same reason given in the previous section can justify this result. At 10 Hz frequency, the rate of damage accumulation per cycle is lower because creep deformation decreases due to the smaller time period for loading. Therefore, fatigue life increases and the concrete can dissipate more energy.

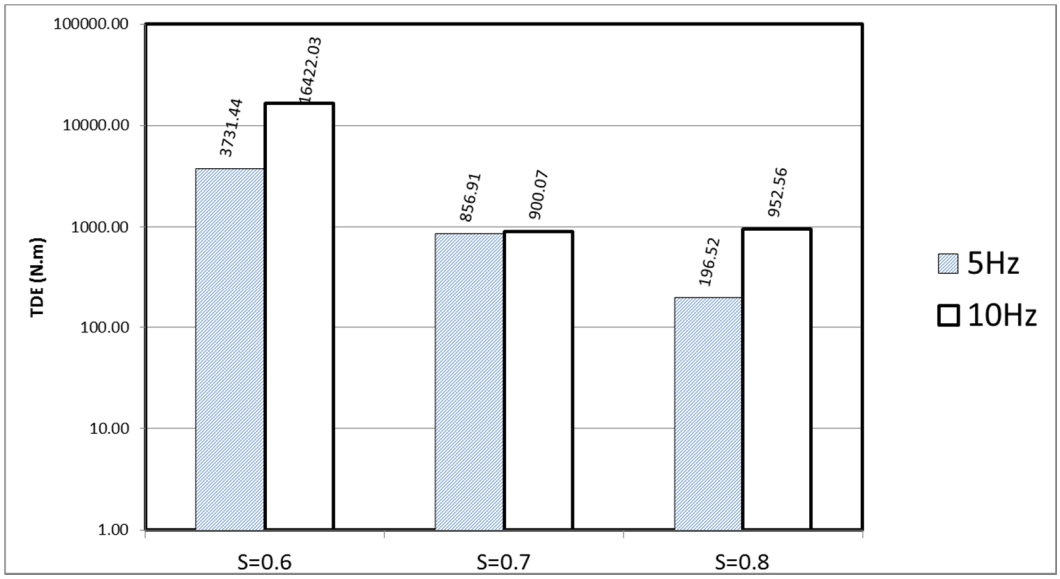

Figure 4.23: Effect of loading frequency on total dissipated energy (FRC8 Mixture)

Table 4-12: Total dissipated energy of FRC8 samples at different loading condition

S-Frequency- ID#	N_f	ADE (N.m)	Stress Level (%)	TDE (N.m)
0.8-5-1	15000	0.02034	80.19	305.1
0.8-5-2	610	0.024	80.28	14.64
0.8-5-3	7950	0.02185	80.36	173.73
0.8-5-4	1245	0.02317	78.69	28.85
0.8-5-5	2310	0.02244	78.95	51.84
0.8-5-6	30520	0.01982	77.48	604.94
Average	9606	0.02194	79.33	196.52
0.7-5-1	29120	0.0171	70.58	497.97
0.7-5-2	41260	0.01812	70.54	747.49
0.7-5-3	30640	0.0165	69.7	505.63
0.7-5-4	42120	0.01699	70.17	715.53
0.7-5-5	20000	0.01719	70.22	343.82
0.7-5-6	66940	0.01301	66.73	871.2
0.7-5-7	153175	0.01829	70.94	2800.94
0.7-5-8	36475	0.01552	70.6	566.11
0.7-5-9	7460	0.02083	70.84	155.36
0.7-5-10	94110	0.0145	70.72	1365.02
Average	52130	0.0168	70.1	856.91
0.6-5-1	302620	0.01206	59.43	3648.13
0.6-5-2	272270	0.01132	58.99	3082.49
0.6-5-3	409800	0.00997	59.09	4084.45
0.6-5-4	118600	0.01006	58.8	1192.79
0.6-5-5	233900	0.01038	58.56	2428.95
0.6-5-6	775000	0.01026	58.18	7951.82
Average	352032	0.01067	58.84	3731.44
0.8-10-1	17150	0.0306	77.44	524.8
0.8-10-2	11532	0.03056	76.76	352.37
0.8-10-3	120928	0.02789	76.07	3372.88
0.8-10-4	24236	0.0333	78.25	807.02
0.8-10-5	5352	0.03409	77.43	182.44
0.8-10-6	15920	0.02989	76.5	475.84
Average	32520	0.03105	77.08	952.56
0.7-10-1	13090	0.0199	68.93	260.49
0.7-10-2	5420	0.02077	71.9	112.57
0.7-10-3	54840	0.02302	70.38	1262.16
0.7-10-4	22740	0.02208	69.76	502.07
0.7-10-5	18340	0.02172	68.28	398.3
0.7-10-6	128000	0.01999	68.29	2866.61
Average	40405	0.02125	69.59	900.07
0.6-10-1	973500	0.01627	59.18	15834.37
0.6-10-2	300000	0.0169	61.01	5069.25
0.6-10-3	1736900	0.01973	61.01	34270.24
0.6-10-4	1277300	0.01751	62.08	22361.74
0.6-10-5	237000	0.0193	62.12	4574.52
Average	904940	0.01794	61.08	16422.03

Figure 4.24 shows the relationship between the fatigue life of concrete and the total energy dissipated in the fatigue test. As can be seen, the difference between total dissipated energy at loading frequencies of 5 and 10 Hz decreases as fatigue life decreases. In other words, when the fatigue life is very small (i.e., the fatigue test is close to becoming a static test because of the stress level close to 1), the difference between total energy dissipation is becomes a relatively small number. Therefore, it can be concluded that the effect of loading frequency on total energy dissipation becomes negligible by increasing the stress level (i.e., decreasing fatigue life).

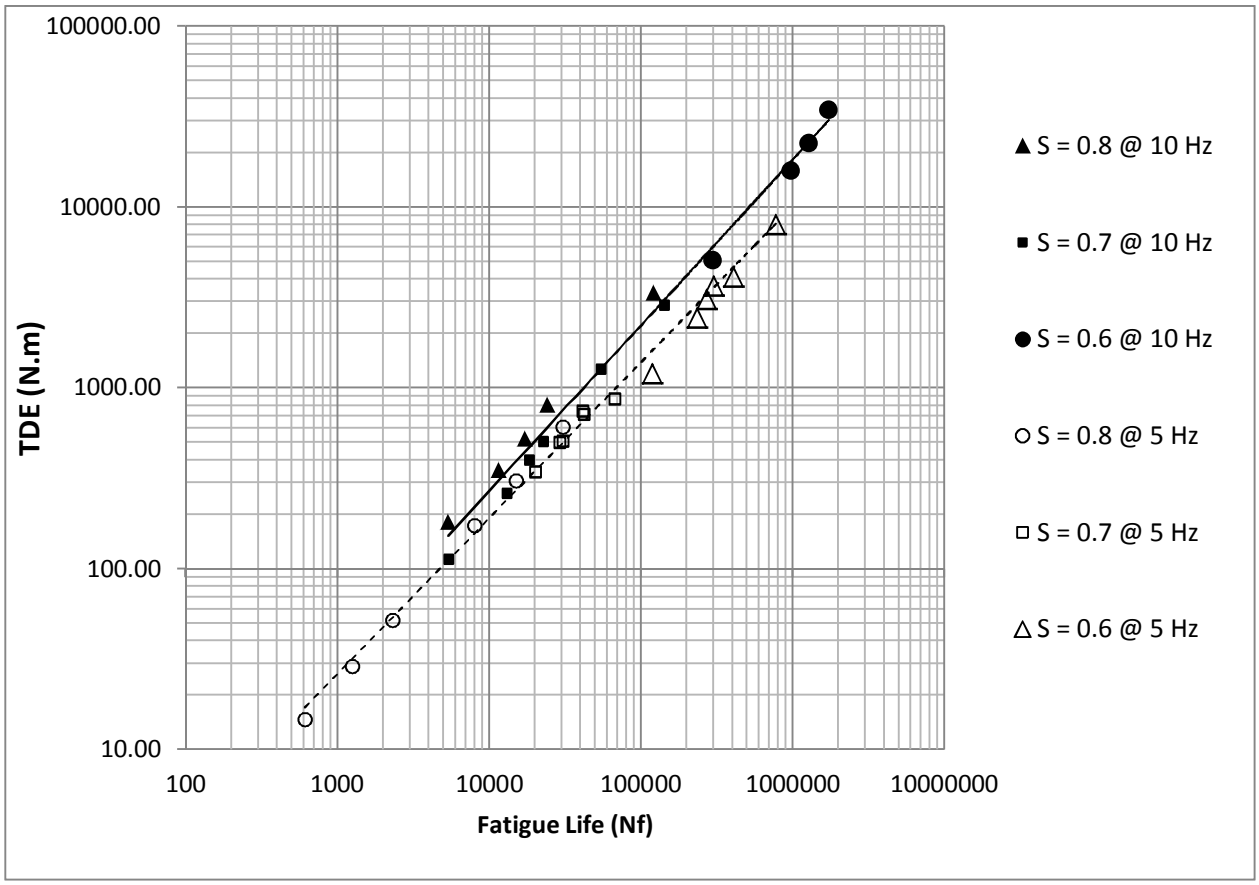

Figure 4.24: Total dissipated energy (TDE) vs. fatigue life (N_f) (FRC8 samples)

4.3.5.4. Effect of Fiber Reinforcement on Total Dissipated Energy

Table 4.13 summarizes the total dissipated energy in the fatigue of concrete with different amounts of fiber content. Results show that application of fiber by 0.4% volume reduces the dissipated energy of the mixture compared to a mixture without fiber. Conversely, addition of 0.8% fiber slightly enhances the energy dissipation properties.

Fiber addition provides reinforcement for the concrete matrix, which reduces the concrete's brittleness and improves the energy dissipation properties. On the other hand, it could have an undesirable effect on the pore size of the matrix, and therefore worsen the energy dissipation properties. It seems that matrix reinforcement is the dominant factor in the case of mixtures containing 0.8% fiber, rather than fiber's undesirable effect of increasing pore size. Previous studies on TDE of polypropylene-reinforced concrete have shown similar results. In a study done by Paskova and Meyer, a mixture containing 1% polypropylene displayed better behavior in terms of energy dissipation during fatigue compared to mixtures with 0.75%, 0.5% and 0% polypropylene fibers (Paskova and Meyer 1997).

Table 4-13: Total dissipated energy at S=0.7 and loading frequency =5 (effect of fiber reinforcement)

Sample ID	TDE (N.m)
FRC8-1	497.97
FRC8-2	747.49
FRC8-3	505.63
FRC8-4	715.53
FRC8-5	343.82
FRC8-6	871.2
FRC8-7	2800.94
FRC8-8	566.11
FRC8-9	155.36
FRC8-10	1365.02
Average	856.91
FRC4-1	720.26
FRC4-2	635.83
FRC4-3	449.52
FRC4-4	11.62
FRC4-5	358.73
FRC4-6	8.63
Average	364.1
Control-1	1934.46
Control-2	1344.25
Control-3	367.72
Control-4	131.58
Control-5	795.31
Control-6	492.06
Average	844.23

4.3.6. Deformational Characteristics

4.3.6.1. Load-Deflection Curve and Post-Failure Behavior

A representative load-deflection curve for FRC8 samples is shown in Figure 4.25. Increasing the maximum cyclic deflection by increasing the cycle count is an indicator of plastic deformation accumulation. The change in the maximum cyclic deflection from N=1 to N=200 (i.e., first 16% of fatigue life) and from N=800 to N_f =1245 (i.e., the last 35% of fatigue life) is almost twice the change in the maximum cyclic deflection from N=200 to N=800 (i.e., middle 50% of fatigue life). This suggests that the rate of increasing plastic deformation is higher at the beginning and the end of the fatigue process. The accumulation of surface deformation, as well as the formation of the first micro-cracks due to flexural fatigue, could be the main reason for the high plastic deformation accumulation rate at the beginning of cyclic loading. On the other hand, increasing the micro-crack network—and hence the movement of the concrete sample to unstable crack networks—could be major cause of increasing the rate of plastic deformation accumulation at the final stage of fatigue life. It has to be added that the contribution of plastic surface deformation in the first stage of fatigue life is beyond the scope of this study, and any definitive statement regarding the magnitude of this deformation will require further investigation.

The concept of the hysteresis damping behavior of concrete is well reflected in the load-deflection curve. The area enclosed in the load-deflection curve, which represents the amount of energy dissipation in a loading cycle, is greater at the beginning and the end of the fatigue process compared to that in the middle cycles. This supports

the observation that the amount of energy dissipation at the start and at the end of the fatigue process is higher than during the middle loading cycles.

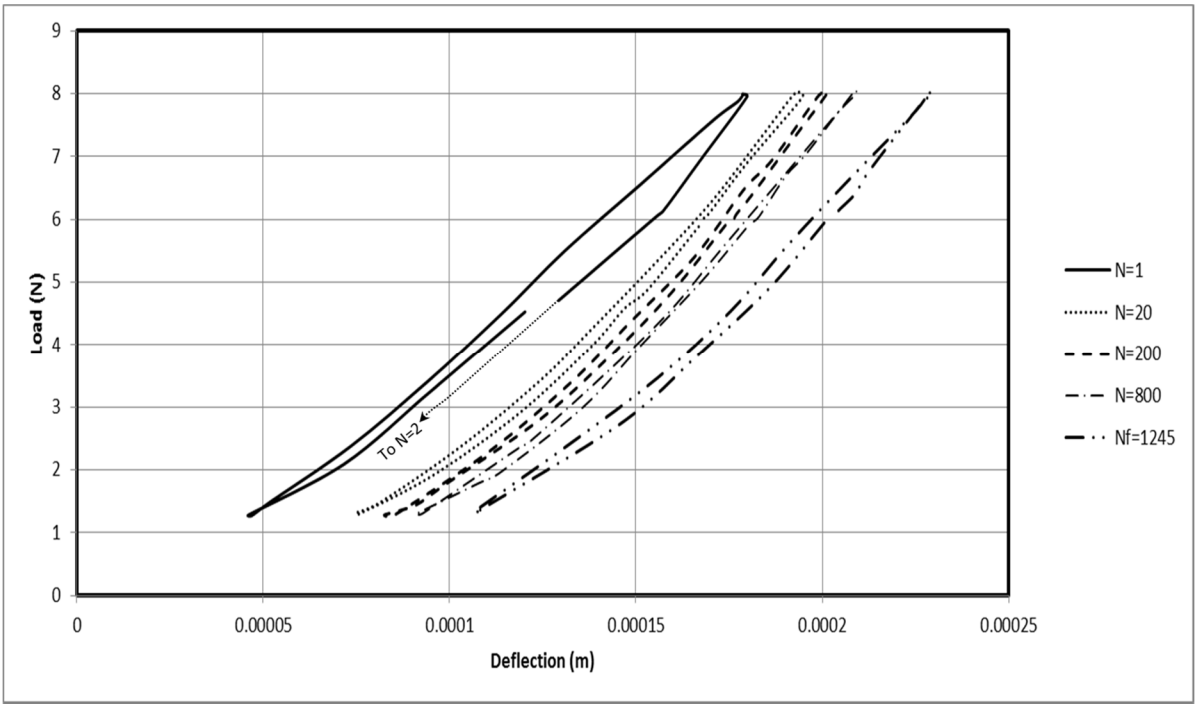

Figure 4.25: Load-deflection curve (S=0.8, frequency of loading=5, FRC8)

Figure 4.26 and Figure 4.27 include the post-failure behavior of an FRC8 and a control sample, respectively. As mentioned previously, in Section 4.1.1, physical damage to the sample happens a few cycles after fatigue failure. In other words, the sample can still take a few loading cycles at lower stress levels before complete destruction (visible cracks) occurs.

The machine is set to generate a certain number of loading cycles per second (i.e., frequency of loading) at a certain stress level. When a sample reaches the point that fatigue failure occurs, the machine automatically decreases the amplitude of loading to be able to provide the specified frequency of loading. In other words, between the input parameters that control the fatigue test (amplitude and frequency of loading), the frequency is set to always be constant. This characteristic of the loading machine give it the capability to record the post-failure cycles.

As seen in Figure 4.26 and Figure 4.27, beyond fatigue the failure point (i.e., $N>N_f$), the load-deflection curve cannot reach the maximum load specified in the test due to strength loss of concrete. However, the sample still takes more loading cycles at a lower stress level.

It is generally accepted that the cyclic load-deflection curve throughout the entire fatigue life, even after failure, is surrounded by a curve similar to the static load-deflection curve (Bahn and Hsu 1998). This is shown in Figure 4.26 and Figure 4.27 for the FRC8 and control sample, respectively. The surrounding curve is drawn by connecting the maximum cyclic deflection points. As can be seen, the surrounding curve of the sample containing 0.8% fiber (Figure 4.26) shows considerable enhancement in terms of post-failure ductility and toughness compared to the control sample (Figure 4.27).

4.3.6.2. Rate of Plastic Deformation Accumulation during the Course of Fatigue Life

The concept of plastic deformation accumulation during fatigue life is presented in Figure 4.28 to Figure 4.33. The ratio of maximum deflection at cycle N to the

maximum deflection at fatigue failure is plotted as a function of cycle ratio (N/N_f) for FRC8 samples at different loading characteristics.

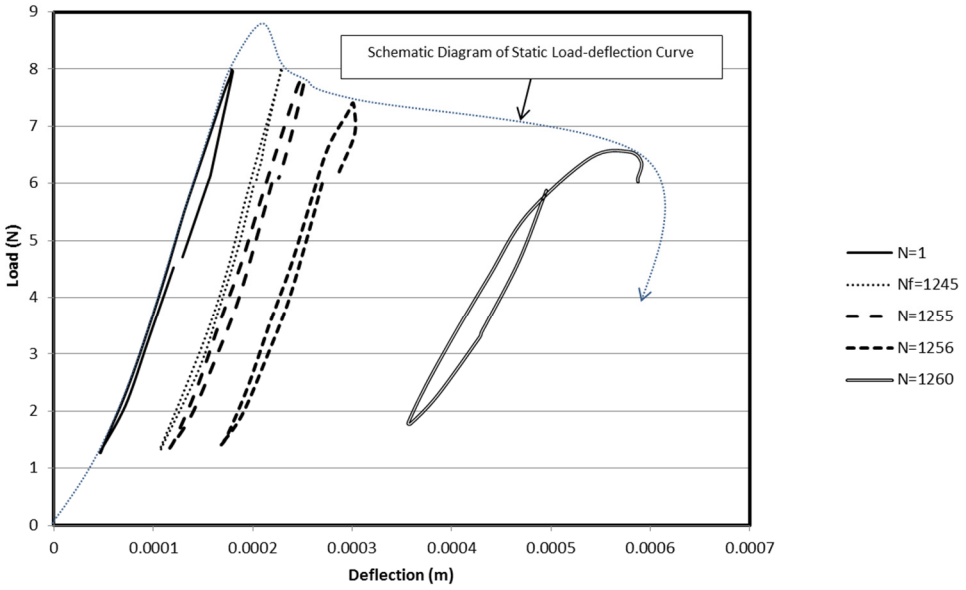

Figure 4.26: Load-Deflection history-FRC8 sample (S=0.8, loading frequency = 5)

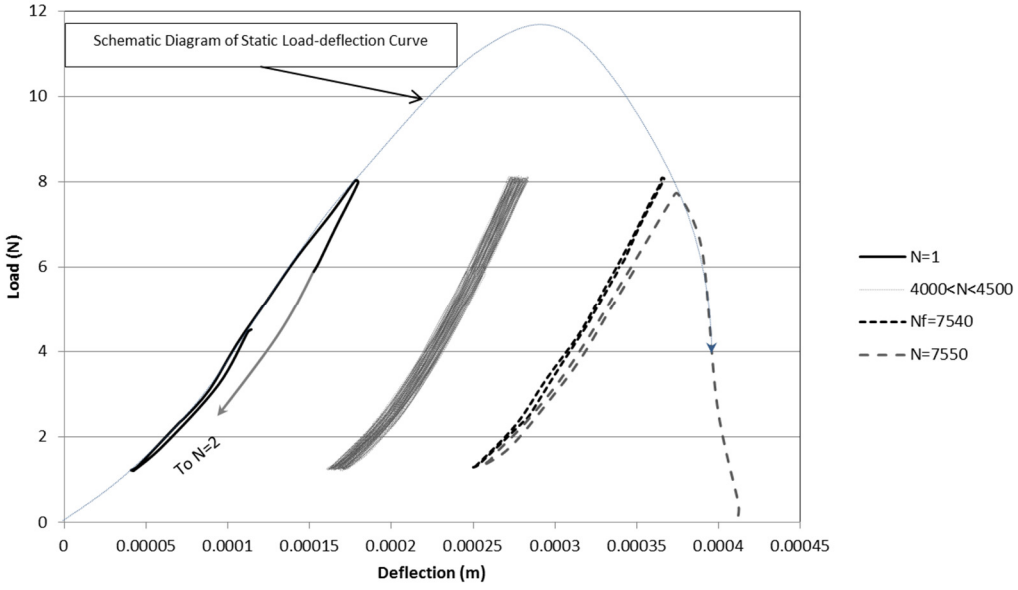

Figure 4.27:Load-Deflection history-Control sample (S=0.7, loading frequency = 5)

As shown, three distinctive stages of fatigue life are noticeable. The first 10% of fatigue life is associated with a fast increase in the maximum deformation of the beam. The deformation then increases at a very slow rate compared to the first stage. This phase continues to 95% of the fatigue life and is followed by a quick increase in deformation until failure.

This behavior has been reported in several studies conducted on the fatigue life of concrete (Tawfiq, Armaghani and Ruiz 1999). The steep rise in accumulated plastic deformation at the first stage is attributed to the initiation of the first micro-cracks. The second stage is described as the constant growth of micro-cracks. At this stage, micro-cracks propagate throughout the concrete matrix until the matrix becomes unstable. The last stage is associated with a sudden increase in the size of micro-cracks, which leads to failure.

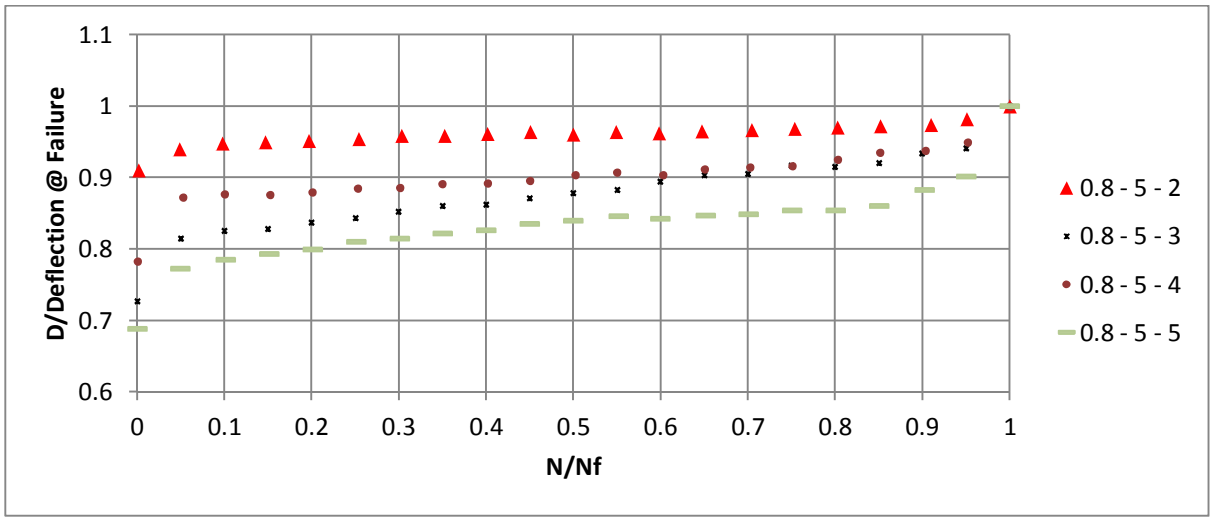

Figure 4.28: Plastic deformation accumulation during fatigue life (S=0.8, loading frequency = 5, FRC8 samples)

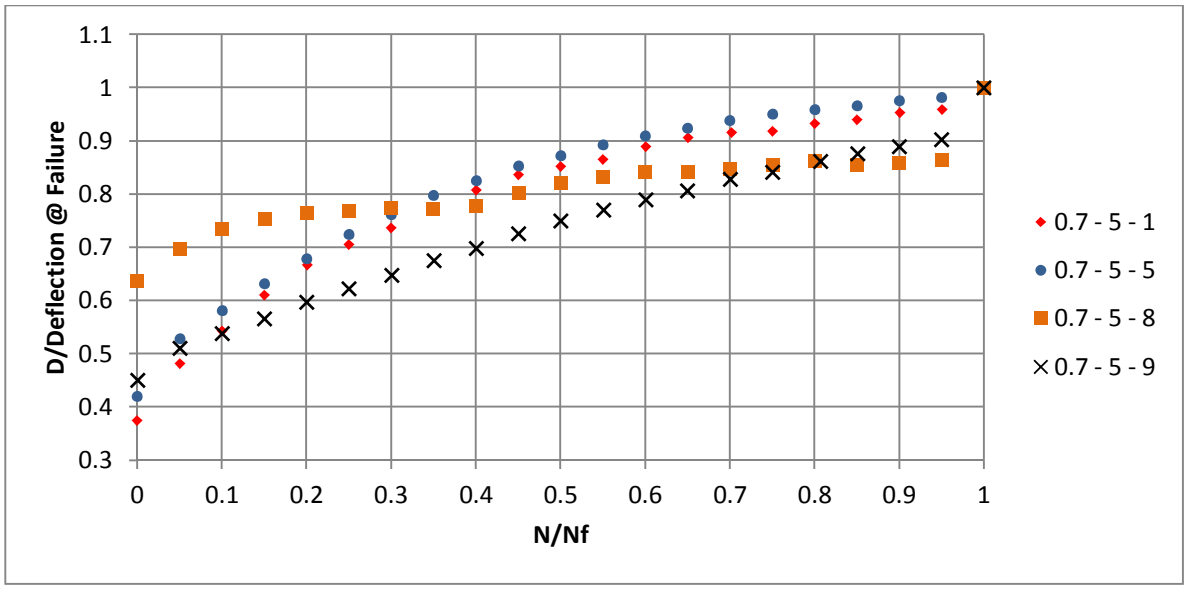

Figure 4.29: Plastic deformation accumulation during fatigue life (S=0.7, loading frequency = 5, FRC8 samples)

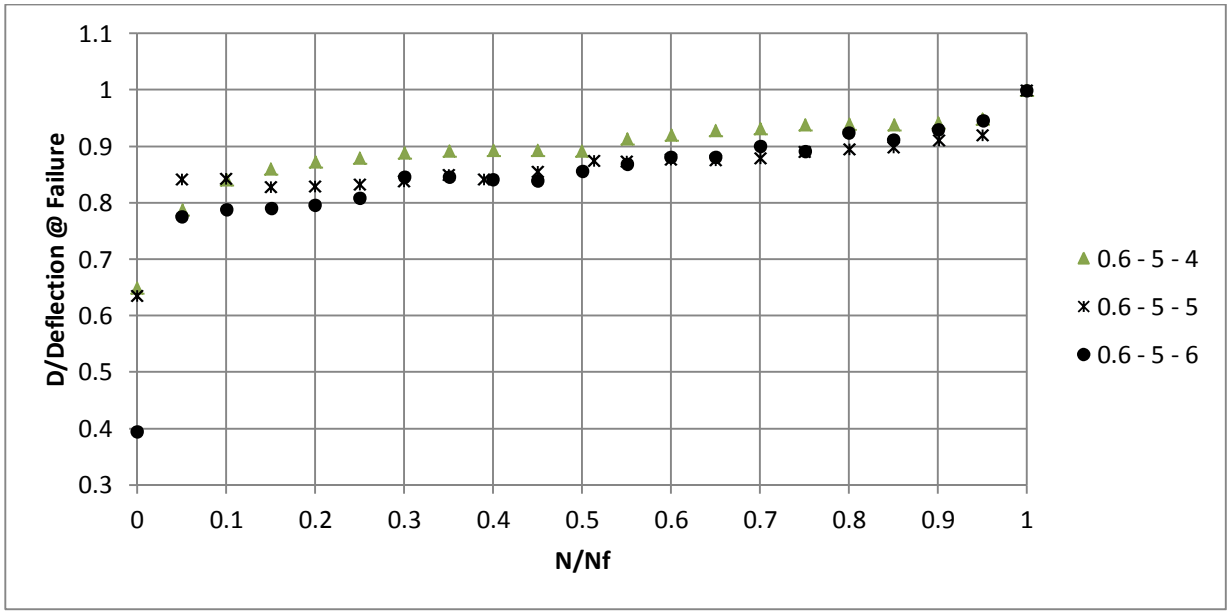

Figure 4.30: Plastic deformation accumulation during fatigue life (S=0.6, loading frequency = 5, FRC8 Samples)

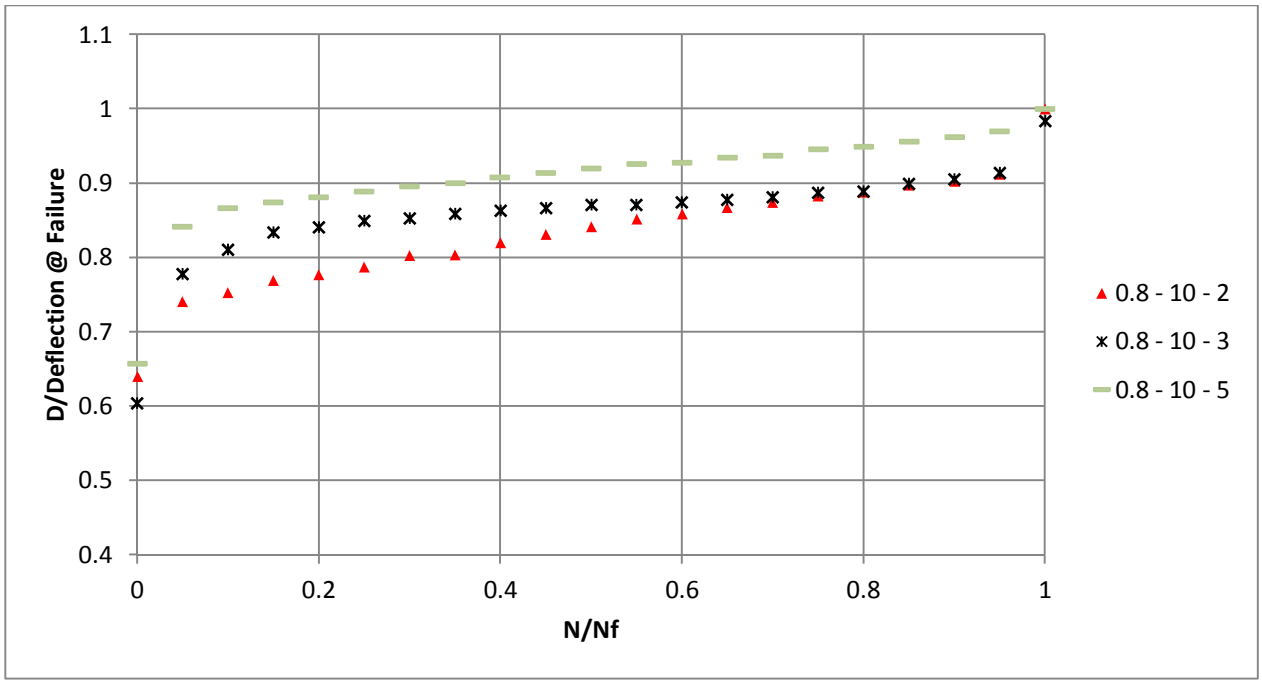

Figure 4.31: Plastic deformation accumulation during fatigue life (S=0.8, loading frequency = 10, FRC8 samples)

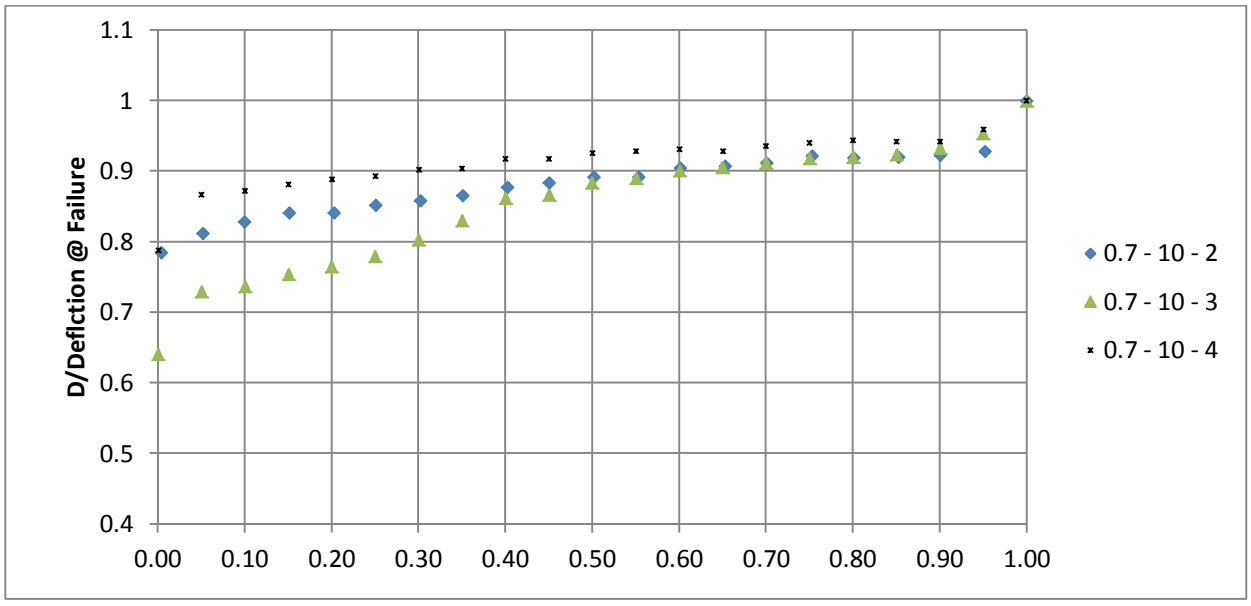

Figure 4.32: Plastic deformation accumulation during fatigue life (S=0.7, loading frequency = 10, FRC8 samples)

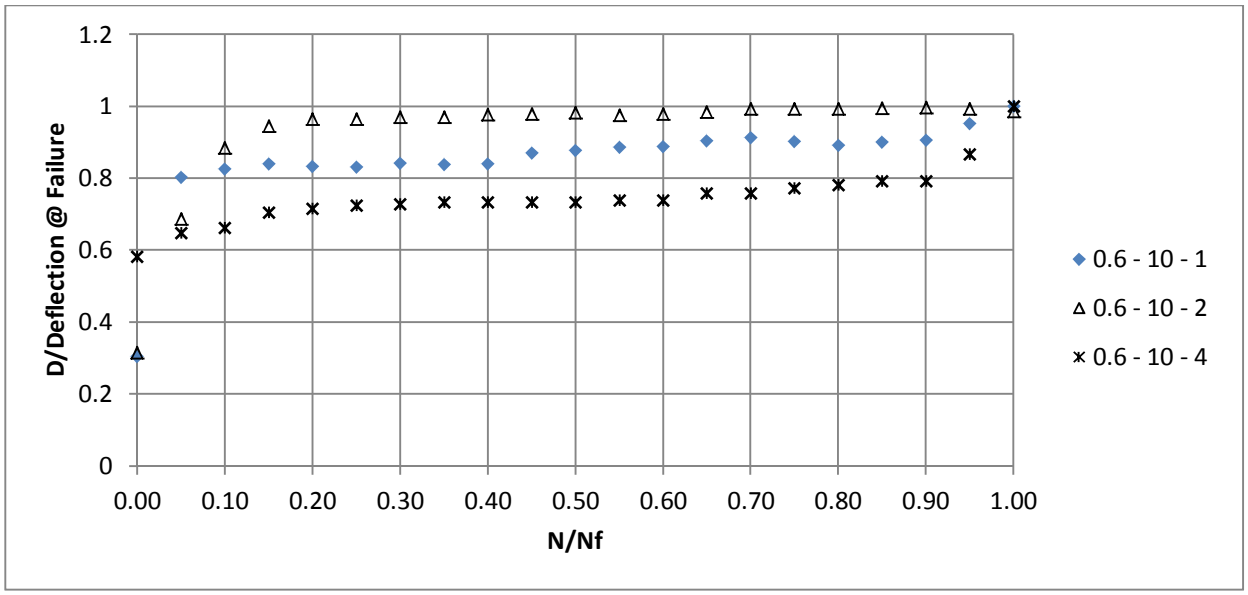

Figure 4.33: Plastic deformation accumulation during fatigue life (S=0.7, loading frequency = 10, FRC8 samples)

4.3.6.3. Effect of Fiber Addition on Plastic Deformation

Figure 4.34 presents the ratio of maximum deformation at cycle N to the maximum deformation at failure as a function of cycle ratio for different mixtures. Each data point represents the average of 6 samples tested at S= 0.7 with a loading frequency of 5 Hz.

There is a clear distinction between plastic deformation accumulation rates of mixtures, particularly at the first stage of fatigue life. It can be seen that as the amount of fibers in the mixture increases, the rate of increasing plastic deformation at the first stage of fatigue life slows. Due to the gradual increase in plastic deformation in FRC8 samples, it becomes harder to distinguish between the first and second stages of fatigue life. The slower rate of plastic deformation accumulation at the first stage can be explained by

fiber reinforcement's effect of controlling the crack size and thereby slowing the process of plastic deformation accumulation.

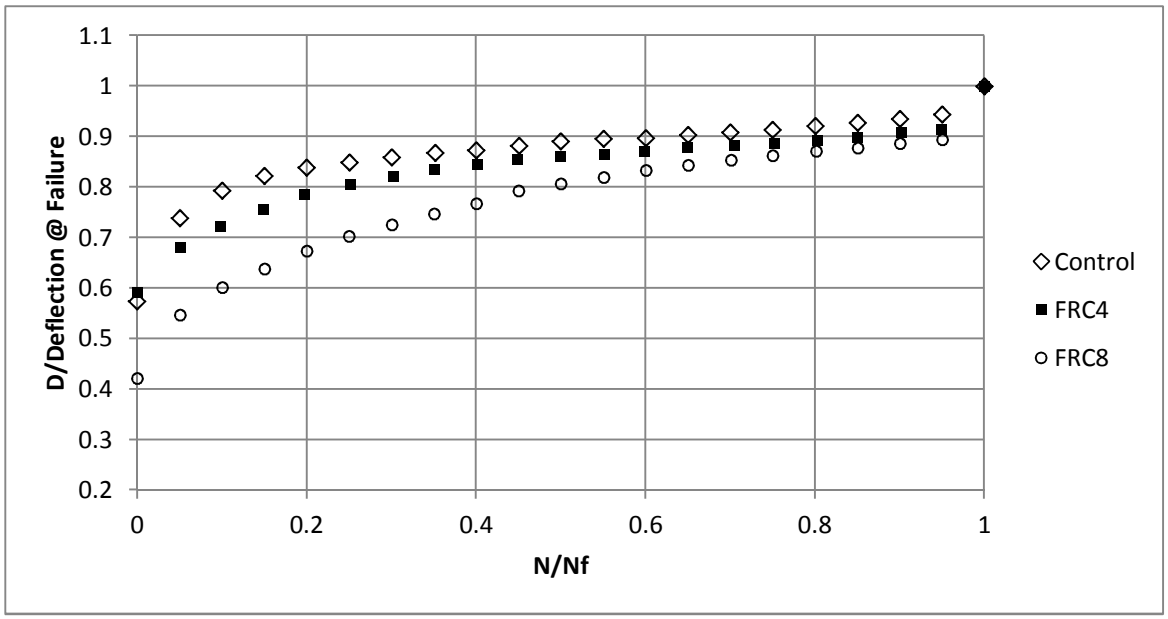

Figure 4.34: Plastic deformation accumulation during fatigue life (effect of fiber reinforcement)

4.3.6.4. Components of Total Dissipated Energy: Plastic Dissipated Energy and Heat Transformation

The maximum plastic deformation of different mixtures tested at S=0.7 and a loading frequency of 5 Hz is shown in Table 4.14. As shown, the FRC samples, particularly the one containing 0.8% fibers, display more plastic deformation at failure

than the control samples. This indicates that the ductility of concrete significantly increases by reinforcing the matrix with fibers.

With regard to the effect of fiber reinforcement on the deformational behavior of concrete exposed to fatigue load, the following conclusions may be drawn. First, fiber reinforcement delays the process of fatigue degradation and therefore decreases the rate of plastic deformation accumulation, particularly at the first stage of fatigue life. And second, the addition of fiber increases ductility, and hence increases the maximum cyclic deflection at failure.

4.3.6.5. Components of Total Dissipated Energy: Plastic Dissipated Energy and Heat Transformation

As pointed out at the beginning of this chapter, the plastic damping mechanism, along with other energy dissipation mechanisms, such as material and sliding damping, are the main reasons for energy dissipation in the concrete fatigue process. Plastic energy dissipation is caused by irreversible deformation, and therefore it can be easily quantified by measuring the accumulation of plastic deformation. On the other hand, the quantification of dissipated energy caused by material and sliding damping requires a device to measure generated heat; it can also be back-calculated from the difference between TDE and plastic energy. In this study, the second method is used to calculate dissipated energy caused by material and slid damping. Table 4.15 summarizes TDE and its components.

Table 4-14: Maximum deflection at failure (effect of fiber reinforcement)

Sample ID	Maximum Deflection at Failure (mm)
FRC8-1	0. 558
FRC8-2	0. 524
FRC8-3	0. 656
FRC8-4	0. 615
FRC8-5	0. 425
FRC8-6	0. 455
FRC8-7	0. 574
FRC8-8	0. 551
FRC8-9	0. 359
FRC8-10	0. 645
Average	0. 536
FRC4-1	0. 46
FRC4-2	0. 243
FRC4-3	0. 306
FRC4-4	0. 198
FRC4-5	0. 498
FRC4-6	0. 269
Average	0. 329
Control-1	0. 351
control-2	0. 464
Control-3	0. 241
Control-4	0. 365
Control-5	0. 262
Control-6	0. 252
Average	0.323

As can be seen in Table 4-15, the contribution of plastic energy dissipation to TDE is not significant compared to other damping sources, such as material and slid damping. In most of the cases the plastic energy is less than 1% of the total dissipated energy in the fatigue test (Table 4.16), which is in accord with previous studies (Tepfers, Sjostrom, et al. 2011).

4.3.6.6. Effect of Fiber Reinforcement on Total Dissipated Energy Caused by Plastic Deformation

As shown in Table 4-17, FRC8 samples dissipated more energy via plastic deformation than the two other mixtures. This implies that fiber reinforcement enhances the energy absorption of concrete matrix.

4.3.6.7. Variation of Amplitude Ratio during the Course of Fatigue Life

The moving average technique is used to examine the variation in amplitude ratio during the fatigue test (Figure 4.35 to Figure 4.38). As can be seen, the value of the amplitude ratio fluctuates within a very small range—around 1—and it rapidly increases in the last 3% of the fatigue life.

As mentioned in section 4.1.2.1, the natural frequency of a vibrating system plays an important role in the value of the amplitude ratio. For systems in which the natural frequency is significantly higher than the frequency of loading and the hysteresis damping constant (β) is very small, the amplitude ratio is expected to be close to 1 (see Figure 4.3).

Table 4-15: TDE, total plastic energy and heat (FRC8 samples)

S-Frequency- ID#	TDE (N.m)	Plastic Energy (N.m)	Heat Transformation (N.m)
0.8-5-1	305.1	2.86	302.24
0.8-5-2	14.64	1.08	13.56
0.8-5-3	173.73	1.5	172.23
0.8-5-4	28.85	1.13	27.72
0.8-5-5	51.84	1.38	50.46
0.8-5-6	604.94	3.8	601.14
0.7-5-1	497.97	3.27	494.7
0.7-5-2	747.49	3.1	744.39
0.7-5-3	505.63	4.08	501.55
0.7-5-4	715.53	3.73	711.79
0.7-5-5	343.82	2.36	341.46
0.7-5-6	871.2	3.38	867.82
0.7-5-7	2800.94	3.59	2797.35
0.7-5-8	566.11	1.36	564.75
0.7-5-9	155.36	2.05	153.31
0.7-5-10	1365.02	2.27	1362.75
0.6-5-1	3648.13	3.68	3644.45
0.6-5-2	3082.49	3.16	3079.33
0.6-5-3	4084.45	1.34	4083.11
0.6-5-4	1192.79	1	1191.79
0.6-5-5	2428.95	1.27	2427.69
0.6-5-6	7951.82	2.66	7949.16
0.8-10-1	524.8	2.8	522
0.8-10-2	352.37	2.15	350.22
0.8-10-3	3372.88	2.07	3370.8
0.8-10-4	807.02	3.76	803.26
0.8-10-5	182.44	2.11	180.33
0.8-10-6	475.84	2.38	473.46
0.7-10-1	260.49	2.79	257.7
0.7-10-2	112.57	2.22	110.35
0.7-10-3	1262.16	3.06	1259.11
0.7-10-4	502.07	2.63	499.43
0.7-10-5	398.3	2.54	395.76
0.7-10-6	2866.61	4.03	2862.58
0.6-10-1	15834.37	2.82	15831.56
0.6-10-2	5069.25	3.49	5065.76
0.6-10-3	34270.24	2.53	34267.71
0.6-10-4	22361.74	1.17	22360.57
0.6-10-5	4574.52	1.71	4572.81

Table 4-16: Ratio of total plastic energy to TDE

Stress level-Frequency	Plastic Energy/TDE (%)
0.8-5	2.73
0.7-5	0.57
0.6-5	0.07
0.8-10	0.55
0.7-10	0.77
0.6-10	0.03

Table 4-17: Plastic energy dissipation (effect of fiber reinforcement)

Sample ID	Total Plastic Energy (N.m)
FRC8-1	3.27
FRC8-2	3.1
FRC8-3	4.08
FRC8-4	3.73
FRC8-5	2.36
FRC8-6	3.38
FRC8-7	3.59
FRC8-8	1.36
FRC8-9	2.05
FRC8-10	2.27
Average	2.92
FRC4-1	2.96
FRC4-2	1.16
FRC4-3	1.44
FRC4-4	0.88
FRC4-5	3.15
FRC4-6	1.29
Average	1.81
Control-1	2.24
control-2	3.04
Control-3	1.23
Control-4	2.23
Control-5	1.4
Control-6	1.26
Average	1.9

The natural frequency of a simply supported beam with a size of 30.5×7.6×7.6 cm (12×3×3 inches) is 700-900 (L=22.9 cm, A=522.6 cm^2, ρ≈4200 kg/m^3, E≈35 Gpa), and the average dimensionless hysteresis constant for the concrete is 0.02-0.05 (extracted from section 4.3.3.5). Therefore, it is expected that the amplitude ratio value will be around 1. Rapid increase in the amplitude ratio at the very end of the fatigue process can be attributed to reduction of natural frequency due to sudden enlargement of micro-cracks.

This suggests that micro-crack formation, which starts at the beginning of the fatigue process, does not affect the natural frequency of the beam until the crack network expands and the concrete matrix becomes unstable

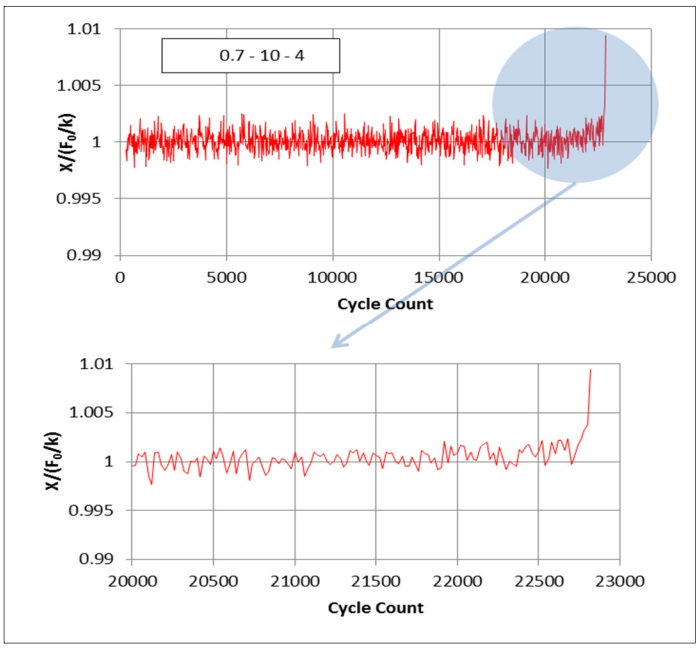

Figure 4.35: Amplitude ratio variation during fatigue life (S=0.7, loading frequency = 10, FRC8)

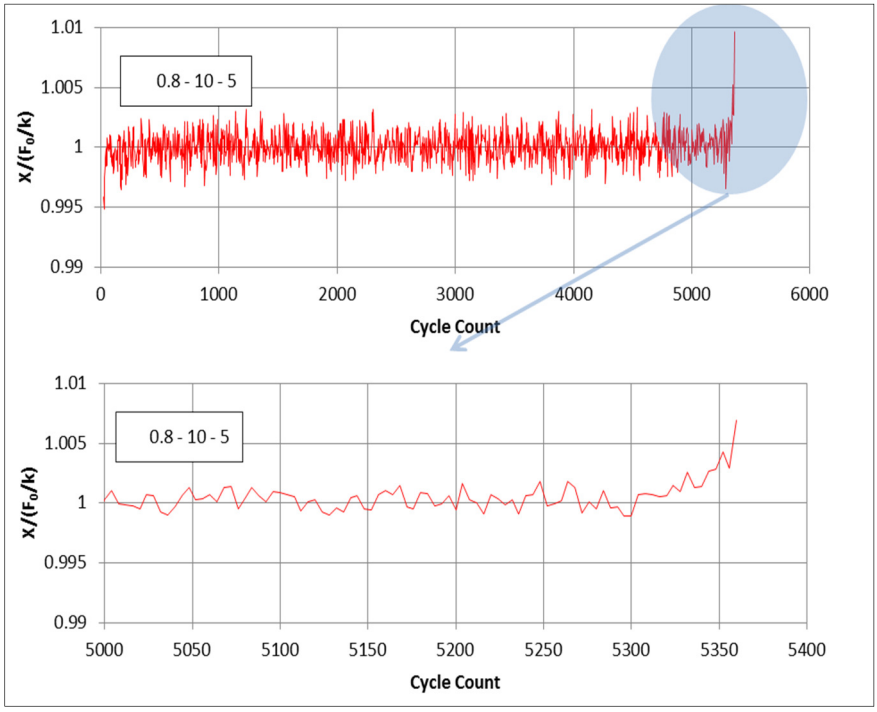

Figure 4.36: Amplitude ratio variation during fatigue life (S=0.8, loading frequency = 10)

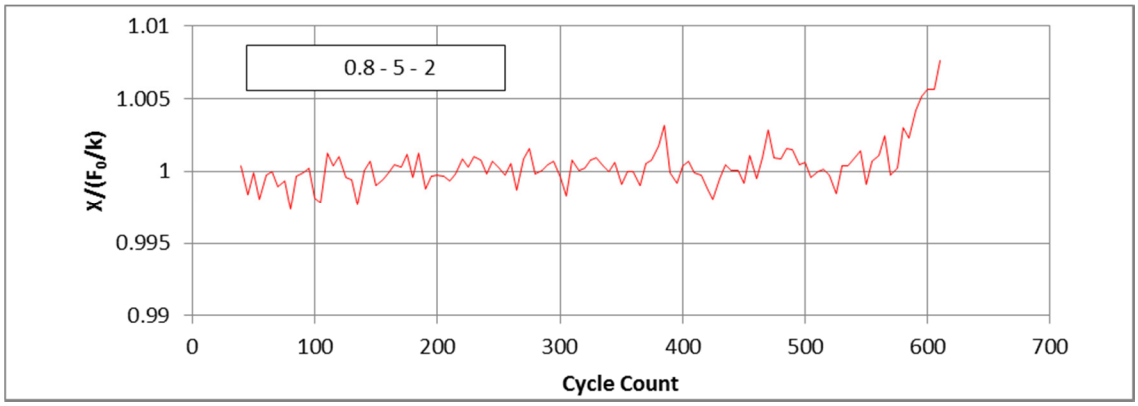

Figure 4.37: Amplitude ratio variation during fatigue life (S=0.8, loading frequency = 5, FRC8)

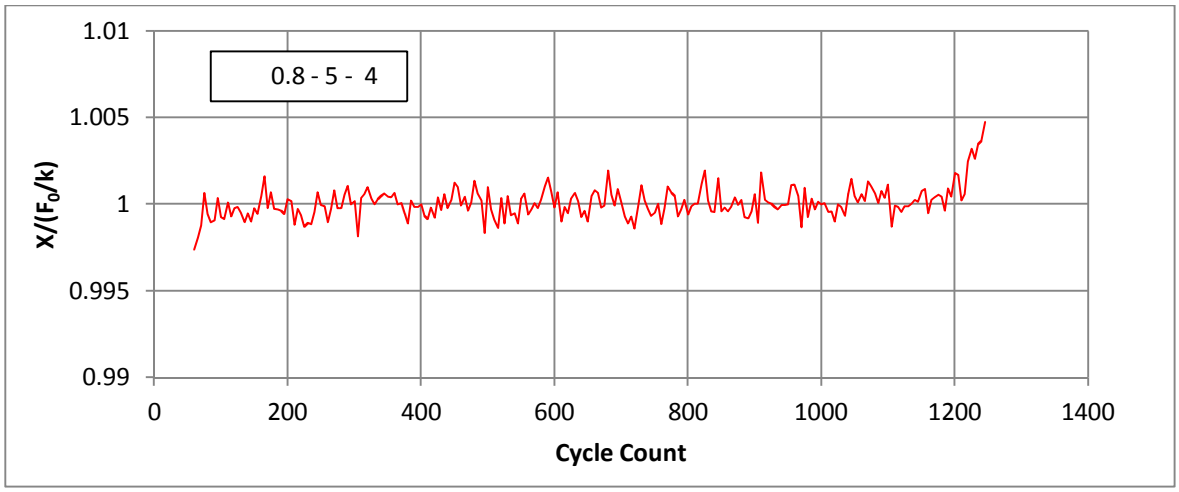

Figure 4.38: Amplitude ratio variation during fatigue life (S=0.8, loading frequency = 5, FRC8)

4.4. Combined Effect of Fatigue and Freeze-Thaw

This section aims to examine the effects of freezing and thawing on the fatigue behavior of FRC concrete containing 0.8% polypropylene fibers. FRC8 samples were exposed to freeze-thaw cycles for up to 400 cycles and tested at the same loading condition as the control samples (i.e., samples that have not experienced freeze-thaw cycles). The effects of freeze-thaw on density and void structure were studied using the method provided by ASTM C642. In addition, the uniformity of the concrete was monitored using an ultrasonic pulse velocity test. Furthermore, fatigue life, energy dissipation behavior, and deformational characteristics of freeze-thaw samples were studied and compared to control samples.

4.4.1. Volumetric Analysis of Samples Exposed to Freeze-Thaw

Figure 4.39 shows the phase diagram of concrete. As can be seen, the concrete matrix consists of four phases. The majority of matrix volume is occupied by cement paste and aggregate, which is denoted by V_s.

There are some voids on the surface and in the body of concrete can be easily filled with water after immersion in water at 21°C. These voids are denoted by V_i. Parts of voids are extremely small and located in the depth of the concrete surface, so they are not accessible to water under normal conditions. However, water can reach these pores at higher temperatures after the sample has been boiled for 5 hours. The permeable voids after boiling are denoted by V_b.

Lastly, some voids in the matrix are not connected to the network of permeable voids and therefore are not accessible to water under any conditions. These impermeable voids are denoted by V_{im}. The mass of each phase is denoted by m.

The density, water absorption capacity, and percent voids of samples were measured in accordance with ASTM C642. Results are shown in Table 4-19. Bulk density is the ratio of the mass to the total volume of sample. Absorption is the mass of absorbed water to the dry mass of concrete, and percent void is the ratio of permeable void to the total volume of concrete. The volumetric definition of these parameters is presented in Table 4-18.

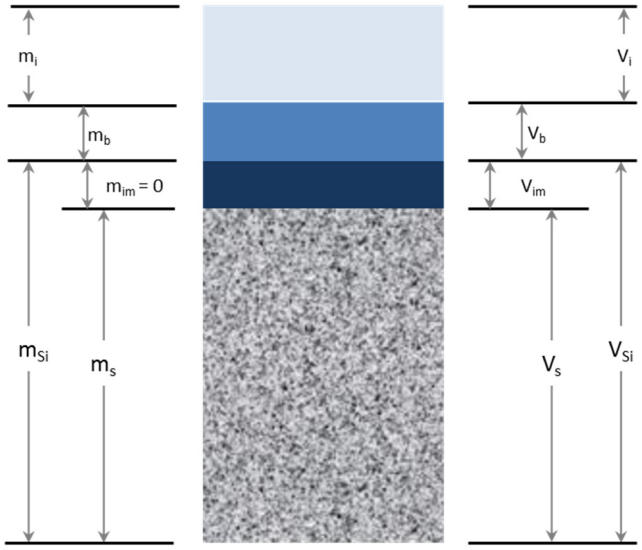

Figure 4.39: Phase diagram of concrete

Table 4-18: Volumetric definition of ASTM C642 parameters

Bulk Dry Density	$\frac{m_s}{V_{si} + V_i + V_b}$
Bulk Density after Immersion	$\frac{m_s + m_i}{V_{si} + V_i + V_b}$
Bulk Density after Boiling	$\frac{m_s + m_i + m_b}{V_{si} + V_i + V_b}$
Apparent Density	$\frac{m_s}{V_{si}}$
Absorption after Immersion	$\frac{m_i}{m_s}$
Absorption after Boiling	$\frac{m_i + m_b}{m_s}$
Voids ratio	$\frac{V_i + V_b}{V_{si} + V_i + V_b}$

The average value of apparent density of concrete, along with 95% confidence intervals, is plotted against the number of F/T cycles in Figure 4.40. The average is calculated after removing outliers from the data set. Outliers are detected through Chauvenet's outlier detection method. A brief explanation of this method is presented in Appendix B.

As can be seen, the apparent density decreases as the F/T cycle increases up to 200 cycles, then starts increasing. The apparent density at 400 F/T cycles is greater than the control samples (i.e., no F/T exposure). Apparent density is defined as the ratio of mass of the solid part ($m_{si} = m_s$) to the volume of the solid plus the impermeable pores located in the solid part (V_{si}) (Equation 4.7).

$$Apparent\ Density = \frac{m_{si}}{V_{si}} = \frac{m_s}{V_s + V_{im}} = \frac{m_s}{\frac{m_s}{\rho_s} + V_{im}} \qquad \textbf{4.7}$$

The apparent density formula can also be written as follows:

$$\frac{1}{Apparent\ Density} = \frac{1}{\rho_s} + \frac{V_{im}}{m_s} \qquad \textbf{4.10}$$

Since density of the solid portion (ρ_s) of the concrete matrix is not affected by frost damage (as is in the case for bulk density), it is assumed to be constant, and therefore the change in apparent density can be explained by the change in the ratio of solid mass (m_s) to volume of impermeable pores (V_{im}). Thus, it can be inferred that the volume of impermeable voids per unit mass of solid increases up to 200 F/T cycles and then decreases.

It seems that internal stress induced by freezing water initiates micro-cracks in the body of concrete. Up to 200 cycles of freezing and thawing, micro-cracks are very small and are not connected to permeable voids. Therefore, any increase in the volume of these micro-cracks decreases apparent density. After 200 cycles of freeze-thaw exposure, micro-cracks become larger and are eventually connected to the permeable voids network, thereby increasing the apparent density. Variation in apparent density clearly indicates that freeze-thaw exposure has caused internal damage in the concrete.

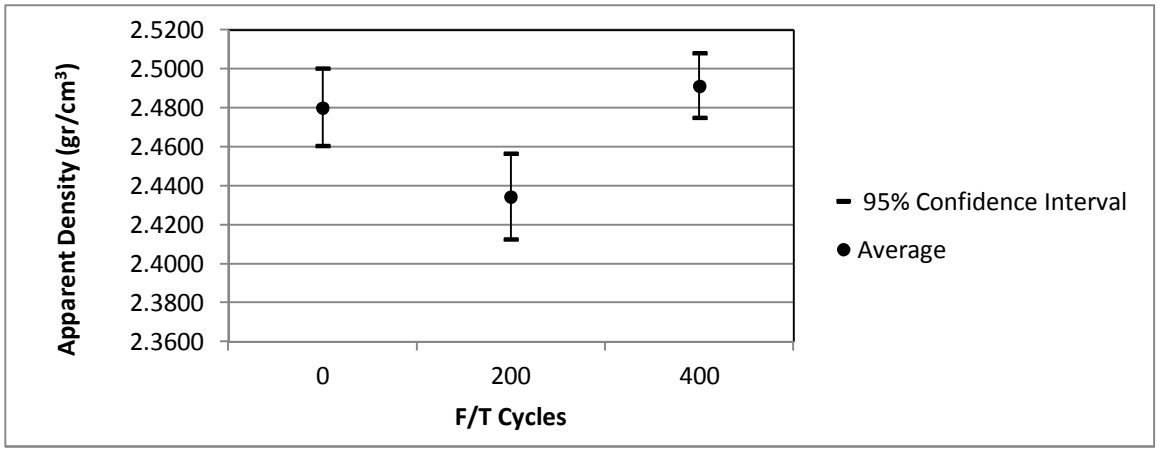

Figure 4.40: Variation of apparent density due to frost damage (FRC8 samples)

Table 4-19: Density, water absorption and %voids of FRC8 samples exposed to freezing and thawing cycle

F/T Cycles-ID	% Absorption after Immersion	% Absorption after boiling	Bulk Dry Density (gr/cm^3)	Bulk Density after Immersion (gr/cm^3)	Bulk Density after Boiling (gr/cm^3)	Apparent Density (gr/cm^3)	% Void
0-1	6.22	6.39	2.08	2.21	2.21	2.39	13.27
0-2	5.93	6.19	2.15	2.27	2.28	2.48	13.29
0-3	6.08	6.51	2.11	2.24	2.25	2.44	13.72
0-4	5.7	5.95	2.18	2.3	2.31	2.5	12.94
0-5	5.91	6.03	2.15	2.28	2.28	2.47	12.99
0-6	5.61	5.81	2.16	2.28	2.29	2.47	12.55
200-1	6.14	6.54	2.12	2.25	2.26	2.47	13.89
200-2	5.94	5.97	2.17	2.3	2.3	2.49	12.94
200-3	6.04	6.15	2.11	2.24	2.24	2.43	12.99
200-4	5.66	5.68	2.15	2.27	2.27	2.45	12.2
200-5	6.4	6.63	2.08	2.22	2.22	2.42	13.81
200-6	6.08	6.37	2.11	2.24	2.25	2.44	13.47
400-1	5.82	6.19	2.14	2.26	2.27	2.46	13.24
400-2	5.55	5.72	2.18	2.3	2.31	2.49	12.49
400-3	5.4	5.67	2.18	2.3	2.31	2.49	12.36
400-4	5.65	5.99	2.16	2.28	2.29	2.48	12.92
400-5	5.67	6.11	2.17	2.29	2.3	2.5	13.27

As can be seen in Figure 4.41, the average of the ratio of the volume of voids accessible to water after boiling (V_b) to the volume of the void accessible water at 21°C (V_i) follows the same trend as the apparent density. The average of (V_b/V_i) is calculated after outlier removal.

It is evident that up to 200 F/T cycles, the volume of large voids—which are easily accessible to water under normal conditions—has slightly increased; this could be attributed to the enlargement of tiny voids (V_b) due to internal stress caused by freezing water. The increase of V_b/V_i after 200 F/T cycles could be due to two major causes. First, surface scaling, which is mass loss of the sample due to frost damage (Table 4.20), leads to reduction in permeable voids (V_i) because the majority of voids that are accessible to water under normal conditions are located on the surface of the concrete. Second, the impermeable voids (V_{im}) located in the matrix become larger and connected to the permeable voids network, and therefore the amount of tiny voids (V_b) increases.

Absorption results (Figure 4.42 and Figure 4.43) at different stages of F/T exposure support the previous claim. Water absorption increases up to 200 F/T cycles due to the increase in the volume of permeable voids. After that, due to scaling, the volume of permeable voids deceases and therefore absorption capacity also decreases.

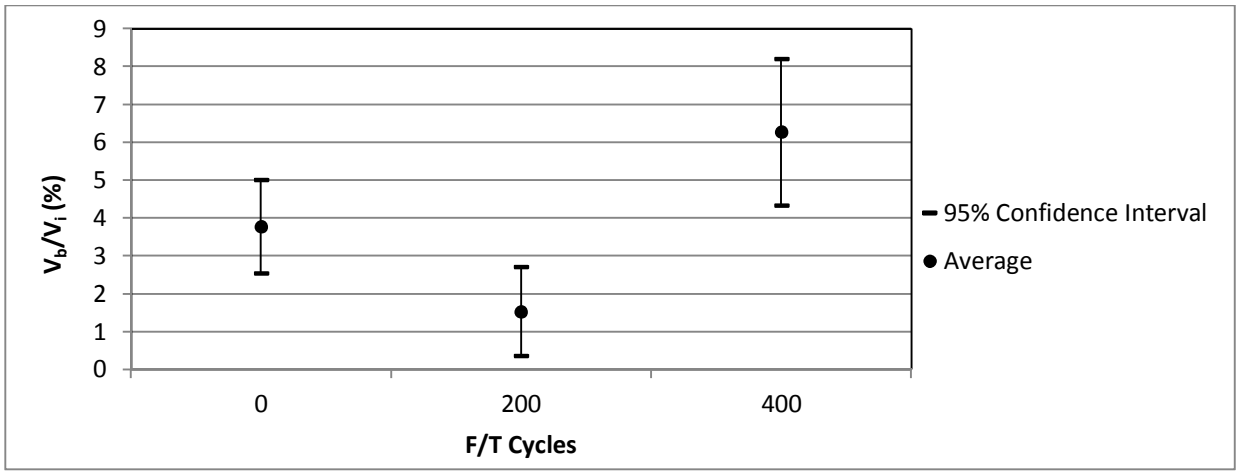

Figure 4.41: Ratio of the volume of permeable voids after boiling (Vb) to the volume of permeable voids after immersion (Vi) (FRC8 samples)

Table 4-20: Mass loss due to scaling

F/T cycle-Sample ID	Mass Loss (grams)
0-1	0
0-2	0
0-3	0
0-4	0
0-5	0
0-6	0
200-1	0
200-2	7.1
200-3	2.7
200-4	0
200-5	0
200-6	0
400-1	21.9
400-2	14.3
400-3	16
400-4	34
400-5	14.9

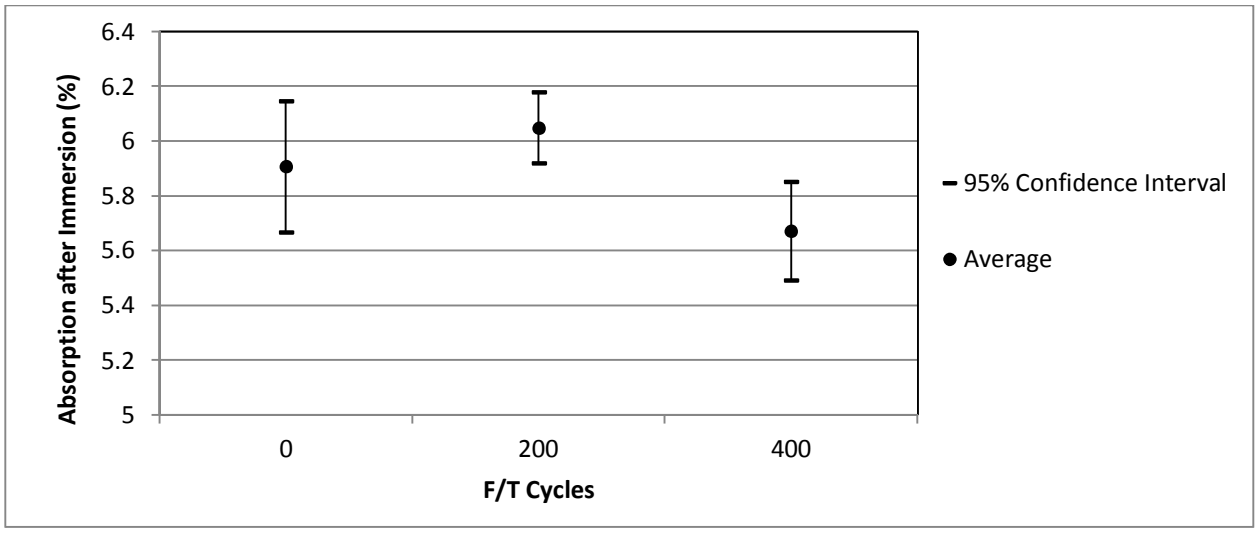

Figure 4.42: Absorption after immersion (FRC8 samples)

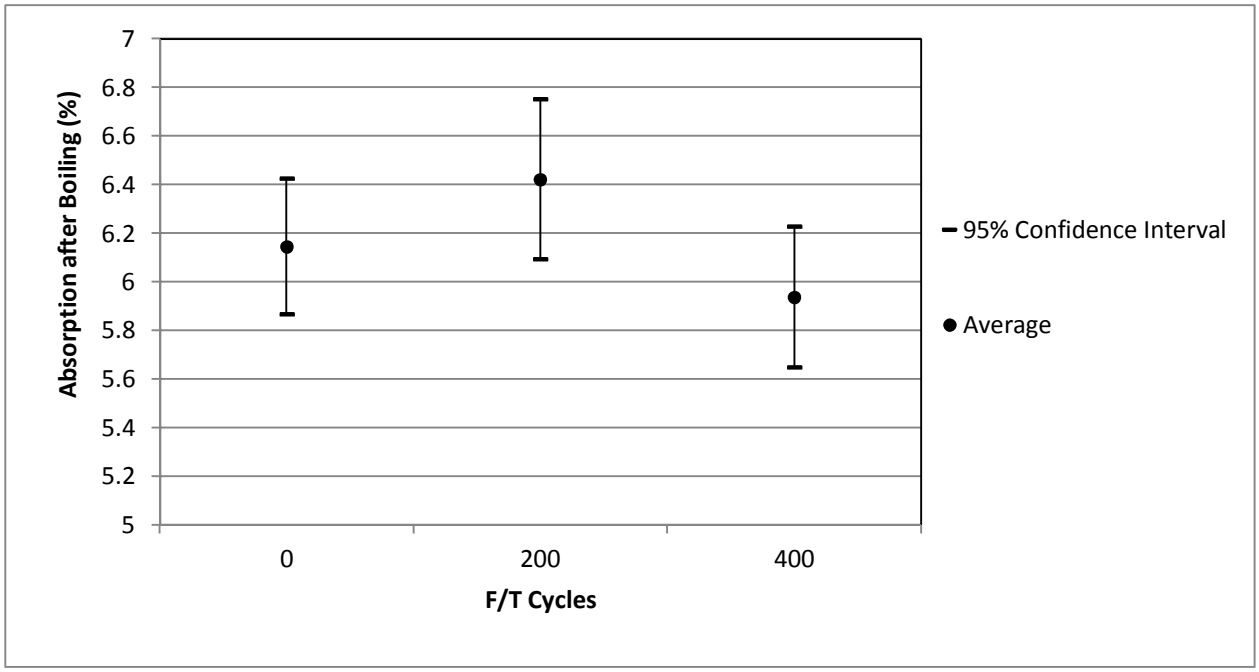

Figure 4.43: Absorption after boiling (FRC8 samples)

4.4.2. Ultrasonic Pulse Velocity Result

The ultrasonic pulse velocity test (UPV), in accordance with ASTM C597, was conducted on the samples after boiling in the water for 5 hours to evaluate the severity of frost damage. Test results are plotted in Figure 4.44. It can be seen that the UPV has an indirect relationship with the void ratio of concrete. Results (Figure 4.44 and Figure 4.45) indicate that pulse velocity is higher in the samples that have fewer voids. Furthermore, the result is thoroughly in agreement with the volumetric analysis performed previously in section 4.4.1, which suggests that at first, the void content of concrete increases up to 200 F/T cycles; beyond that, as frost damage progresses, the void content decreases.

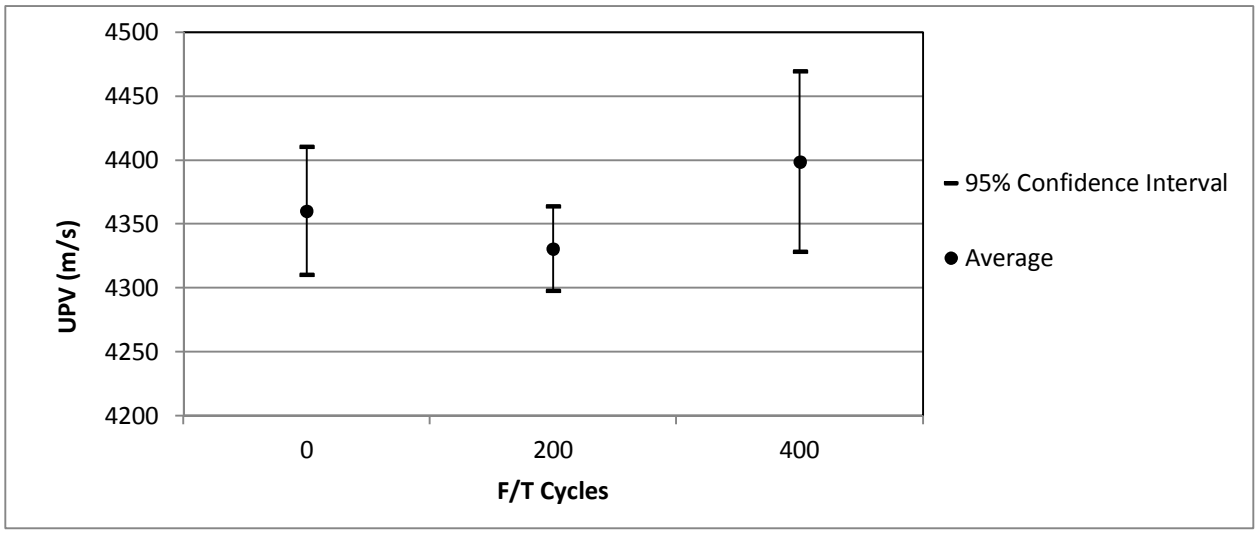

Figure 4.44: Ultrasonic pulse velocity vs. freeze-thaw exposure

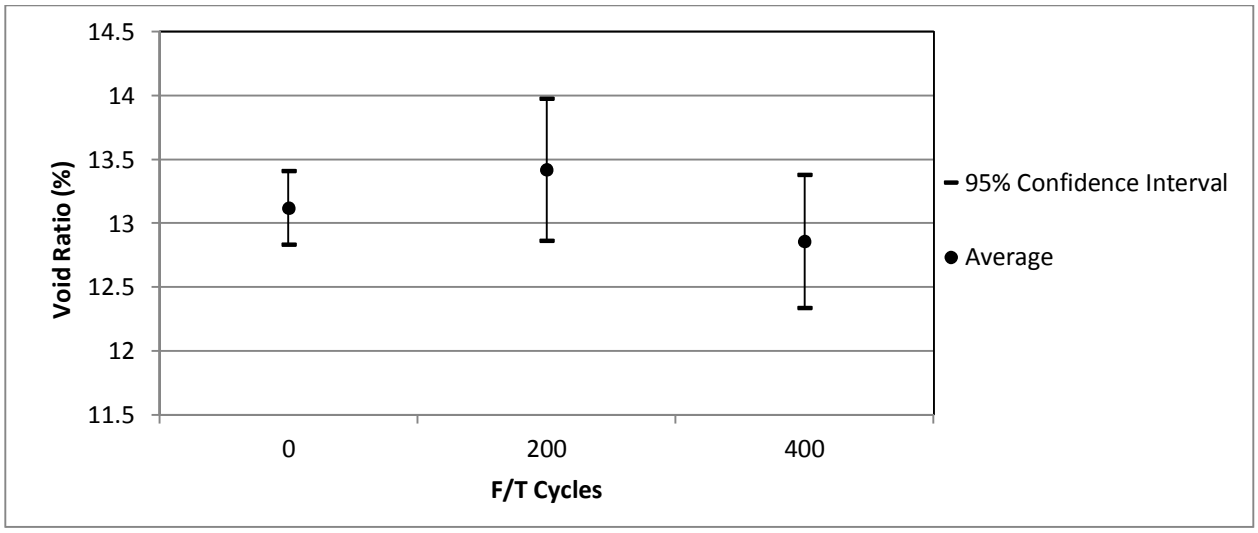

Figure 4.45: Void Ratio vs. freeze-thaw cycle

4.4.3. Effect of Freeze-Thaw Exposure on Fatigue Life

The average fatigue life of all the specimens exposed to freezing and thawing cycle, as well as the coefficient of variation of fatigue life, is shown in Figure 4.46. It can be seen that frost damage has significantly decreased fatigue life, particularly at 400 cycles. This is not surprising, considering the damage due to cyclic internal stress caused by the freezing and thawing of water in the form of internal cracks and external deterioration (i.e., mass loss).

Higher variability was observed within the fatigue results of frost-damaged samples compared to control samples (i.e., 0 F/T exposures). This indicates that the severity of freeze-thaw damage is variable among the samples that have experienced the same freeze-thaw cycles. This means that F/T cycle count is not a good indicator of the severity of frost damage.

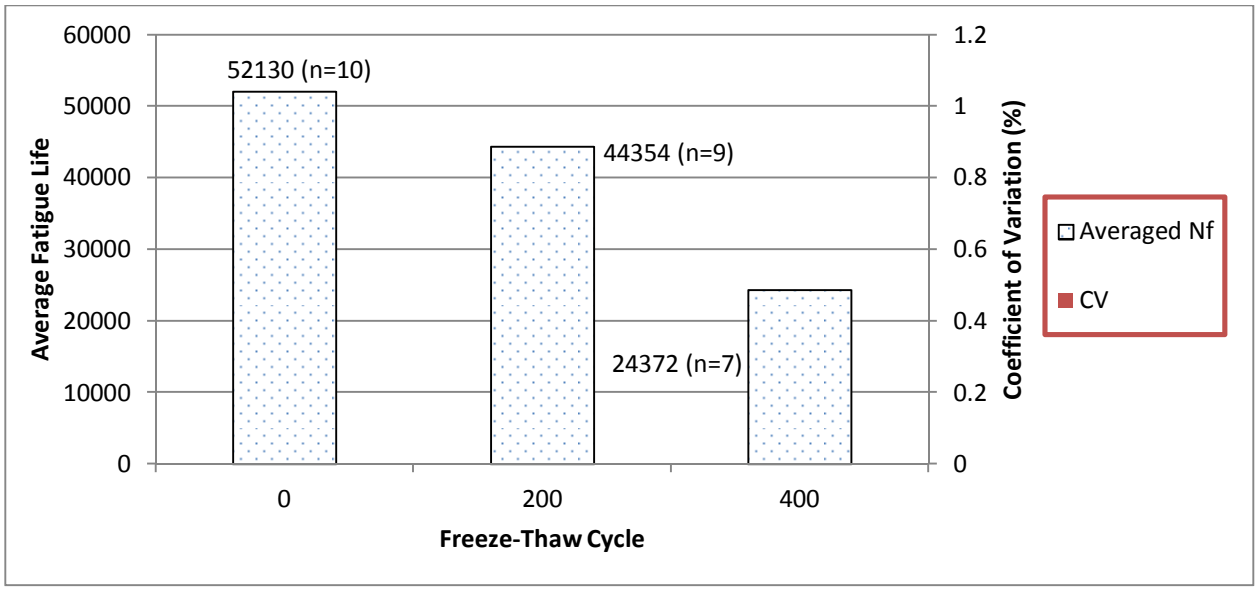

Figure 4.46: Average fatigue life at different freeze-thaw exposure (FRC8 Sample)

4.4.4. Effect of Freeze-Thaw Exposure on Averaged and Total Dissipated Energy

The averaged-dissipated energy (ADE) per loading cycle versus freeze-thaw cycles is shown in Figure 4.47. As mentioned in the previous chapter, all frost-damaged specimens were tested for fatigue at stress levels corresponding to 70% of maximum flexural strength of the control samples, which have experienced no freezing and thawing. Thus, the actual stress level that the frost-damaged samples experienced during fatigue was higher than 70%, considering the flexural strength loss due to damage caused by freezing and thawing. Therefore, an increase in ADE due to frost damage can attributed to higher stress levels during the fatigue test.

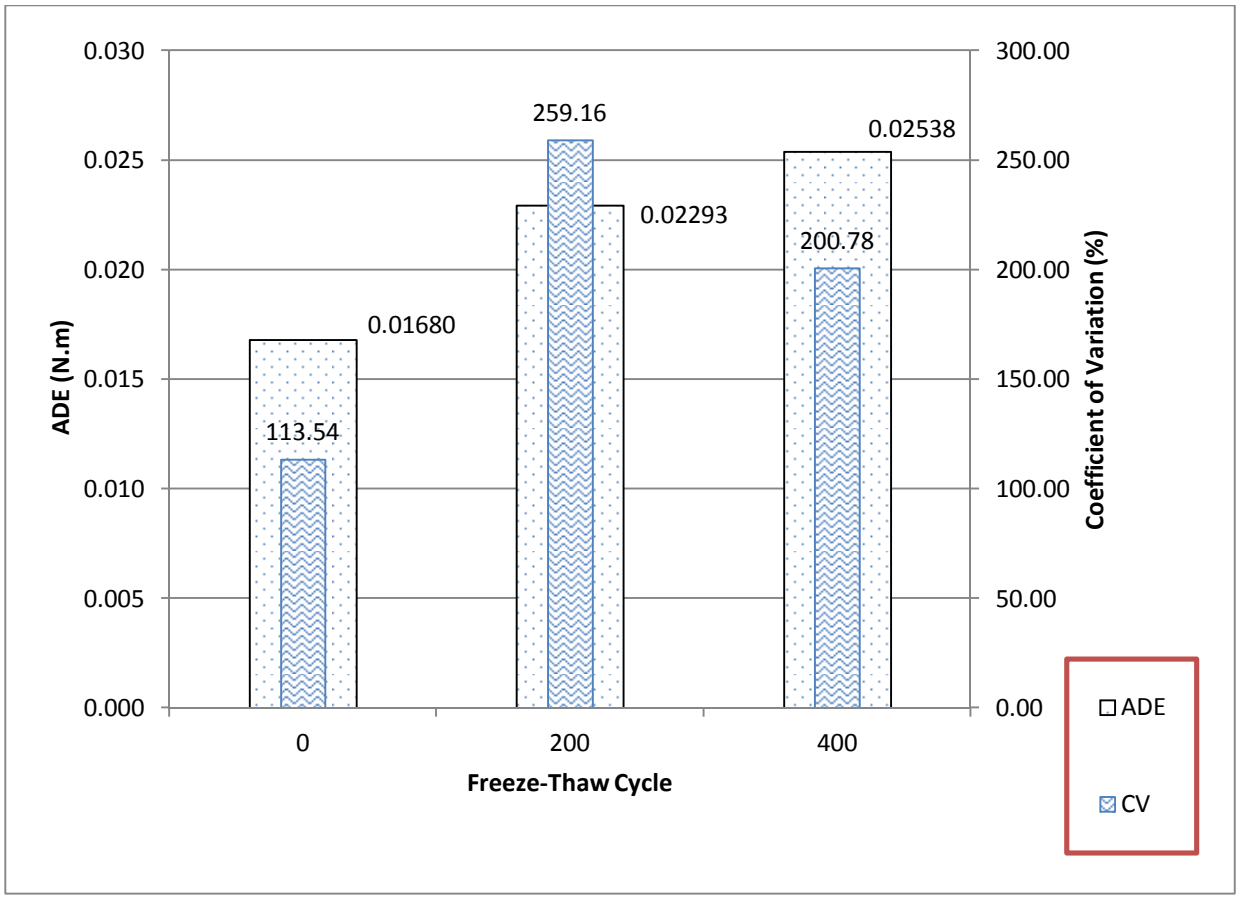

Figure 4.47: Averaged dissipated energy per loading cycle at different freeze-thaw exposure (FRC8 Samples)

As shown in Figure 4.48, the total dissipated energy during the fatigue test decreases as the number of freeze-thaw cycles increases. As shown previously in this chapter, there is a significant drop in the fatigue life (N_f) of frost-damaged samples. This will directly decrease total dissipated energy. Freezing water expansion in the boundary of different phases of concrete may detach the connections between aggregate-paste and paste-fiber, loosen the entire matrix, and reduce the energy dissipation capability.

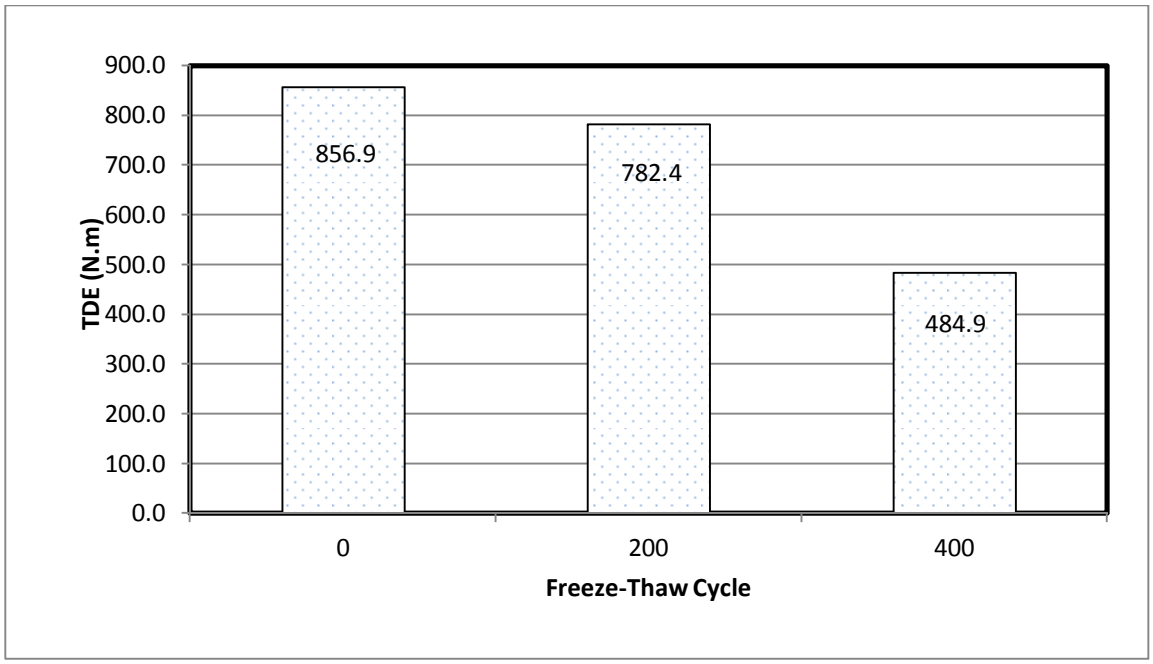

Figure 4.48: Total dissipated energy at different freeze-thaw cycle (FRC8 samples)

Figure 4.49 reveals that the ADE-N_f curves of frost-damaged samples do not follow the same trend as the samples that have experienced no freezing and thawing cycles, even though they are from the same mixture. This suggests that any environmental condition that affects the concrete matrix could change the ADE-N_f relationship. The same observation was made in the case of different mixtures (Section 4.3.4).

The main conclusion to be drawn is that the ADE-N_f curve trend is highly dependent on the properties of the mixture, as well external factors that affect concrete behavior, such as environmental conditions, loading conditions, and fiber reinforcement.

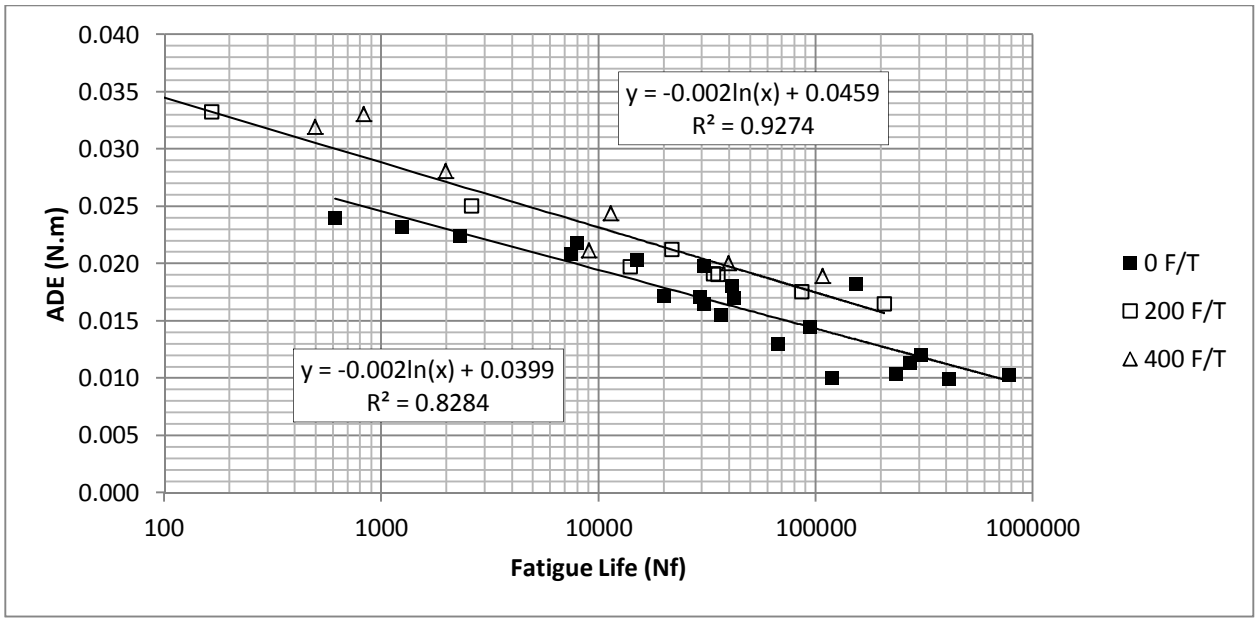

Figure 4.49: ADE-N_f trend (0 F/T vs. frost-damaged samples, FRC8)

4.4.5. Effect of Freeze-Thaw Exposure on Damping Force

4.4.5.1. Effect of Freeze-Thaw Exposure on Cyclic Stiffness (k)

The average values for the cyclic stiffness of samples with different F/T exposure are shown in Table 4-21. As mentioned earlier, frost-damaged samples were tested under higher stress levels than control samples (i.e., 0 F/T exposures). Considering the increasing effect of stress level on cyclic stiffness (Section 4.3.3.3) it is expected that frost-damaged samples will have higher cyclic stiffness.

Experimental results, however, reveal the opposite trend. Frost-damaged samples have experienced more cyclic deflection compared to control samples (i.e., 0 F/T exposure), and thereby display lower cyclic stiffness. This indicates that frost damage

may have a negative effect on dissipated energy, considering the direct relation between stiffness and damping coefficient.

Table 4-21: Effect of frost damage on cyclic stiffness (k)

F/T Cycles	k (kN/m)
0	55351
200	53976
400	49396

4.4.5.2. Effect of Freeze-Thaw Exposure on Dimensionless Hysteresis Damping Constant

Average of hysteresis damping constant per cycle of loading at different freeze-thaw cycles is tabulated in Table 4-22. As can be seen, the hysteresis damping constant increases as F/T cycles increase.

An increase in the β value could be attributed to a change in loading characteristics due to change in the size of the sample resulting from scaling, a change in the matrix of the concrete due to freeze-thaw deterioration, or a combination of these factors. If the former was the only reason for the increase in β and there was no internal deterioration that would cause a change in the matrix, the N_f-β trend for frost-damaged samples would follow the N_f-β trend for control samples (i.e., 0 F/T exposure). As Figure 4.50 shows, however, the N_f-β relationship for frost-damaged concrete samples is

different from that for control samples. Therefore, it can be concluded that both the change in loading characteristics and the change in the concrete matrix caused by internal cracks play an important role in the damping behavior of concrete.

Table 4-22: Effect of frost damage on hysteresis damping constant

F/T Cycles	Averaged β
0	0.0325
200	0.0391
400	0.0403

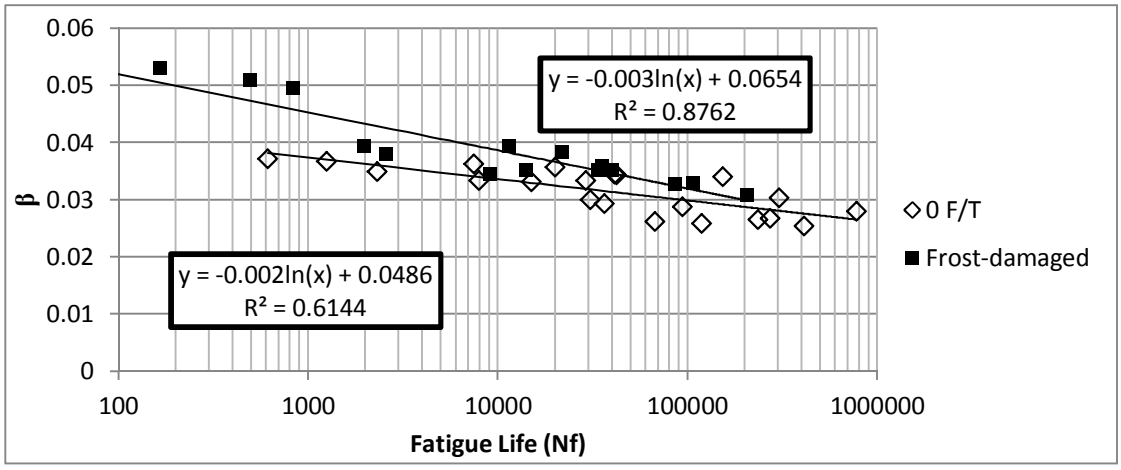

Figure 4.50: Hysteresis damping constant vs. fatigue Life (effect of frost damage, FRC8)

4.4.6. Effect of Freeze-Thaw Exposure on Deformational Characteristics

4.4.6.1. Effect of Freeze-Thaw Exposure on Load-Deflection Curve and Post-Failure Behavior

Representative load-deflection curves for frost-damaged samples are shown in Figure 4.51 to Figure 4.54. The maximum cyclic deflection at N=1, N=N_f and total plastic deformation during fatigue of frost-damaged samples are summarized in Table 4.23.

As can be seen, although the maximum cyclic deflection of frost-damaged samples at N=1 is higher than the control sample, total plastic deformation during the fatigue life (i.e., the difference between maximum cyclic deflection at N=N_f and maximum cyclic deflection at N=1, which is labeled by *b* in Figure 4.51) and the total deflection that a concrete sample experiences up to fatigue failure (Portion c in Figure 4.51) decreases as a result of frost damage.

Frost damage has increased the ductility of the sample (i.e., higher deformation under cyclic load). However, the amount of plastic deformation experienced by concrete during fatigue has significantly decreased due to frost damage, which can directly affect the damping behavior of concrete.

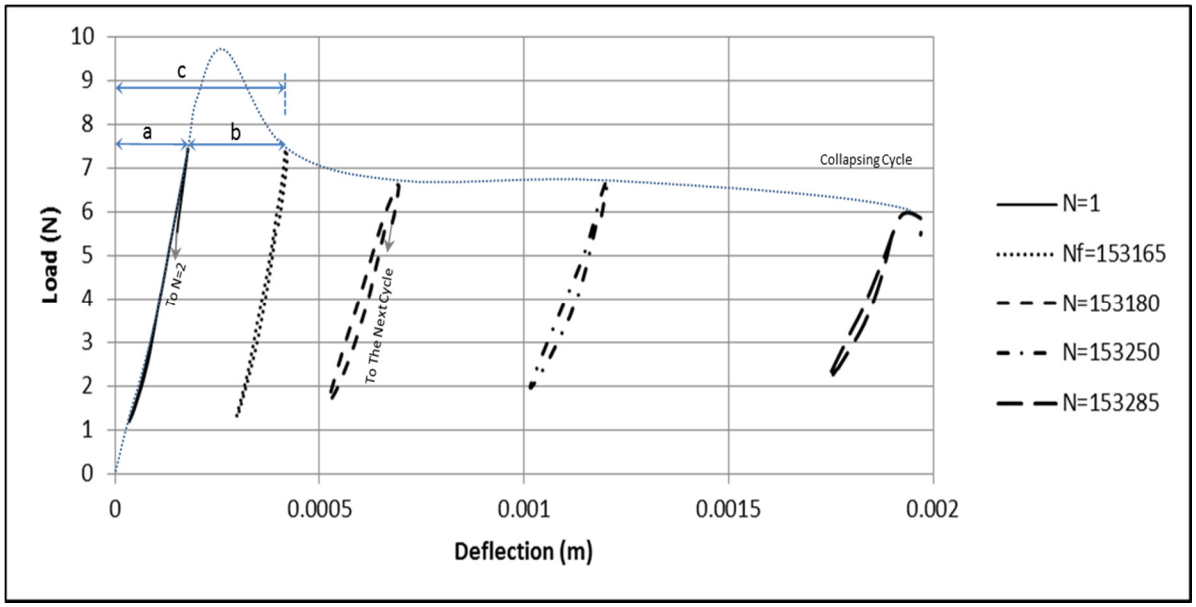

Figure 4.51: Load-Deflection history (0 F/T, FRC8)

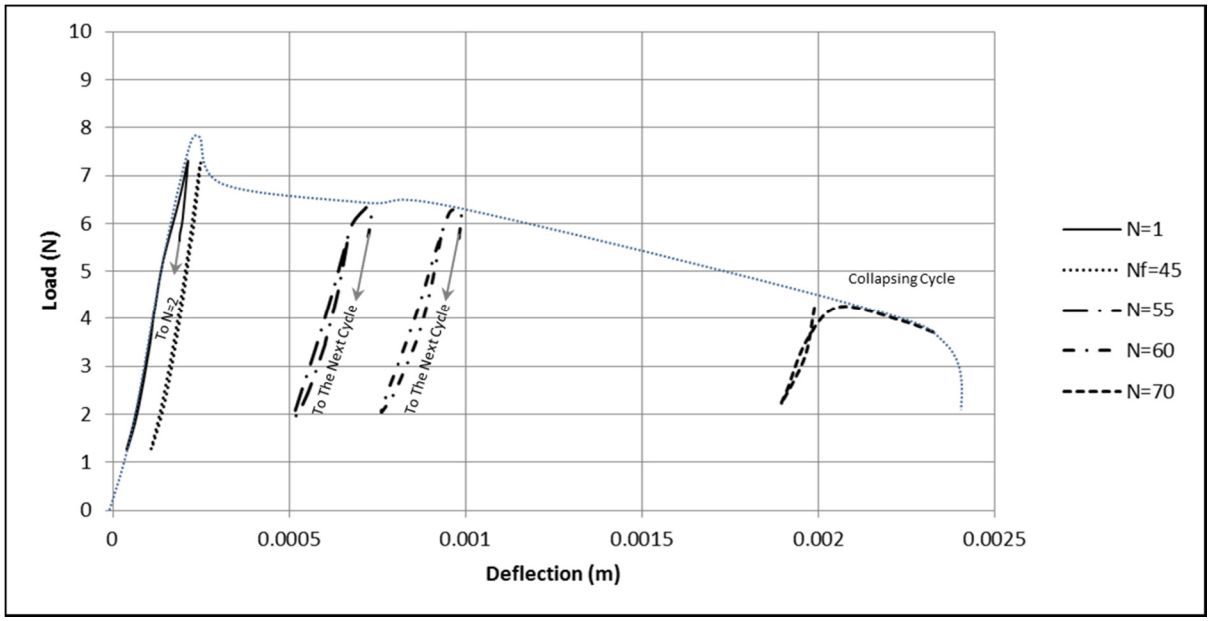

Figure 4.52: Load-Deflection history (200 F/T, FRC8)

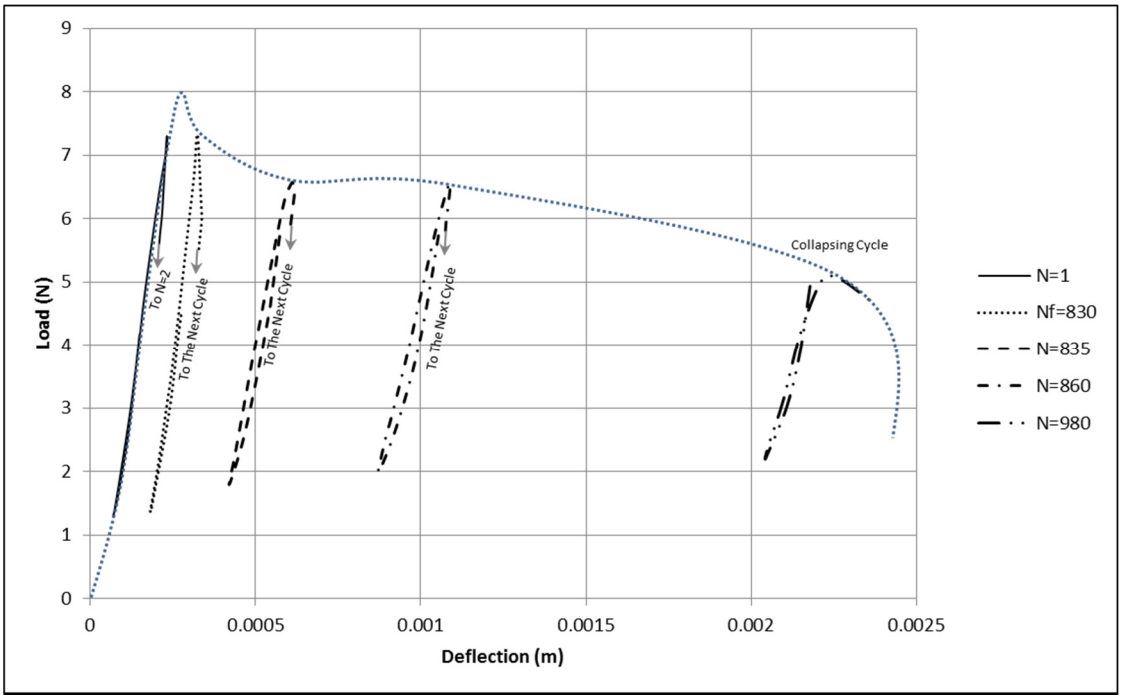

Figure 4.53: Load-Deflection history (400 F/T, FRC8)

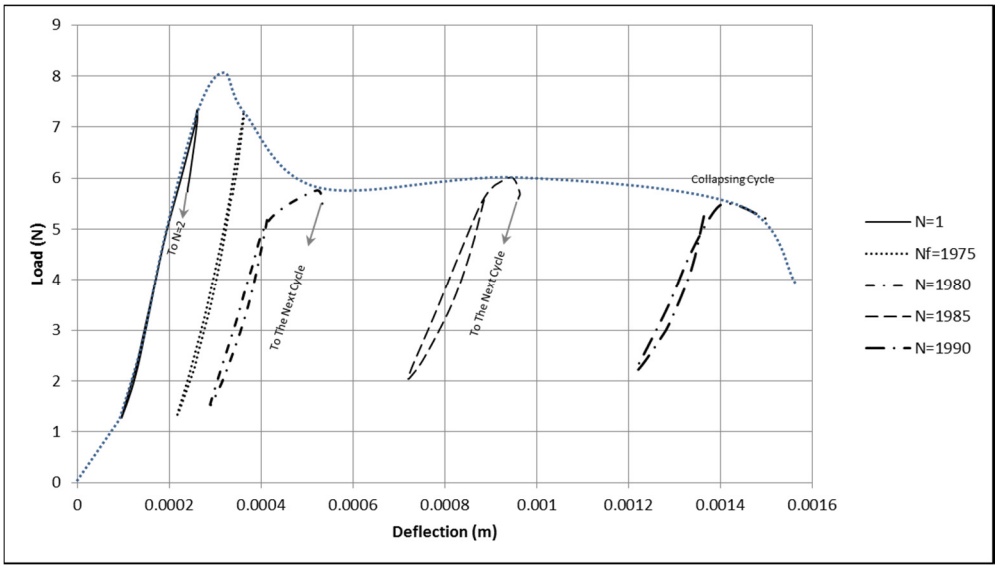

Figure 4.54: Load-Deflection history (400 F/T, FRC8)

Table 4-23: Maximum deflection at failure (effect of frost damage)

Sample ID	Maximum Cyclic Deflection at N=1 (mm)	Maximum Cyclic Deflection at $N=N_f$ (mm)	Total Plastic Deformation (mm)
	Refers to a in Figure 4.51	Refers to c in Figure 4.51	Refers to b in Figure 4.51
0-1	0.209	0.559	0.35
0-2	0.176	0.523	0.347
0-3	0.16	0.655	0.495
0-4	0.175	0.615	0.439
0-5	0.177	0.424	0.247
0-6	0.187	0.455	0.268
0-7	0.179	0.574	0.395
0-8	0.176	0.551	0.375
0-9	0.162	0.358	0.196
0-10	0.165	0.645	0.48
Average	0.177	0.536	0.359
200-1	0.159	0.203	0.044
200-2	0.183	0.274	0.092
200-3	0.174	0.363	0.189
200-4	0.171	0.597	0.426
200-5	0.465	0.511	0.046
200-6	0.153	0.47	0.316
200-7	0.211	0.249	0.038
200-8	0.162	0.368	0.206
200-9	0.176	0.259	0.083
Average	0.206	0.366	0.16
400-1	0.176	0.272	0.096
400-2	0.186	0.338	0.152
400-3	0.252	0.343	0.091
400-4	0.26	0.363	0.103
400-5	0.275	0.419	0.145
400-6	0.232	0.338	0.105
400-7	0.208	0.33	0.123
Average	0.227	0.343	0.116

4.4.6.2. Effect of Freeze-Thaw Exposure on the Rate of Plastic Deformation Accumulation

As mentioned earlier, F/T cycle count is not a proper indicator of the severity of frost damage. Therefore, to study the effect of frost damage on the rate of plastic deformation accumulation, freeze-thaw samples were divided into three categories based on their fatigue life. Figure 4.55 shows the selected intervals based on average fatigue life and 80% confidence intervals. According to Figure 4.55, samples with fatigue life of N_f>15000 are considered either mildly deteriorated or not deteriorated. Samples with 3000<N_f<15000 are assumed to be moderately deteriorated, and samples with N_f<3000 are severely deteriorated. It should be noted that the proposed intervals represent an approximation of severity of damage based on fatigue life.

The ratio of maximum deflection at cycle N to maximum deflection at fatigue failure for each category is plotted against cycle ratio (N/N_f) in Figure 4.56. Each data point is derived from the average of at least 5 samples' points.

A different trend is observed for the rate of plastic deformation for each of these deterioration categories at the beginning of fatigue life. However, after 60% of fatigue life, the rate of increase in plastic deformation converges.

4.4.6.3. Effect of Freeze-Thaw Exposure on Plastic Energy and Heat Transformation

Table 4.24 shows the total dissipated energy (TDE) and its components. As can be seen, frost damage has significantly decreased the damping characteristic of FRC concrete. Both plastic energy and generated heat have significantly decreased. The

presence of internal and external frost damage has resulted in a weaker concrete matrix in terms of damping properties.

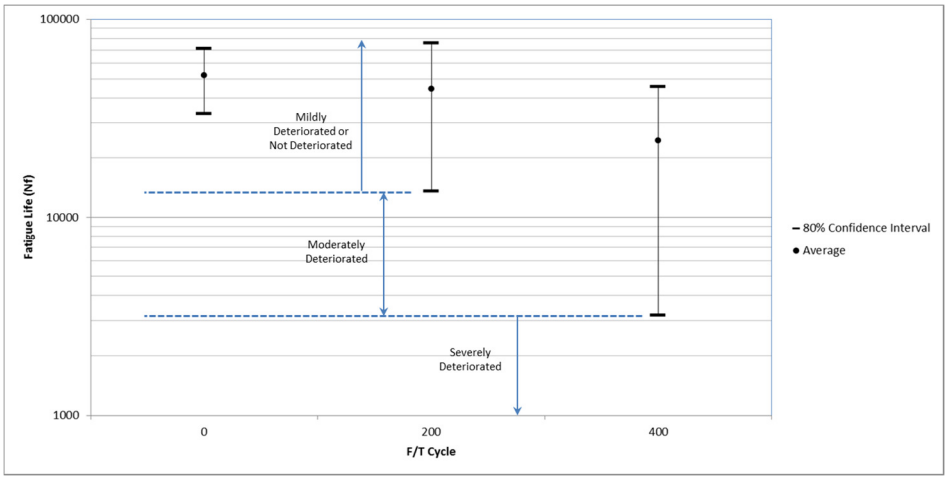

Figure 4.55: Categorization of severity of frost damage based on the fatigue life

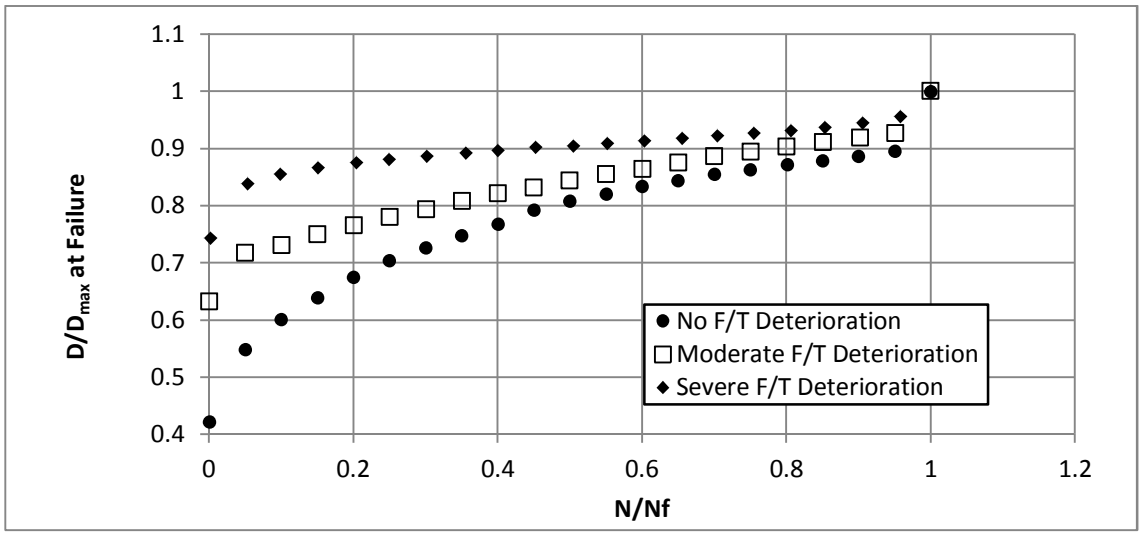

Figure 4.56: Plastic deformation accumulation during fatigue life (effect of freeze-thaw exposure, FRC8)

Table 4-24: TDE, plastic energy and heat (effect of freeze-thaw exposure, FRC8)

F/T Cycle - ID#	TDE (N.m)	Plastic Energy(N.m)	Heat Transformation (N.m)
0-1	497.97	3.27	494.7
0-2	747.49	3.1	744.39
0-3	505.63	4.08	501.55
0-4	715.53	3.73	711.79
0-5	343.82	2.36	341.46
0-6	871.2	3.39	867.81
0-7	2800.94	3.59	2797.35
0-8	566.11	1.36	564.75
0-9	155.36	2.05	153.31
0-10	1365.02	2.27	1362.75
Average	856.91	2.92	853.99
200-1	462.35	0.95	461.4
200-2	64.68	1.39	63.29
200-3	3405.48	2.66	3402.81
200-4	643.98	3.77	640.22
200-5	5.49	2.05	3.45
200-6	673.34	2.9	670.44
200-7	1.56	1.05	0.51
200-8	1508.71	1.23	1507.47
200-9	275.6	1.26	274.34
Average	782.35	1.92	780.43
400-1	797.51	1.46	796.05
400-2	190.8	1.87	188.93
400-3	2029.01	2.3	2026.71
400-4	55.46	1.7	53.76
400-5	15.82	2.05	13.76
400-6	27.46	1.63	25.83
400-7	278.07	1.67	276.4
Average	484.88	1.81	483.06

Chapter 5. Research Analysis and Modeling

5.1. Introduction

In this chapter, the analytic methods and statistical modeling procedures used to develop a reliable model to predict a dependent variable based on one or more independent variables are presented. The data set used in the modeling was gathered from several experiments conducted in the Civil and Environmental Engineering lab of the University of Maryland.

Section 5.3 is dedicated to the statistical models developed to predict the fatigue life (N_f) of concrete. Several independent variables, such as stress level (S; i.e., the ratio of maximum cyclic stress to flexural strength) and averaged-dissipated energy (ADE; i.e., the average value of dissipated energy per loading cycle throughout the entire fatigue life), were incorporated into prediction models. Finally, traditional S-N_f models were developed and compared to the proposed ADE-N_f models.

In Section 5.4, it is tried to assess the effects of loading characteristics, such as stress level and loading frequency, on ADE. Several models that incorporate ADE, stress level and loading frequency have been developed and are evaluated statistically.

Section 5.5 addresses the combined effects of freeze-thaw exposure and fatigue. Several models were developed and evaluated to predict fatigue life of frost-damaged samples using the volumetric properties of samples, such as void content and ADE, as independent variables.

In Section 5.6, a prediction model for the deformation of concrete samples during fatigue testing is proposed, which includes cycle ratio (N/Nf) and fiber content (%f) as independent variables.

Section 5.7 aimed to the relation between fatigue life and dynamic motion parameters such as cyclic stiffness (k) and hysteresis damping constant (β) is studied.

Finally, in the last section a new approach to find the endurance limit of FRC concrete is presented based on the load-deflection envelope curve.

5.2. Least Squares Methods

The statistical models proposed in this chapter were developed based on regression analysis using the least squares method. Based on the least squares method, calibration coefficients are selected in such a way that the sum of squared error (SSE) becomes a minimum possible value (Graybill and Iyer 1994). In a multivariate population of data with size n, if P_i is the predicted value of the dependent variable using a regression model and y_i is the observed value of the dependent variable obtained from sampling, the SSE is defined as follows:

$$SSE = \sum_{i=1}^{n} (P_i - y_i)^2 \qquad \textbf{5.1}$$

5.3. Fatigue Life Modeling

One of the main objectives of this research is to develop a prediction model for the fatigue life of concrete that not only yields greater predictability than the existing fatigue life models, but also requires fewer fatigue tests for calibration. In order to achieve this goal a series of fatigue tests were performed on polypropylene fiber

reinforced concrete (FRC8) under various loading conditions, as discussed in previous chapters. The results presented in Table 5-1 were used as data points to develop a regression model.

Table 5-1: Fatigue Modeling Dataset

Fatigue Life (Nf)	Frequency of Loading	Stress Level (%)	ADE (N.m)	TDE (N.m)
15000	5	80.19	0.02034	305.10
610	5	80.28	0.02400	14.64
7950	5	80.36	0.02185	173.73
1245	5	78.69	0.02317	28.85
2310	5	78.95	0.02244	51.84
30520	5	77.48	0.01982	604.94
29120	5	70.58	0.01710	497.97
41260	5	70.54	0.01812	747.49
30640	5	69.70	0.01650	505.63
42120	5	70.17	0.01699	715.53
20000	5	70.22	0.01719	343.82
66940	5	66.73	0.01301	871.20
153175	5	70.94	0.01829	2800.94
36475	5	70.60	0.01552	566.11
7460	5	70.84	0.02083	155.36
94110	5	70.72	0.01450	1365.02
302620	5	59.43	0.01206	3648.13
272270	5	58.99	0.01132	3082.49
409800	5	59.09	0.00997	4084.45
118600	5	58.80	0.01006	1192.79
233900	5	58.56	0.01038	2428.95
775000	5	58.18	0.01026	7951.82
17150	10	77.44	0.03060	524.80
11532	10	76.76	0.03056	352.37
120928	10	76.07	0.02789	3372.88
24236	10	78.25	0.03330	807.02
5352	10	77.43	0.03409	182.44
15920	10	76.50	0.02989	475.84
13090	10	68.93	0.01990	260.49
5420	10	71.90	0.02077	112.57
54840	10	70.38	0.02302	1262.16
22740	10	69.76	0.02208	502.07
18340	10	68.28	0.02172	398.30
128000	10	68.29	0.01999	2866.61
973500	10	59.18	0.01627	15834.37
300000	10	61.01	0.01690	5069.25
1736900	10	61.01	0.01973	34270.24
1277300	10	62.08	0.01751	22361.74
237000	10	62.12	0.01930	4574.52

5.3.1. Fatigue Life Prediction Using ADE

As mentioned earlier, stress level may not be a proper independent variable in the fatigue life prediction model, since it represents only the strength of material and does not reflect its damping properties. However, incorporating a new parameter that can reflect both the strength and damping properties of concrete during fatigue testing may increase the predictability of fatigue life models.

Averaged-dissipated energy per loading cycle (ADE), which is the average value dissipated energy per loading cycle during the fatigue life, has not only been found to represent the damping properties of concrete but is also directly correlated to stress level (see Section 5.4). Several models, including linear and nonlinear, were assessed to find the best model to describe the relationship between fatigue life and ADE. The statistical analysis of these models is presented below.

5.3.2. Linear Model

The Nf-ADE plot shows that there is no linear trend between fatigue life and ADE (Figure 5.1). The correlation coefficient value between two random variables (i.e., Nf and ADE) also confirms that there is a weak linear correlation between these two variables (Table 5-2). Therefore, the linear regression model was excluded from further assessment.

Table 5-2: Linear correlation coefficient between Nf and ADE

Loading frequency	Linear correlation coefficient
5	-0.69
10	-0.50

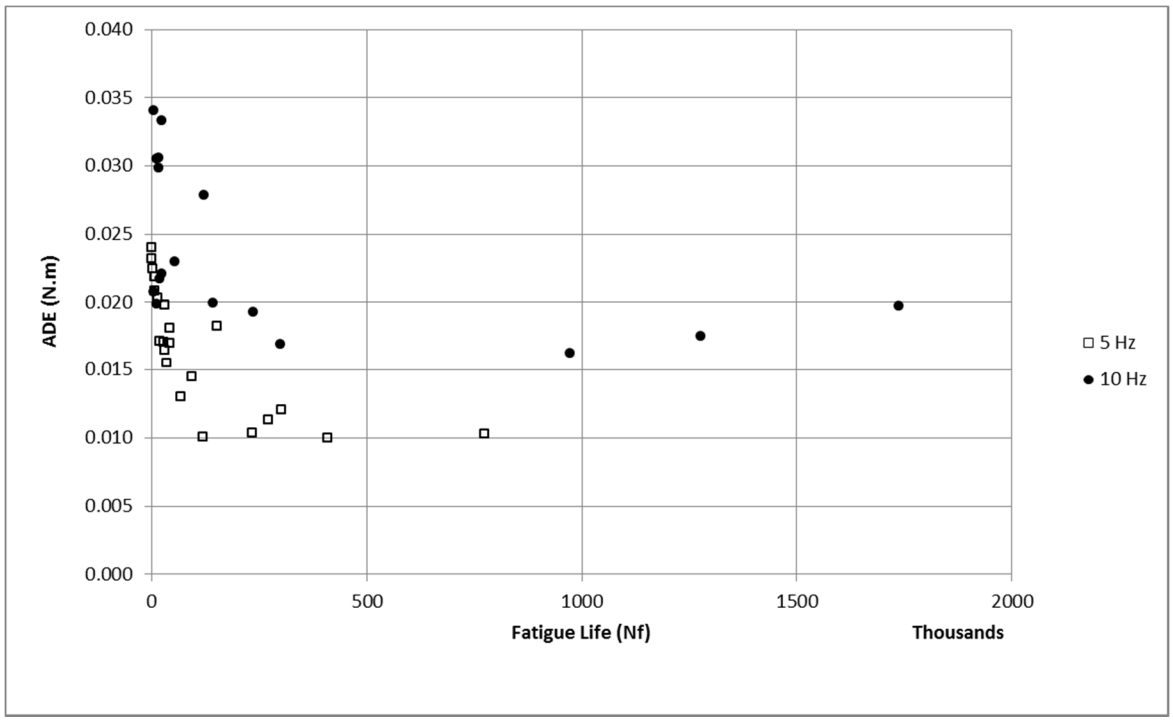

Figure 5.1: Fatigue life vs. ADE (FRC8)

5.3.3. Exponential Model

An exponential model, as shown in Equation 5.2, was assessed and proved to be statistically meaningful for a fatigue life (Nf) prediction model.

$$N_f = a\, b^{\,ADE} \qquad \textbf{5.2}$$

The exponential model was linearized by transforming the dependent variable to a logarithmic function. The linearized model is shown by Equation 5.3. The least square linear regression analysis method was applied to find the linearized exponential regression function coefficients (i.e., *Ln a* and *Ln b* in Equation 5.3).

$$\mathrm{Ln}\left(N_f\right) = \mathrm{Ln}\, a + ADE\, \mathrm{Ln}\, b \qquad \textbf{5.3}$$

5.3.3.1. Analysis of Variance

The analysis of variance (ANOVA) of the regression analysis of the sample tested at frequencies of 5 and 10 Hz are shown in Table 5-3 and Table 5-4, respectively. The result of an overall F-test for the regression model for samples tested at a frequency of 5 Hz indicates that the model is significant (i.e., $F_{statistic}$=96.58>$F_{critical}$=4.35, from Table 5-3). The null hypothesis in the overall F-test for the regression model is that all regression coefficients of the model (i.e., *Ln a* and *Ln b*) are equal to zero. The null hypothesis is rejected ($F_{statistic}$>$F_{critical}$) when there is at least one regression coefficient

that not zero. In other words, the probability that the proposed model is obtained by chance is very low if the null hypothesis is rejected. The *significance F* in Table 5-3 is the *p*-value or significance probability of the test. When the *p*-value is smaller than the significance level of the test (in this case α=0.05), the null hypothesis is rejected. The result of the F-test for samples tested at a frequency of 10 Hz also indicates that the proposed model is significant ($F_{statistic}$=10.35>$F_{critical}$=4.54. from Table 5-4).

Table 5-3: Analysis of variance (exponential model, Nf-ADE, FRC8, 5 Hz, α=0.05)

	df	*SS*	*MS*	$F_{statistic}$	*Significance F*	$F_{critical}$
Regression	1	61.11	61.11	96.58	4.2E-09	4.35
Residual	20	12.65	0.63			
Total	21	73.77				

Table 5-4: Analysis of variance (exponential model, Nf-ADE, FRC8, 10 Hz, α=0.05)

	df	*SS*	*MS*	$F_{statistic}$	*Significance F*	$F_{critical}$
Regression	1	23.41	23.41	10.35	0.006	4.54
Residual	15	33.92	2.26			
Total	16	57.34				

5.3.3.2. t-test of the Independent Variable and Regression Coefficients (Ln a and Ln b)

A *t*-test of the independent variable was performed to determine whether the independent variable was significant or not. The null hypothesis for the *t*-test is that the coefficient is equal to zero. Rejection of null hypothesis means that the independent

variable is significant. Results of the *t*-test on independent variables, as well as calculated exponential model coefficients (i.e., *Ln a* and *Ln b*), are presented in Table 5-5 and Table 5-6, respectively. The *p*-values for the independent variable are significantly lower than the power of the test (i.e., α=0.05), and therefore the effect of both the intercept (Ln a) and the independent variable (ADE) on the response variable (N_f) are significant. The absolute value of $t_{statistic}$ (i.e., $|t_{statistic}|$) is larger than the $t_{critical}$ for both intercept and ADE which confirms the significance of independent variables.

Table 5-5: Calibration coefficients and *t*-test of independent variable (exponential model, N_f-ADE, FRC8, 5 Hz, α=0.05)

	Coefficients	*Standard Error*	$T_{statistic}$	*P-value*	$T_{critical}$
Intercept	16.69	0.65	25.70	8.6E-17	2.42
ADE	-372.59	37.91	-9.83	4.2E-09	

Table 5-6: Calibration coefficients and *t*-test of independent variable (exponential model, N_f-ADE, FRC8, 10 Hz, α=0.05)

	Coefficients	*Standard Error*	$T_{statistic}$	*P-value*	$T_{critical}$
Intercept	15.82	1.54	10.27	3.5E-08	2.49
ADE	-202.78	63.03	-3.22	5.8E-03	

5.3.3.3. Evaluation of Regression Assumption Validity

Linear regression analysis is based on several assumptions. The first and most important is that the data set must be selected from a normal population using a simple random sampling method. The second assumption is the homogeneity of standard deviation, which means that all subpopulations of the dependent variable corresponding to a given independent variable must have the same standard deviation (Graybill and Iyer 1994). Figure 5.2 shows the assumption of linear regression analysis. Any subpopulation of data (i.e., X_i and X_j) is a random sample taken from a normal distribution (first assumption) with the same standard deviation (homogeneity of standard deviation).

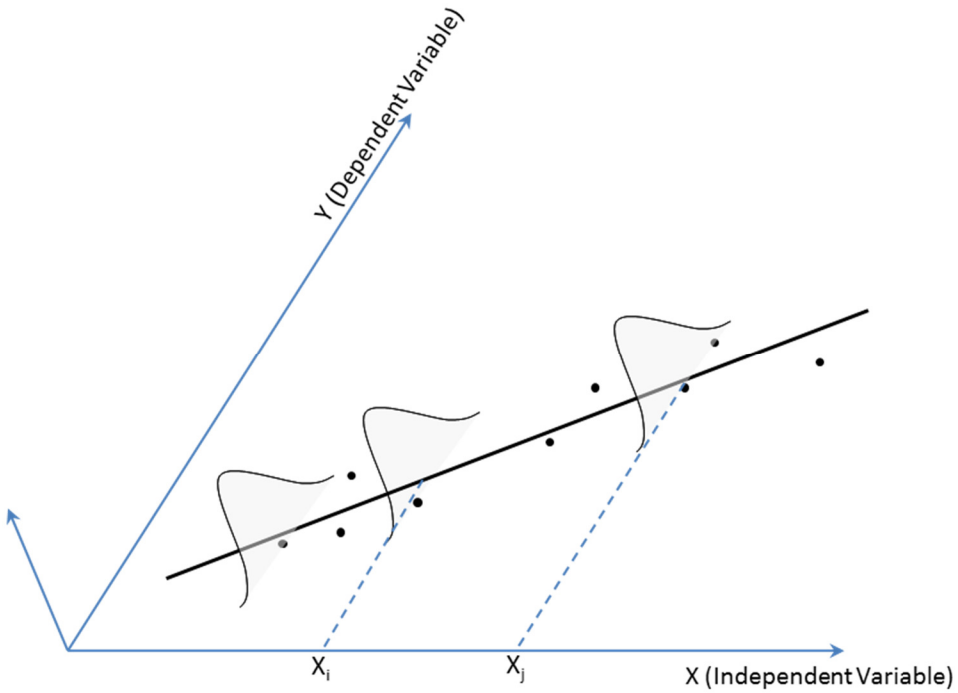

Figure 5.2: Assumption of linear regression

The Gaussian rankit plot is one of the most acceptable methods for determining whether data are taken from a normal distribution using random sampling. In the rankit plot, standardized residuals are plotted against Gaussian scores. By definition, the residual is the difference between the observed dependent variable and the predicted dependent variable. The standardized residual is obtained by dividing the residual by the standard deviation of the residual. In other words, the standardized residual has a standard deviation of 1. Gaussian scores with a sample size of *n* are random samples from a normal distribution, with zero mean and unit standard deviation. Given the above, if the rankit plot follows a linear trend that passes through the origin, the standardized residuals possess a normal distribution with zero mean and unit standard deviation.

As cited by Graybill and Iyer, if the standardized residuals resemble a normal distribution with zero mean and standard deviation of 1, assumptions of linear regression analysis are satisfied (1994).

By looking at Figure 5.3 and Figure 5.4, which are the rankit plots for frequencies of 5 and 10 Hz, respectively, it can be concluded that the assumption of normality of the data set is valid, since the rankit plot shows a linear relation between Gaussian scores and standardized residuals. Some data points do not appear to follow the linear trend and must be assessed as potential outliers. The process of outlier detection is explained in the next section.

Figure 5.3: Rankit plot (Exponential Model, Nf vs. ADE, 5Hz)

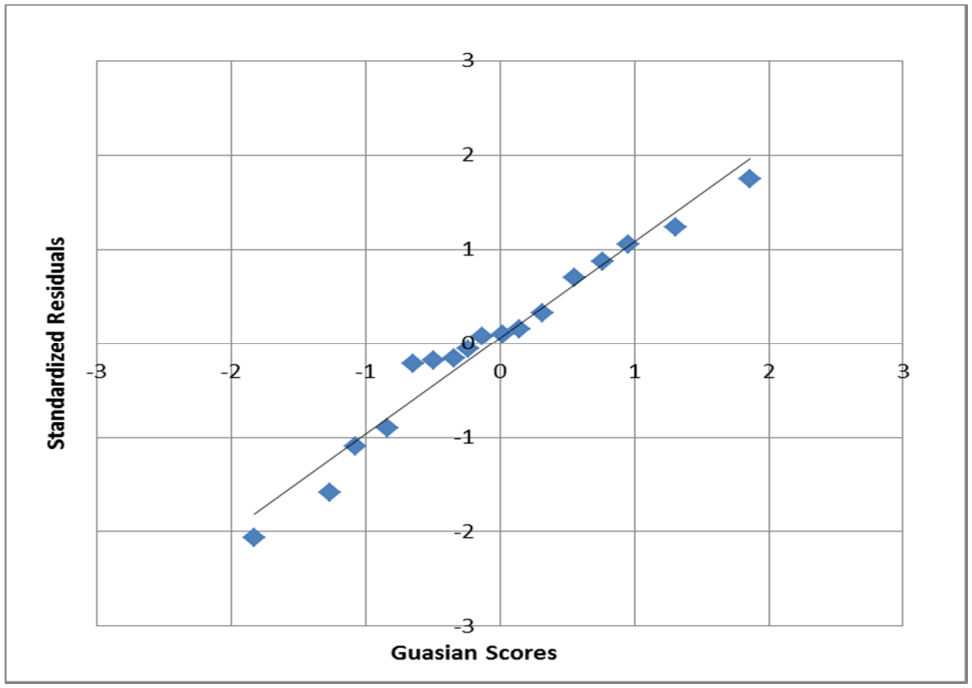

Figure 5.4: Rankit plot (Exponential Model, Nf vs. ADE, 10Hz)

5.3.3.4. Outlier Detection

Detection of influential observations—so called outliers—is based on Cook's distance method, which assesses the influence of any data point on regression coefficient (i.e., *Ln a* and *Ln b*). In other words, the presence of an outlier in data would significantly affect the regression coefficients. Cook's distance, which is defined by Equation 5.4, is the measure of difference between coefficients of regression analysis before and after removal of the *ith* observation.

$$c_i = \frac{1}{p}\left(\frac{h_{i,i}}{1 - h_{i,i}}\right) {r_i}^2 \qquad \textbf{5.4}$$

p is the number of coefficients in the regression model (in this case 2), $h_{i,i}$ is the hat value of the *ith* observation, and r_i is the standardized residual of the *ith* observation. The hat values ($h_{i,i}$) are the diagonal elements of the hat matrix (H). The matrix format of the regression equation is shown by Equation 5.5, where X is the independent variable matrix, β is the regression coefficient matrix, and e is the error matrix.

$$y = X\beta + e = \begin{pmatrix} 1 & \cdots & x_p \\ \vdots & \ddots & \vdots \\ 1 & \cdots & x_{p+n} \end{pmatrix} \begin{pmatrix} \beta_0 \\ \vdots \\ \beta_{p-1} \end{pmatrix} + \begin{pmatrix} e_1 \\ \vdots \\ e_n \end{pmatrix} \qquad \textbf{5.5}$$

The hat matrix (H) is defined by Equation 5.6. X^T is the transposition of matrix *X*.

$$H = X(X^T X)^{-1} X^T \quad \textbf{5.6}$$

The value of c_i, indicates whether the observation is influential or not. As recommended by the literature, a value of c_i greater than $F_{0.5:p,n-p}$ should be treated as an outlier (Graybill and Iyer 1994).

The Cook's distance for all data points is shown in Table 5-7 and Table 5-8. As can be seen, no outliers are and therefore the regression analysis for this model is complete.

Table 5-7: Outlier detection (Exponential Model, Nf vs ADE, 5 Hz)

Observation	*Predicted Ln (Nf)*	*Residuals*	*Std Residuals*	*hi*	*ci*	$F_{0.5:p,n-p}$
1	9.108	0.508	0.654	0.078	0.018	0.718
2	7.745	-1.332	-1.716	0.172	0.306	0.718
3	8.544	0.436	0.562	0.110	0.019	0.718
4	8.052	-0.926	-1.192	0.146	0.121	0.718
5	8.326	-0.581	-0.748	0.125	0.040	0.718
6	9.301	1.025	1.320	0.070	0.066	0.718
7	10.315	-0.036	-0.046	0.046	0.000	0.718
8	9.937	0.691	0.890	0.051	0.021	0.718
9	10.538	-0.208	-0.268	0.045	0.002	0.718
10	10.357	0.291	0.375	0.046	0.003	0.718
11	10.281	-0.378	-0.487	0.046	0.006	0.718
12	11.837	-0.726	-0.935	0.074	0.035	0.718
13	12.195	0.425	0.548	0.091	0.015	0.718
14	12.468	0.046	0.060	0.107	0.000	0.718
15	12.973	-0.050	-0.064	0.143	0.000	0.718
16	12.939	-1.256	-1.618	0.141	0.214	0.718
17	12.817	-0.455	-0.586	0.131	0.026	0.718
18	12.864	0.697	0.898	0.135	0.063	0.718
19	9.873	2.066	2.661	0.052	0.196	0.718
20	10.904	-0.399	-0.515	0.048	0.007	0.718
21	8.927	-0.010	-0.013	0.087	0.000	0.718
22	11.282	0.170	0.219	0.055	0.001	0.718

Table 5-8: Outlier detection (Exponential Model, Nf vs ADE, 10 Hz)

Observation	*Predicted Ln(Nf)*	*Residuals*	*Std Residuals*	*hi*	*ci*	$F_{0.5:p,n-p}$
1	9.612	0.137	0.094	0.142	0.001	0.726
2	9.622	-0.269	-0.184	0.141	0.003	0.726
3	10.162	1.541	1.058	0.089	0.055	0.726
4	9.065	1.030	0.708	0.219	0.070	0.726
5	8.905	-0.320	-0.220	0.247	0.008	0.726
6	9.757	-0.081	-0.056	0.125	0.000	0.726
7	11.782	-2.303	-1.581	0.085	0.116	0.726
8	11.606	-3.008	-2.066	0.074	0.171	0.726
9	11.151	-0.238	-0.164	0.060	0.001	0.726
10	11.340	-1.309	-0.899	0.064	0.027	0.726
11	11.414	-1.597	-1.097	0.066	0.042	0.726
12	11.764	0.109	0.075	0.083	0.000	0.726
13	12.519	1.269	0.872	0.157	0.071	0.726
14	12.391	0.220	0.151	0.141	0.002	0.726
15	11.817	2.551	1.752	0.087	0.146	0.726
16	12.267	1.793	1.231	0.127	0.110	0.726
17	11.904	0.472	0.324	0.093	0.005	0.726

5.3.3.5. Goodness of Model

As shown in Table 5-9 and Table 5-10, the coefficients of determination (R^2), which is a measure of overall goodness of fit, are 0.828 and 0.408 for the proposed model at frequencies of 5 and 10 Hz, respectively. It is evident that the model has revealed a reasonable correlation for a loading frequency of 5 Hz. Therefore, the fatigue life of concrete samples tested at a frequency of 5 Hz can be modeled by Equation 5.7. The graphical format of the model is presented in Figure 5.5. The predictability of the model at a frequency of 10 Hz is extremely low, and therefore not statistically reliable.

$$N_f = e^{16.69-372.58\ ADE} \quad \textbf{5.7}$$

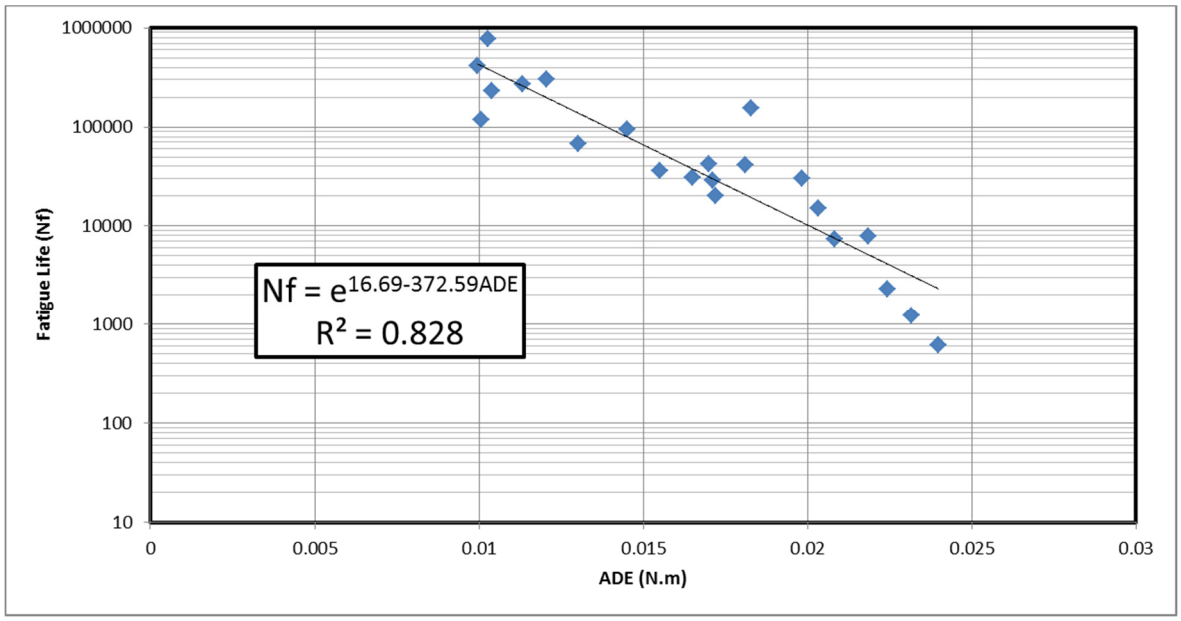

Figure 5.5: Exponential model of fatigue for samples tested at a frequency of 5 Hz

Standard error is the estimated standard deviation of errors. The adjusted R^2 (Equation 5.8) takes into account the effect of addition of a new independent variable in increasing R^2. Sometimes the addition of a new independent variable to the regression model falsely increases the R^2 by decreasing the unexplained errors (residuals) of the model. This is usually the case when the sample size is small or when collinearity exists in the data set. The large difference between R^2 and adjusted R^2 implies that the regression equation is overfitted with too many independent variables. In the equation below, *n* represents the sample size and *p* is the number of independent variables. As can be seen, large sample size and a limited number of independent variables (i.e., lower complexity of model) decrease the difference between R^2 and adjusted R^2.

$$Adjusted\ R^2 = 1 - (1 - R^2)\frac{n-1}{n-p-1} \quad \textbf{5.8}$$

Table 5-9: Measure of Goodness of Model (Exponential Model, Nf vs ADE, 5 Hz)

Regression Statistics	
R Square	0.828
Adjusted R Square	0.820
Standard Error	0.795
Observations	22

Table 5-10: Measure of Goodness of Model (Exponential Model, Nf vs ADE, 10 Hz)

Regression Statistics	
R Square	0.408
Adjusted R Square	0.369
Standard Error	1.504
Observations	17

5.3.3.6. Evaluation of Validity of Model

Leave-one-out cross validation (LOOCV) is used to check how accurately the prediction model performs. The method involves removing one data point from the data set, fitting a model to the remaining data points, and then plugging the removed data point into the new model. The process is repeated for all data points, and finally the mean square error (MSE) is used as a measure of fit. Mean square error is the average value of squared errors. LOOCV was not performed on the proposed model for a frequency of 10 Hz, since the model has not demonstrated high predictability.

Table 5-11 shows the process of LOOCV for the proposed exponential model at a frequency of 5 Hz. To produce Model 1 (see Table 5-11), observation 1 (from Table 5-7) is removed from the data set and the exponential model is calibrated using the 21 remaining data points. The removed data point is then plugged into the calibrated model (i.e., model 1) and the predicted value for *Ln Nf* is found. The square of the difference between the actual *Ln Nf* (i.e., the one obtained from sampling) and the predicted one is then calculated. The same process is followed to calculate the squared error of all models in Table 5-11.

The low value of MSE indicates that the model possesses a good accuracy in real application. As can be seen in Table 5-11, some models have larger squared errors than the MSE. A large value for squared errors implies that the data point is far from the regression line and may be a potential outlier. Although none of these data points are detected as an outlier, it can be seen that the Cook's distance for these data points (i.e., the ones that have large squared errors) is relatively large.

Table 5-11. LOO CV for Exponential Model at 5 Hz Frequency (Nf vs ADE)

Ln (Nf) = A+B ADE	A = Ln a	B = Ln b	R^2	Adj. R^2	Predicted Ln(Nf)	Actual Ln(Nf)	$(\text{Actual-Predicted})^2$
Model 1	16.740	-377.350	0.83	0.82	9.06	9.62	0.303
Model 2	16.309	-345.310	0.81	0.80	8.02	6.41	2.588
Model 3	16.762	-378.502	0.83	0.82	8.49	8.98	0.240
Model 4	16.466	-356.236	0.83	0.82	8.21	7.13	1.174
Model 5	16.570	-363.674	0.81	0.80	8.41	7.75	0.441
Model 6	16.773	-380.807	0.84	0.84	9.22	10.33	1.213
Model 7	16.687	-372.529	0.83	0.82	10.32	10.28	0.001
Model 8	16.697	-375.198	0.84	0.83	9.90	10.63	0.530
Model 9	16.697	-372.592	0.83	0.82	10.55	10.33	0.048
Model 10	16.678	-372.893	0.83	0.82	10.34	10.65	0.093
Model 11	16.695	-371.985	0.83	0.82	10.30	9.90	0.157
Model 12	16.826	-378.840	0.84	0.83	11.90	11.11	0.614
Model 13	16.587	-367.819	0.82	0.81	12.15	12.62	0.219
Model 14	16.674	-371.965	0.82	0.81	12.46	12.51	0.003
Model 15	16.703	-373.441	0.81	0.80	12.98	12.92	0.003
Model 16	17.108	-394.076	0.85	0.84	13.15	11.68	2.136
Model 17	16.831	-379.889	0.82	0.81	12.89	12.36	0.274
Model 18	16.460	-361.100	0.81	0.80	12.76	13.56	0.649
Model 19	16.731	-381.260	0.89	0.88	9.76	11.94	4.752
Model 20	16.722	-373.542	0.83	0.82	10.92	10.50	0.176
Model 21	16.685	-372.472	0.82	0.81	8.93	8.92	0.000
Model 22	16.665	-371.749	0.83	0.82	11.27	11.45	0.032
						MSE	0.71

5.3.4. Power Model

The other possible model to describe the relationship between fatigue life (N_f) and ADE is the power model, as shown by Equation 5.9.

$$N_f = a\, ADE^b \qquad \textbf{5.9}$$

The power model can be linearized by taking the logarithm of each side of the equation. The linearized model is shown below.

$$Ln\left(N_f\right) = Ln(a) + b\,Ln(ADE) \quad \textbf{5.10}$$

The result of least square linear regression analysis for loading frequencies of 5 and 10 Hz are presented in Table 5-12 and Table 5-13, respectively. The results for overall F of the model and *t*-test indicate that both the model and the independent variable are significant at α=0.05, except for the *t*-test for intercept of the model at a loading frequency of 10 Hz ($t_{statistic}$=1.48<$t_{critical}$=2.49).

The coefficients of determination (R^2) are 0.78 and 0.44 for loading frequencies of 5 and 10 Hz, respectively, which shows a relatively good predictability of the power model for the fatigue test at a frequency of 5 Hz. However, the proposed model for the frequency of 10 Hz does not possess good predictability. The power model for predicting fatigue life at a frequency of 5 Hz is shown by Equation 5.11. The graphical format of the model is presented in Figure 5.6.

$$N_f = e^{-12.82} ADE^{-5.64} \quad \textbf{5.11}$$

The generated rankit plots for the power models (Figure 5.7 and Figure 5.8) indicate that the basic assumptions of the linear regression model (i.e., normal population and homogeneity of standard deviation) are valid.

Outlier detection was performed based on Cook's distance value (c_i). The results are tabulated in Table 5-14 and Table 5-15. As can be seen, none of the Cook's values for data points was larger than $F_{0.5:p,n-p}$, and therefore no outliers were detected.

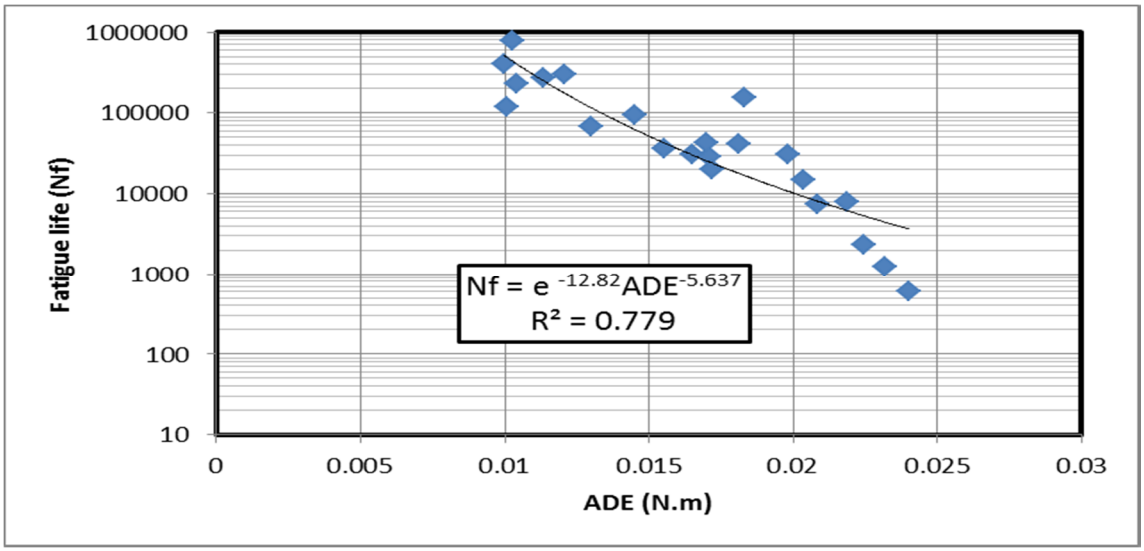

Figure 5.6:Power model (Nf vs ADE, 5Hz)

Table 5-12 Regression Analysis of the Power Model (Nf vs. ADE, 5Hz, α=0.05)

Regression Statistics	
R Square	0.779
Adjusted R Square	0.768
Standard Error	0.902
Observations	22

	Degree of Freedom	*SS*	*MS*	*F*	*Significance F*	$F_{critical}$
Regression	1	57.48	57.48	70.61	5.4E-08	4.35
Residual	20	16.28	0.81			
Total	21	73.77				

	Coefficients	*Std Error*	$T_{statistic}$	*P-value*	$T_{critical}$
Intercept	-12.820	2.785	-4.603	0.000172	2.42
Ln ADE	-5.637	0.671	-8.403	5.41E-08	

Table 5-13 Regression Analysis of the Power Model (Nf vs. ADE, 10Hz, α=0.05)

Regression Statistics	
R Square	0.441
Adjusted R Square	0.404
Standard Error	1.461
Observations	17

	Degree of Freedom	*SS*	*MS*	$F_{statistic}$	*Significance F*	$F_{critical}$
Regression	1	25.3000	25.3000	11.8462	3.63E-03	4.54
Residual	15	32.0358	2.1357			
Total	16	57.3358				

	Coefficients	*Std Error*	$T_{statistic}$	*P-value*	$T_{critical}$
Intercept	-8.35	5.6352	-1.4822	0.1590	2.49
Ln ADE	-5.14	1.4920	-3.4418	0.0036	

Figure 5.7: Rankit Plot (Power Model, Nf vs. ADE, 5Hz)

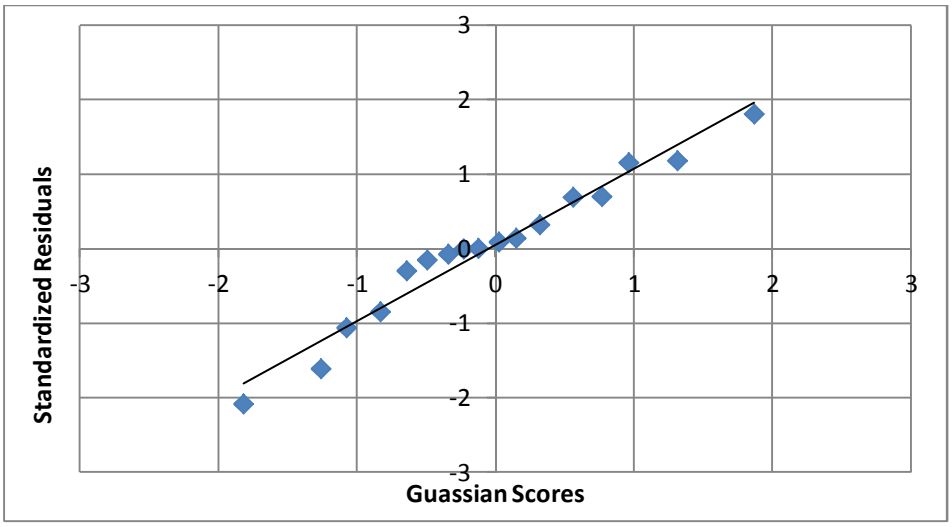

Figure 5.8: Rankit Plot (Power Model, Nf vs. ADE, 10Hz)

Table 5-14 Outlier Detection (Power Model, Nf vs ADE, 5 Hz)

Observation	*Predicted Ln Nf*	*Residuals*	*Std Residuals*	$h_{i,i}$	C_i	$F_{0.5:p,n-p}$
1	9.14	0.48	0.54	0.079	0.013	0.718
2	8.20	-1.79	-2.03	0.139	0.335	0.718
3	8.73	0.25	0.28	0.102	0.005	0.718
4	8.40	-1.27	-1.45	0.124	0.148	0.718
5	8.58	-0.84	-0.95	0.111	0.057	0.718
6	9.28	1.04	1.19	0.072	0.055	0.718
7	10.11	0.17	0.19	0.048	0.001	0.718
8	9.79	0.84	0.95	0.055	0.026	0.718
9	10.31	0.02	0.02	0.046	0.000	0.718
10	10.15	0.50	0.56	0.048	0.008	0.718
11	10.08	-0.18	-0.21	0.049	0.001	0.718
12	11.65	-0.54	-0.61	0.068	0.014	0.718
13	12.08	0.54	0.61	0.088	0.018	0.718
14	12.44	0.08	0.09	0.109	0.000	0.718
15	13.16	-0.23	-0.26	0.166	0.007	0.718
16	13.11	-1.42	-1.62	0.161	0.251	0.718
17	12.93	-0.56	-0.64	0.146	0.035	0.718
18	12.99	0.57	0.64	0.151	0.037	0.718
19	9.74	2.20	2.50	0.056	0.187	0.718
20	10.66	-0.16	-0.18	0.046	0.001	0.718
21	9.00	-0.09	-0.10	0.086	0.000	0.718
22	11.04	0.41	0.47	0.050	0.006	0.718

Table 5-15 Outlier Detection (Power Model, Nf vs ADE, 10 Hz)

Observation	*Predicted Ln Nf*	*Residuals*	*Standard Residuals*	$h_{i,i}$	C_i	$F_{0.5:p,n-p}$
1	9.553	0.197	0.139	0.142	0.002	0.726
2	9.560	-0.207	-0.146	0.141	0.002	0.726
3	10.029	1.674	1.183	0.096	0.075	0.726
4	9.119	0.977	0.690	0.199	0.059	0.726
5	8.998	-0.413	-0.292	0.218	0.012	0.726
6	9.673	0.002	0.001	0.129	0.000	0.726
7	11.762	-2.283	-1.613	0.082	0.115	0.726
8	11.543	-2.945	-2.081	0.070	0.164	0.726
9	11.015	-0.103	-0.073	0.059	0.000	0.726
10	11.229	-1.197	-0.846	0.061	0.023	0.726
11	11.313	-1.497	-1.058	0.063	0.037	0.726
12	11.739	0.134	0.095	0.080	0.000	0.726
13	12.798	0.991	0.700	0.186	0.056	0.726
14	12.602	0.010	0.007	0.160	0.000	0.726
15	11.806	2.562	1.810	0.084	0.151	0.726
16	12.420	1.640	1.159	0.138	0.108	0.726
17	11.919	0.457	0.323	0.092	0.005	0.726

5.3.5. Traditional S-N_f Approach versus ADE-N_f Approach

As mentioned earlier in this chapter, the main purpose of this study is to introduce a new approach that not only has better predictive quality, but also reduces the time required for fatigue testing. The normalized ADE (N) at various cycle ratios (N/N_f) of samples tested at different stress levels are shown in Figure 5.9 to Figure 5.14. ADE (N) denotes the average of dissipated energy up to loading cycle N. As can be seen, ADE (N) has large values at the beginning of the fatigue test and approaches ADE (i.e., average dissipated energy per cycle for all cycles until fatigue failure) after a certain loading cycle, then remains almost constant. This indicates that the ADE of each sample can be estimated with a reasonable accuracy after a few cycles. In other words, there is no need to continue fatigue testing up to failure to find the ADE value; testing can be stopped

after a few cycles without damaging the sample. Therefore, not only can a good amount of fatigue testing time be saved, but the fatigue life of the sample can also be predicted without destroying the sample.

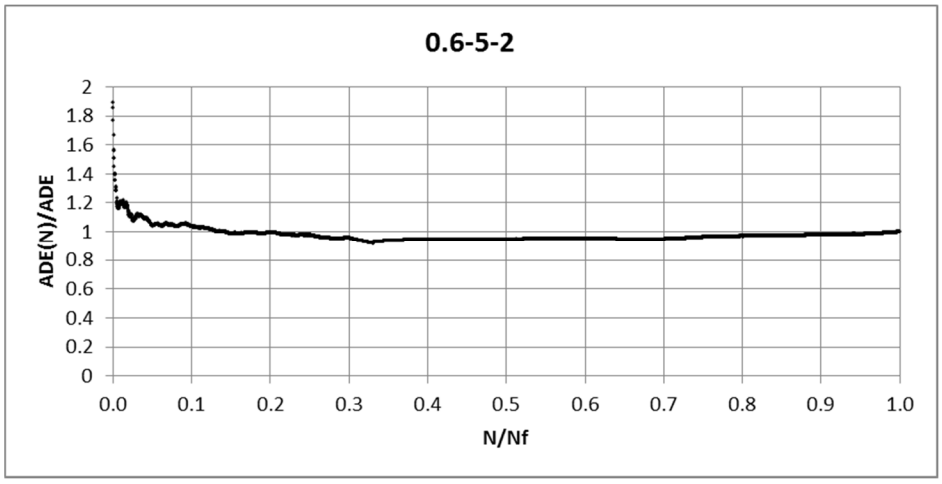

Figure 5.9: Normalized ADE(N) during the fatigue life (FRC8, S=0.6, 5Hz)

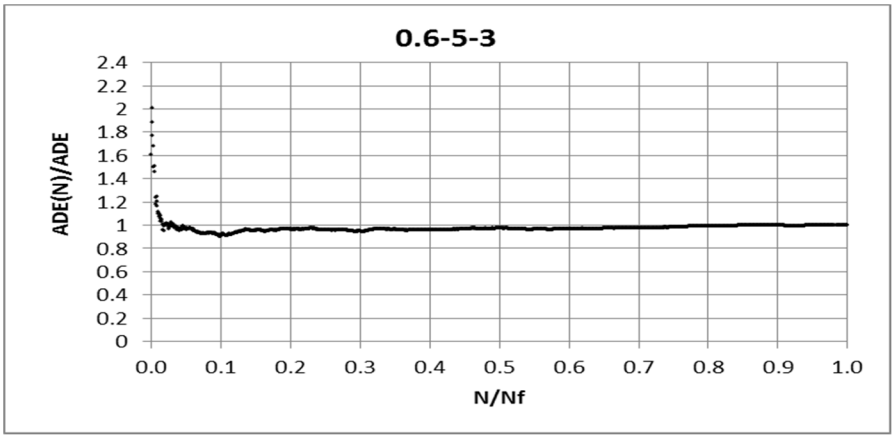

Figure 5.10: Normalized ADE(N) during the fatigue life (FRC8, S=0.6, 5Hz)

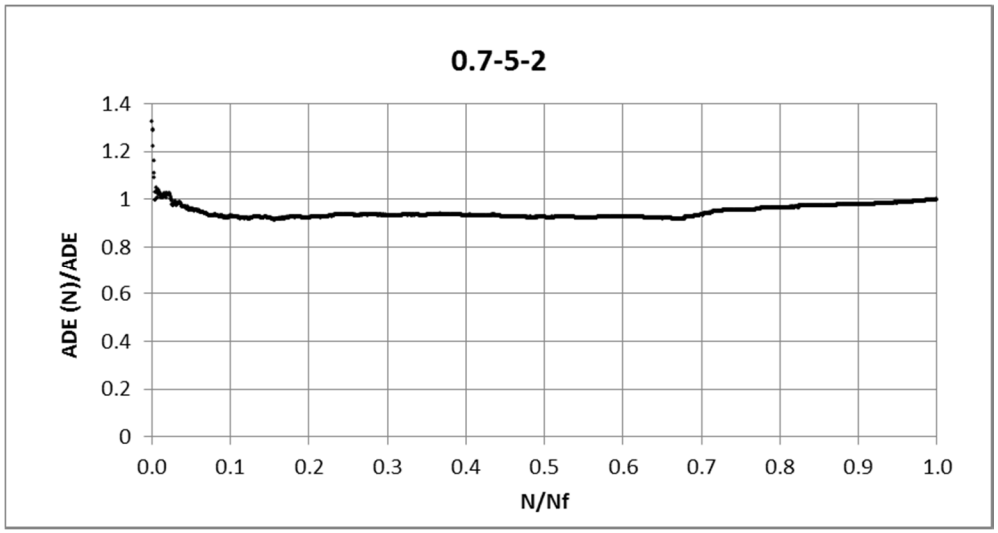

Figure 5.11: Normalized ADE(N) during the fatigue life (FRC8, S=0.7, 5Hz)

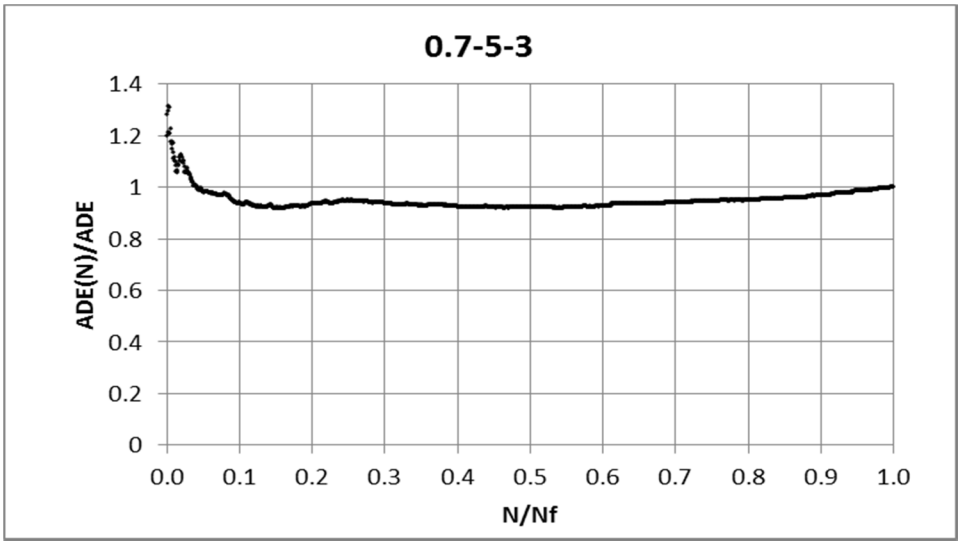

Figure 5.12: Normalized ADE(N) during the fatigue life (FRC8, S=0.7, 5Hz)

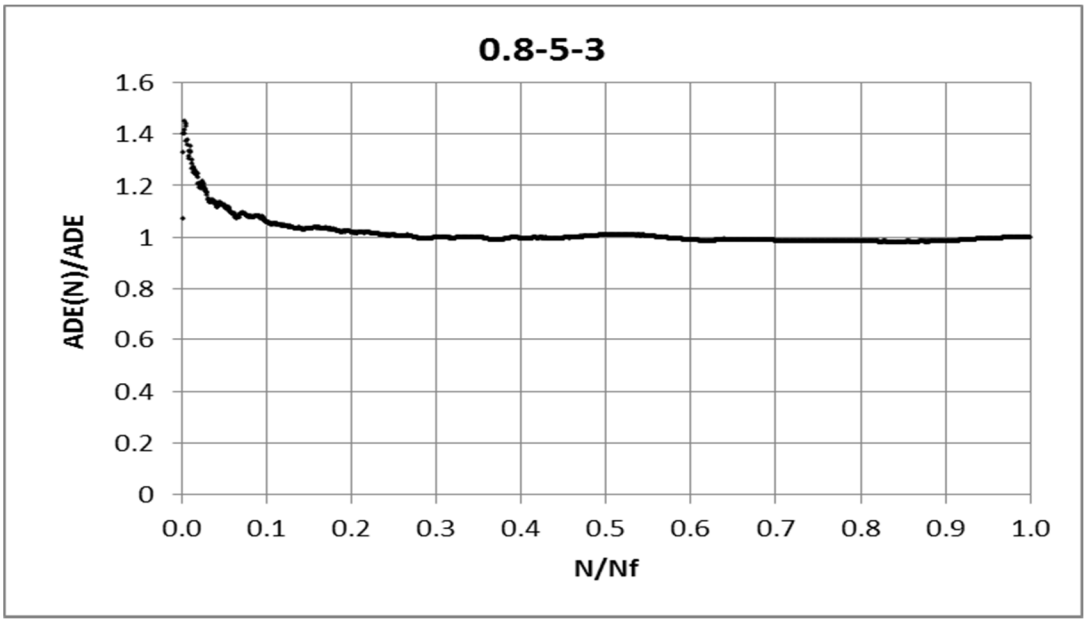

Figure 5.13: Normalized ADE(N) during the fatigue life (FRC8, S=0.8, 5Hz)

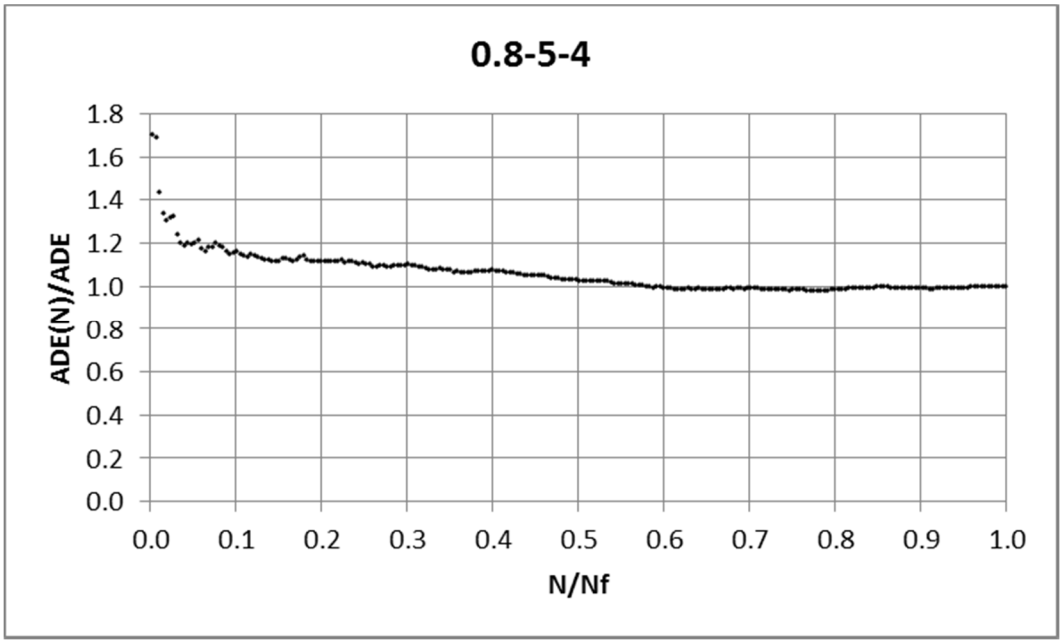

Figure 5.14: Normalized ADE(N) during the fatigue life (FRC8, S=0.8, 5Hz)

Each curve in Figure 5.15 shows an average of five samples tested at the same stress levels. As can be seen, after almost 10% of fatigue life, the ADE (N) of samples tested at stress levels of 0.6 and 0.7 is within the range of 0.97 ADE to 1.03 ADE. This is also valid for samples tested at stress levels of 0.8 after 30% of fatigue life. In other words, the maximum deviation of ADE (N) from the actual ADE value is ± 3% when the ADE is estimated from ADE (N), which seems to be an acceptable error for estimating fatigue life. Figure 5.16 shows the effect of a ± 3% error in ADE in the ratio of *Ln Nf* predicted from ADE, with a ± 3% error to *Ln Nf* predicted from actual ADE. This figure is developed from Equation 5.7 by changing the actual ADE. As can be seen, the error in predicting ADE from estimated ADE with ± 6% error in the worst scenario (i.e., at higher ADE values when fatigue life is low) is not more than 7%. This level of error is negligible considering the high variation in fatigue test results.

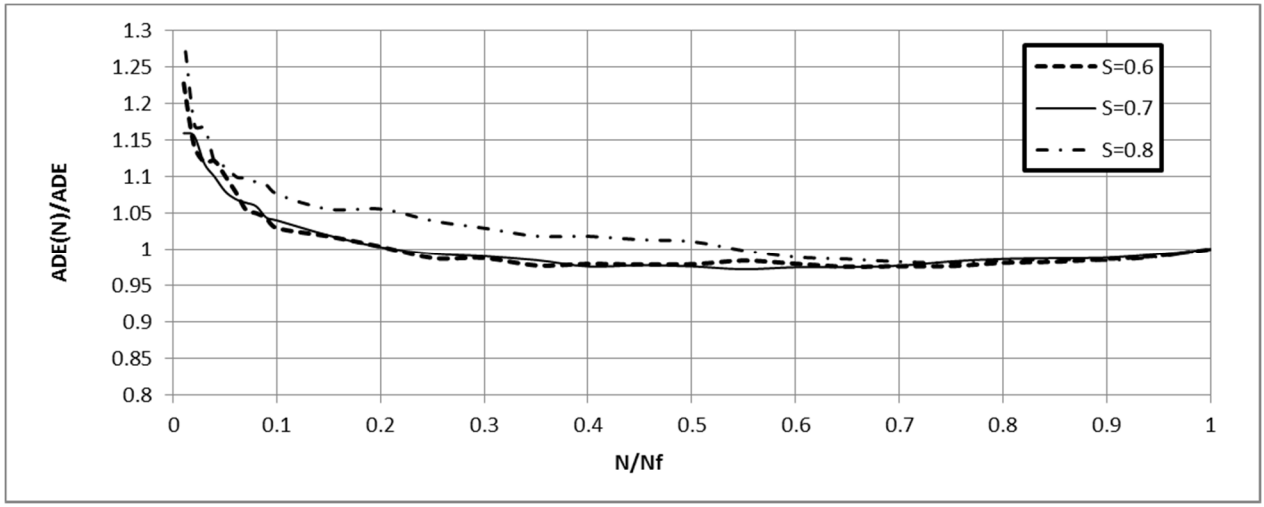

Figure 5.15: Normalized ADE (N) during the fatigue life (FRC8, 5Hz, average of 5 samples)

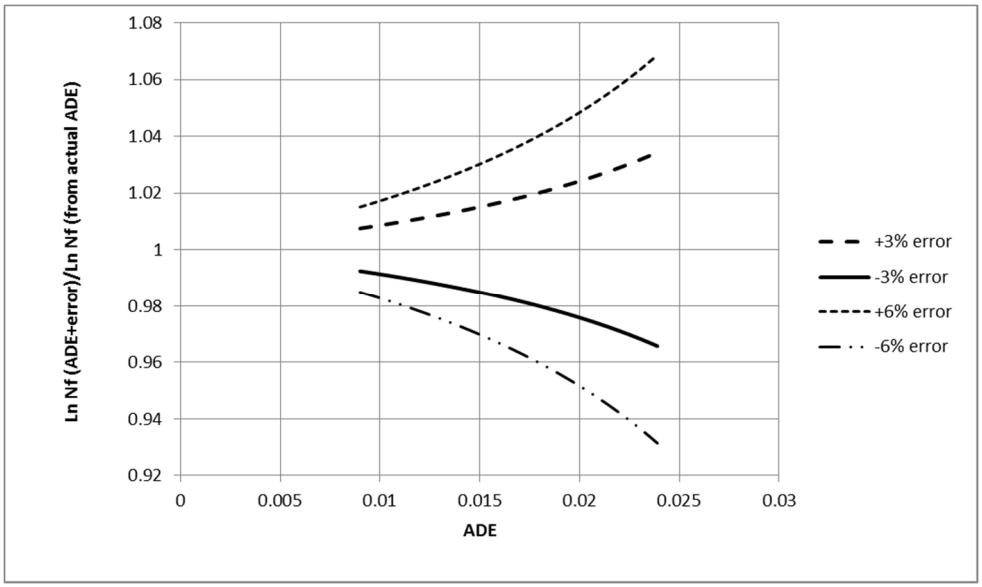

Figure 5.16: Ratio of Ln Nf from estimated ADE with error to Ln Nf from actual ADE

To compare predicted fatigue life from ADE and ADE (N), the values for ADE (N) are found and plugged into the proposed exponential model (Equation 5.7) to predict fatigue life from ADE. The absolute error of prediction, which is the ratio of difference between the actual value of *Ln Nf* and the predicted value of *Ln Nf* to the actual value of *Ln Nf,* is calculated for both ADE and ADE (N). The results of the comparison are presented in Table 5-16. As can be seen, the averages of absolute error for both methods are almost the same, which indicates that ADE (N) is a good estimation of ADE and can be used in fatigue life prediction models as a replacement for ADE.

The algorithm applied to find ADE (N) is shown in Figure 5.17. In the proposed algorithm, fatigue loading stops at cycle N, where the ADE (N) is smaller than 0.024 *N.m* and the difference between Ln Nf(ADE(N)) and Ln N is smaller than 2 standard deviations of the model. The graphical explanation of the algorithm is presented in Figure 5.18 to Figure 5.20. As can be seen, these figures include the actual fatigue model presented for FRC8 samples tested at a frequency of 5 Hz, as well as two boundary lines. The vertical distance of any point within these boundaries to the prediction line is less than *m* standard deviations of the model. The solid gray line in the figures shows the ADE (N) versus the loading cycle (N). As can be seen, the value of ADE (N) after a certain loading cycle does not change significantly, and therefore any point within this period of fatigue life can be a good estimate for ADE. The starting point of this plateau (i.e., where ADE (N) stops changing significantly) is where the fatigue test can be stopped. The algorithm suggests that this plateau starts where the vertical distance of the prediction line and the N-ADE(N) line are equal to 2 standard deviations of the model (i.e., m=2). As can be seen in Figure 5.21, the larger the value of m is, the larger the prediction error in ADE and the shorter the fatigue test time (i.e., %N/Nf). At *m=2*, the error in estimating ADE from ADE (N) is 6% and the testing time is 25% of the total testing time.

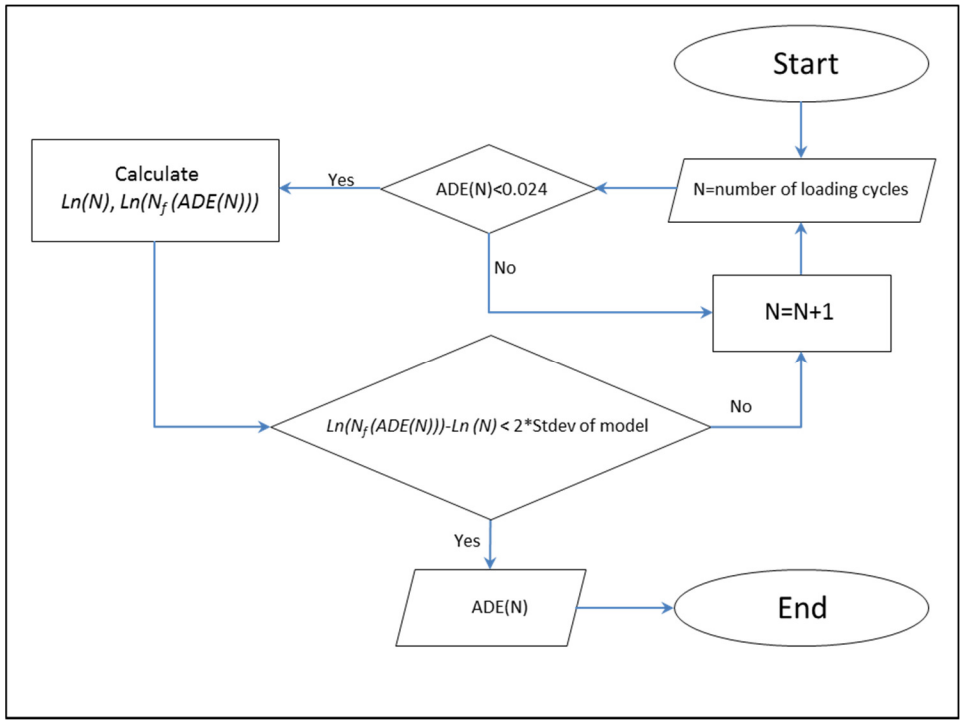

Figure 5.17: Algorithm to find ADE (N)

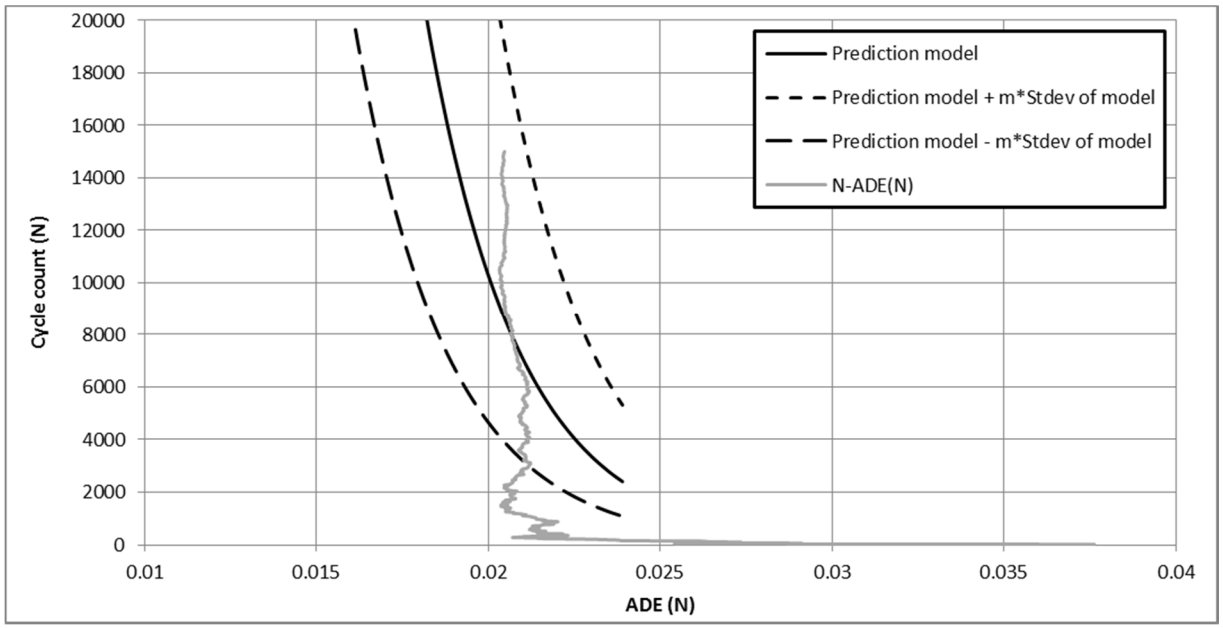

Figure 5.18: Estimation of ADE from N-ADE(N) curve (FRC8,0.8-5-1)

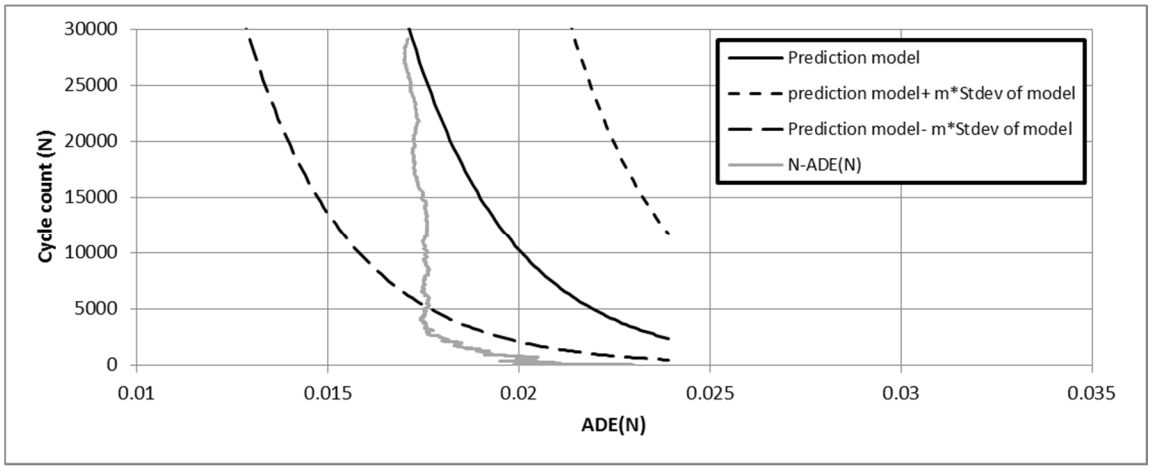

Figure 5.19: Estimation of ADE from N-ADE(N) curve (FRC8,0.7-5-1)

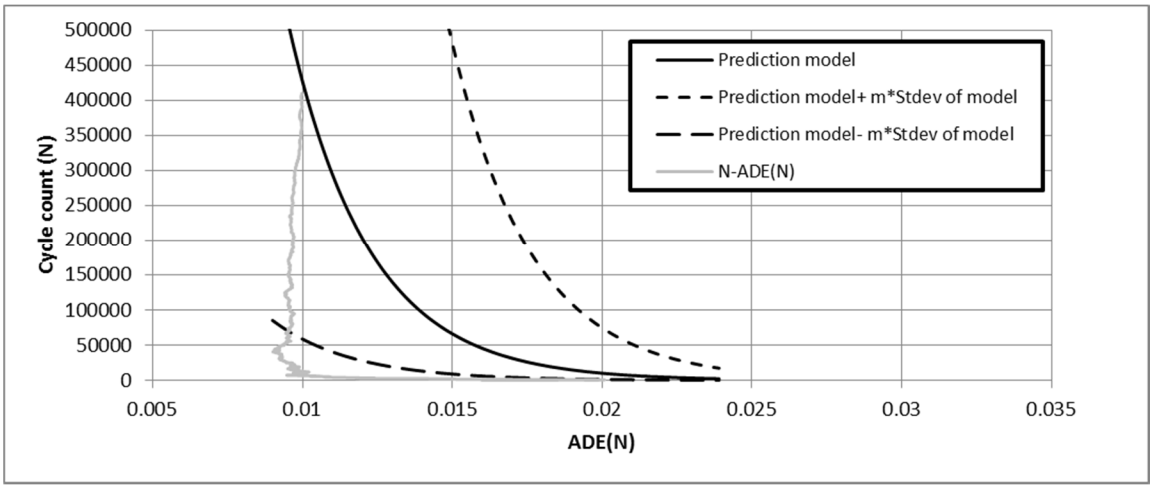

Figure 5.20: Estimation of ADE from N-ADE (N) curve (FRC8, 0.6-5-3)

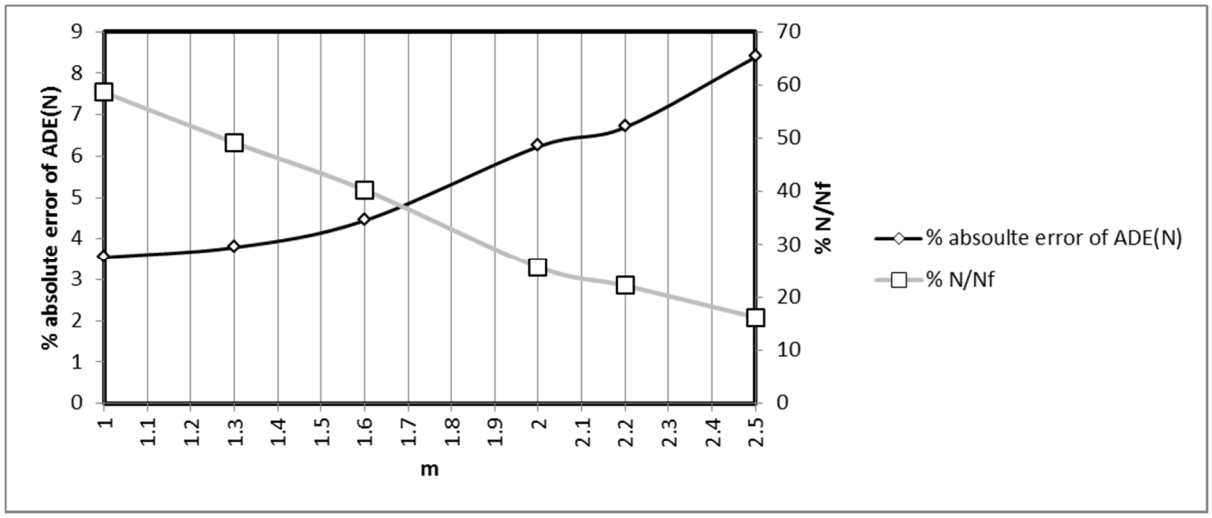

Figure 5.21: Effect of m on the absolute error of ADE (N) and the stopping time of fatigue test

Table 5-16: Comparison of fatigue life prediction results using ADE and ADE (N)

Stress Level	Sample ID	ADE (N)	ADE	Predicted Ln(Nf) (from ADE(N)) using Equation 7	Predicted Ln (Nf) (from ADE) using Equation 7	Actual Ln (Nf)	%Absolute error in Ln Nf (ADE(N))	%Absolute error in Ln Nf (ADE)
0.6	1	0.012236	0.012055	12.13	12.20	12.62	3.88	3.34
	2	0.011248	0.011321	12.50	12.47	12.51	0.12	0.34
	3	0.009569	0.009967	13.12	12.98	12.92	1.56	0.41
	4	0.010252	0.010057	12.87	12.94	11.68	10.16	10.78
	5	0.011111	0.010385	12.55	12.82	12.36	1.52	3.71
	6	0.010933	0.010260	12.62	12.87	13.56	6.96	5.11
0.7	1	0.017612	0.017101	10.13	10.32	10.28	1.47	0.38
	2	0.016744	0.018117	10.45	9.94	10.63	1.66	6.47
	3	0.015195	0.016502	11.03	10.54	10.33	6.76	2.05
	4	0.018841	0.016988	9.67	10.36	10.65	9.19	2.70
	5	0.020513	0.017191	9.05	10.28	9.90	8.65	3.85
	6	0.013349	0.013015	11.72	11.84	11.11	5.44	6.57
0.8	1	0.020623	0.020340	9.01	9.11	9.62	6.34	5.24
	2	0.023540	0.023997	7.92	7.75	6.41	23.48	20.82
	3	0.023794	0.021853	7.82	8.55	8.98	12.87	4.82
	4	0.025701	0.023173	7.11	8.06	7.13	0.18	13.04
	5	0.022115	0.022440	8.45	8.33	7.75	9.11	7.55
	6	0.022718	0.019821	8.23	9.31	10.33	20.34	9.89
						Average	7.20	5.95

A traditional S-N_f curve, the so-called Wohler's equation (i.e., $Ln\, N_f = a + b\, S$), along with Shi's formula (1993) (i.e., $Ln\,(EN) = a + b\, Ln\, S$, EN= N_f^{1-R}), which incorporates the effect of stress ratio on fatigue life, were calibrated for samples tested at 5 Hz frequency and compared to the new ADE-N_f approach. The regression analysis results of Wohler's equation (Equation 5.13) and Shi's formula (Equation 5.14) are presented in Table 5-17 and Table 5-18. Results for the overall F-test and *t*-test for both models indicate that both the regression model and the independent variables are significant (i.e., $F_{statistic}>F_{critical}$, $|t_{statistic}|>t_{critical}$).

Comparison of coefficients of determination (R^2) is one the most common methods of determining the predictive quality of two regression functions in which the independent variables are not the same. To compare the R^2 of these three methods, the new R^2 must be calculated for Shi's model, because the dependent variable in this model is not *Ln Nf* (instead, it is *Ln EN*), as opposed to the dependent variables of the other two methods. The process of adjusting R^2 is presented in Table 5-19. In this table, *Ln Nf* if calculated by dividing *Ln EN* by *1-R*. Unexplained and total variation of the model is calculated in columns 6 and 7. The R^2 is then calculated using Equation 5.12.

$$R^2 = 1 - \frac{Unexplaied\ variation}{Total\ variation} \qquad \textbf{5.12}$$

Table 5-17: Wohler's equation calibration (Nf vs. S, 5 Hz, α=0.05)

Regression Statistics	
R Square	0.740
Adjusted R Square	0.727
Standard Error	0.979
Observations	22

	df	*SS*	*MS*	$F_{statistic}$	*Significance F*	$F_{critical}$
Regression	1	54.59	54.59	56.92	2.8E-07	4.35
Residual	20	19.18	0.96			
Total	21	73.77				

	Coefficients	*Standard Error*	$T_{statistic}$	*P-value*	$T_{critical}$
Intercept	24.856	1.911	13.009	3.2E-11	2.42
S	-0.206	0.027	-7.545	2.8E-07	

$$Ln\ N_f = 24.856 - 0.206\ S \qquad \textbf{5.13}$$

Table 5-18: Shi's equation calibration (EN vs. S, 5 Hz, α=0.05)

Regression Statistics	
R Square	0.689
Adjusted R Square	0.674
Standard Error	0.837
Observations	22

	df	*SS*	*MS*	$F_{statistic}$	*Significance F*	$F_{critical}$
Regression	1	31.08	31.08	44.33	1.8E-06	4.35
Residual	20	14.02	0.70			
Total	21	45.10				

	Coefficients	*Std Error*	$T_{statistic}$	*P-value*	$T_{critical}$
Intercept	4.79	0.62	7.78	1.8E-07	2.42
Ln S	-10.62	1.60	-6.66	1.8E-06	

$$Ln\ EN = 4.79 - 10.62\ Ln\ S \qquad \textbf{5.14}$$

Table 5-19: Calculation of R^2 for Shi's formula (Equation 5.14) when *Ln Nf* is the dependent variable

Column Number	*1*	*2*	*3*	*4*	*5*	*6*	*7*
Observation	*Predicted Ln EN*	*R (stress ratio)*	*Predicted Ln Nf*	*Actual Ln Nf*	*Residuals*	*Unexplaned Variation*	*Total Variation*
1	7.135	0.157	8.468	9.616	1.147	1.317	0.830
2	7.123	0.159	8.468	6.413	-2.055	4.222	16.918
3	7.113	0.160	8.466	8.981	0.515	0.265	2.389
4	7.336	0.159	8.727	7.127	-1.600	2.561	11.558
5	7.301	0.158	8.674	7.745	-0.929	0.863	7.738
6	7.501	0.163	8.961	10.326	1.365	1.863	0.040
7	8.491	0.166	10.178	10.279	0.101	0.010	0.061
8	8.497	0.169	10.227	10.628	0.401	0.161	0.010
9	8.625	0.178	10.487	10.330	-0.157	0.025	0.039
10	8.553	0.174	10.351	10.648	0.297	0.088	0.015
11	8.546	0.167	10.264	9.903	-0.360	0.130	0.388
12	9.087	0.156	10.768	11.112	0.344	0.118	0.342
13	10.318	0.176	12.522	12.620	0.099	0.010	4.383
14	10.397	0.192	12.867	12.515	-0.353	0.124	3.952
15	10.379	0.184	12.721	12.923	0.203	0.041	5.744
16	10.431	0.182	12.755	11.684	-1.071	1.148	1.338
17	10.474	0.193	12.978	12.363	-0.615	0.378	3.371
18	10.544	0.191	13.039	13.561	0.521	0.272	9.205
19	8.437	0.167	10.129	11.939	1.811	3.278	1.996
20	8.488	0.171	10.244	10.504	0.260	0.068	0.000
21	8.452	0.166	10.138	8.917	-1.221	1.491	2.590
22	8.470	0.167	10.165	11.452	1.287	1.658	0.857
					Sum	20.090	73.765
						R square	0.728

The coefficient of determination of the exponential model incorporating ADE and N_f, the traditional Wohler's S-N_f equation, and Shi's formula are 0.83, 0.74, and 0.73, respectively. Relatively large R^2 value for the new ADE-N_f model compared to the other two models indicates that the new approach has better predictability.

The other method of comparison is the chi-square goodness of fit test. Chi-square, which is shown by Equation 5.15, is the measure of discrepancy between the

expected value of fatigue life (e_i) (i.e., fatigue life predicted by the model) and the observed value of fatigue life (O_i) obtained from experimental results.

$$\chi^2 = \sum_{i=1}^{N} \frac{(o_i - e_i)^2}{e_i} \quad \textbf{5.15}$$

The critical $\chi 2$ value at a significance level of α=0.05 with a degree of freedom of n=21 is 32.67. As can be seen from Table 5-20 to Table 5-22, the $\chi 2$ values of all three models are smaller than the critical value. This means that the null hypothesis is rejected and all three models are good estimators of observed data points. The lower $\chi 2$ value of the ADE-N_f model compared to the other two models is an indicator of this model's better predictability.

Table 5-20:Chi-square calculation (Wohler's S-Nf model)

Observation	Predicted Ln Nf (e_i)	Observed Ln Nf (O_i)	$\frac{(o_i - e_i)^2}{e_i}$
1	8.33	9.62	0.197
2	8.32	6.41	0.435
3	8.30	8.98	0.056
4	8.64	7.13	0.266
5	8.59	7.75	0.083
6	8.89	10.33	0.231
7	10.31	10.28	0.000
8	10.32	10.63	0.009
9	10.50	10.33	0.003
10	10.40	10.65	0.006
11	10.39	9.90	0.023
12	11.11	11.11	0.000
13	12.61	12.62	0.000
14	12.70	12.51	0.003
15	12.68	12.92	0.005
16	12.74	11.68	0.088
17	12.79	12.36	0.014
18	12.87	13.56	0.037
19	10.24	11.94	0.282
20	10.31	10.50	0.004
21	10.26	8.92	0.176
22	10.29	11.45	0.132
		Chi-square	2.049

Table 5-21: Chi-square calculation (Shi's S-Nf model)

Observation	Predicted Ln Nf (e_i)	Observed Ln Nf (O_i)	$\frac{(o_i - e_i)^2}{e_i}$
1	8.47	9.62	0.155
2	8.47	6.41	0.499
3	8.47	8.98	0.031
4	8.73	7.13	0.293
5	8.67	7.75	0.100
6	8.96	10.33	0.208
7	10.18	10.28	0.001
8	10.23	10.63	0.016
9	10.49	10.33	0.002
10	10.35	10.65	0.009
11	10.26	9.90	0.013
12	10.77	11.11	0.011
13	12.52	12.62	0.001
14	12.87	12.51	0.010
15	12.72	12.92	0.003
16	12.75	11.68	0.090
17	12.98	12.36	0.029
18	13.04	13.56	0.021
19	10.13	11.94	0.324
20	10.24	10.50	0.007
21	10.14	8.92	0.147
22	10.16	11.45	0.163
		Chi-square	2.131

Table 5-22: Chi-square calculation (ADE-Nf model)

Observation	Predicted Ln Nf (e_i)	Observed Ln Nf (O_i)	$\frac{(o_i - e_i)^2}{e_i}$
1	9.11	9.62	0.028
2	7.75	6.41	0.229
3	8.54	8.98	0.022
4	8.05	7.13	0.106
5	8.33	7.75	0.041
6	9.30	10.33	0.113
7	10.32	10.28	0.000
8	9.94	10.63	0.048
9	10.54	10.33	0.004
10	10.36	10.65	0.008
11	10.28	9.90	0.014
12	11.84	11.11	0.045
13	12.19	12.62	0.015
14	12.47	12.51	0.000
15	12.97	12.92	0.000
16	12.94	11.68	0.122
17	12.82	12.36	0.016
18	12.86	13.56	0.038
19	9.87	11.94	0.432
20	10.90	10.50	0.015
21	8.93	8.92	0.000
22	11.28	11.45	0.003
		Chi-square	1.299

5.3.6. Fatigue life prediction model incorporating fiber content

To examine the validity of the ADE-Nf approach for other mixtures, the exponential ADE-Nf model was calibrated for the mixture containing %0.4 fiber (FRC4), a combination of FRC4 and FRC8m and a combination of all three mixtures (i.e., Control, FRC4, and FRC8) .

The results of regression analysis and the calibrated model for the FRC4 mixture are shown in Table 5-23 and Equation 5.16. The graphical format of the model is presented in Figure 5.22. As can be seen, results for the *t*-test of the independent variable and also the F-test of the entire model (($F_{statistic}>F_{critical}$, $|t_{statistic}|>t_{critical}$) indicates that both the model and that independent variables are significant at α=0.05. Furthermore, the model has a very high coefficient of determination (R^2=0.956), which is an indicator of good predictability.

Table 5-23: Exponential model (Nf vs. ADE, FRC4, α=0.05)

Regression Statistics	
R Square	0.956
Adjusted R Square	0.945
Standard Error	0.526
Observations	6

	Degree of freedom	*SS*	*MS*	$F_{statistic}$	*Significance F*	$F_{critical}$
Regression	1	24.143	24.143	87.353	0.001	7.71
Residual	4	1.106	0.276			
Total	5	25.249				

	Coefficients	*Std Error*	$T_{statistic}$	*P-value*	$T_{critical}$
Intercept	19.854	1.178	16.848	7.28E-05	3.50
ADE	-633.507	67.782	-9.346	7.30E-04	

$$N_f = e^{19.854-633.5\,ADE} \qquad \textbf{5.16}$$

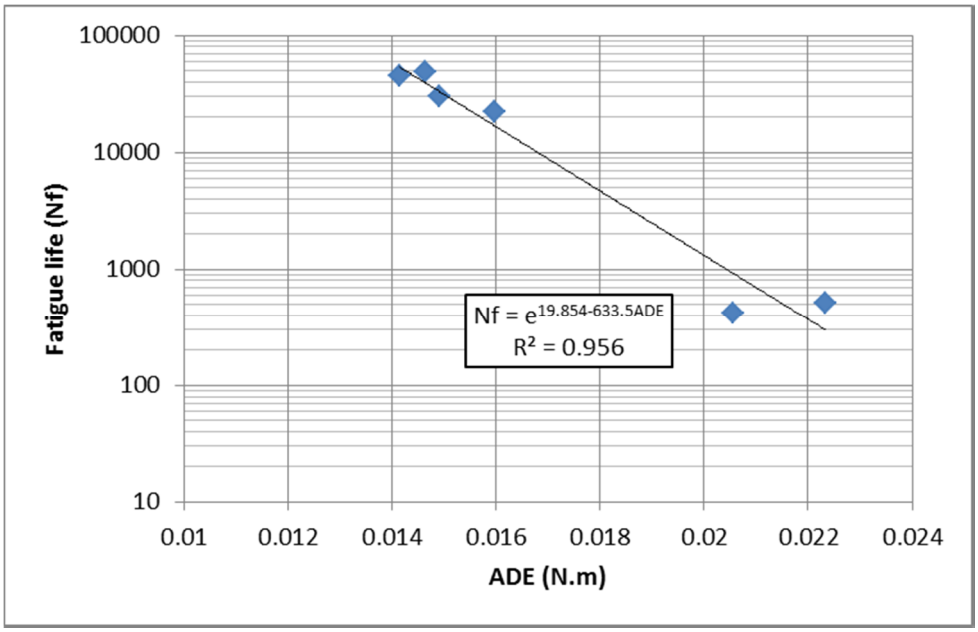

Figure 5.22: Exponential model (Nf vs. ADE, FRC4)

ADE-Nf for the exponential model is then calibrated for the FRC4 and FRC8 samples together. The regression analysis and the calibrated model are shown in Table 5-24 and Equation 5.17. The graphical format of the model is presented in Figure 5.23. The result of the overall F-test on the model shows that the null hypothesis is rejected (i.e., $F_{statistic}$= 88.00 >$F_{critical}$=4.23), and therefore there is no evidence that the model was obtained by chance. The null hypothesis of the *t*-test for the intercept and independent variable (i.e., ADE) is rejected (i.e., $t_{statistic}$>$t_{critical}$), and therefore the independent variables are significant. Although the R^2 of the exponential fatigue life model that includes the FRC8 samples (Equation 5.7, R^2=0.83) has been decreased to 0.77 by incorporating FRC4 samples in the model (i.e., the combination of FRC4 and FRC8), the model is still shown to be statistically reliable.

Table 5-24: Exponential model (Nf vs. ADE, FRC4 and FRC8, α=0.05)

Regression Statistics	
R Square	0.772
Adjusted R Square	0.763
Standard Error	0.981
Observations	28

	df	*SS*	*MS*	$F_{statistic}$	*Significance F*	$F_{critical}$
Regression	1	84.65	84.65	88.00	7.89E-10	4.23
Residual	26	25.01	0.96			
Total	27	109.66				

	Coefficients	*Std Error*	$T_{statistic}$	*P-value*	$T_{critical}$
Intercept	17.04	0.75	22.66	1.21E-18	2.38
ADE	-410.70	43.78	-9.38	7.89E-10	

$$N_f = e^{17.04-410.70\ ADE} \qquad \textbf{5.17}$$

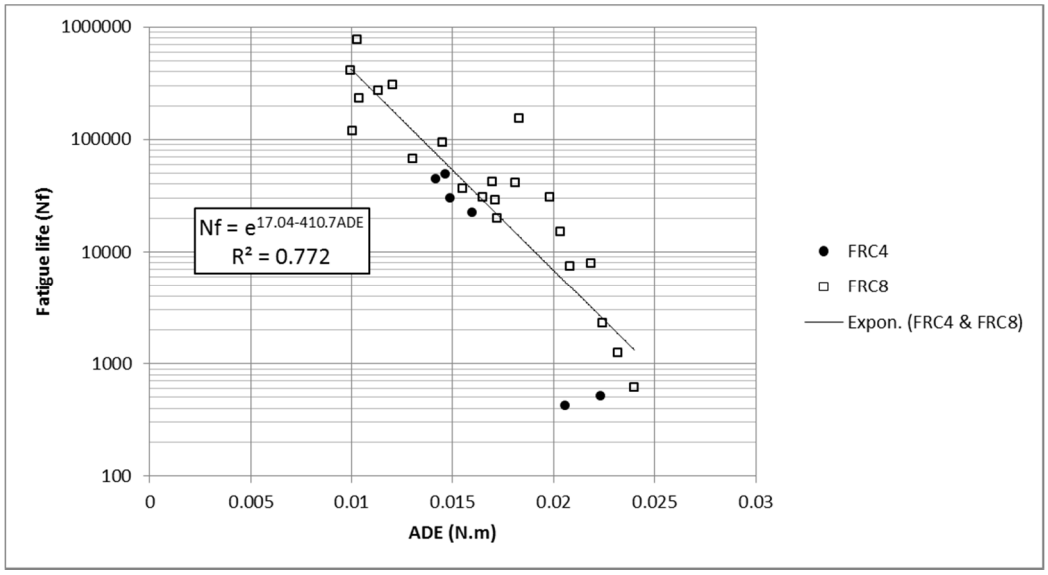

Figure 5.23: Exponential model (Nf vs. ADE, FRC4 and FRC8)

Incorporating control samples in the exponential fatigue life model reduces the R^2 even more. However, the model (Equation 5.18) still has an acceptable prediction quality (R^2=0.753, Table 5-25). The regression analysis and calibrated exponential model for all samples (i.e., Control, FRC4, and FRC8) are shown in Table 5-25 and Equation 5.18. The graphical format of the model is presented in Figure 5.24.

Table 5-25: Exponential model (Nf vs. ADE, control, FRC4 and FRC8, α=0.05)

Regression Statistics	
R Square	0.753
Adjusted R Square	0.745
Standard Error	0.943
Observations	34

	df	*SS*	*MS*	*F*	*Significance F*	$F_{critical}$
Regression	1	86.71	86.71	97.56	3.07E-11	4.15
Residual	32	28.44	0.89			
Total	33	115.15				

	Coefficients	*Standard Error*	$T_{statistic}$	*P-value*	$T_{critical}$
Intercept	17.124	0.713	24.008	4.9E-22	2.35
ADE	-414.218	41.937	-9.877	3.1E-11	

$$N_f = e^{17.124-414.218\ ADE} \qquad \textbf{5.18}$$

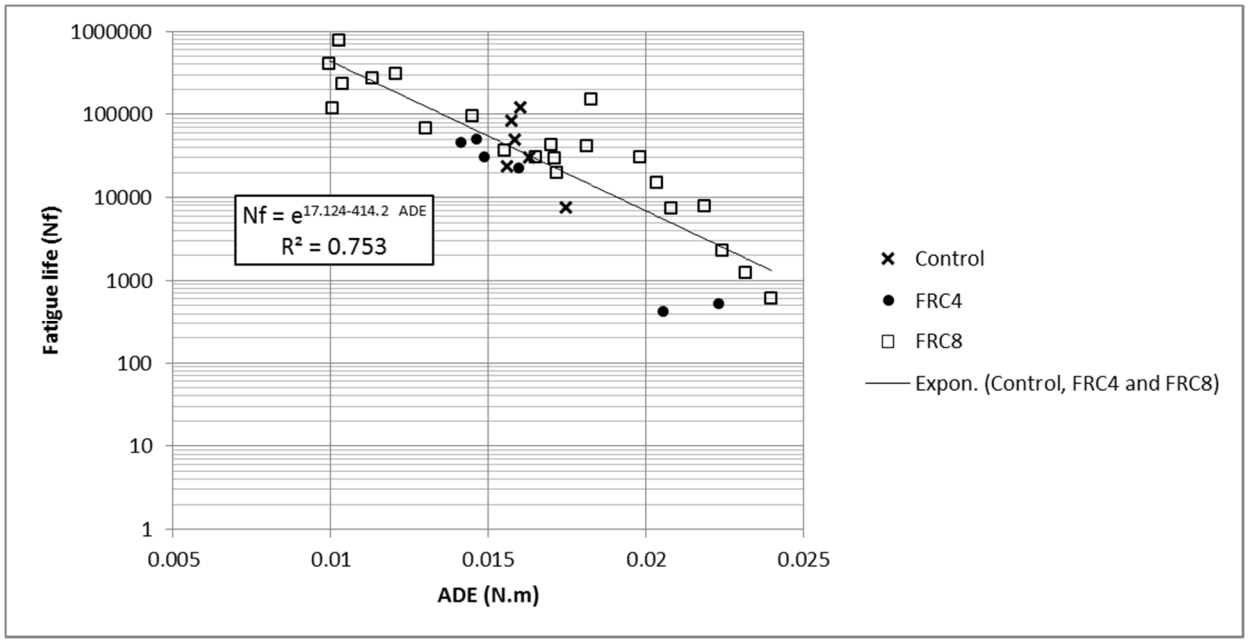

Figure 5.24: Exponential model (Nf vs. ADE, Control, FRC4, and FRC8)

5.4. Loading Characteristics and ADE Relationship

In this section it is tried to develop a statistical model to relate ADE to loading characteristics such as stress level (S) and frequency of loading (f). Different mathematical models such as linear, exponential, and power were assessed as possible regression models for ADE versus stress level.

5.4.1. Linear Model

Regression analysis was performed to find the coefficients of the linear model (i.e., *a* and *b* in Equation 5.19), and the results are shown in Table 5-26 and Table 5-28 for samples tested at frequencies of 5 and 10 Hz, respectively. The overall F-test confirms the validity of the model, as $F_{statistic}$ is larger than $F_{critical}$. The *t*-test on the independent variable also shows the significance of the variable in the model. Relatively high values

for the coefficient of determination (R^2) for both models shows very good predictability of the linear model.

No influential data point was detected, as all Cook's distance values are smaller than $F_{0.5,p,n-p}$ (Table 5-27 and Table 5-29).

$$ADE = a\,S + b \qquad \textbf{5.19}$$

Table 5-26: Regression analysis for linear model (ADE vs. S, 5 Hz, α=0.05)

Regression Statistics	
R Square	0.904
Adjusted R Square	0.899
Standard Error	0.001
Observations	22

	Degree of freedom	*SS*	*MS*	$F_{statistic}$	*Significance F*	$F_{critical}$
Regression	1	0.000	0.000	187.96	1.2E-11	4.35
Residual	20	0.000	0.000			
Total	21	0.000				

	Coefficients	*Std Error*	$T_{statistic}$	*P-value*	$T_{critical}$
Intercept	-0.02215	0.003	-7.804	1.71E-07	2.42
S (%)	0.000556	0.000	13.710	1.25E-11	

Table 5-27: Outlier detection, linear model (ADE vs. S, 5 Hz)

Observation	*Predicted ADE*	*Residuals*	*Std Residuals*	$h_{i,i}$	C_i	$F_{0.5:p,n-p}$
1	0.02245	-0.00211	-1.488	0.1335	0.1706	0.718
2	0.02250	0.00149	1.053	0.1350	0.0865	0.718
3	0.02255	-0.00069	-0.489	0.1364	0.0189	0.718
4	0.02162	0.00156	1.095	0.1105	0.0745	0.718
5	0.02176	0.00068	0.477	0.1142	0.0146	0.718
6	0.02095	-0.00112	-0.792	0.0944	0.0327	0.718
7	0.01711	-0.00001	-0.005	0.0463	0.0000	0.718
8	0.01708	0.00103	0.727	0.0462	0.0128	0.718
9	0.01662	-0.00012	-0.081	0.0455	0.0002	0.718
10	0.01688	0.00011	0.077	0.0458	0.0001	0.718
11	0.01691	0.00028	0.200	0.0458	0.0010	0.718
12	0.01497	-0.00195	-1.374	0.0516	0.0514	0.718
13	0.01090	0.00115	0.810	0.1251	0.0469	0.718
14	0.01066	0.00066	0.466	0.1321	0.0165	0.718
15	0.01072	-0.00075	-0.527	0.1305	0.0209	0.718
16	0.01055	-0.00050	-0.350	0.1353	0.0096	0.718
17	0.01042	-0.00004	-0.026	0.1393	0.0001	0.718
18	0.01021	0.00005	0.036	0.1459	0.0001	0.718
19	0.01731	0.00098	0.689	0.0470	0.0117	0.718
20	0.01712	-0.00160	-1.125	0.0463	0.0308	0.718
21	0.01725	0.00357	2.517	0.0468	0.1554	0.718
22	0.01719	-0.00268	-1.888	0.0465	0.0870	0.718

$$ADE = 5.56 * 10^{-4} S - 2.215 * 10^{-2} \quad \textbf{5.20}$$

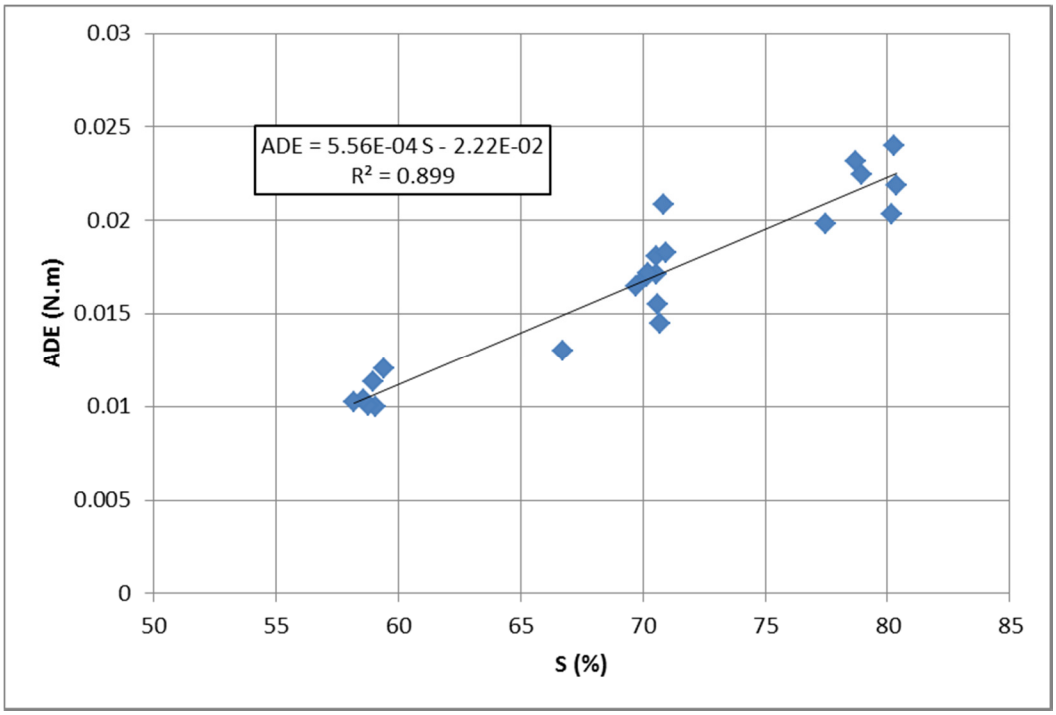

Figure 5.25: Linear model (ADE vs. S, FRC8, 5 Hz)

Table 5-28: Regression analysis for linear model (ADE vs. S, 10 Hz, α=0.05)

Regression Statistics	
R Square	0.851
Adjusted R Square	0.841
Standard Error	0.002
Observations	17

	Degree of freedom	*SS*	*MS*	$F_{statistic}$	*Significance F*	$F_{critical}$
Regression	1	0.00048	0.0004846	85.77	1.36E-07	4.54
Residual	15	0.00008	0.0000057			
Total	16	0.00057				

	Coefficients	*Standard Error*	$T_{statistic}$	*P-value*	$T_{critical}$
Intercept	-0.033608	0.006	-5.40	7.31E-05	2.49
S	0.000822	0.000	9.26	1.36E-07	

Table 5-29: Outlier detection, linear model (ADE vs. S, 10 Hz)

Observation	*Predicted ADE*	*Residuals*	*Standard Residuals*	$h_{i,i}$	C_i	$F_{0.5:p,n-p}$
1	0.0301	0.0005	0.2277	0.1418	0.0043	0.7262
2	0.0295	0.0010	0.4510	0.1278	0.0149	0.7262
3	0.0289	-0.0011	-0.4598	0.1149	0.0137	0.7262
4	0.0307	0.0026	1.1104	0.1602	0.1176	0.7262
5	0.0301	0.0040	1.7467	0.1416	0.2516	0.7262
6	0.0293	0.0006	0.2546	0.1228	0.0045	0.7262
7	0.0231	-0.0032	-1.3809	0.0597	0.0606	0.7262
8	0.0255	-0.0048	-2.0645	0.0654	0.1491	0.7262
9	0.0243	-0.0013	-0.5454	0.0594	0.0094	0.7262
10	0.0238	-0.0017	-0.7309	0.0588	0.0167	0.7262
11	0.0225	-0.0008	-0.3590	0.0618	0.0042	0.7262
12	0.0226	-0.0026	-1.1130	0.0617	0.0407	0.7262
13	0.0151	0.0012	0.5237	0.2141	0.0374	0.7262
14	0.0166	0.0003	0.1445	0.1649	0.0021	0.7262
15	0.0166	0.0032	1.3755	0.1649	0.1868	0.7262
16	0.0174	0.0001	0.0270	0.1405	0.0001	0.7262
17	0.0175	0.0018	0.7925	0.1396	0.0510	0.7262

$$ADE = 8.22 * 10^{-4} S - 3.361 * 10^{-2} \quad \textbf{5.21}$$

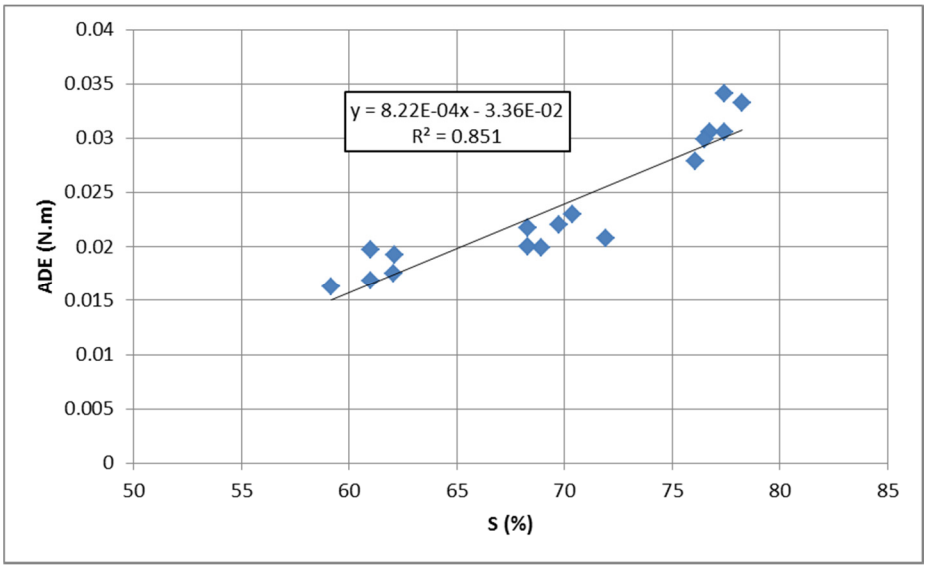

Figure 5.26: Linear model (ADE vs. S, FRC8, 10 Hz)

5.4.2. Exponential Model

The exponential model shown by Equation 5.22 is linearized (Equation 5.23) by taking the logarithm of each side, then the coefficients of the linearized model (i.e., *Ln a* and *Ln b*) are calculated using the least squares regression method. Regression analysis results are presented in Table 5-30 and Table 5-32 for samples tested at frequencies of 5 and 10 Hz, respectively. The calibrated formula and the graphical format of models are shown in Equation 5.24 and 5.25 and Figure 5.27 and Figure 5.28. Results for the overall F-test of the model and the *t*-test of the independent variable show that both the model and the independent variables are significant at α=0.05 (i.e., $F_{statistic}>F_{critical}$ and $|t_{statistic}|>t_{critical}$. The coefficients of determination (R^2) for 5 and 10 Hz exponential models are 0.91 and 0.88, respectively. This reflects the excellent predictability of the exponential model.

Outlier detection was performed based on Cook's distance method and is presented in Table 5-31 and Table 5-33. No influential data points are detected.

$$ADE = a\, b^S \qquad \textbf{5.22}$$

$$Ln\, ADE = Ln\, a + S\, Ln\, b \qquad \textbf{5.23}$$

Table 5-30: Regression analysis for exponential model (ADE vs. S, 5 Hz, α=0.05)

Regression Statistics	
R Square	0.911
Adjusted R Square	0.907
Standard Error	0.090
Observations	22

	df	*SS*	*MS*	$F_{statistic}$	*Significance F*	$F_{critical}$
Regression	1	1.648	1.648	205.03	5.65E-12	4.35
Residual	20	0.161	0.008			
Total	21	1.809				

	Coefficients	*Standard Error*	$T_{statistic}$	*P-value*	$T_{critical}$
Intercept	-6.6320	0.1750	-37.91	4.21E-20	2.42
S	0.0358	0.0025	14.32	5.65E-12	

Table 5-31: Outlier detection, exponential model (ADE vs. S, 5 Hz)

Observation	*Predicted Ln ADE*	*Residuals*	*Std Residuals*	$h_{i,i}$	C_i	$F_{0.5:p,n-p}$
1	-3.761	-0.1343	-1.535	0.1335	0.1816	0.718
2	-3.758	0.0278	0.318	0.1350	0.0079	0.718
3	-3.755	-0.0687	-0.785	0.1364	0.0487	0.718
4	-3.815	0.0498	0.569	0.1105	0.0201	0.718
5	-3.805	0.0083	0.095	0.1142	0.0006	0.718
6	-3.858	-0.0632	-0.722	0.0944	0.0272	0.718
7	-4.105	0.0363	0.414	0.0463	0.0042	0.718
8	-4.106	0.0954	1.090	0.0462	0.0288	0.718
9	-4.136	0.0322	0.368	0.0455	0.0032	0.718
10	-4.120	0.0443	0.507	0.0458	0.0062	0.718
11	-4.118	0.0544	0.622	0.0458	0.0093	0.718
12	-4.243	-0.0989	-1.131	0.0516	0.0348	0.718
13	-4.504	0.0859	0.981	0.1251	0.0688	0.718
14	-4.520	0.0388	0.444	0.1321	0.0150	0.718
15	-4.516	-0.0922	-1.053	0.1305	0.0833	0.718
16	-4.527	-0.0728	-0.832	0.1353	0.0541	0.718
17	-4.535	-0.0321	-0.367	0.1393	0.0109	0.718
18	-4.549	-0.0306	-0.349	0.1459	0.0104	0.718
19	-4.092	0.0904	1.033	0.0470	0.0263	0.718
20	-4.104	-0.0614	-0.702	0.0463	0.0120	0.718
21	-4.096	0.2240	2.560	0.0468	0.1607	0.718
22	-4.100	-0.1334	-1.524	0.047	0.0567	0.718

$$ADE = e^{0.0358\,S-6.632} \quad \textbf{5.24}$$

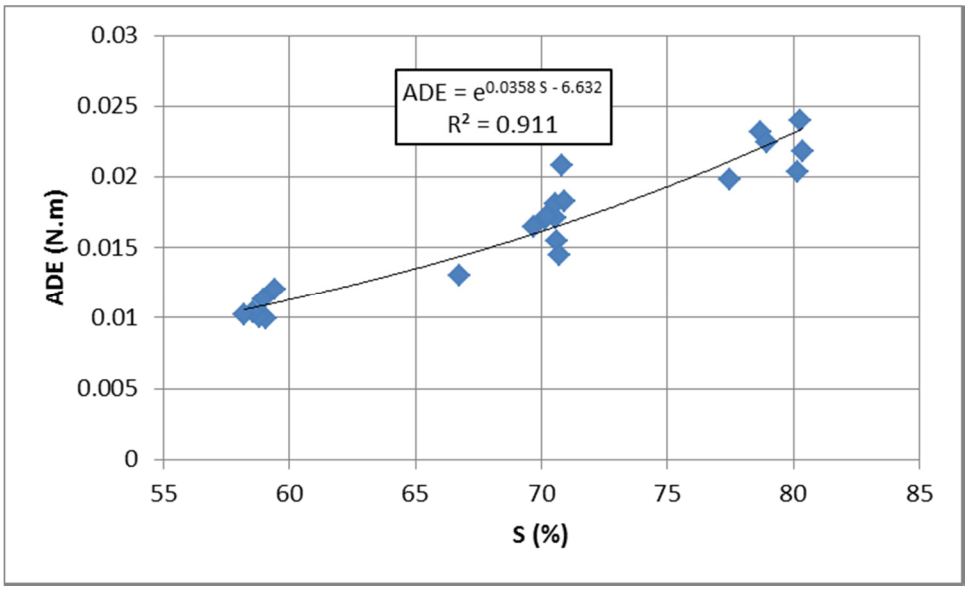

Figure 5.27: Exponential model (ADE vs. S, FRC8, 5 Hz)

Table 5-32: Regression analysis for exponential model (ADE vs. S, 10 Hz, α=0.05)

Regression Statistics	
R Square	0.884
Adjusted R Square	0.877
Standard Error	0.086
Observations	17

	Degree of freedom	*SS*	*MS*	$F_{statistic}$	*Significance F*	$F_{critical}$
Regression	1	0.849	0.849	114.78	2.00E-08	4.54
Residual	15	0.111	0.007			
Total	16	0.959				

	Coefficients	*Standard Error*	$T_{statistic}$	*P-value*	$T_{critical}$
Intercept	-6.1691	0.2249	-27.42	3.12E-14	2.49
S	0.0344	0.0032	10.71	2.00E-08	

Table 5-33: Outlier detection, Exponential model (ADE vs. S, 10 Hz)

Observation	*Predicted Ln ADE*	*Residuals*	*Std Residuals*	$h_{i,i}$	C_i	$F_{0.5:p,n-p}$
1	-3.504	0.017	0.209	0.142	0.004	0.726
2	-3.528	0.039	0.472	0.128	0.016	0.726
3	-3.551	-0.028	-0.338	0.115	0.007	0.726
4	-3.476	0.074	0.889	0.160	0.075	0.726
5	-3.504	0.126	1.510	0.142	0.188	0.726
6	-3.536	0.026	0.315	0.123	0.007	0.726
7	-3.797	-0.120	-1.442	0.060	0.066	0.726
8	-3.695	-0.180	-2.156	0.065	0.163	0.726
9	-3.747	-0.025	-0.294	0.059	0.003	0.726
10	-3.768	-0.045	-0.537	0.059	0.009	0.726
11	-3.819	-0.010	-0.124	0.062	0.001	0.726
12	-3.819	-0.093	-1.123	0.062	0.041	0.726
13	-4.133	0.014	0.166	0.214	0.004	0.726
14	-4.070	-0.011	-0.133	0.165	0.002	0.726
15	-4.070	0.144	1.729	0.165	0.295	0.726
16	-4.033	-0.012	-0.149	0.140	0.002	0.726
17	-4.031	0.084	1.006	0.140	0.082	0.726

$$ADE = e^{0.0344\ S - 6.1691} \qquad \textbf{5.25}$$

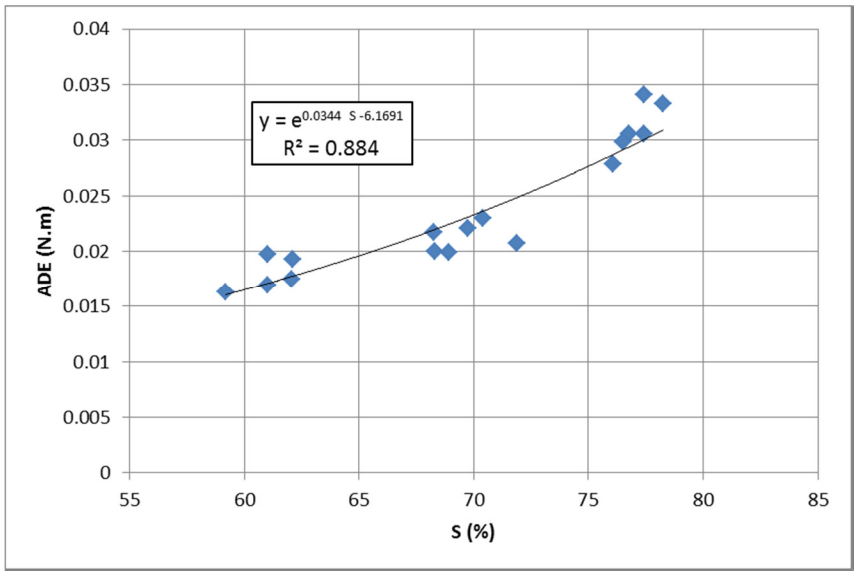

Figure 5.28: Exponential model (ADE vs. S, FRC8, 10 Hz)

5.4.3. Power Model

The power model, as shown by Equation 5.26, was assessed to find the relationship between ADE and S. The model was linearized by taking the logarithm of each side, as shown in Equation 5.27. Least squares regression analysis was performed to find the coefficient of the linearized model (i.e., *Ln a* and *b*). Regression analysis results are shown in Table 5-34 and Table 5-36 for frequencies of 5 and 10 Hz, respectively. As can be seen, for both models, the $F_{statistic}$ of the model and the $t_{statistic}$ of the independent variable are larger than the critical value, and hence the model and independent variable are significant. A relatively large coefficient of determination is an indicator of goodness of fit of the power model. As the outlier detection procedure presented in Table 5-35 and Table 5-37shows, no outlier was detected based on Cook's distance method.

$$ADE = a\,S^{b} \qquad \textbf{5.26}$$

$$Ln\,ADE = Ln\,a + b\,Ln\,S \qquad \textbf{5.27}$$

Table 5-34: Regression analysis for power model (ADE vs. S, 5 Hz, α=0.05)

Regression Statistics	
R Square	0.918
Adjusted R Square	0.914
Standard Error	0.086
Observations	22

	Degree of freedom	*SS*	*MS*	$F_{statistic}$	*Significance F*	$F_{critical}$
Regression	1	1.661	1.661	224.00	2.51E-12	4.35
Residual	20	0.148	0.007			
Total	21	1.809				

	Coefficients	*Standard Error*	$T_{statistic}$	*P-value*	$T_{critical}$
Intercept	-14.544	0.695	-20.92	4.57E-15	2.42
Ln S	2.456	0.164	14.97	2.51E-12	

Table 5-35: Outlier detection, power model (ADE vs. S, 5 Hz)

Observation	*Predicted Ln ADE*	*Residuals*	*Std Residuals*	$h_{i,i}$	C_i	$F_{0.5:p,n-p}$
1	-3.7770	-0.1181	-1.4058	0.1256	0.1419	0.718
2	-3.7743	0.0445	0.5290	0.1268	0.0203	0.718
3	-3.7718	-0.0516	-0.6141	0.1279	0.0277	0.718
4	-3.8234	0.0586	0.6978	0.1065	0.0290	0.718
5	-3.8153	0.0184	0.2186	0.1097	0.0029	0.718
6	-3.8614	-0.0596	-0.7088	0.0928	0.0257	0.718
7	-4.0905	0.0219	0.2602	0.0470	0.0017	0.718
8	-4.0919	0.0810	0.9634	0.0470	0.0229	0.718
9	-4.1213	0.0171	0.2031	0.0457	0.0010	0.718
10	-4.1048	0.0295	0.3516	0.0463	0.0030	0.718
11	-4.1031	0.0397	0.4723	0.0464	0.0054	0.718
12	-4.2282	-0.1134	-1.3499	0.0499	0.0479	0.718
13	-4.5128	0.0945	1.1245	0.1283	0.0930	0.718
14	-4.5310	0.0500	0.5944	0.1366	0.0280	0.718
15	-4.5268	-0.0816	-0.9714	0.1347	0.0734	0.718
16	-4.5389	-0.0605	-0.7203	0.1404	0.0424	0.718
17	-4.5490	-0.0185	-0.2197	0.1452	0.0041	0.718
18	-4.5650	-0.0145	-0.1725	0.1532	0.0027	0.718
19	-4.0780	0.0764	0.9089	0.0479	0.0208	0.718
20	-4.0898	-0.0758	-0.9019	0.0471	0.0201	0.718
21	-4.0815	0.2099	2.4977	0.0477	0.1561	0.718
22	-4.0856	-0.1477	-1.7571	0.0474	0.0767	0.718

$$ADE = e^{-14.544} S^{2.456} \quad \textbf{5.28}$$

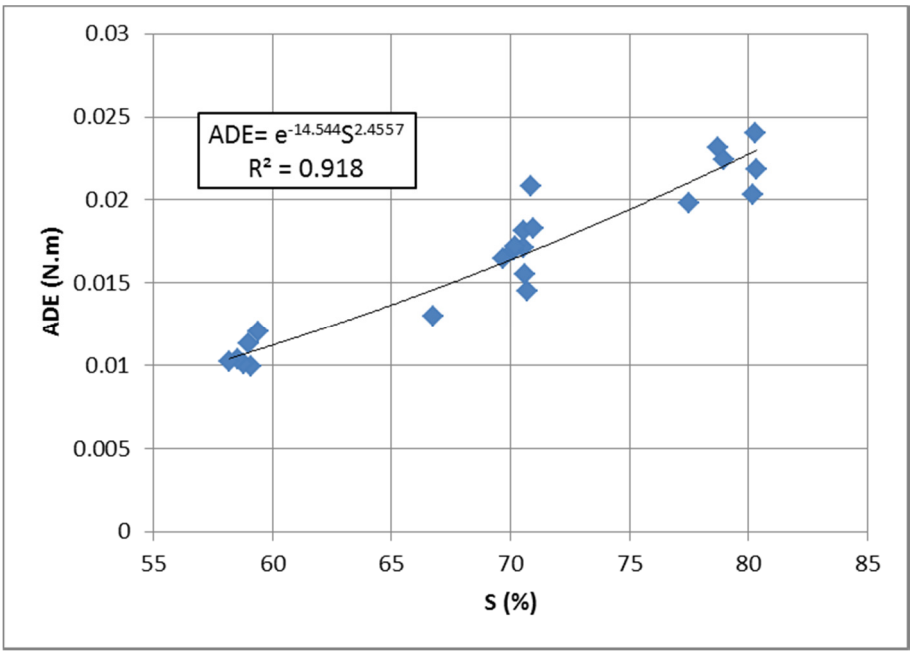

Figure 5.29: Power model (ADE vs. S, FRC8, 5 Hz)

Table 5-36: Regression analysis for power model (ADE vs. S, 10 Hz, α=0.05)

Regression Statistics	
R Square	0.868
Adjusted R Square	0.859
Standard Error	0.092
Observations	17

	Degree of freedom	*SS*	*MS*	$F_{statistic}$	*Significance F*	$F_{critical}$
Regression	1	0.833	0.833	98.39	5.56E-08	4.54
Residual	15	0.127	0.008			
Total	16	0.959				

	Coefficients	*Standard Error*	$T_{statistic}$	*P-value*	$T_{critical}$
Intercept	-13.699	1.001	-13.68	7.07E-10	2.49
Ln S	2.342	0.236	9.92	5.56E-08	

Table 5-37: Outlier detection, Power model (ADE vs. S, 10 Hz)

Observation	*Predicted Ln ADE*	*Residuals*	*Std Residuals*	$h_{i,i}$	C_i	$F_{0.5:p,n-p}$
1	-3.514	0.027	0.301	0.138	0.007	0.726
2	-3.534	0.046	0.516	0.125	0.019	0.726
3	-3.555	-0.024	-0.271	0.114	0.005	0.726
4	-3.489	0.087	0.976	0.153	0.086	0.726
5	-3.514	0.135	1.516	0.137	0.183	0.726
6	-3.542	0.032	0.358	0.121	0.009	0.726
7	-3.786	-0.131	-1.470	0.059	0.068	0.726
8	-3.687	-0.187	-2.099	0.067	0.158	0.726
9	-3.737	-0.034	-0.384	0.060	0.005	0.726
10	-3.758	-0.055	-0.618	0.059	0.012	0.726
11	-3.808	-0.021	-0.239	0.061	0.002	0.726
12	-3.808	-0.105	-1.174	0.061	0.044	0.726
13	-4.143	0.025	0.276	0.227	0.011	0.726
14	-4.072	-0.009	-0.097	0.169	0.001	0.726
15	-4.072	0.146	1.643	0.169	0.274	0.726
16	-4.031	-0.014	-0.156	0.141	0.002	0.726
17	-4.030	0.082	0.923	0.140	0.069	0.726

$$ADE = e^{-13.699}S^{2.342} \qquad \textbf{5.29}$$

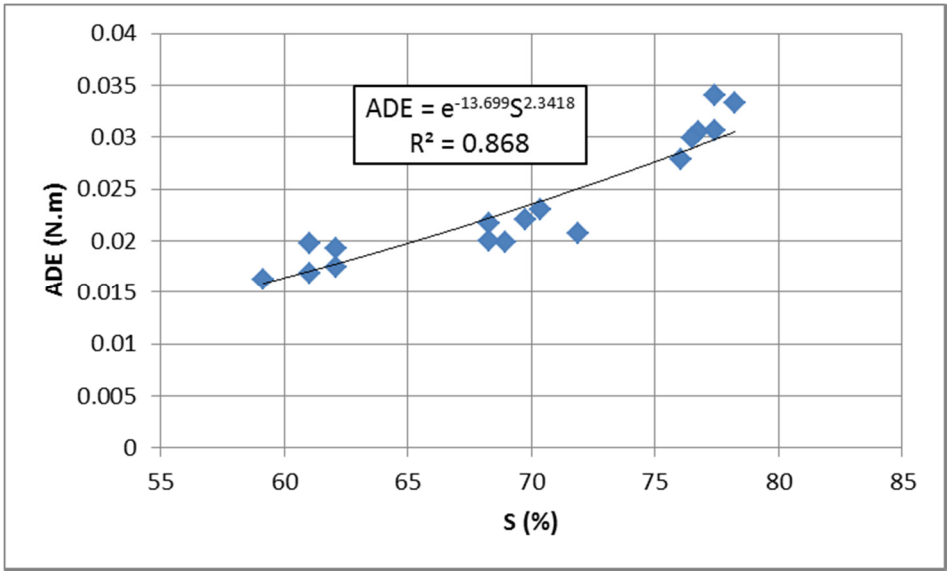

Figure 5.30: Power model (ADE vs. S, FRC8, 10 Hz)

5.4.4. Evaluating the effect of frequency of loading on ADE

To evaluate the effect of loading frequency (f) on ADE, a multivariate linear model was formed, as shown by Equation 5.30. Regression analysis results are presented in Table 5-38. As can be seen, the $t_{statistic}$=10.42 of loading frequency is smaller than the $t_{critical}$=3.34. This indicates that loading frequency is significant in the model. The positive coefficient of loading frequency (b=0.0014) shows that there is direct relationship between ADE and loading frequency. In other words, increasing the loading frequency increases the ADE.

$$ADE = a\,S + b\,f + c \qquad \textbf{5.30}$$

Table 5-38: Multivariate regression analysis (ADE, S, and f, α=0.05)

Regression Statistics	
R Square	0.894
Adjusted R Square	0.888
Standard Error	0.002
Observations	39

	Degree of freedom	*SS*	*MS*	$F_{statistic}$	*Significance F*	$F_{critical}$
Regression	2	0.001347342	0.000674	151.9	2.83E-18	3.26
Residual	36	0.000159674	4.44E-06			
Total	38	0.001507015				

	Coefficients	*Std Error*	$T_{statistic}$	*P-value*	$T_{critical}$
Intercept	-0.0359	0.0034	-10.47	1.78E-12	2.34
S	0.0007	0.0000	13.84	5.49E-16	
f	0.0014	0.0001	10.42	2.07E-12	

$$ADE = 0.0007\,S + 0.0014\,f - 0.0359 \quad \textbf{5.31}$$

5.5. Combined effect of freeze-thaw and fatigue

To study the effect of frost damage on the fatigue behavior of fiber-reinforced concrete, concrete samples were exposed to freezing and thawing cycles of 200 and 400 and then tested at a loading condition of S=0.7 and frequency of 5 Hz. The maximum cyclic load is determined based on 70% of the maximum load that an undamaged sample (i.e., the sample that has not experienced a freeze-thaw cycle) of the same age can take. After completion of the fatigue test, the two ends of the broken samples were cut and tested in accordance with ASTM C642 to determine density, absorption, and void content. The testing approach is detailed in Chapter 3. The results of fatigue testing, as well as the density, absorption, and void content of concrete samples, are presented in Table 5-39.

Table 5-39. Fatigue Test and Volumetric Analysis (reeze-thaw exposed samples)

F/T Cycle	Nf	ADE (N.m)	Absorption after Immersion (%)	Absorption after Boiling (%)	Bulk Dry Density (gr/cm^3)	Bulk Density after Immersion (gr/cm^3)	Bulk Density after Boiling (gr/cm^3)	Apparent Density (gr/cm^3)	Void Content (%)
0	94110	0.01450	5.70	5.95	2.18	2.30	2.31	2.50	12.94
0	153175	0.01829	6.22	6.39	2.08	2.21	2.21	2.39	13.27
0	7460	0.02083	6.08	6.51	2.11	2.24	2.25	2.44	13.72
0	36475	0.01552	5.93	6.19	2.15	2.27	2.28	2.48	13.29
200	13960	0.01974	6.14	6.54	2.12	2.25	2.26	2.47	13.89
200	33580	0.01918	5.94	5.97	2.17	2.30	2.30	2.49	12.94
200	35235	0.01911	6.04	6.15	2.11	2.24	2.24	2.43	12.99
200	85845	0.01757	5.66	5.68	2.15	2.27	2.27	2.45	12.20
200	165	0.03329	6.40	6.63	2.08	2.22	2.22	2.42	13.81
200	45	0.03463	6.08	6.37	2.11	2.24	2.25	2.44	13.47
400	11400	0.02439	5.82	6.19	2.14	2.26	2.27	2.46	13.24
400	107125	0.01894	5.55	5.72	2.18	2.30	2.31	2.49	12.49
400	1975	0.02808	5.40	5.67	2.18	2.30	2.31	2.49	12.36
400	830	0.03308	5.65	5.99	2.16	2.28	2.29	2.48	12.92
400	495	0.03196	5.67	6.11	2.17	2.29	2.30	2.50	13.27

5.5.1. Application of ADE in Fatigue Life Prediction Model of Freeze-thaw Exposed Concrete

In this section the new fatigue life model (Nf-ADE) is calibrated for the freeze-thaw exposed samples to examine the validity of this approach. All data points, including the frost-damaged samples and the samples that have not experienced any freezing and thawing, were treated as one data set (Table 5-40). It must be added that all these samples are from the same mixture (i.e., FRC8) and were tested at S=0.7 and a frequency of 5 Hz; therefore, treating them as one data set regardless of severity of frost damage is the first step in evaluating whether the same ADE-N_f model that was developed for undamaged samples is capable of predicting the fatigue life of frost-damaged samples.

Then it is tried to incorporate other parameters, such as number of freeze-thaw cycles and void content, to create a more precise fatigue-life prediction model for the combined effects of fatigue and freeze-thaw damage.

5.5.2. Exponential Model (Freeze-thaw Exposed Samples)

Regression analysis results for the exponential model, which incorporate ADE as an independent variable, are presented in Table 5-41. The proposed model is created using the data points presented in Table 5-40. The calibrated equation and the model's graphical format are presented in Equation 5.32 and Figure 5.31, respectively.

As can be seen, the overall F-test of the model confirms the significance of the model, as $F_{statistic}$=135.86 is larger than $F_{critical}$=4.28. The independent variable is also shown to be significant (i.e., $|t_{statistic}|>t_{critical}$). The relatively high coefficient of determination (R^2=0.855) demonstrates the model's excellent predictability.

As shown, an exponential Nf-ADE model is valid in the case of freeze-thaw exposed concrete. Comparison of the exponential fatigue life model for undamaged samples (i.e., Equation 5.7) with the exponential model for freeze-thaw exposed samples (i.e., Equation 5.32) reveals that frost damage has slightly changed the slope of the model. As can be seen in Figure 5.32, the difference between the ADE of the freeze-thaw exposed samples and the undamaged samples increases as the fatigue life decreases. This implies that as the severity of frost damage increases (i.e., fatigue life deceases), the data points are located farther from the original undamaged ADE-Nf model.

Table 5-40: Data Points for Exponential Model, Including the F/T Exposed Samples

F/T Cycle	Nf	ADE (N.m)
0	29120	0.01710
0	41260	0.01812
0	30640	0.01650
0	42120	0.01699
0	20000	0.01719
0	66940	0.01301
0	153175	0.01829
0	36475	0.01552
0	7460	0.02083
0	94110	0.01450
0	94110	0.01450
0	153175	0.01829
0	7460	0.02083
0	36475	0.01552
200	13960	0.01974
200	33580	0.01918
200	35235	0.01911
200	85845	0.01757
200	165	0.03329
200	45	0.03463
400	11400	0.02439
400	107125	0.01894
400	1975	0.02808
400	830	0.03308
400	495	0.03196

Table 5-41: Regression Analysis of Freeze-thaw Exposed Samples (Exponential Model, α=0.05)

Regression Statistics	
R Square	0.855
Adjusted R Square	0.849
Standard Error	0.840
Observations	25

	df	*SS*	*MS*	$F_{statistic}$	*Significance F*	$F_{critical}$
Regression	1	95.81	95.81	135.86	3.94E-11	4.28
Residual	23	16.22	0.71			
Total	24	112.03				

	Coefficients	*Std Error*	$T_{statistic}$	*P-value*	$T_{critical}$
Intercept	16.08	0.579	27.79	3.36E-19	2.40
ADE	-312.06	26.773	-11.66	3.94E-11	

$$N_f = e^{16.08-312.06\ ADE} \qquad \textbf{5.32}$$

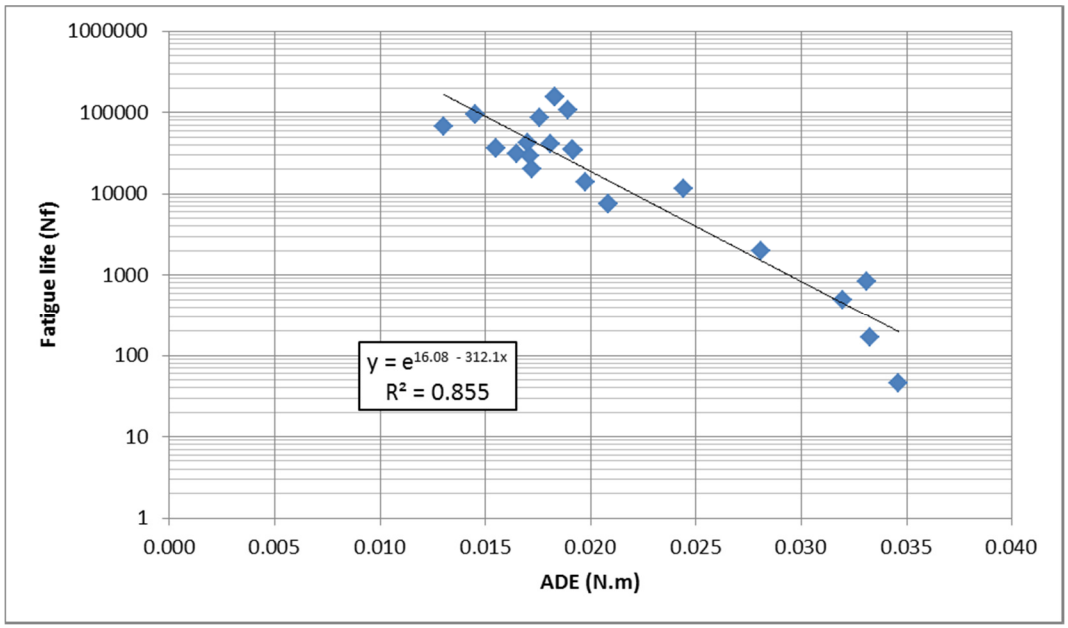

Figure 5.31: Exponential model (Nf vs. ADE, Freeze-thaw exposed samples)

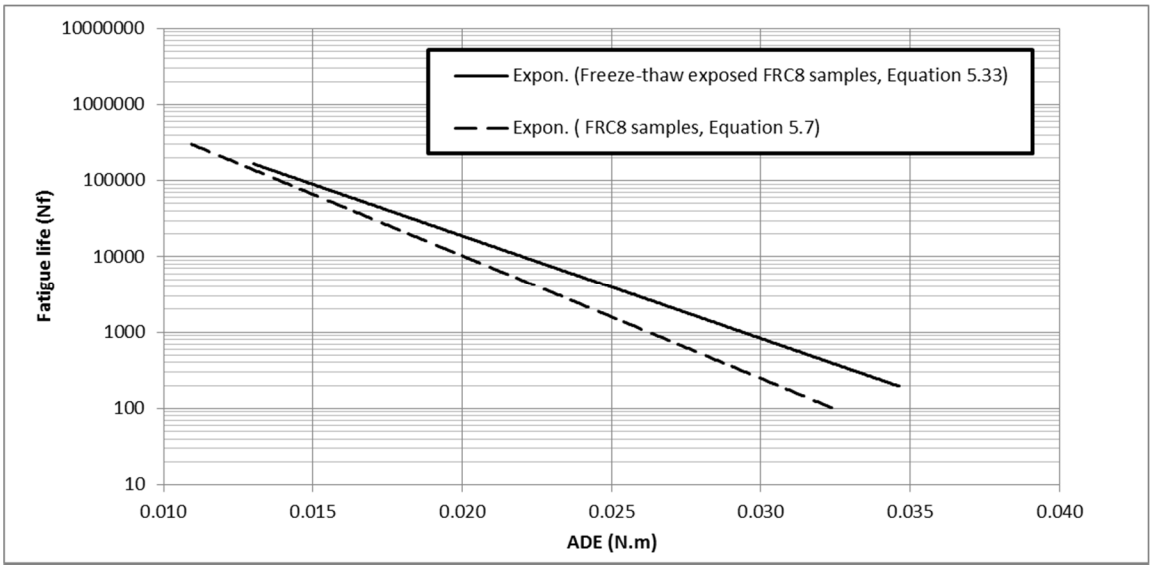

Figure 5.32: Exponential fatigue life model (Freeze-thaw exposed samples vs. undamaged samples)

5.5.3. Prediction Model Incorporating Freeze-thaw Cycles and ADE

In this section, the number of freezing and thawing cycle (FT) is added to a regression model as an independent value along with ADE and the developed model is compared to the model using ADE as the only independent variable (i.e., Equation 5.32). A multiple linear regression is performed to find the regression coefficients of Equation 5.33 (i.e., *a*, *b,* and *c*).

$$Ln\left(N_f\right) = a.ADE + b.FT + c \qquad \textbf{5.33}$$

Results of the multiple linear regression analysis are presented in Table 5-42. The calibrated model is shown by Equation 5.34. $F_{statistic}$ and $t_{statistic}$ are both larger than the critical value, which is an indicator of the significance of both the regression model and the independent variables. The coefficient of determination (R^2=0.897) shows an improvement in the model's predictability after incorporating the number of freezing and thawing cycles (FT) as an independent variable in the model.

Table 5-42: Regression Analysis of Frost-Damage Sample (α=0.05)

Regression Statistics	
R Square	0.897
Adjusted R Square	0.887
Standard Error	0.725
Observations	25

	df	*SS*	*MS*	$F_{statistic}$	*Significance F*	$F_{critical}$
Regression	2	100.45	50.23	95.43	1.44E-11	3.42
Residual	22	11.58	0.53			
Total	24	112.03				

	Coefficients	*Std Error*	$T_{statistic}$	*P-value*	$T_{critical}$
Intercept	16.945	0.578	29.30	4.03E-19	2.40
F/T Cycle	0.004	0.001	2.97	0.00709	
ADE	-376.852	31.798	-11.85	5.05E-11	

$$N_f = e^{-376.85\ ADE + 0.004\ FT + 16.945} \quad \textbf{5.34}$$

5.5.4. Prediction Model Incorporating Void Content and ADE

The void content of the concrete is expected to increase as the severity of frost damage increases, and therefore it can be a good parameter to characterize the fatigue behavior of frost-damaged samples. To improve the predictive quality of the ADE-Nf model, the void content of concrete samples, along with ADE, were incorporated in a multivariate linear model, as shown by Equation 5.35. The data set of multiple linear regressions is presented in Table 5-43. Results of the multiple linear regression analysis are presented in Table 5-44. The relatively low *p*-values of independent variables (i.e., ADE and void ratio) indicate that both variables are significant at α=0.05. Increasing the value of the coefficient of determination from 0.855 (model without void ratio) to 0.927 (model with void ratio) shows that addition of the void ratio as an independent variable has improved the model's predictability.

$$Ln(N_f) = a\ ADE + b\ Void\ Ratio + c \quad \textbf{5.35}$$

Table 5-43 Multivariate Linear Regression (Nf, ADE, and Void ratio)

Nf	F/T Cycle	ADE (N.m)	Viod Ratio (%)
94110	0	0.01450	12.94
153175	0	0.01829	13.27
7460	0	0.02083	13.72
36475	0	0.01552	13.29
13960	200	0.01974	13.89
33580	200	0.01918	12.94
35235	200	0.01911	12.99
85845	200	0.01757	12.20
165	200	0.03329	13.81
45	200	0.03463	13.47
11400	400	0.02439	13.24
107125	400	0.01894	12.49
1975	400	0.02808	12.36
830	400	0.03308	12.92
495	400	0.03196	13.27

Table 5-44 Multivariate Regression Analysis (Nf, ADE, and Void Ratio, α=0.05)

Regression Statistics	
R Square	0.927
Adjusted R Square	0.914
Standard Error	0.746
Observations	15

	df	*SS*	*MS*	$F_{statistic}$	*Significance F*	$F_{critical}$
Regression	2	84.21	42.10	75.64	1.57612E-07	3.81
Residual	12	6.68	0.56			
Total	14	90.89				

	Coefficients	*Std Error*	$T_{statistic}$	*P-value*	$T_{critical}$
Intercept	28.63	5.21	5.49	0.000138	2.53
Voids	-0.91	0.41	-2.25	0.043728	
ADE	-328.02	3.29	-11.26	9.79E-08	

5.6. Prediction model for plastic deformation accumulation of mixture with various amounts of fiber content (%f)

Variations in *D/Dmax* during the fatigue life for different mixtures are shown in Table 5-33. Data points were obtained by averaging at least five samples. As was mentioned in the previous chapter, *D* denotes the deflection of beam and *Dmax* expresses the maximum deflection of beam at failure. Therefore, a change in the *D/Dmax* can be a measure of the accumulation of plastic deformation in the sample during the fatigue life. In this section it is tried to develop a prediction model for *D/Dmax*, incorporating cycle ratio (N/Nf) and fiber content (%f) as independent variables.

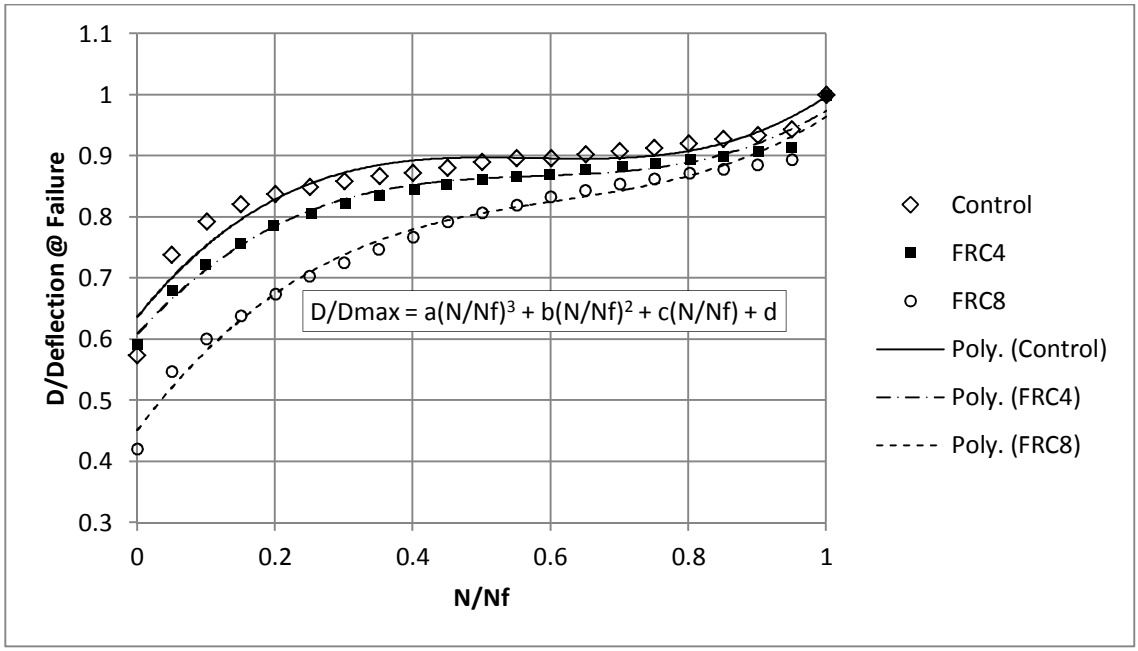

Figure 5.33: Plastic deformation accumulation during fatigue life (mixtures with various fiber contents)

The strategy was to find a shift factor that multiplies by the plastic deformation accumulation model of the control mixture (as a master curve) and yields the plastic deformation accumulation model of the other two mixtures (i.e., FRC4 and FRC8), as shown in Figure 5.37. As the first step, the best polynomial model is fitted to of each set of data points. A third-degree polynomial function is found to be the best function to describe the trend of *D/Dmax* versus cycle ratio (N/Nf). The models are presented in Table 5-45. The dependent variable (i.e., *D/Dmax*) of each regression model is normalized by the dependent variable of the control mixture's regression model at different cycle ratios. Table 5-46 presents the normalized deformation of each mixture at different cycle ratios.

Table 5-45: Plastic deformation polynomial models

Fiber Content (%)	Plastic deformation model
0	$\frac{D}{D_{max}} = 1.4327\left(\frac{N}{N_f}\right)^3 - 2.4711\left(\frac{N}{N_f}\right)^2 + 1.3994\left(\frac{N}{N_f}\right) + 0.6365$
0.4	$\frac{D}{D_{max}} = 1.2036\left(\frac{N}{N_f}\right)^3 - 2.0927\left(\frac{N}{N_f}\right)^2 + 1.2551\left(\frac{N}{N_f}\right) + 0.6083$
0.8	$\frac{D}{D_{max}} = 1.1960\left(\frac{N}{N_f}\right)^3 - 2.1888\left(\frac{N}{N_f}\right)^2 + 1.5057\left(\frac{N}{N_f}\right) + 0.4512$

Table 5-46: Normalized deformation models at various cycle ratios (i.e., shift factors)

N/Nf	$\frac{D/D_{max}(FRC4)}{D/D_{max}(Control)}$	$\frac{D/D_{max}(FRC8)}{D/D_{max}(Control)}$	$\frac{D/D_{max}(Control)}{D/D_{max}(Control)}$
0	0.956	0.709	1
0.05	0.951	0.744	1
0.1	0.948	0.772	1
0.15	0.947	0.794	1
0.2	0.947	0.813	1
0.25	0.948	0.831	1
0.3	0.950	0.846	1
0.35	0.952	0.860	1
0.4	0.955	0.874	1
0.45	0.958	0.886	1
0.5	0.962	0.898	1
0.55	0.965	0.910	1
0.6	0.969	0.921	1
0.65	0.972	0.931	1
0.7	0.975	0.940	1
0.75	0.978	0.948	1
0.8	0.979	0.955	1
0.85	0.980	0.961	1
0.9	0.980	0.964	1
0.95	0.979	0.966	1
1	0.977	0.967	1

The values in Table 5-46 are the shift factors of plastic deformation accumulation models. In other words, the *D/Dmax* of FRC4 and FRC8 at certain cycle ratios (N/Nf) can be easily found by multiplying the *D/Dmax* of the control sample at a corresponding cycle ratio by the corresponding shift factor. For example, to find the *D/Dmax* of the

FRC8 sample at cycle ratio N/N_f=0.65, the *D/Dmax* of the control sample at N/N_f=0.65 is multiplied by 0.931. As can be seen, the values of shift factors depend on the mixture (i.e., fiber content) and cycle ratio, and therefore the shift factor can be shown as a function with two independent variables, cycle ratio and fiber content (% f). The dependency of the shift factor on these two variables is shown in Figure 5.34. As can be seen, the shift factor has an indirect relationship with increases in fiber content and a direct relationship with cycle ratio (N/Nf).

It can be seen (Figure 5.34) that a polynomial model is a precise model to describe the trend of normalized *D/Dmax* (i.e., shift factor) at different cycle ratios (N/N_f). Knowing that the value of the normalized *D/Dmax* (i.e., shift factor) at a fiber content of 0% (i.e., control sample, which is the master curve) is equal to 1, the simplest polynomial that can describe the trend is shown by Equation 5.36. The model (Equation 5.36) is calibrated at different cycle ratios and the calibration coefficients (i.e., *a* and *b* in Equation 5.36) are presented in Table 5-47.

$$Shift\ factor = 1 - a\ \%f^{b} \quad \textbf{5.36}$$

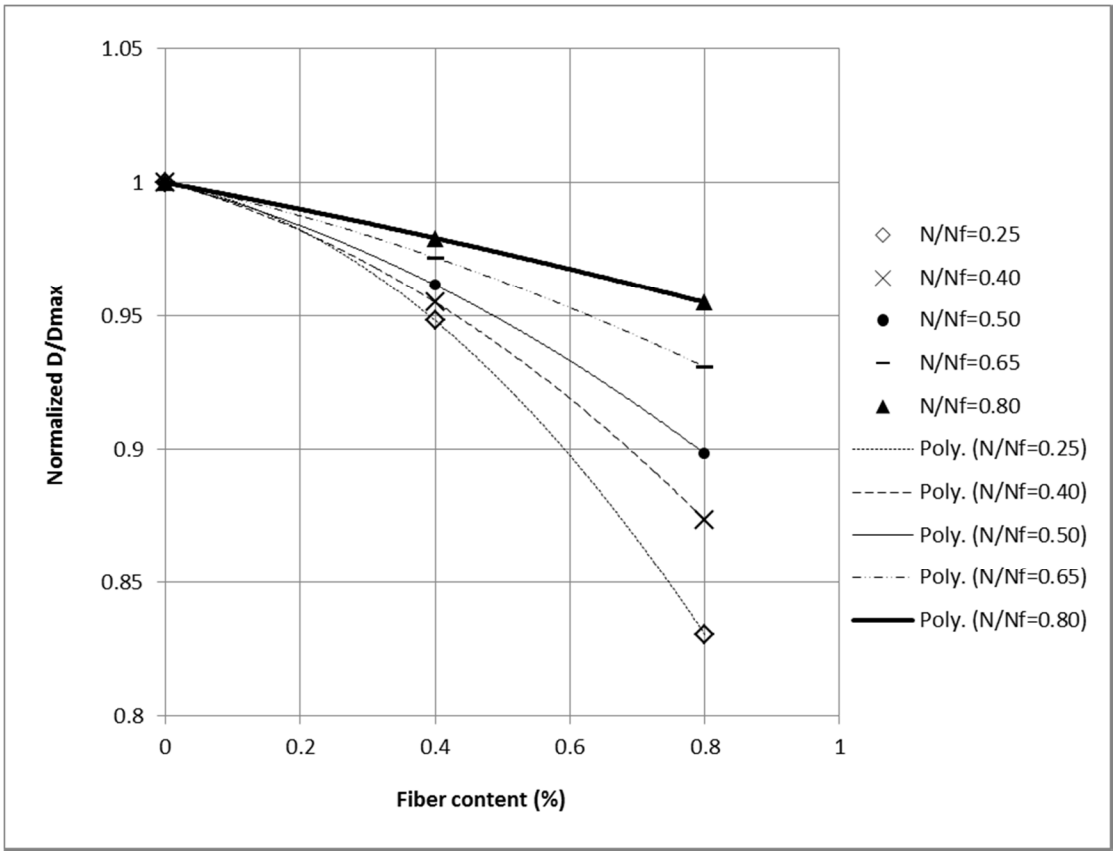

Figure 5.34: Normalized D/Dmax vs. fiber content

The calibration coefficients of Equation 5.36 (i.e., *a* and *b*) are determined as a function of cycle ratio (Figure 5.35 and Figure 5.36) and plugged into the shift factor equation (Equation 5.36). The final format for the shift factor is shown by Equation 5.37, in which the shift factor multiplies by the plastic deformation accumulation model of the control mixture (as a master curve) and yields the plastic deformation accumulation of the other mixtures with different fiber contents. The proposed prediction model is compared to the actual data in Figure 5.37.

Table 5-47: Calibration coefficients of Equation 5.36 at different cycle ratios

N/Nf	a	b
0.01	0.533	2.716
0.05	0.435	2.378
0.1	0.368	2.139
0.15	0.319	1.960
0.2	0.280	1.821
0.25	0.248	1.711
0.3	0.221	1.623
0.35	0.198	1.552
0.4	0.176	1.494
0.45	0.157	1.446
0.5	0.139	1.407
0.55	0.122	1.372
0.6	0.107	1.341
0.65	0.093	1.307
0.7	0.079	1.264
0.75	0.068	1.205
0.8	0.058	1.141
0.85	0.049	1.050
0.9	0.043	0.931
0.95	0.039	0.795
1	0.038	0.656

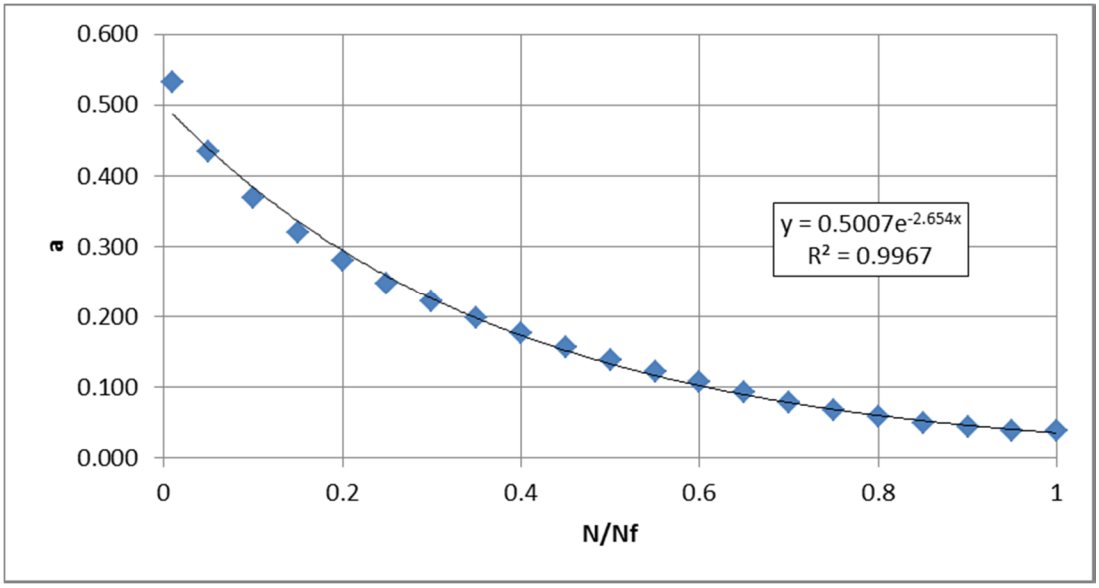

Figure 5.35: Calibration coefficient (a) vs. cycle ratio

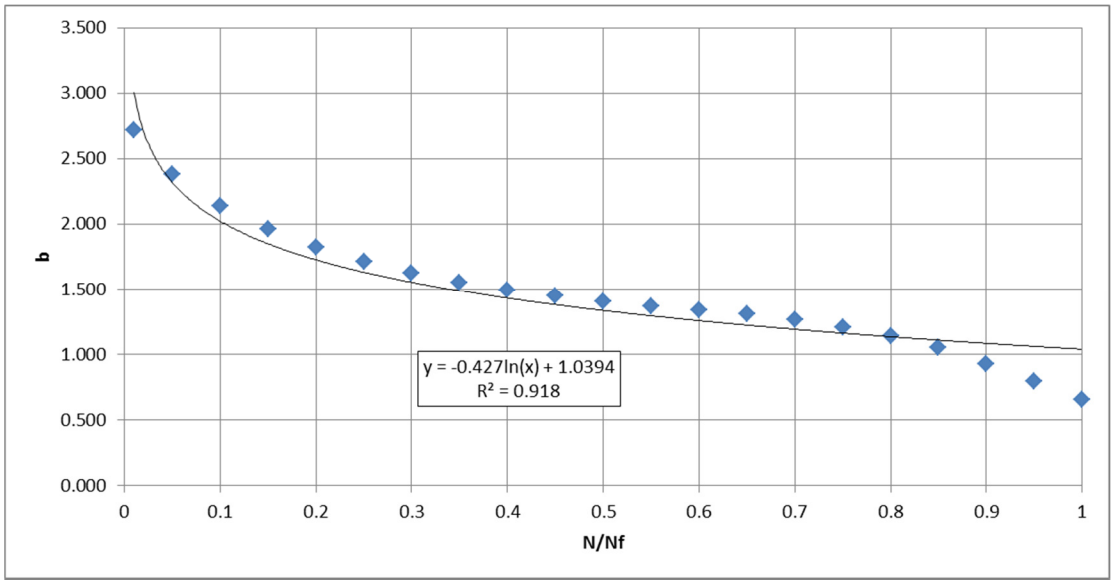

Figure 5.36: Calibration coefficient (b) vs. cycle ratio

$$Shift\ factor = 1 - \left(0.5007e^{-2.654\frac{N}{N_f}}\right) * \%f^{-0.427Ln\left(\frac{N}{N_f}\right)+1.039} \quad \textbf{5.37}$$

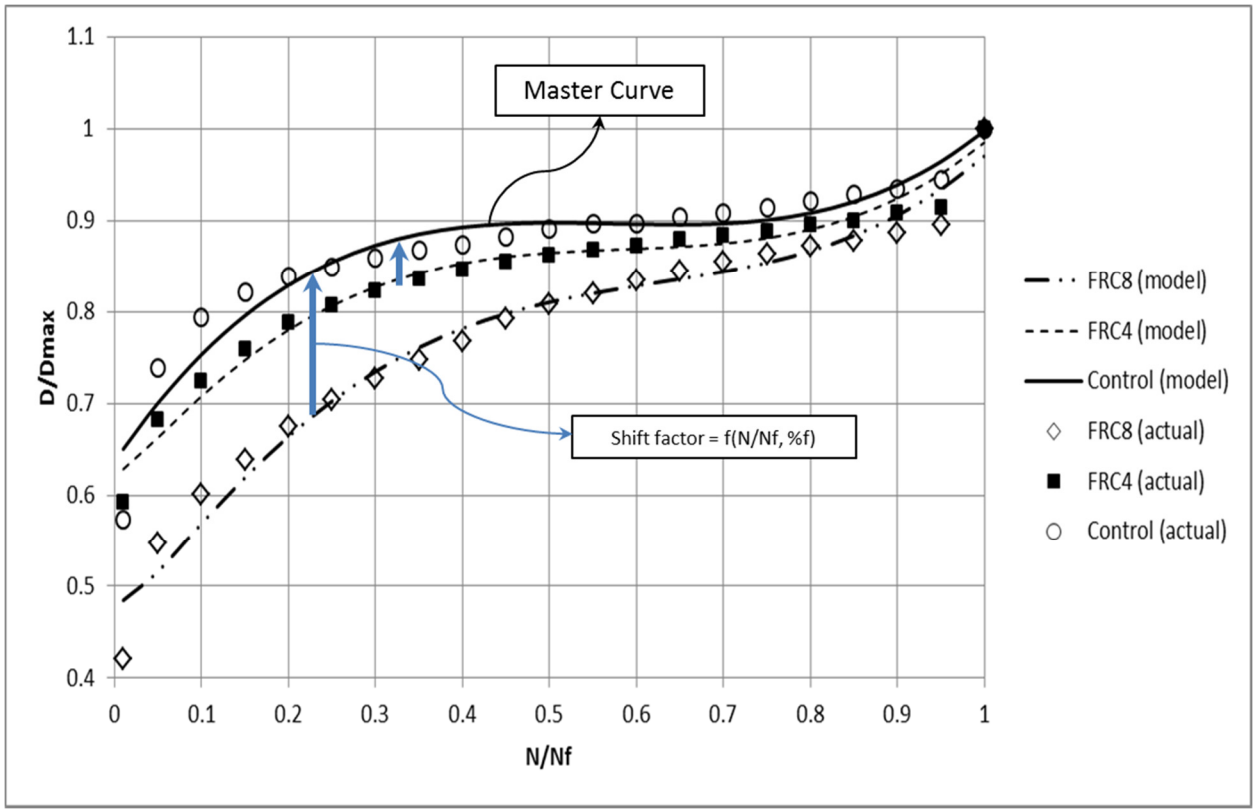

Figure 5.37: Comparison of deformation prediction model and actual data

5.7. Relation between Dynamic Motion Parameters and Fatigue Life and Stress Level

As shown previously, ADE is a proper parameter to characterize the fatigue life of concrete. The N_f-ADE model is shown to have better predictive quality than the traditional S-N_f model; this is because ADE is not only a measure of the damping properties of concrete but also a measure of concrete strength, because it is highly correlated to stress level. Two other parameters directly affect the damping properties of concrete: cyclic stiffness (k) and the dimensionless hysteresis damping constant (β). This

section is dedicated to develop a statistical model to describe the relationship between cyclic stiffness (k) and dimensionless hysteresis damping constant (β) to fatigue life (N_f) and stress level (S). The data points used in the regression analysis are presented in Table 5-48. The proposed models, along with the summary of regression analysis results, are presented in Table 5-49. Regression analysis of these models are presented in Appendix C. The models are calibrated for the FRC8 mixture, and in some cases the model's validity is evaluated for the FRC4 mixture.

As can be seen in Table 5-49, three models were developed to describe the relationship between stress level (S) and cyclic stiffness (k) (i.e., model 1, model 2 and model 3). All three models have a relatively high R^2 (R^2>0.8), which indicates that the stress level at which the sample is tested can be estimated precisely using the results for cyclic stiffness. The overall F-test for all three models confirms the significance of the model, as the *p*-value is smaller than α=0.05. The null hypothesis of the *t*-test is rejected for all three models. This means that the independent variables are significant. In other words, the independent variable is useful in predicting and controlling for the dependent variable.

Unlike ADE, cyclic stiffness has been shown to be a useful parameter to characterize fatigue life. As can be seen, models 4 and 5 presented in Table 5-49 reveal a relatively low coefficient of determination (R^2<0.6).

As discussed previously in Chapter 4, the damping force in a hysteresis damper is directly related to cyclic stiffness, and therefore cyclic stiffness can affect the amount of energy dissipation. This is investigated in models 6 and 7. As can be seen, the relationship between ADE and cyclic stiffness (k) is described by an exponential model

with a R^2=0.806. The model's validity is also confirmed for FRC4. The overall model and the independent variable are shown to be significant at α=0.05.

The dimensionless hysteresis damping constant (β) is not found to be a proper parameter to estimate stress level and fatigue life. The relatively low coefficients of determination of models 8 to 11 (R^2<0.6) indicate that prediction models including β as an independent variable are not statistically reliable.

Several multivariate models (i.e., model 13 to model 17) were developed to predict fatigue life from parameters such as hysteresis damping constant (β), cyclic stiffness (k), and stress level (S). To improve the model's predictability, many dependent variable transformations were incorporated in the model and Ln (Nf) and $Nf^{0.2}$ and $Nf^{0.1}$ were found to be beneficial in terms of increasing the R^2 and significance level of the model. Including both cyclic stiffness and dimensionless hysteresis damping constant in the fatigue life model has improved the predictability of the model compared to the fatigue models, which include only one independent variable. However, the predictive quality of these models is still worse than the ADE-Nf models (i.e., R2 of model 13 and model 15<R2 of Equation 5.7 and 5.11).

Table 5-48: Data set for fatigue modeling using dynamic motion parameters (5 Hz)

%fiber	S (%)	Nf	β	k (kN/m)	ADE (N.m)
0	72.19	120690	0.0266	61275	0.01603
0	72.18	85370	0.0267	61891	0.01575
0	72.09	23590	0.0263	61681	0.01559
0	72.14	7540	0.0287	60735	0.01745
0	72.21	50220	0.0266	61335	0.01584
0	72.18	30210	0.0267	59754	0.01629
0.4	72.87	49160	0.0272	57866	0.01465
0.4	72.83	44920	0.0265	58215	0.01415
0.4	72.43	30170	0.0279	58303	0.01490
0.4	72.81	520	0.034	56894	0.02234
0.4	72.41	22460	0.0297	57779	0.01597
0.4	72.25	420	0.0354	57377	0.02055
0.8	80.19	15000	0.0331	58180	0.02034
0.8	80.28	610	0.0372	55872	0.02400
0.8	80.36	7950	0.0334	56979	0.02185
0.8	78.69	1245	0.0367	57148	0.02317
0.8	78.95	2310	0.035	57369	0.02244
0.8	77.48	30520	0.03	57410	0.01982
0.8	70.58	29120	0.0334	56293	0.01710
0.8	70.54	41260	0.0345	54586	0.01812
0.8	69.7	30640	0.0321	55351	0.01650
0.8	70.17	42120	0.0344	54461	0.01699
0.8	70.22	20000	0.0357	55730	0.01719
0.8	66.73	66940	0.0262	53850	0.01301
0.8	70.94	153175	0.034	55809	0.01829
0.8	70.6	36475	0.0294	55754	0.01552
0.8	70.84	7460	0.0363	56918	0.02083
0.8	70.72	94110	0.0288	54763	0.01450
0.8	59.43	302620	0.0303	51983	0.01206
0.8	58.99	272270	0.0268	49533	0.01132
0.8	59.09	409800	0.0254	50237	0.00997
0.8	58.8	118600	0.0259	52396	0.01006
0.8	58.56	233900	0.0265	47432	0.01038
0.8	58.18	775000	0.028	48963	0.01026

Table 5-49: Summary of regression analysis of proposed models (Nf, ADE, S, k and β, α=0.05)

Model #	Mixture	Model	Coefficients			R^2	Adj. R^2	T test (α=0.05)	F test (P-value)
			a	b	c				
1	FRC8	$S = a\,k + b$	-5.693E+01	2.300E-03		0.817	0.808	Null is rejected	8.10E-09
2	FRC8	$S = a\,e^{b\,k}$	1.060E+01	3.400E-05		0.838	0.83	Null is rejected	2.38E-09
3	FRC8	$S = a\,k^{b}$	1.837E-07	1.811E+00		0.827	0.819	Null is rejected	4.49E-09
4	FRC8	$Nf = a\,e^{bk}$	4.994E+15	-4.709E-04		0.584	0.563	Null is rejected	3.44E-05
5	FRC8	$Nf = a\,k^{b}$	5.376E+121	-2.474E+01		0.577	0.556	Null is rejected	4.16E-05
6	FRC8	$ADE = a\,e^{bk}$	1.428E-04	8.661E-05		0.806	0.796	Null is rejected	1.46E-08
7	FRC4	$ADE = a\,e^{bk}$	6.147E+00	-1.037E-04		0.96	0.951	Null is rejected	5.21E-03
8	FRC8	$S = a\,\beta + b$	2.227E+01	1.501E+03		0.556	0.534	Null is rejected	6.76E-05
9	FRC8	$S = a\,e^{b\,\beta}$	3.437E+01	2.218E+01		0.567	0.546	Null is rejected	5.22E-05
10	FRC8	$S = a\,\beta^{b}$	7.558E+02	6.903E-01		0.577	0.556	Null is rejected	4.15E-05
11	FRC8	$Nf = a\,e^{b\beta}$	5.500E+09	-3.778E+02		0.615	0.595	Null is rejected	1.58E-05
12	FRC4	$Nf = a\,e^{b\beta}$	4.304E+11	-5.898E+02		0.96	0.95	Null is rejected	6.10E-04
13	FRC8	$Nf^{0.2} = a\,k + b\,\beta + c$	-5.763E-04	-2.769E+02	4.882E+01	0.763	0.738	Null is rejected	1.16E-06
14	FRC4	$Nf^{0.2} = a\,k + b\,\beta + c$	4.033E-04	-4.739E+02	-2.122E+00	0.987	0.978	Null is not rejected	1.48E-03
15	FRC8	$Ln\,Nf = a\,k + b\,\beta + c$	-2.540E-04	-2.331E+02	3.169E+01	0.694	0.662	Null is rejected	1.29E-05
16	FRC8	$Nf^{0.1} = a\,\beta + b\,S + c$	-5.752E+01	-6.570E-02	1.000E+01	0.813	0.793	Null is rejected	1.21E-07
17	FRC8	$Ln\,Nf = a\,\beta + b\,S + c$	-1.546E+02	-1.487E-01	2.574E+01	0.786	0.763	Null is rejected	4.42E-07

5.8. Endurance limit

The endurance limit of concrete, by definition, is the maximum stress level under which the concrete can withstand 2 million cycles of fatigue loading (Ramakrishnan, Wu and Hosalli 1989). At a stress level below the endurance limit, the fatigue life is assumed to be significantly large (i.e., it approaches to infinity). The traditional approach to finding the endurance limit is to form the S-Nf curve and determine the value of the stress level at 2 million cycles of loading. In this section, it is tried to related the endurance limit to the deformational characteristics of concrete and potentially find a new approach to defining the endurance limit.

5.8.1. Traditional approach to determining endurance limit

The S-Nf curve for FRC8 samples tested at frequencies of 5 Hz and 10 Hz are presented in Figure 5.38. The stress-level value at 2 million loading cycles, the so-called endurance limit, is equal to 55% for samples tested at 5 Hz and 60% for samples tested at 10 Hz. Specifying a confidence interval for the endurance limit seems to be more accurate mathematically, because of high variability in the fatigue test results. Therefore, the confidence interval for the endurance limit is specified and shown in Figure 5.38. The higher endurance limit for the FRC8 sample at a frequency of 10 Hz can be explained by smaller creep deformation at faster loading rates.

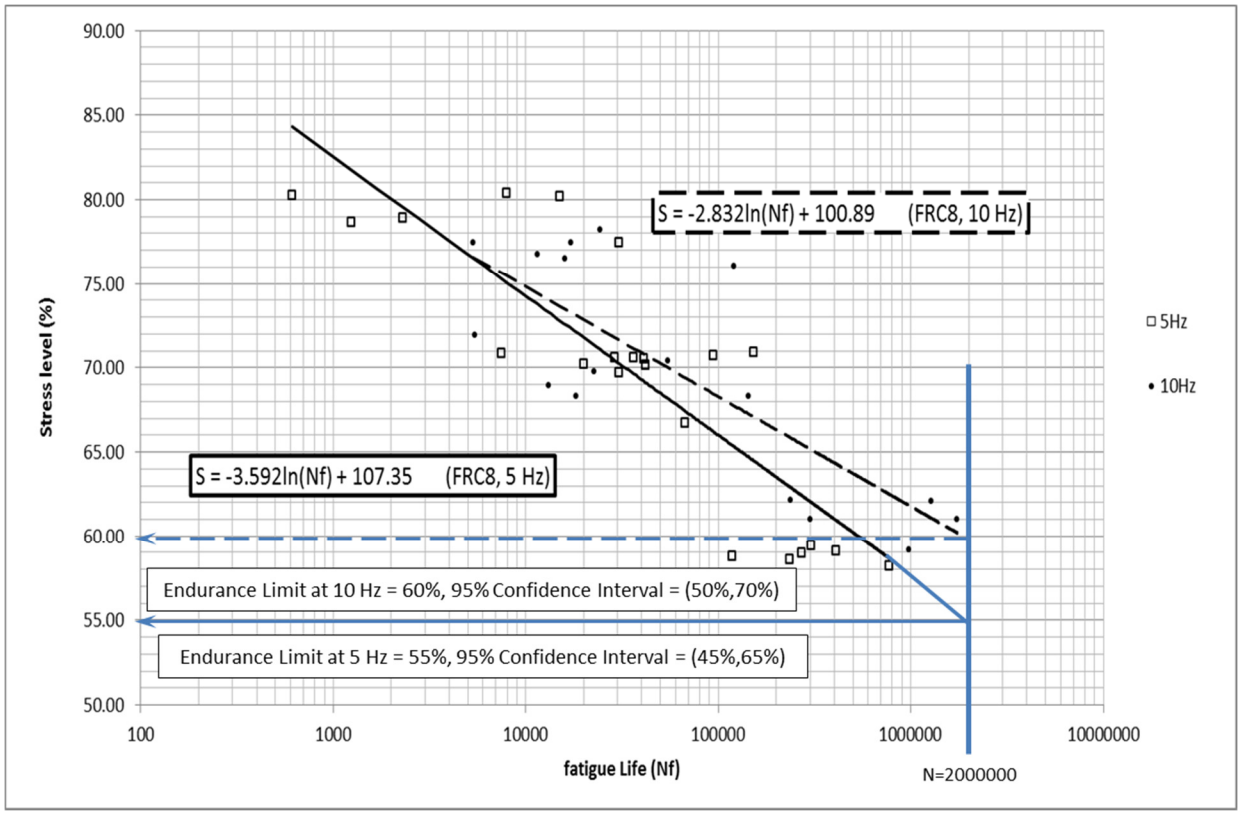

Figure 5.38: Endurance limit of FRC8 samples tested at frequencies of 5 Hz and 10 Hz

The endurance limit of fiber-reinforced concrete can also be expressed as a percentage of the flexural strength of plain concrete (Ramakrishnan, Wu and Hosalli 1989). To find the endurance limit as a percentage of the flexural strength of plain concrete, the stress levels of the FRC8 sample are calculated based on the modulus of rupture of the control mixture. The modified S-Nf curves are then plotted, and the stress-level value at 2 million loading cycles is determined. Figure 5.39 presents the modified S-N_f curves for samples tested at frequencies of 5 and 10 Hz. The value of the endurance

limit as a percentage of the flexural strength of control sample is equal to 47% and 51% for 5 Hz and 10 Hz, respectively.

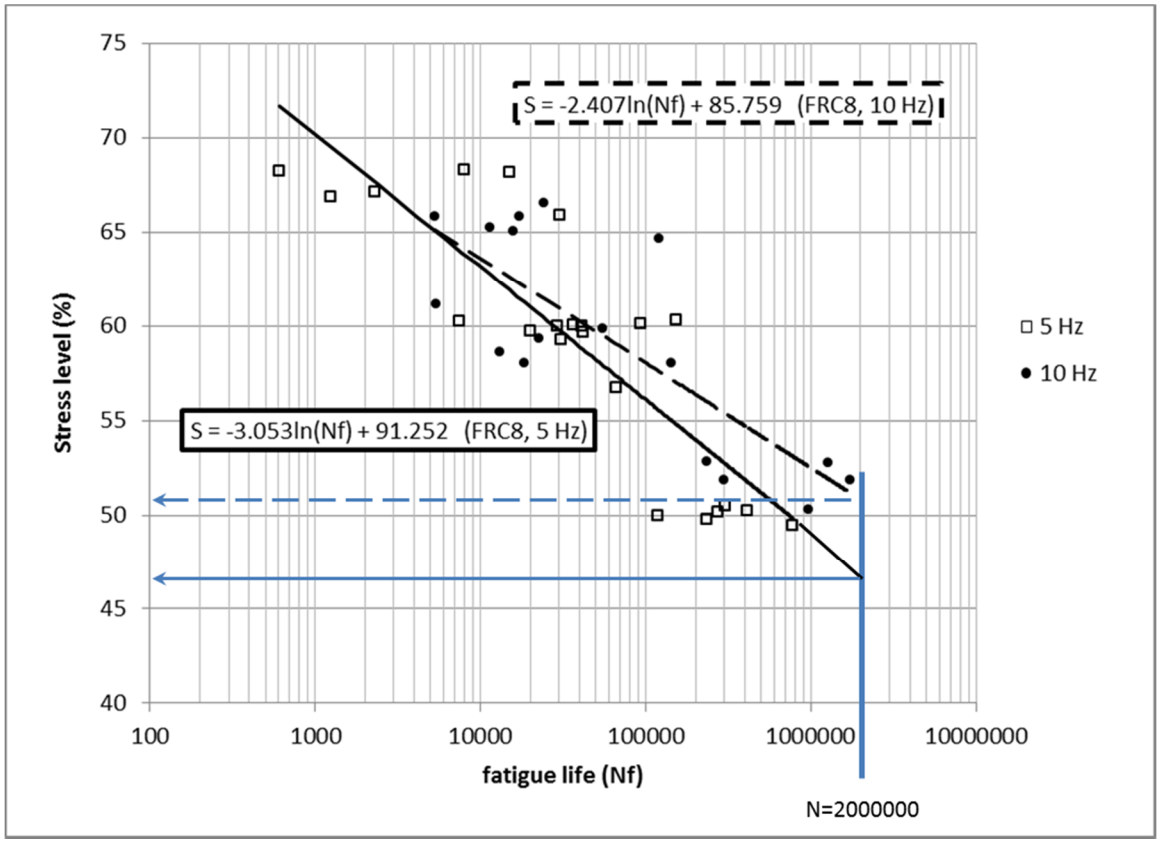

Figure 5.39: Endurance limit of FRC8 samples tested at frequencies of 5 Hz and 10 Hz expressed as percentage of plain concrete flexural strength

5.8.2. Load-deformation curve and endurance limit

As discussed in Chapter 4, the cyclic load-deflection curve is surrounded by a curve that is similar to the static load-deflection curve. The envelope curve was developed for different samples and is shown in Figure 5.40 to Figure 5.43.

The envelope curve suggests that the higher the maximum cyclic load, the smaller the total plastic deformation due to fatigue loading will be. In other words, the amount of plastic deformation that samples experience up to failure (i.e., between maximum deflection at fatigue failure and maximum deflection at cycle 1, denoted by *b* in Figure 5.40) increases as the stress level decreases. This is expected, since more cracks must develop to destabilize the concrete matrix at lower loads. This finding is also in agreement with the study of creep phenomenon in concrete (Bazant 1975).

The envelope curve also shows a plateau where the load-deflection curve becomes flat. At the load level, the total plastic deformation (i.e., b in Figure 5.40) that must be induced in the sample to make the matrix unstable significantly increases. It seems that the endurance limit corresponds to this point at which the load-deflection envelope shows a drastic increase in total plastic deformation.

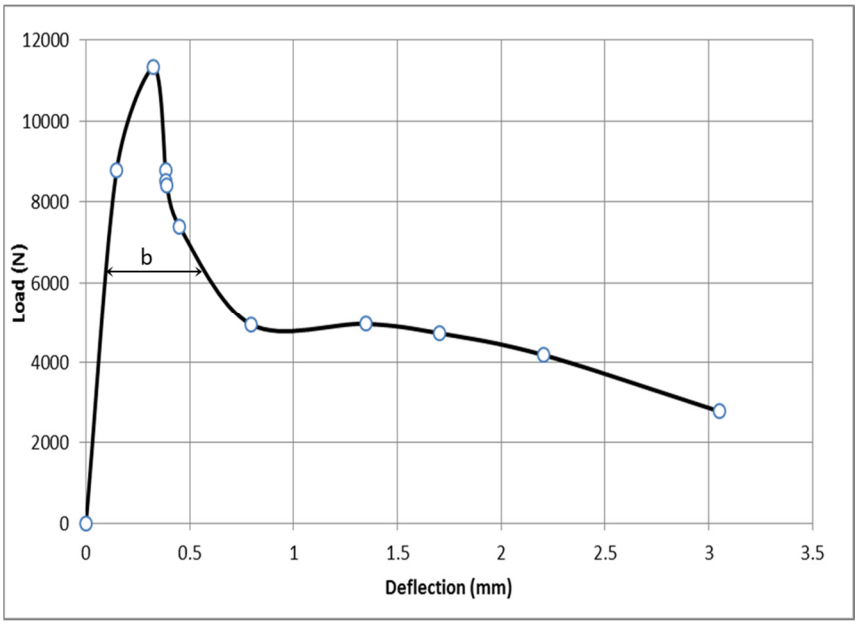

Figure 5.40: Load-deflection envelope (FRC8, 0.8-10-1)

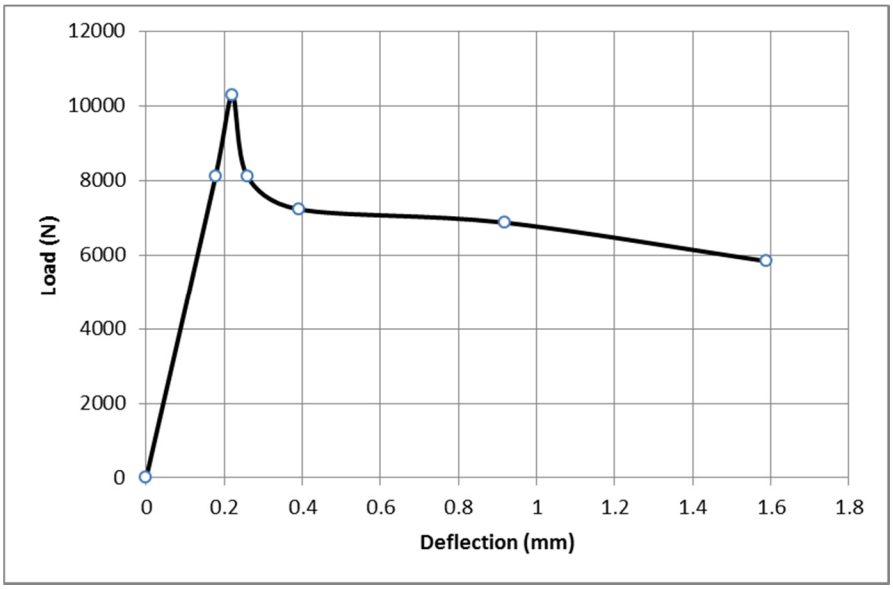

Figure 5.41: Load-deflection envelope (FRC8, 0.8-5-5)

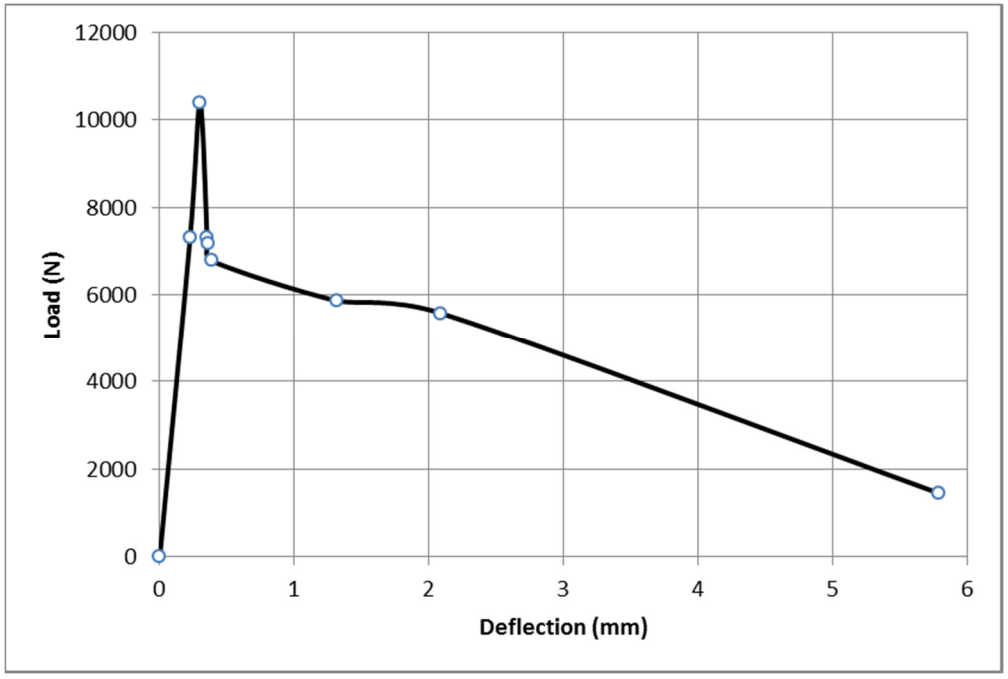

Figure 5.42: Load-deflection envelope (FRC8, 0.7-10-3)

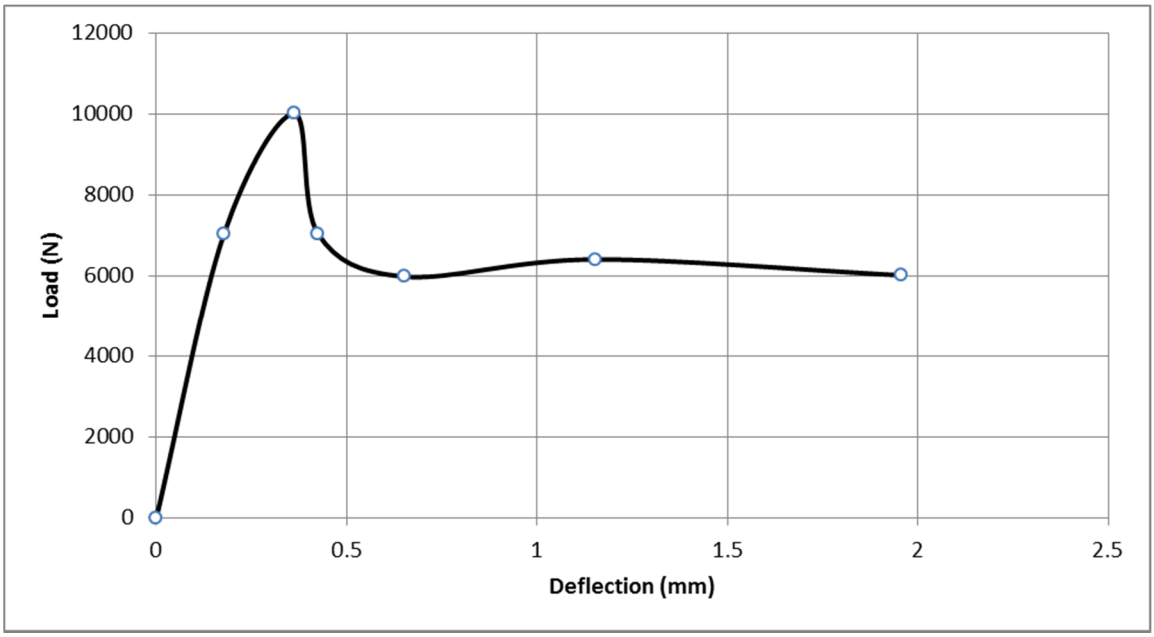

Figure 5.43: Load-deflection envelope (FRC8, 0.7-5-5)

To investigate this, the envelope curve of the FRC8 mixture at different loading frequencies was determined and is shown in Figure 5.44 and Figure 5.45. The X-axis of the envelope curve is converted to stress level by normalizing with maximum load.

As can be seen in Figure 5.44, the plateau of the FRC8 samples at a frequency of 5 Hz is mostly located between 50% and 70%. In the averaged-envelope, the plateau is located between 55% and 65%. The plateau range of the averaged-envelope for samples tested at a frequency of 10 Hz is between 50% and 60% (Figure 5.45).

As was expected, the estimated value of the endurance limit using a traditional approach (i.e., 55% for 5 Hz and 60% for 10 Hz) falls within the plateau range. This indicates that formation of an envelope curve could be an alternative method to determine endurance limit. It must be mentioned that the validity of this approach must be examined

for many other mixtures before a definite conclusion can be reached about the method's usefulness.

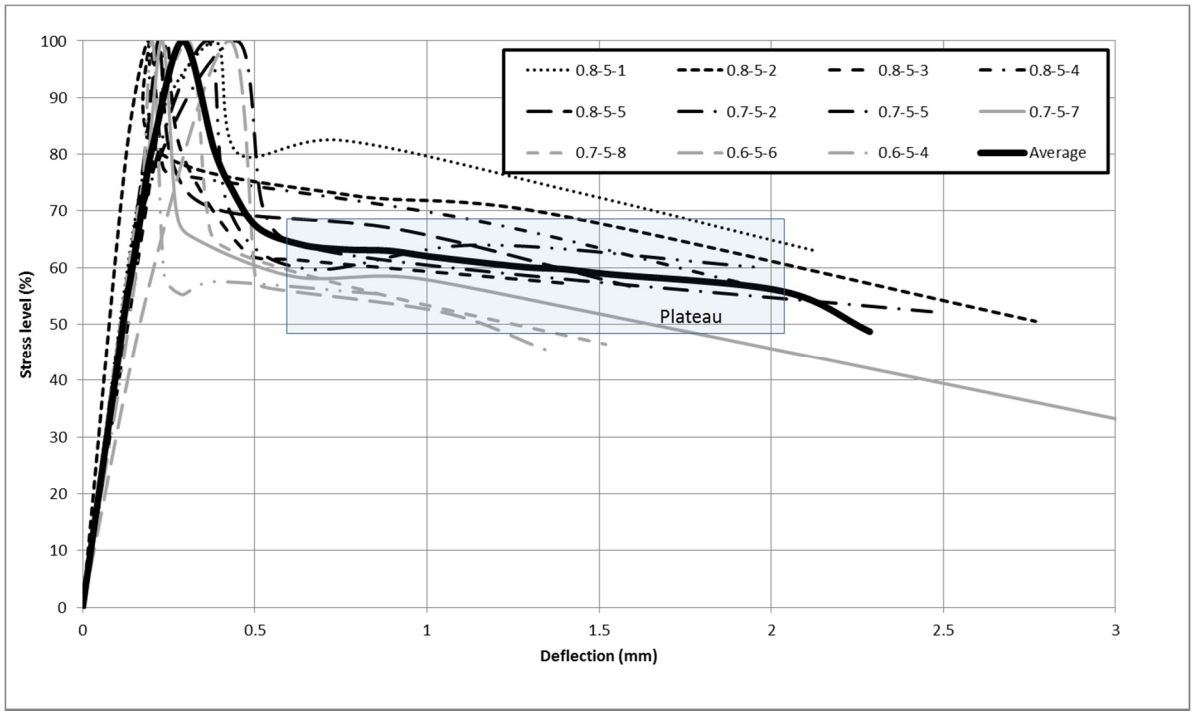

Figure 5.44: Envelope curve of FRC8 mixture tested at a frequency of 5 Hz

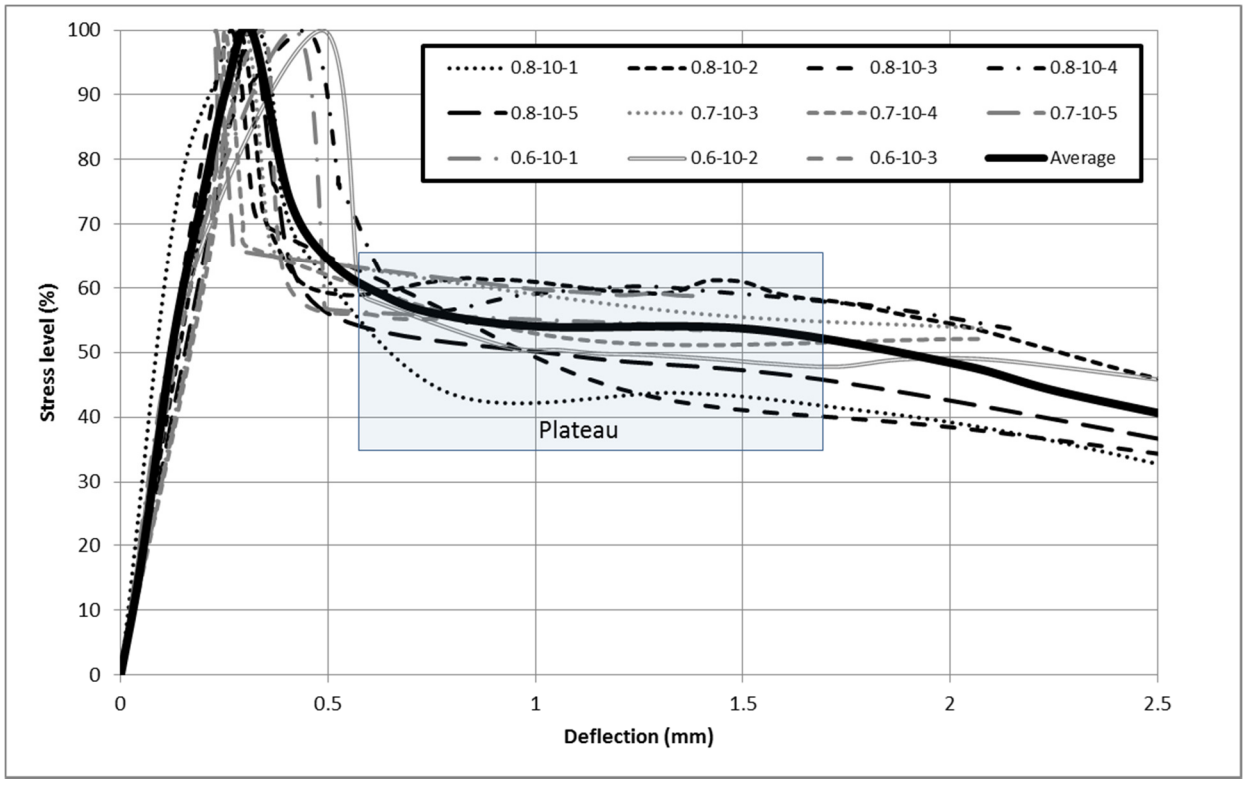

Figure 5.45: Envelope curve of FRC8 mixture tested at frequency of 10 Hz

Chapter 6. Conclusions and Recommendations

6.1. Conclusions

The objective of this research was to develop fatigue modeling based on energy dissipation principles. The results of this study provided the following conclusions.

In regards to the effects of polypropylene fiber reinforcement on fresh concrete properties the following conclusion were observed:

- The addition of polypropylene fiber into plain concrete has a significant effect on the rheological properties of fresh concrete. The slump of concrete is reduced by increasing the fiber content in the mixture. The use of higher amount of water reducer in the FRC mixture did not compensate for the negative effects of fibers on workability, although the slump of FRC mixtures were within the target range of 4-7.5 cm. There was no fiber balling and aggregate segregation during the mixing process. The fibers were uniformly distributed, and the FRC mixtures were easy to consolidate;
- The air content test results indicated that FRC mixtures have higher amount of air content. Existence of fiber in the fresh concrete hinders the process of movement of entrapped air to the surface of concrete during consolidation. This leads to a higher amount of entrapped air in the hardened concrete.

Regarding the effects of fiber-reinforcement on mechanical properties of concrete the following conclusions were drawn:

- As expected polypropylene fiber reinforcement did not contribute to compressive strength of concrete. The use of fibers in concrete has led to 15% decrease in the 28 days compressive strength. No difference was observed between the 28 days compressive strength of fiber reinforced concrete with 0.4% and 0.8% fiber content. However, higher variability in the compressive strength of the 0.8% fiber content mixture;
- There was no significant difference between the flexural strength of plain concrete and the FRC mixture containing 0.4% polypropylene fiber. However, increasing the fiber content to 0.8% has led to a 15% reduction in the flexural strength of plain concrete. Although fiber reinforcement at 0.8% does not improve the flexural strength (perhaps reflecting the weak transition zone between fibers and cement matrix), it increases the ductility of the concrete matrix since an increase in the amount of the area under the load-deflection curve was observed;
- No effect on the static elastic modulus of concrete was observed with the addition of 0.4% polypropylene fiber. However, increasing the fiber content from 0.4% to 0.8% decreased the elastic modulus by 20%.

In regards to the effects of fatigue loading conditions and fiber reinforcement the following conclusions were observed:

- Fatigue life has indirect relationship with stress level. As the stress level increases the fatigue life of concrete decreases. It is also observed that increasing the loading frequency leads to an increase in the fatigue life of concrete. The impact of loading frequency on fatigue life at lower stress level is more noticeable.

- The loading rate directly affects the variability of the test results, with higher variability observed at higher stress level and loading frequency;
- The polypropylene fiber content (at these low fiber content levels) had no effects on increasing fatigue life of concrete.
- The endurance limit of FRC was higher at higher loading frequencies.

In regards to the effects of fatigue loading conditions and fiber reinforcement on the hysteresis damping properties of concrete the following conclusions were reached:

- All concrete mixtures, with or without fiber reinforcement, have revealed a hysteresis behavior under cyclic loading. The hysteresis loop properties such as cyclic stiffness, dissipated energy per loading cycle and etc. are affected by the fatigue test setup parameters (i.e., stress level and loading frequency) and fiber reinforcement;
- The dissipation energy (DE) analysis per loading cycle indicated that DE is variable throughout the fatigue life of concrete regardless of loading condition and mixture type. However, the moving average of DE has shown three distinctive stages of fatigue life. The analysis have shown that at the beginning (i.e., the first 20% of fatigue life) and the end (i.e., the last 10% of fatigue life) of fatigue life the rate of energy dissipation is higher compared to the average energy dissipation throughout the fatigue life;
- FRC mixtures have shown higher energy dissipation rates at the final stage compared to the control mixture;
- The general trend for cyclic stiffness during the course of fatigue life reveals that at the first 10% of fatigue life cyclic stiffness is increasing. This stage is followed

by a stage during which the change in cyclic stiffness is gradual, and finally, during the final 10% of fatigue life, a steep drop in stiffness is observed;

- The experimental results show a positive correlation between the cyclic stiffness of concrete and stress level and loading frequency. The same trend was observed in the case of the dimensionless hysteresis damping constant. Fiber reinforcement has decreased the cyclic stiffness (k) of the samples. On the other hand, the dimensionless hysteresis damping constant (β) has increased by increasing the fiber content;
- Even though the fiber content did not increase the fatigue life of concrete it did increase the damping properties;
- Although the accumulation of plastic deformation is the primary reason of fatigue failure, the contribution of plastic energy on the total dissipated energy is less than 1%. The majority of energy dissipation in fatigue process is through heat generation.

In regards to effects of fatigue loading conditions and fiber reinforcement on the rate and amount of plastic deformation the following conclusion were reached:

- It was observed that the cyclic load-deflection curve throughout the entire fatigue life is surrounded by a curve similar to the static load-deflection curve. The envelope curve of the concrete containing 0.8% fiber shows considerable enhancement in terms of post-failure ductility and toughness compared to the control mixture;
- Three distinctive stages of fatigue life are noticeable in terms of plastic deformation growth. The first 10% of fatigue life is associated with a fast increase

in the maximum deformation of the beam. The deformation then increases at a very slow rate compared to the first stage. This phase continues to 95% of the fatigue life and is followed by a quick increase in deformation until failure. Fiber reinforcement has significantly decreased the rate of plastic deformation increase at the early ages fatigue life;

- Fiber reinforcement increases the maximum deflection at fatigue failure. In other words, the brittleness of plain concrete matrix is reduced by fiber reinforcement.
- The analysis of the amplitude ratio (i.e., the ratio of maximum cyclic deflection to the maximum static deflection) of concrete have shown that that micro-crack formation, which start at the beginning of the fatigue process, does not affect the natural frequency of the beam until the crack network expands and the concrete matrix becomes weak;
- A new definition of endurance limit based on hysteresis envelope was proposed. The analysis and modeling indicated that the endurance limit (according to the traditional definition of 2 million cycles) corresponds to the same stress level of the load-deflection curve of the hysteresis envelope when an increase in deflection is observed with no increase in load;
- Among the objectives of this study was to examine the accumulation of plastic deformation during fatigue life of concrete. A master curve was developed representing such relationship for the conventional and FRC mixtures. To be able to model so, a shift factor that multiplies by the plastic deformation accumulation model of the control mixture (as a master curve) and yields the plastic

deformation accumulation model of the other two mixtures is used. The shift factor is dependent on fiber content and cycle ratio (N/N_f).

The fatigue modeling analysis in regards to hysteresis properties provided the following conclusions:

- ADE was found to be a good estimator of fatigue life for fiber reinforced concrete. The exponential model was able to better relate fatigue life of FRC with ADE. The proposed fatigue model (i.e., the model based on the dissipated energy approach) has greater predictive quality compared to the traditional fatigue life model (i.e., S-Nf curve);
- The value of ADE can be estimated after 25% of fatigue life and therefore there is no need to continue fatigue test to failure. This can significantly reduce the time of fatigue testing.
- ADE has a good correlation with stress level and therefore it is not only a measure of damping properties of concrete, but also represents well concrete strength. The relation between ADE and stress level is well explained by an exponential model. This relationship can be useful to estimate the flexural strength of concrete using the ADE;
- Cyclic stiffness is shown to be a good estimator of fatigue life for FRC. An exponential model was developed to relate the fatigue life of FRC with cyclic stiffness.

In regards to the combined effect of freeze-thaw and fatigue of FRC the following conclusions were obtained.

- A significant variability in the freeze-thaw results was observed due to non-uniform temperature exposure in the freeze-thaw chamber combined with the variability in concrete properties (air content, strength, etc.);
- Freeze-thaw deterioration starts from the surface layer. The porosity of the surface layer increases with freeze-thaw exposure up to when scaling happens. The average porosity after scaling decreased to a value which is smaller than the undamaged samples. This indicates that the inner part of concrete body is not affected by freeze-thaw and freeze-thaw damage is limited at the concrete surface;
- Because of the above conclusion, UPV was not responsive for concrete conditions were scaling was observed;
- It was observed that frost damage and fatigue deterioration are cumulative. Generally, Frost-damaged samples had lower fatigue life.
- The amount of cumulative plastic deformation that frost-damaged samples can resist during fatigue testing was smaller than undamaged ones, providing thus lower fatigue life.
- Cyclic stiffness of frost-damaged samples was lower than undamaged ones. The crack network developed in the concrete matrix of frost-damaged samples was evident during this testing.
- The dimensionless hysteresis damping constant was larger in the frost-damaged samples, implying thus higher energy dissipation. Formation of new sliding surfaces (i.e., micro cracks) in the concrete matrix can be the main reason of increased dissipated energy through friction.

- As expected, frost-damaged samples revealed higher ADE values than the undamaged sample. However since TDE is the product of ADE by Nf, the undamaged samples have higher TDE values.

6.2. Recommendations for Future Research

- Larger size of beam samples and concrete slabs can better represent the real structure. On the other hand, smaller samples are easier to prepare and test. It is recommended that the effect of sample size and shape on the damping properties and fatigue life of concrete is evaluated. Perhaps this could be helpful to better predict the fatigue behavior of real size structures through using more representative prototype sample dimensions;
- Different stress ratios (R) should be used to evaluate the effect of minimum cyclic stress on fatigue life and damping properties of concrete;
- More experimental work is required to validate, the proposed method for predicting the endurance limit using the load-deflection envelope. Different mixtures with or without fiber have to be examined for this purpose;
- To study the post-failure load deflection curve, it is recommended that the load-deflection data are recorded for every loading cycle. This could be very helpful in case of mixtures that are very brittle and does not last long after fatigue failure;
- To further validate the fatigue life models that include the fiber content, additional mixtures with variable fiber content need to be tested at additional stress levels.

- The of moisture condition on the hysteresis damping properties of concrete should be investigated;
- It is recommended that the dynamic modulus of elasticity of frost-damaged samples is measured using the longitudinal and transverse natural frequency instead of the ultra-sonic pulse velocity method.

Appendix A.

Surface Deformation

One of the reported experimental issues related to recording the net deflection of beam at a third-point flexural loading configuration is the existence of extraneous deformation (δ) at the contact surface loading point (Gopalaratnam 1995). The recorded deflection at the loading point includes both the elasto-plastic flexural deflection of beam and the elasto-plastic compression at the surface of the beam under the loading point. Figure A.1 schematically demonstrates the extraneous deformations at the loading point.

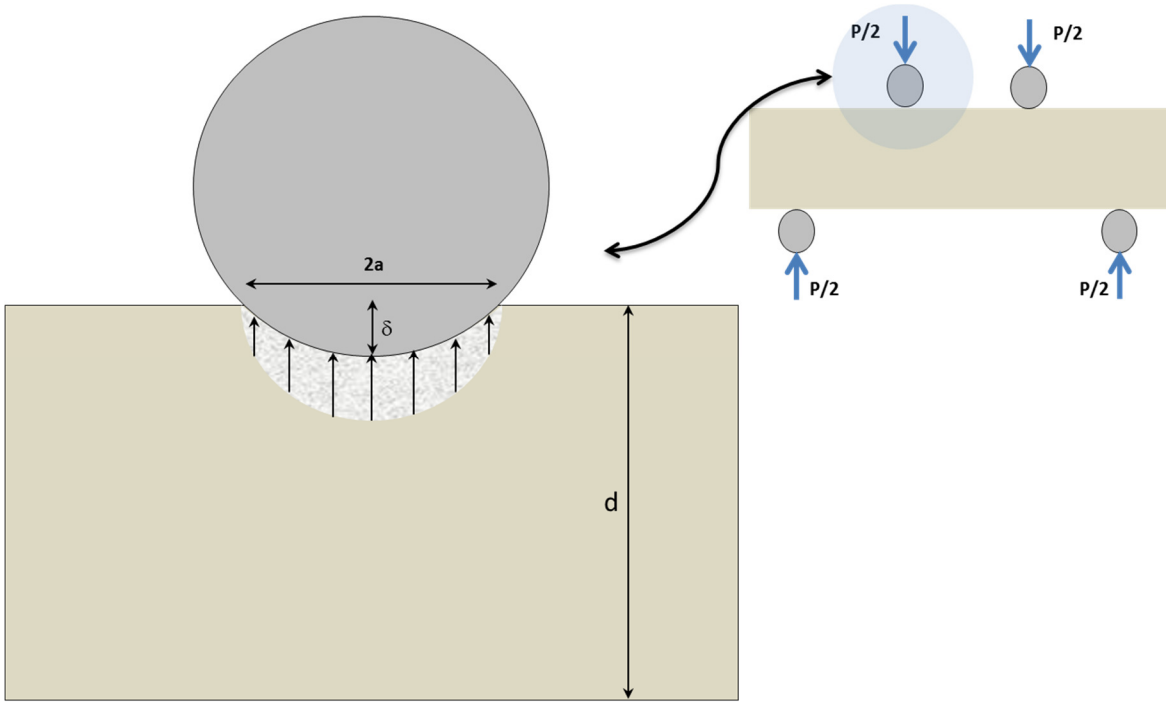

Figure A.1: Elasto-plastic deformation at loading points

In a static loading condition (i.e., a flexural strength test), before the load is applied to the sample the length of the contact zone (i.e., 2a in Figure A.1) is very small (almost zero). Therefore, the contact stress at the beginning of loading is significantly large. As the load gradually increases, contact stress also increases and leads to creation of elasto-plastic deformation on the surface of the concrete. The increase in surface deformation is associated with an increase in the length of the contact zone and, consequently, contact stress decreases. The process of increasing permanent deformation on the surface continues until contact stress is well below the strength of the concrete. After that point, the growth rate of plastic deformation at the surface significantly decreases. However, elastic deformation still grows as the load increases.

In this study it can be seen that large surface deformation occurs in cyclic loading, especially during the beginning cycles. Although there was no measurement device to distinguish between surface deformation and flexural deflection, several forms of evidence are available that confirm the existence of large surface deformation at the beginning of the fatigue test.

It can also be seen that large surface deformation has led to higher energy dissipation in the first cycle. As shown in Table A-1, dissipated energy at cycle 1 is almost 10 times larger than ADE. The reason for higher energy dissipation in cycle 1 is the formation of large surface deformation at the beginning of the fatigue test.

Table A-1: ADE vs. Dissipated energy at cycle 1

Sample ID	ADE (N.m)	Dissipated energy at cycle 1 (N.m)
0.8-5-1	0.0203	0.2358
0.7-5-1	0.0171	0.2318
0.6-5-1	0.0121	0.1891
0.8-10-1	0.0306	0.2774
0.7-10-1	0.0199	0.2966
0.6-10-1	0.0163	0.2052
200-1	0.0213	0.2080
400-7	0.0244	0.3091

Other evidence of the development of large surface deformation at the beginning of the fatigue test is the increasing trend of cyclic stiffness during the first 2% of fatigue life. Since the amplitude of loading (i.e., the difference between maximum and minimum cyclic load) was kept constant during the test, the only reason for the low cyclic stiffness of initial cycles is a large deflection in amplitude due to the development of surface permanent deformation (i.e., the difference between maximum and minimum cyclic deflection).

Contribution of Surface Deformation to Dissipated Energy per Loading Cycle

It has been proven that recorded deflection during fatigue testing not only includes flexural bending deflection but also surface compression, including both plastic and elastic deformation. The contribution of surface compression to dissipated energy per loading cycle is investigated in this section. For this purpose, the amount of surface

deformation is approximated by an elasticity-based model (Equation A.1) obtained by El-Shakra and Gopalaratnam (1993) to estimate the total surface compression and is then compared to the deflection caused by flexural bending.

$$\delta = \frac{P}{2\pi E_c}\left(2\,\mathrm{Ln}\left(\frac{a}{d}\right) - 2 + \vartheta\right) \qquad \textbf{A.1}$$

In the above equation, δ represent surface compression, maximum load is denoted by *P/2*, length of contact zone is denoted by *a*, depth of the beam is denoted by d, E_c is the elastic modulus in compression, and *v* represents the Poisson ratio of concrete. The amount of surface compression (δ) is approximately equal to:

$$\delta = 1.377\frac{P}{E_c} \qquad \textbf{A.2}$$

Assuming ν=0.15, d=76.2 mm, a=2mm (the length of contact zone found by measuring the width of samples' contact zones). The amount of bending deflection at loading point in a third-point loading configuration is also found to be

$$Deflection\ due\ to\ bending = 2.444\frac{P}{E_{flexure}} \qquad \textbf{A.3}$$

.

The ratio of flexural bending to surface compression is shown by Equation A.4.

$$\frac{Flexural\ Deflection}{Surface\ Compression} = 1.775\frac{E_c}{E_{flexure}} \quad \textbf{A.4}$$

Knowing that the elastic modulus of concrete in compression (E_c) is much large than elastic modulus in flexure ($E_{flexure}$), it can be concluded that the contribution of surface compression to net deflection is very small, and therefore most of the energy dissipation occurs through bending deflection.

Appendix B.

Outlier Detection (Chauvenet's method)

Chauvenet's outlier detection method is based on the specification of a probability range around the mean of a set of data which has a two-tailed normal probability equal to (see Figure B.1):

$$P = 1 - \frac{1}{2n} \qquad \textbf{B.1}$$

Where n is the number of data points. If a data point falls outside this boundary, it is called a possible outlier and can be eliminated from the data set. The process is then continued by calculation of new mean and probability range. The ending point of the method is when no data point is rejected. The results of volumetric analysis of freeze-thaw exposed sample were examined to find the potential outliers. Figure B.1 to Figure B.6 are shown the original data, outliers and, the average data after removing the outliers.

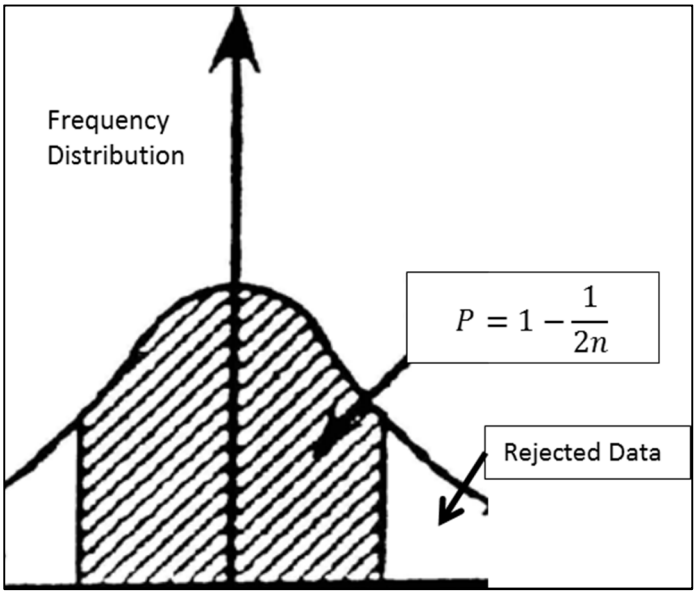

Figure B.1: Process of outlier detection based on Chauvenet's criteria

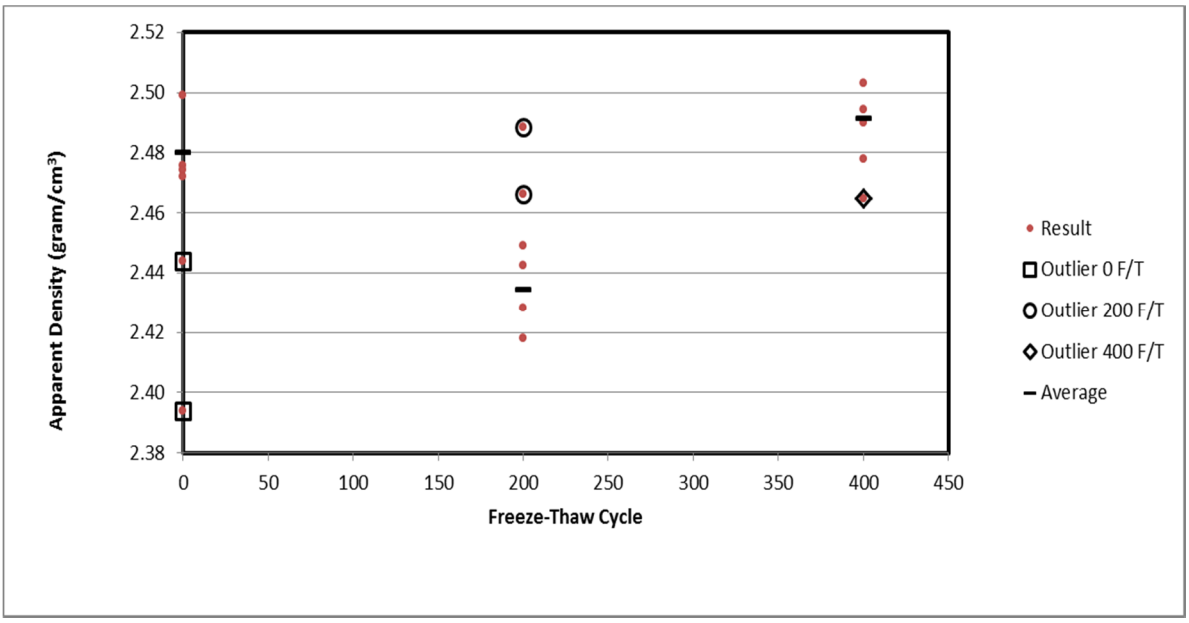

Figure B.2: Apparent density of freeze-thaw exposed samples (outlier detection)

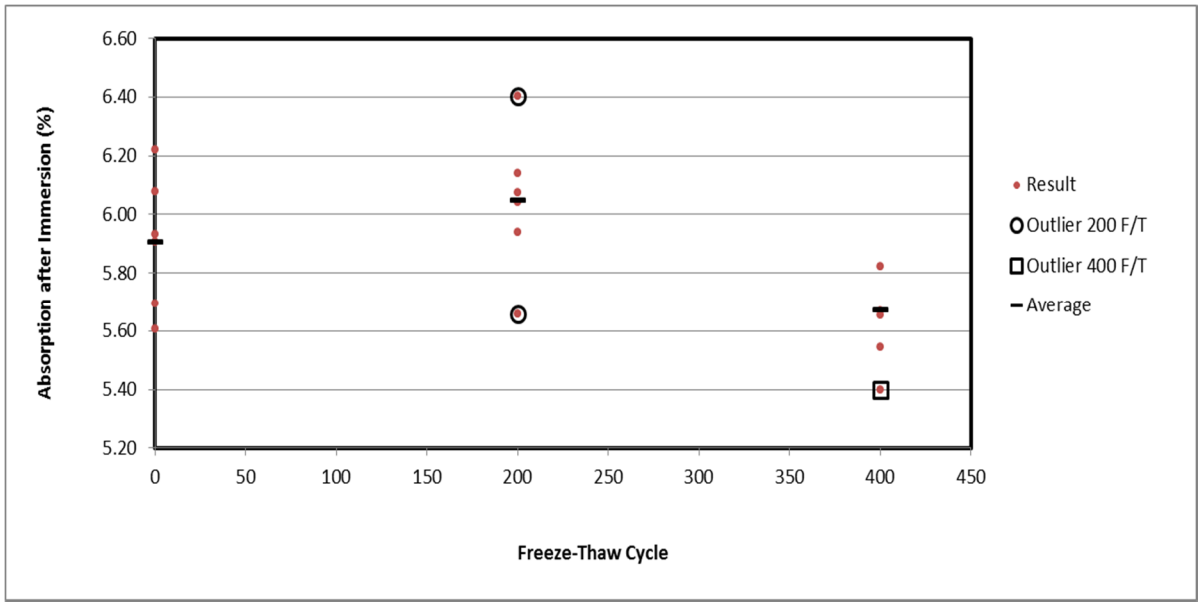

Figure B.3: Absorption after immersion of freeze-thaw exposed samples (outlier detection)

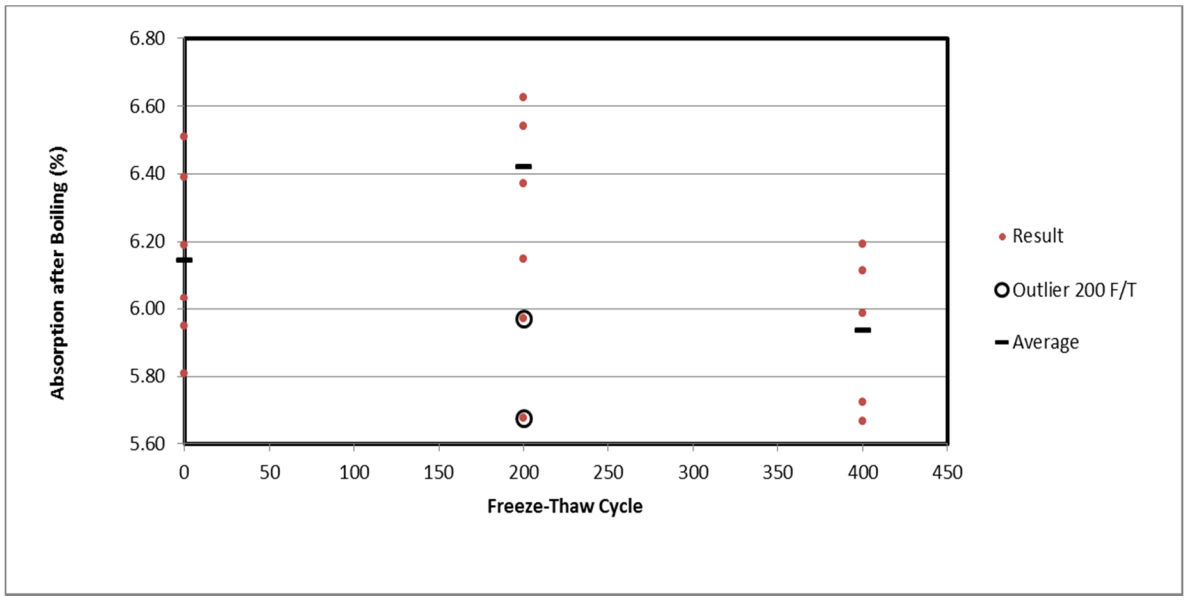

Figure B.4: Absorption after boiling of freeze-thaw exposed samples (outlier detection)

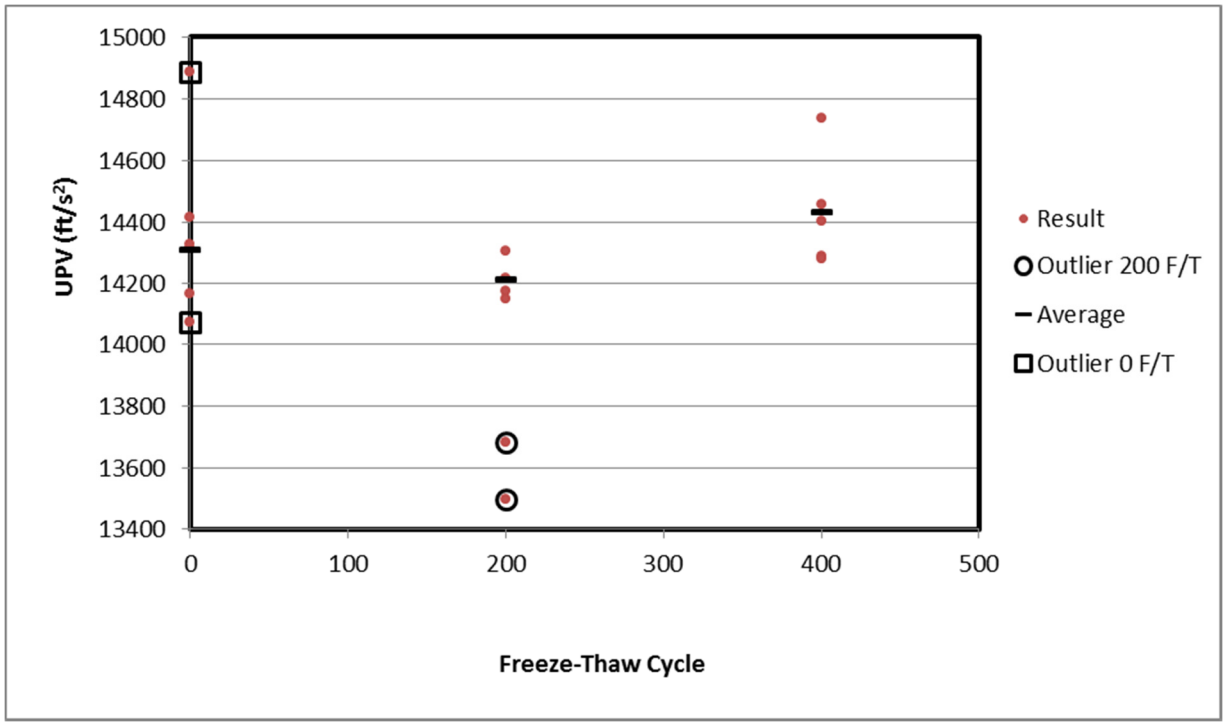

Figure B.5: UPV of freeze-thaw exposed samples (outlier detection)

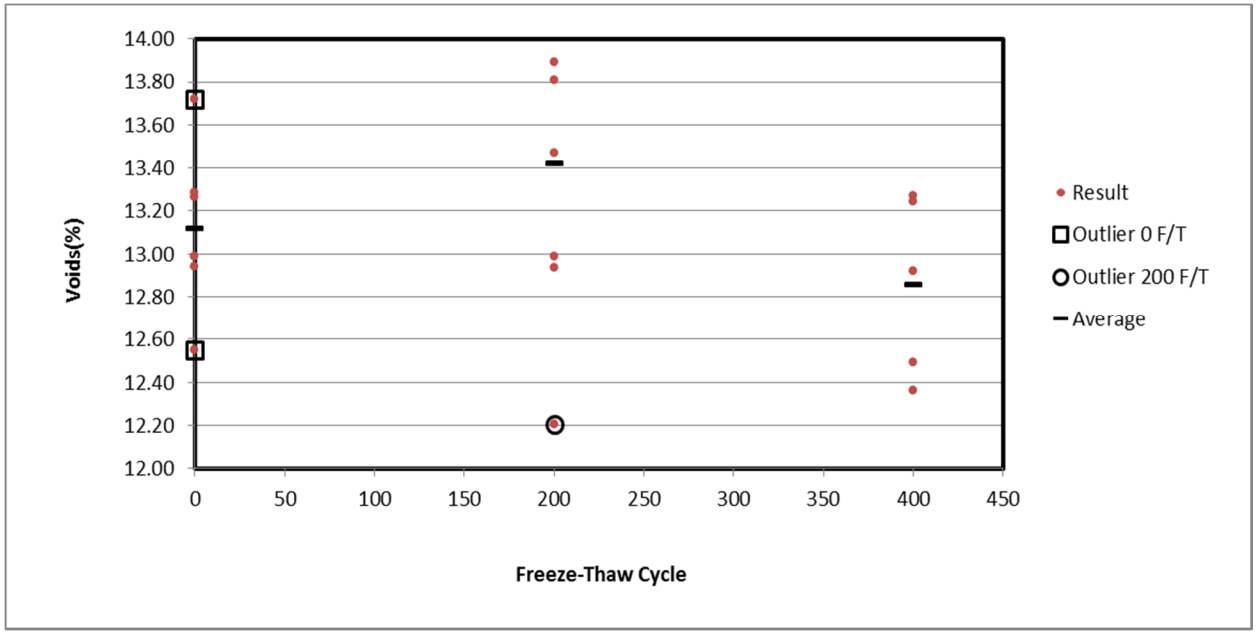

Figure B.6: Void ratio of freeze-thaw exposed samples (outlier detection)

Appendix C.

Table C-1: Regression analysis of model 1-table 5.49

Regression Statistics	
R Square	0.817
Adjusted R Square	0.808
Standard Error	3.429
Observations	22

	df	*SS*	*MS*	$F_{statistic}$	*Significance F*	$F_{critical}$
Regression	1	1050.63	1050.63	89.33	8.10E-09	4.35
Residual	20	235.23	11.76			
Total	21	1285.86				

	Coefficients	*Std Error*	$T_{statistic}$	*P-value*	$T_{critical}$
Intercept	-56.9326	13.402	-4.25	0.000	2.42
K	0.0023	0.000	9.45	0.000	

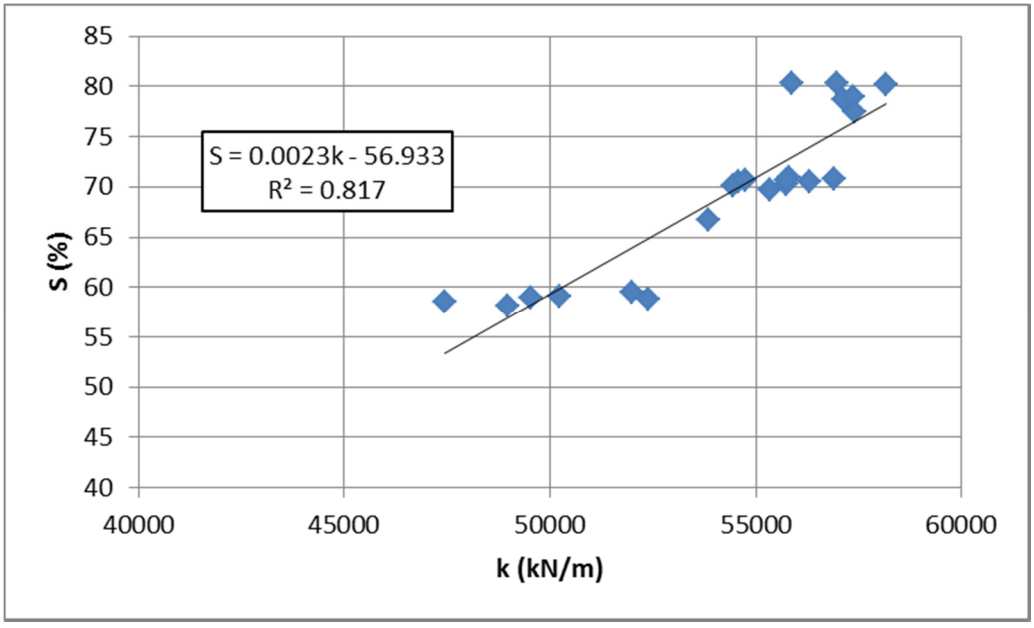

Figure C.1: Graphical format of model 1-table 5:49

Table C-2: Regression analysis of model 2-table 5.49

Regression Statistics	
R Square	0.838
Adjusted R Square	0.830
Standard Error	0.047
Observations	22

	df	*SS*	*MS*	$F_{statistic}$	*Significance F*	$F_{critical}$
Regression	1	0.231	0.231	103.448	2.38E-09	4.35
Residual	20	0.045	0.002			
Total	21	0.275				

	Coefficients	*Std Error*	$T_{statistic}$	*P-value*	$T_{critical}$
Intercept	2.361	0.185	12.792	4.36E-11	2.42
K	3.45E-05	0.000	10.171	2.38E-09	

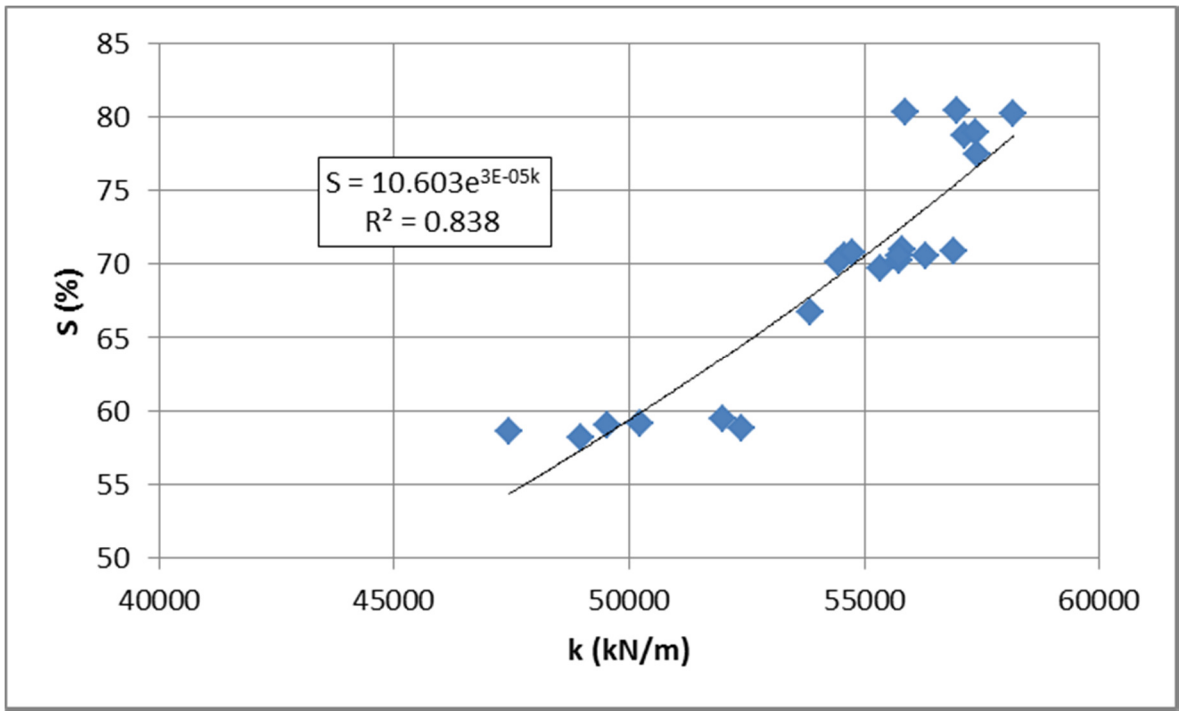

Figure C.2: Graphical format of model 2-table 5:49

Table C-3: Regression analysis of model 3-table 5.49

Regression Statistics	
R Square	0.827
Adjusted R Square	0.819
Standard Error	0.049
Observations	22

	df	*SS*	*MS*	$F_{statistic}$	*Significance F*	$F_{critical}$
Regression	1	0.2279	0.2279	95.92	4.49E-09	4.35
Residual	20	0.0475	0.0024			
Total	21	0.2754				

	Coefficients	*Std Error*	$T_{statistic}$	*P-value*	$T_{critical}$
Intercept	-15.510	2.016	-7.69	2.1E-07	2.42
Ln k	1.811	0.185	9.79	4.5E-09	

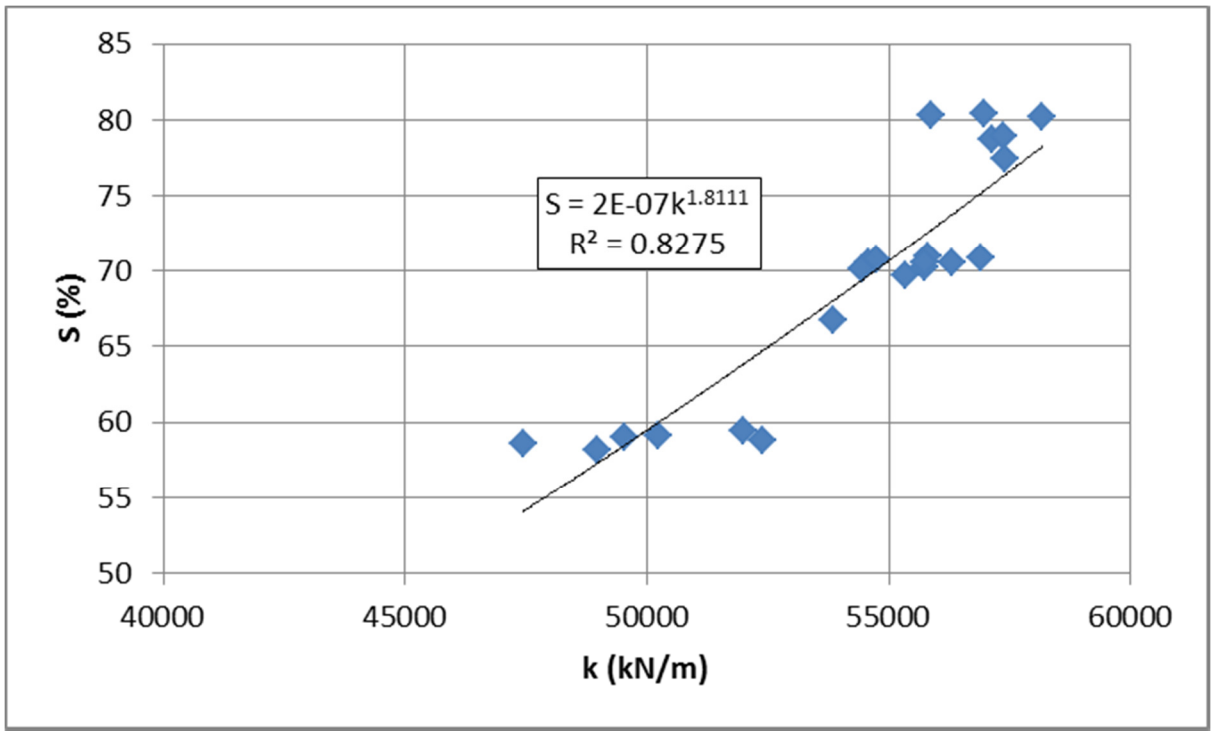

Figure C.3: Graphical format of model 3-table 5:49

Table C-4: Regression analysis of model 4-table 5.49

Regression Statistics	
R Square	0.584
Adjusted R Square	0.564
Standard Error	1.238
Observations	22

	df	*SS*	*MS*	$F_{statistic}$	*Significance F*	$F_{critical}$
Regression	1	43.11	43.110	28.1	3.43591E-05	4.35
Residual	20	30.66	1.533			
Total	21	73.77				

	Coefficients	*Std Error*	$T_{statistic}$	*P-value*	$T_{critical}$
Intercept	36.15	4.84	7.47	3.3E-07	2.42
K	0.00	0.00	-5.30	3.4E-05	

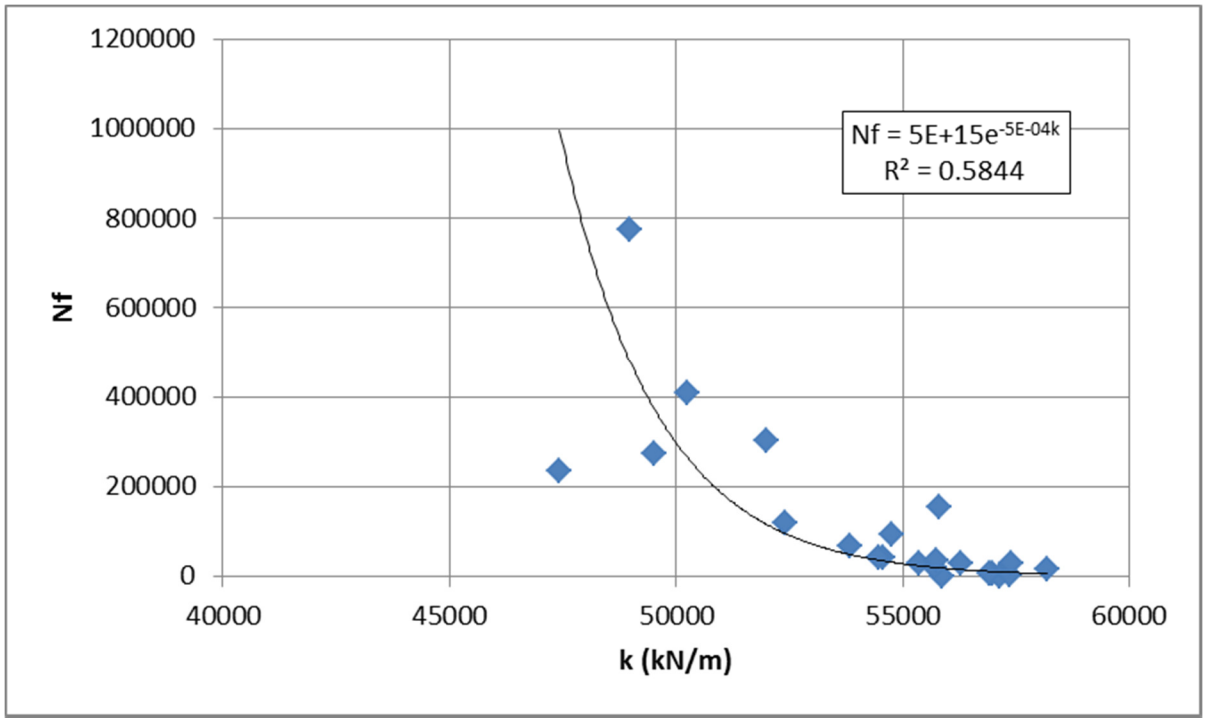

Figure C.4: Graphical format of model 4-table 5:49

Table C-5: Regression analysis of model 5-table 5.49

Regression Statistics	
R Square	0.577
Adjusted R Square	0.556
Standard Error	1.250
Observations	22

	df	*SS*	*MS*	$F_{statistic}$	*Significance F*	$F_{critical}$
Regression	1	42.54	42.54	27.24	4.16E-05	4.35
Residual	20	31.23	1.56			
Total	21	73.77				

	Coefficients	*Std Error*	$T_{statistic}$	*P-value*	$T_{critical}$
Intercept	280.29	51.68	5.42	2.62E-05	2.42
Ln k	-24.74	4.74	-5.22	4.16E-05	

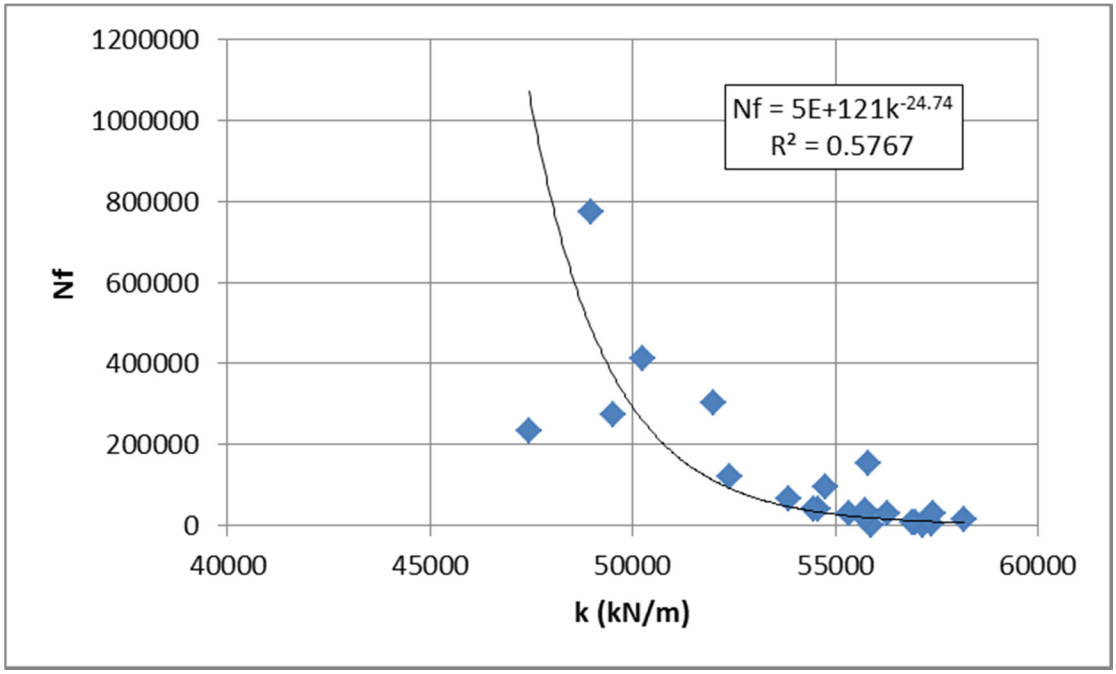

Figure C.5: Graphical format of model 5-table 5:49

Table C-6: Regression analysis of model 6-table 5.49

Regression Statistics	
R Square	0.806
Adjusted R Square	0.796
Standard Error	0.132
Observations	22

	df	*SS*	*MS*	$F_{statistic}$	*Significance F*	$F_{critical}$
Regression	1	1.46	1.46	83.15	1.46E-08	4.35
Residual	20	0.35	0.02			
Total	21	1.81				

	Coefficients	*Std Error*	$T_{statistic}$	*P-value*	$T_{critical}$
Intercept	-8.85	0.518	-17.11	2.08E-13	2.42
K	8.661E-05	0.000	9.12	1.46E-08	

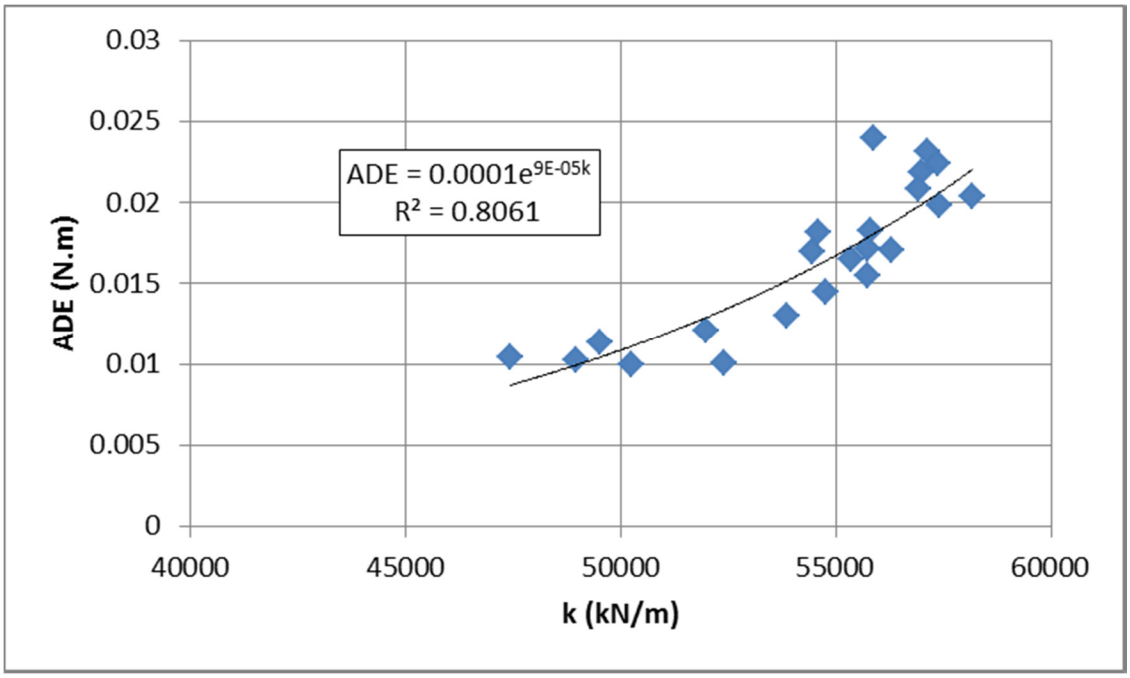

Figure C.6: Graphical format of model 6-table 5:49

Table C-7: Regression analysis of model 7-table 5.49

Regression Statistics	
R Square	0.960
Adjusted R Square	0.951
Standard Error	0.043
Observations	6

	df	*SS*	*MS*	$F_{statistic}$	*Significance F*	$F_{critical}$
Regression	1	0.180	0.180	97.144	0.0006	7.71
Residual	4	0.007	0.002			
Total	5	0.187				

	Coefficients	*Std Error*	$T_{statistic}$	*P-value*	$T_{critical}$
Intercept	1.817	0.5990	3.0325	0.0387	3.50
k	-0.00010	0.0000	-9.8562	0.0006	

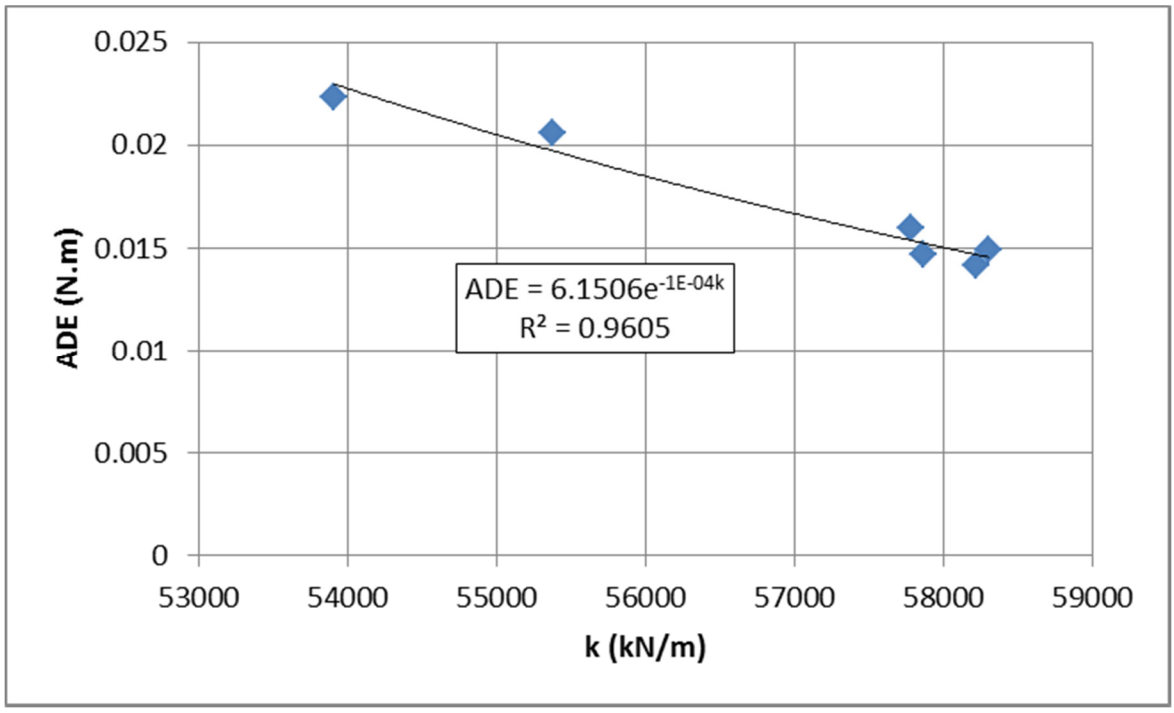

Figure C.7: Graphical format of model 7-table 5:49

Table C-8: Regression analysis of model 8-table 5.49

Regression Statistics	
R Square	0.556
Adjusted R Square	0.534
Standard Error	5.341
Observations	22

	df	*SS*	*MS*	$F_{statistic}$	*Significance F*	$F_{critical}$
Regression	1	715.28	715.28	25.07	6.8E-05	4.35
Residual	20	570.58	28.53			
Total	21	1285.86				

	Coefficients	*Std Error*	$T_{statistic}$	*P-value*	$T_{critical}$
Intercept	22.27	9.51	2.34	0.030	2.42
β	1500.59	299.69	5.01	0.000	

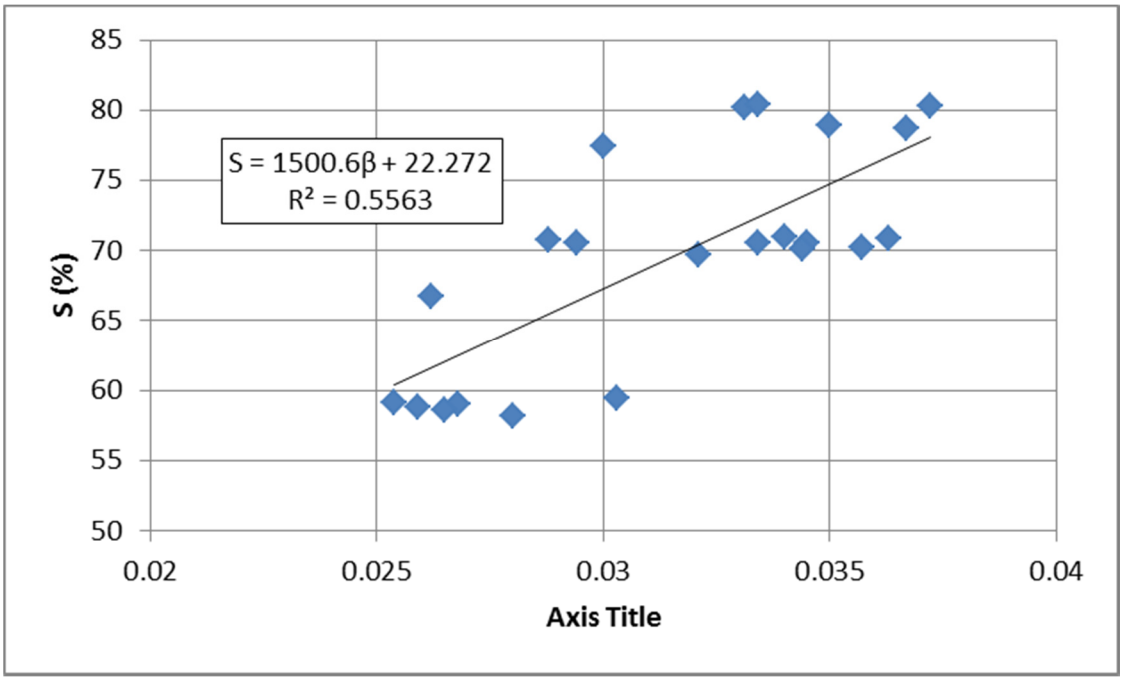

Figure C.8: Graphical format of model 8-table 5:49

Table C-9: Regression analysis of model 9-table 5.49

Regression Statistics	
R Square	0.567
Adjusted R Square	0.546
Standard Error	0.077
Observations	22

	df	*SS*	*MS*	$F_{statistic}$	*Significance F*	$F_{critical}$
Regression	1	0.16	0.16	26.21	5.2E-05	4.35
Residual	20	0.12	0.01			
Total	21	0.28				

	Coefficients	*Std Error*	$T_{statistic}$	*P-value*	$T_{critical}$
Intercept	3.54	0.14	25.73	8.4E-17	2.42
β	22.18	4.33	5.12	5.2E-05	

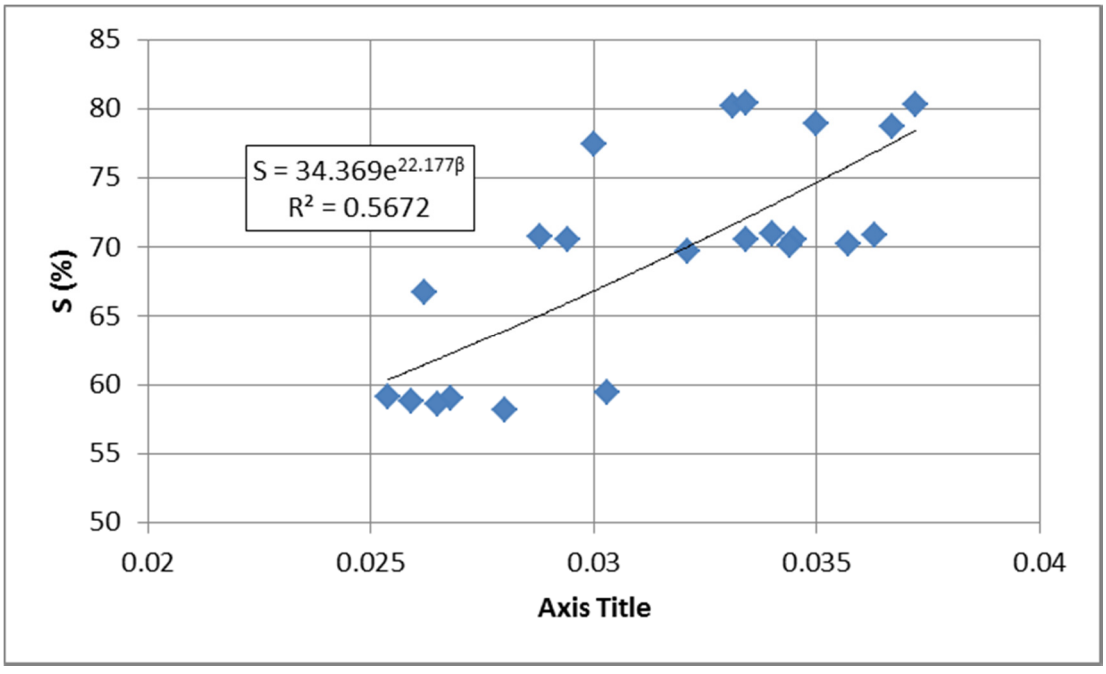

Figure C.9: Graphical format of model 9-table 5:49

Table C-10: Regression analysis of model 10-table 5.49

Regression Statistics	
R Square	0.577
Adjusted R Square	0.556
Standard Error	0.076
Observations	22

	df	*SS*	*MS*	$F_{statistic}$	*ignificance*	$F_{critical}$
Regression	1	0.159	0.159	27.257	4.15E-05	4.35
Residual	20	0.117	0.006			
Total	21	0.275				

	Coefficients	*Std Error*	$T_{statistic}$	*P-value*	$T_{critical}$
Intercept	6.63	0.46	14.46	4.74E-12	2.42
Ln β	0.69	0.13	5.22	4.15E-05	

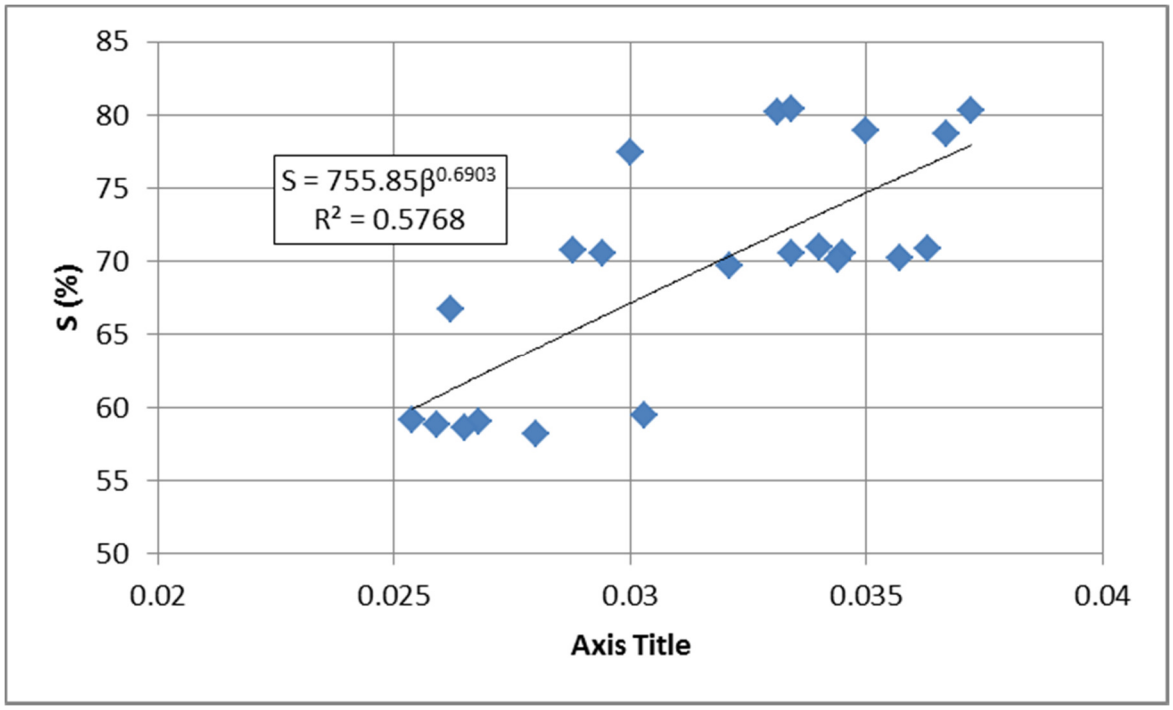

Figure C.10: Graphical format of model 10-table 5:49

Table C-11: Regression analysis of model 11-table 5.49

Regression Statistics	
R Square	0.615
Adjusted R Square	0.595
Standard Error	1.192
Observations	22

	df	*SS*	*MS*	$F_{statistic}$	*Significance F*	$F_{critical}$
Regression	1	45.33	45.33	31.89	1.58E-05	4.35
Residual	20	28.43	1.42			
Total	21	73.77				

	Coefficients	*Std Error*	$T_{statistic}$	*P-value*	$T_{critical}$
Intercept	22.4	2.1	10.6	1.25E-09	2.42
β	-377.8	66.9	-5.6	1.58E-05	

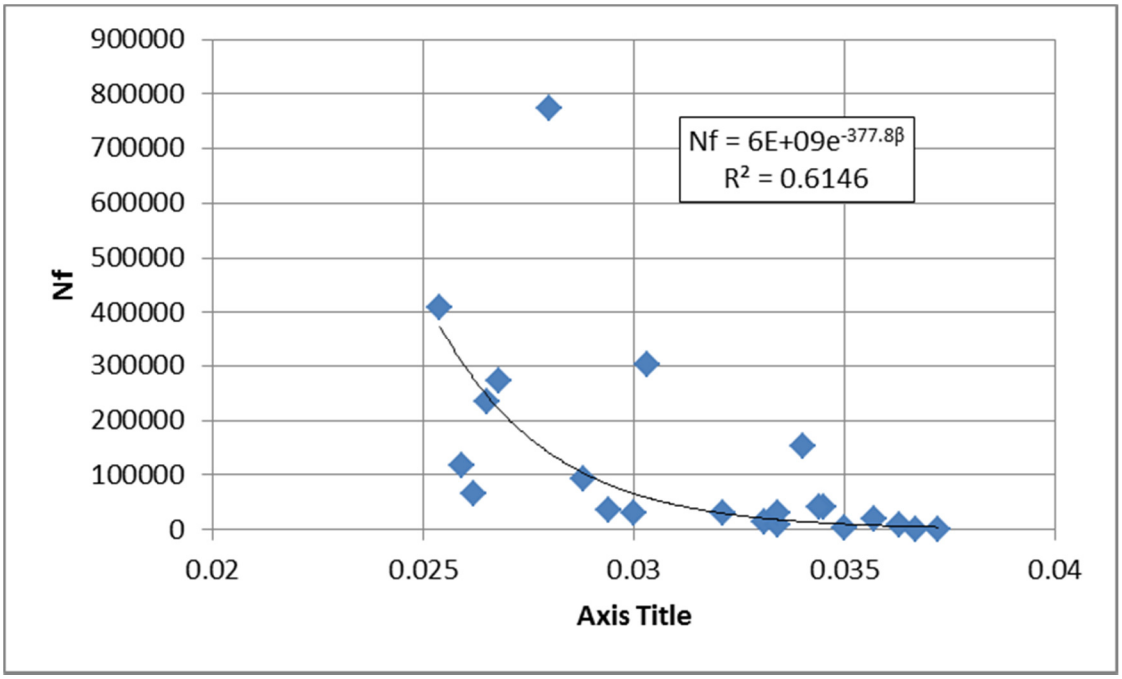

Figure C.11: Graphical format of model 11-table 5:49

Table C-12: Regression analysis of model 12-table 5.49

Regression Statistics	
R Square	0.960
Adjusted R Square	0.950
Standard Error	0.503
Observations	6

	df	*SS*	*MS*	$F_{statistic}$	*Significance F*	$F_{critical}$
Regression	1	24.24	24.24	95.89	0.001	7.71
Residual	4	1.01	0.25			
Total	5	25.25				

	Coefficients	*Std Error*	$T_{statistic}$	*P-value*	$T_{critical}$
Intercept	26.79	1.83	14.67	0.0001	3.50
beta	-589.83	60.23	-9.79	0.0006	

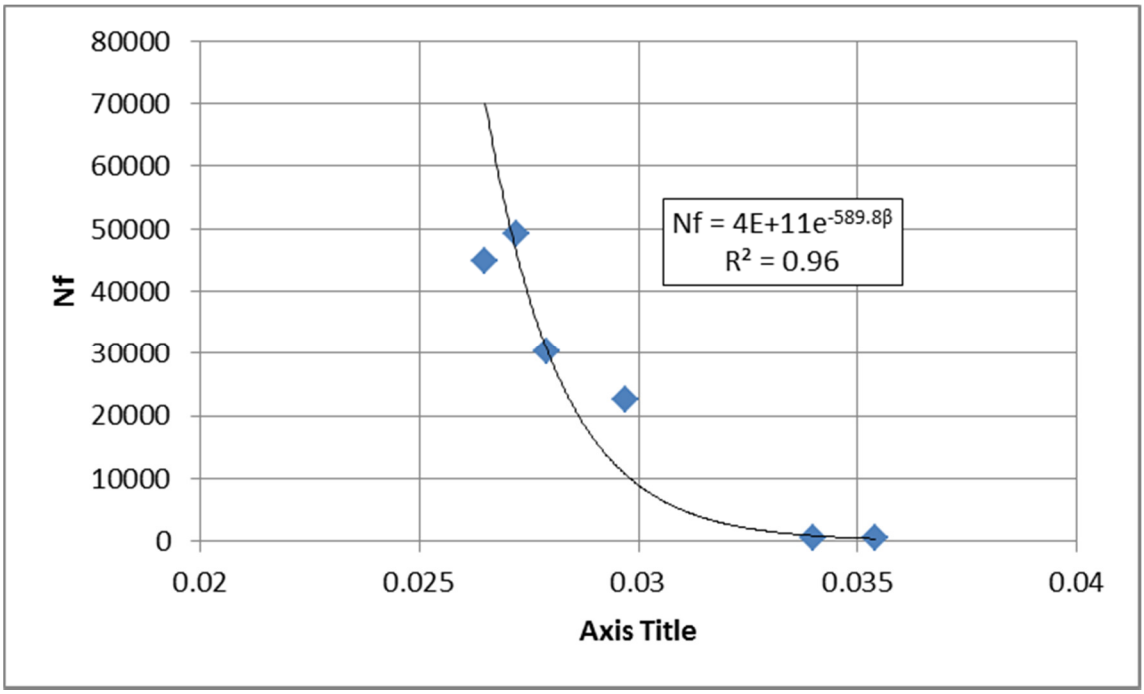

Figure C.12: Graphical format of model 12-table 5:49

Table C-13: Regression analysis of model 13-table 5.49

Regression Statistics	
R Square	0.763
Adjusted R Square	0.738
Standard Error	1.550
Observations	22

	df	*SS*	*MS*	$F_{statistic}$	*Significance F*	$F_{critical}$
Regression	2	146.70	73.35	30.55	1.16E-06	3.49
Residual	19	45.62	2.40			
Total	21	192.32				

	Coefficients	*Std Error*	$T_{statistic}$	*P-value*	$T_{critical}$
Intercept	48.824	6.524	7.484	4.45E-07	2.42
K	-0.001	0.000	-3.555	2.12E-03	
Beta	-276.910	126.852	-2.183	4.18E-02	

Table C-14: Regression analysis of model 14-table 5.49

Regression Statistics	
R Square	0.987
Adjusted R Square	0.978
Standard Error	0.363
Observations	6

	df	*SS*	*MS*	$F_{statistic}$	*Significance F*	$F_{critical}$
Regression	2	30.106	15.053	114.056	0.001	6.94
Residual	3	0.396	0.132			
Total	5	30.502				

	Coefficients	*Std Error*	$T_{statistic}$	*P-value*	$T_{critical}$
Intercept	-2.122	14.463	-0.147	0.893	3.50
beta	-473.897	100.435	-4.718	0.018	
k	0.000	0.000	1.965	0.144	

Table C-15: Regression analysis of model 15-table 5.49

Regression Statistics	
R Square	0.694
Adjusted R Square	0.662
Standard Error	1.089
Observations	22

	df	*SS*	*MS*	$F_{statistic}$	*Significance F*	$F_{critical}$
Regression	2	51.22	25.61	21.58	1.3E-05	3.49
Residual	19	22.54	1.19			
Total	21	73.77				

	Coefficients	*Std Error*	$T_{statistic}$	*P-value*	$T_{critical}$
Intercept	31.6850	4.5862	6.9087	1.38E-06	2.42
K	-0.0003	0.0001	-2.2273	3.82E-02	
Beta	-233.1442	89.1756	-2.6144	1.71E-02	

Table C-16: Regression analysis of model 16-table 5.49

Regression Statistics	
R Square	0.813
Adjusted R Square	0.793
Standard Error	0.352
Observations	22

	df	*SS*	*MS*	$F_{statistic}$	*Significance F*	$F_{critical}$
Regression	2	10.21	5.11	41.28	1.21334E-07	3.49
Residual	19	2.35	0.12			
Total	21	12.56				

	Coefficients	*Std Error*	$T_{statistic}$	*P-value*	$T_{critical}$
Intercept	10.00	0.71	14.15	1.52E-11	2.42
Beta	-57.51	29.62	-1.94	6.72E-02	
S	-0.07	0.01	-4.47	2.65E-04	

Table C-17: Regression analysis of model 17-table 5.49

Regression Statistics	
R Square	0.786
Adjusted R Square	0.763
Standard Error	0.912
Observations	22

	df	*SS*	*MS*	$F_{statistic}$	*Significance F*	$F_{critical}$
Regression	2	57.96	28.98	34.83	4.41766E-07	3.49
Residual	19	15.81	0.83			
Total	21	73.77				

	Coefficients	*Std Error*	$T_{statistic}$	*P-value*	$T_{critical}$
Intercept	25.74	1.83	14.04	1.75E-11	2.42
Beta	-154.60	76.83	-2.01	5.86E-02	
S	-0.15	0.04	-3.89	9.75E-04	

References

Aas-Jakobsen, Knut. *Fatigue of Concrete Beams and Columns.* Tapir, 1970.

Abd el Aty, Metwally Abd Allah . "Performance of Fibrous Concrete as Affected by Flexural Loading Rate." *Contemporary Engineering Sciences* 5 (2012): 325-340.

ACI Committee 201. "ACI 201.2R-Guide to durable concrete." 2008.

ACI Committee 215. "ACI215-R Considerations for Design of Concrete Structures Subjected to Fatigue Loading (ACI 215R-74)." 1997.

ASTM C127. *Standard Test Method for Density, Relative Density (Specific Gravity), and Absorption of Coarse Aggregate.* ASTM International, 2004.

ASTM C128. *Standard Test Method for Density, Relative Density (Specific Gravity), and Absorption of Fine Aggregate.* ASTM International, 2004.

ASTM C136. *Standard Test Method for Sieve Analysis of Fine and Coarse Aggregates.* ASTM International, 2005.

ASTM C143/C143M. *Standard Test Method for Slump of Hydraulic-Cement Concrete.* ASTM International, 2004.

ASTM C150. *Standard Specification for Portland Cement.* ASTM International, 2004.

ASTM C192/C192M . *Standard Practice for Making and Curing Concrete Test Specimens in the Laboratory.* ASTM International, 2007.

ASTM C260. *Standard Specification for Air-Entraining Admixtures for Concrete.* ASTM International, 2004.

ASTM C33/C33 M. *Standard Specification for Concrete Aggregates.* ASTM international, 2013.

ASTM C39/C39M. *Standard Test Method for Compressive Strength of Cylindrical Concrete Specimens.* ASTM International, 2005.

ASTM C469. *Standard Test Method for Static Modulus of Elasticity and Poisson's Ratio of Concrete in Compression.* ASTM International, 2002.

ASTM C494-04. *Standard Specification for Chemical Admixtures for Concrete.* ASTM International, 2004.

ASTM C642. *Standard Test Method for Density, Absorption, and Voids in Hardened Concrete.* ASTM International, 1997.

ASTM C666/C666M. *Standard Test Method for Resistance of Concrete to Rapid Freezing and Thawing.* ASTM International, 2003.

ASTM C78. *Standard Test Method for Flexural Strength of Concrete (Using Simple Beam with Third-Point Loading).* ASTM International, 2004.

ASTM C995. *Standard Test Standard Test Method for Time of Flow of Fiber Reinforced Concrete Through Inverted Slump Cone.* ASTM International, 2001.

Awad, M. E, and H. K Hilsdorf. *Strength and Deformation Characteristics of Plain Concrete Subjected to High Repeated and Sustained Loads.* Urbana: University of Illinois, 1971.

Bahn, Byong Youl, and Cheng-Tzu Thomas Hsu. "Stress-Strain Behavior of Concrete under Cyclic Loading." *ACI Material Journal*, 1998: 178-193.

Ballinger, C.A. "Cumulative Fatigue Damage Characteristics." *Highway Research Record*, 1972: 48-60.

Bazant, Z. B. *Theory of Creep and Shrinkage in Concrete Structures.* Vol. 2. Pergamon Press, 1975.

Carpenter, S. H, and M Jansen. "Fatigue Behavior Under New Aircraft Loading Conditions." *Proceedings of Aircraft Pavement Technology: In the Midst of Change.* Seattle, 1997. 259-271.

Chen, H, R Azzam, W Shao, H Han, and Z Yin. "Experimental research on high-frequency fatigue behavior of concrete." In *Challenges, Opportunities and Solutions in Structural Engineering and Construction*, by N Ghafoori, 63-68. Taylor and Francis Group, 2009.

Daniel, J. S, and W. M Bisirri. "Characterizing Fatigue in Pavement Materials Using a Dissipated Energy Parameter." *Proceedings of the Geo-Frontiers 2005* . Austin: ASCE, 2005. 1-10.

Darter, M I, and E J Barenberg. *Design of Zero-Maintenance Plain Jointed Concrete Pavement.* Federal Highway Administration, 1977.

EI-Shakra, Zeyad M, and Vellore S Gopalaratnam. "Deflection Measurement and Toughness Evaluations for FRC." *Cement and Concrete Research* 23 (1993): 1455-1466.

El-Shakra, Zayed M, Gopalarantam, Vellore S. "Deflection Measurement and Toughness Evaluation for FRC." *Cement and Concrete Research* 23 (1993): 1455-1466.

Forgeron, D. P, and J. F Trottier. "Evaluating the effects of combined freezing and thawing and flexural fatigue loading cycles on the fracture properties of FRC." *2nd International conference, High performance structures and materials.* WIT Press, 2004. 177-188.

Furtak, K. "Ein verfahren zur berechnung der betonfestigkeit unter schwellenden belastungen (In German)." *Cement and Concrete Research*, 1984: Vol. 14, Issue 6, page 855-865.

Gopalaratnam, Vellore S. "On the Characterization of Flexural Toughness in Fiber Reinforced Concrete." *Cement and Concrete Composite* 17, no. 3 (1995): 239-254.

Graybill, Franklin A., and Hariharan K. Iyer. *Regression Analysis: Concepts and Applications.* Duxbury Press, 1994.

Grzybowski, Miroslaw, and Christian Meyer. "Damage Accumulation in Concrete with and without Fiber Reinforcement." *ACI Material Journal*, 1993: Vol.90, Issue.6, page 594-604.

Hasan, Muttaqin, Tamon Ueda, and Yasuhiko Sato. "Stress-Strain Relationship of Frost-Damaged Concrete Subjected to Fatigue Loading." *Journal of Materials in Civil Engineering*, 2008: 37-45.

Helmuth, R. A. "Capillary Size Restrictions on Ice in Hardened Portland Cement Pastes." Washington D. C.: Portland Cement Association, Research and Development Laboratories, 1960a. 855-869.

—. "Frost Action in Concrete." Washington D. C., 1960b. 829-833.

Holmes, J. W, and S. F Shuler. "Temperature rise during fatigue of fibre-reinforced ceramics." *Journal OF Materials Science*, 1990: 1290-1291.

Hsu, T. T. C. "Fatigue of plain concrete." *Proceedings,American Concrete Institute Journal*, 1981: Vol. 78, No. 4, page 292-305.

Joly, De. *La resístanse et l'étasticité des ciments.* Annales dês Pons ET Chaussee, 1898.

Kesler, C. E. *Effect of Speed of Testing on Flexural Fatigue Strength of Plain Concrete.* Proceedings, Highway Research Board, 1953, Vol. 32, page 251-258.

Kim, Haejin. *Behavior and Performance of High Performance Concrete for Pavements.* Master of Science Thesis, College Park: University of Maryland at College Park, 2003.

Li, Wenting, Wei Sun, and Jinyang Jiang. "Damage of concrete experiencing flexural fatigue load and closed freeze/thaw cycles simultaneously." *Construction and Building Materials*, 2011: 2604-2610.

Manolis, G. D, P. J Gareis, A. D Tsono, and J. A Neal. "Dynamic Properties of Polypropylene Fiber-Reinforced Concrete Slabs." *Cement and Concrete Composites* , 1997: 341-349.

McCall, J. "Probability of Fatigue Failure of Plain Concrete in Flexure." *Journal of ACI*, 1958: 233-244.

Mohammadi, Y, and S.K Kaushik. "Flexural Fatigue-Life Distributions of Plain and Fibrous in various stress levels." *Journal Of Materials in civil engineering*, 2005: Vol. 17, No. 6, page 650-658.

Murdock, J. W, and C. E Kesler. "Effect of Range of Stress on Fatigue Strength of Plain Concrete Beams." *Journal of the American Concrete Institute*, 1958: Vol.30, No.2, page 221-231.

Murdock, John W. *A Critical Review of Research on Plain Concrete.* University Of Illinois at Urbana-champaign, 1965.

Oh, Byung H. "Fatigue analysis of plain concrete in flexure." *Journal of Structural Engineering*, 1986: Volume 112, Issue 2, 273-288.

Packard, R. G, and S. D Tayabji. "New PCA Thickness Design Procedure for Concrete Highway and Street Pavements." *3rd International Conference on Concrete Pavement Design.* West Lafayette, 1985. 225-236.

Paskova, Todorka, and Christian Meyer. "Low-cycle fatigue of Plain and Fiber-Reinforced Concrete." *ACI Material Journal*, 1997: Vol. 94, No.4, page 273-285.

Powers, T. C. "Basic consideration Pertaining to Freezing and Thawing Test." West Conshohocken: American Society for Testing and Materials, 1955. 1132-1155.

—. "Freezing Effect in Concrete." Farmington Hills: American Concrete Institiute, 1975. 1-11.

—. "Resistance of Concret to Frost at Early Ages." *RILEM Symposium on Winter Concreting.* Copenhagen, 1956. 1-50.

Raithby, K.D., and J.W. Galloway. *Effects of Moisture Condition, Age and Rate of Loading on Fatigue of Plain Concrete.* ACI Publication SP-41, 1974.

Ramakrishnan, V, George Y Wu, and G Hosalli. "Flexural Fatigue Strength, Endurance Limit and Impact Strength of Fiber Reinforced Concretes." *Transportation Reaserch Record 1226*, 1989: 17-24.

Rao, Singiresu S. *Mechanical Vibration.* Addison-Wesley Publishing Company, 1990.

Richardson, A. E, K. A Coventry, and S Wilkinson. "Freeze/thaw durability of concrete with synthetic fibre additions." *Cold Regions Science and Technology*, 2012: 49-56.

Roesler, J. R. *Fatigue of Concrete Beams and Slabs.* PhD Thesis, Urbana: University of Illinois, 1998.

Sahmaran, Mustafa, Erdogan Özbay, Hasan E Yücel, Mohamed Lachemi, and Victor C Li. "Frost resistance and microstructure of Engineered Cementitious Composites: Influence of fly ash and micro poly-vinyl-alcohol fiber." *Cement & Concrete Composites*, 2012: 156-165.

Shi, X. P, T. F Fwa, and S. A Tan. "Flexural fatigue strength of plain Concrete." *ACI Materials Journal* (ACI Material Journal), 1993: Vol. 90, Issue 5, page 435-440.

Singh, S. P, Sanjay Goel, Roshan Lal, and S. K Kaushik. "Prediction of Mean and Design Fatigue Lives of Steel Fibrous Cconcrete Using S-N Relationships." *Asian Journal of Civil Engineering (Building AND Housing)*, 2004: Vol. 5, page 175-190.

Singh, S.P, and S.K Kaushik. "Fatigue strength of steel fibre reinforced concrete in flexure." *Cement & Concrete Composites*, 2003.

Singh, Surinder P. "Fatigue Strength of Hybrid Steel-Polypropylene Fibrous Concrete Beams in Flexure." *Procedia Engineering*, 2011: 2446-2452.

Spirito, P, CE Seidman, and WJ Mckenna. "The management of hypertrophic cardiomyopathy." 1997.

Steidel, Robert F. *An Introduction to Mechanical Vibration.* John Wiley and Sons, 1989.

Tawfiq, Kamal, Jamshid Armaghani, and Rodolfo Ruiz. "Fatigue Cracking of Polypropylene Fiber Reinforced Concrete." *ACI Material Journal* 96, no. 2 (1999): 226-233.

Tepfers, R, and T Kutti. "Fatigue Strength of Plain, Ordinary, and Lightweight Concrete." *Journal of the American Concrete Institute*, 1979: Vol. 76, page 635-52.

Tepfers, R, G. O Sjostrom, Svensson I. J, and Herrmann G. "Developement of a Method for Measuring Destruction Energy and Generated Heat at Fatigue of Concrete."

3rd Inernational Conference, Civil Engineering 11. Latvia University of Agricultute, 2011. 117-124.

Torvik, Peter J. "Material Damping and Slid Damping." In *Harris' Shock and Vibration Handbook*, by Allan Piersol and Thomas Paez. McGraw-Hill, 2002.

Trainor, Kevin J, Bradley W Foust, and Eric N Landis. "Measurement of Energy Dissipation Mechanisms in Fracture of Fiber-Reinforced Ultrahigh-Strength Cement-Based Composites." *Journal of Engineering Mechanics* 139, no. 7 (2013): 771–779.

Vesic, A. S, and S. K Saxena. *Analysis of Structural Behavior of Road Test Rigid Pavements.* Whasington, D.C.: Highway Research Board, No. 291, 1969.

Yan, Dongming, and Gao Lin. "Dynamic Properties of Concrete in Direct Tension." *Cement and Concrete Research*, 2006: 1371-1378.

Yun, Hyun-Do, and Keitetsu Rokugo. "Freeze-thaw influence on the flexural properties of ductile fiber-reinforced cementitious composites (DFRCCs) for durable infrastructures." *Cold Regions Science and Technology*, 2012: 82-88.

Zheng, Zhihong, and Dorel Feldman. "Synthetic Fibre-Reinforced Concrete." *Progress in Polymer Science* 20, no. 2 (1995): 185–210.